LIPOPEPTIDE-COATED IRON OXIDE NANOPARTICLES AND ENGINEERED Qβ VIRUS LIKE PARTICLES AS POTENTIAL GLYCOCONJUGATE-BASED SYNTHETIC ANTICANCER VACCINES

By

Suttipun Sungsuwan

A DISSERTATION

Submitted to
Michigan State University
in partial fulfillment of the requirements
for the degree of

Chemistry – Doctor of Philosophy

2017

ABSTRACT

LIPOPEPTIDE-COATED IRON OXIDE NANOPARTICLES AND ENGINEERED Qβ VIRUS LIKE PARTICLES AS POTENTIAL GLYCOCONJUGATE-BASED SYNTHETIC ANTICANCER VACCINES

By

Suttipun Sungsuwan

Due to genetic and/or epigenetic alteration, glycan markers on tumor cells structurally differ from those on the normal cells. These unique glycans, termed tumor associated carbohydrate antigens (TACAs), have been utilized to educate the immune system to specifically recognize and eliminate cancer cells, a concept known as cancer immunotherapy or anticancer vaccine. The major challenge of developing an anti-TACA vaccine is the low immunogenicity of TACAs as they are self-antigens and not sufficiently immunogenic when administered alone.

In chapter 1, iron oxide magnetic nanoparticles (NPs) have been evaluated as carriers for glycoconjugate-based anticancer vaccines. With their high biocompatibilities and large surface areas, magnetic NPs were synthesized for TACA delivery. The magnetic NPs were coated with phospholipid-functionalized TACA glycopeptides through hydrophobic−hydrophobic interactions without the need for any covalent linkages. Multiple copies of glycopeptides were presented on NPs, potentially leading to enhanced interactions with antibody-secreting B cells through multivalent binding. Mice immunized with the NPs generated strong antibody responses, and the glycopeptide structures important for high antibody titers were identified. The antibodies produced were capable of recognizing both mouse and human tumor cells expressing the glycopeptide, resulting in tumor cell death through complement-mediated cytotoxicities. These results demonstrate that magnetic NPs can be a new and simple platform for multivalently

displaying TACA and boosting anti-TACA immune responses without the need for a typical protein carrier.

Besides iron oxide magnetic nanoparticles (NPs), bacteriophage Qβ is another excellent immunogenic carrier able to break self-tolerance to induce strong antibody response against TACA. One potential drawback of bacteriophage Qβ is its strong immunogenicity, which also induces a strong antibody response against itself. This unwanted anti-carrier immune response can lead to carrier-induced epitopic suppression (CIES), which can limits the full potential of the Qβ in inducing maximum desired immune response against TACA.

In chapter 2, Qβ viral capsid was engineered to reduce the unwanted immune response against the carrier protein, thus refocusing the immunity towards generating higher potency of desired immune response against TACAs. Non-native disulfide bonds were introduced into the capsid to enhance the stability of the engineered capsids. Our results showed that the new Qβ mutants can reduce the unwanted anti-carrier immune response, yet enhance the wanted titers of antibodies against TACA. The approaches presented in this study provide a fundamental implication for rational design of engineered virus-like-particle-based carrier to maximize the potency of vaccines targeting TACA expressing cancers as well as other diseases.

To my beloved family
and
His Majesty King Bhumibol Adulyadej.

ACKNOWLEDGEMENTS

The way led to the completion of this dissertation would be more difficult or would have not been accomplished without the support from many people. I would like to express my respect and appreciation to these people who guided and helped me along the way. The most influential person of my dissertation was my advisor, Professor Xuefei Huang, who generously gave me his invaluable guidance, supports, supervision and kind encouragement throughout this study. Even though I disappointed him many times to get good results or make experiments work, he never failed to inspire and challenge me to experience many of new research areas I had never been exposed to, which drove my perspective and capability in conducting research to another level. I would also like to thank all my guidance committee members, Dr. Heedeok Hong, for his helpful suggestions involving molecular biology aspects and his kind permission to let me use instruments in his lab; Dr. Kevin Walker, for his assistance, good suggestions and kindness, and Dr. Robert Abramovitch for his helpful suggestions and kind collaboration in anti-M. tuberculosis vaccine project.

I would like to thank all instrumental specialists who assisted me to run all experiments involving sophisticate analytical instruments. My special thanks are to Dr. Dan Holmes who kindly trained me to set up and run all kinds of NMR experiments; Professor Dan Jones, Lijun Chen, Scott Smith and Tony Schilmiller, who trained me to run high-end mass spectrometers and assisted me to process all data; Dr. Xudong Fan, who helped me run TEM and made all the images look fantastic and Dr. Xianshu Jin, who kindly helped me run and analyzed X-ray crystallography of Qβ VLPs.

My great appreciation is also expressed to fellowships from Royal Thai Government, graduate school and department of chemistry in Michigan State University for opportunities and all supports throughout my study in doctoral degree.

I am indebted to all of my friends and colleagues from Huang group, especially Dr. Zhaojun Yin, who patiently spent his time mentoring me to develop my research knowledge and skills in immunology. I would not come this far without him. Besides, I thank Moe, Hovig, Herbert, Philip, Jingguang, Xuanjun, Qian, Shuyao and Mehdi for their invaluable assistance in biological experiments. I also thank Vivian, Bo, Keisuke, Steve, Weizhun, Sherif, Kedar, Changxin, Peng, Jicheng, Zeren, Jia for introducing me to the beauty of carbohydrate synthesis and great assistance in my chemical synthesis parts. These people well demonstrated how the hard work pays off. In addition to research assistance, I have deep appreciation for their warm friendship and cheering me up when I am discouraged. They helped me expand my perspective tremendously about their interesting cultures, personalities and positive attitudes.

Finally, I would like to express my deepest gratitude to my family and my beloved girlfriend, Cho, for their unconditional love, care, understanding and encouragement through the duration of my research.

Thank you.

Suttipun Sungsuwan

TABLE OF CONTENTS

LIST OF TABLES x

LIST OF FIGURES xi

LIST OF SCHEMES xix

KEY TO ABBREVIATIONS xx

CHAPTER 1 : Lipopeptide-Coated Iron Oxide Nanoparticles as Potential Glycoconjugate-Based Synthetic Anticancer Vaccines[1] 1

1.1 Introduction 1

1.1.1 Cancer immunotherapy 1

1.1.2 Mechanism behind immunity 3

1.1.3 Protein post-translation modification by glycosylation 7

1.1.4 Mucin1 8

1.1.5 Aberrant glycosylation in cancer cells 11

1.1.6 Evidences supporting MUC1 based vaccine 14

1.1.7 Anti-MUC1 vaccine development 16

1.1.8 Particulate Vaccine 18

1.1.9 Physical properties of a particulate vaccine determine the immune response profile. 20

1.1.10 Anti-MUC1 particulate vaccines 21

1.1.11 Superparamagnetic iron oxide nanoparticle: SPION 25

1.1.12 Self-assembly of amphiphilic-molecule coated iron oxide nanoparticles 26

1.2 Results and discussion 27

1.2.1 Synthesis of magnetic NPs coated with MUC1 lipopeptides and lipo-glycopeptides 27

1.2.2 *In vitro* activation of dendritic cells and detection of NP draining into local lymph nodes *in vivo*. 33

1.2.3 Immunization with MUC1 coated NPs elicited strong anti-MUC1 IgG responses. 36

1.2.4 The antibodies from immunized mice showed binding and complement dependent cytotoxicity against MUC1-expressing tumor cells. 39

1.2.5 Discussion 41

1.3 Conclusions 43

1.4 Materials and methods 45

1.4.1 Materials and instrumentation 45

1.4.2 Synthesis of Fmoc-*p*Tn-Thr-OH 46

1.4.3 Synthesis of MUC1 1 and Tn-MUC1 2-4 50

1.4.4 Purification and characterization of (glyco)-peptides 1–4 51

1.4.5 Synthesis of lipo-(Tn)-peptide (DPPE-MUC1 5 and DPPE-Tn-MUC1 6-8) 56

1.4.6 Purification and characterization of lipo-(glyco)-peptide 5–8 56

1.4.7 Preparation of iron oxide NPs (OA-IONPs) 61
1.4.8 The number of OA-IONP nanoparticle was estimated by TEM and TGA analysis. 61
1.4.9 Preparation of NP5-9 62
1.4.10 Verification of the glyco-lipopeptide (DSPE-MUC1(Tn) 6, 7 and 8 on the coated nanoparticles 63
1.4.11 Quantification of the lipopeptide (DSPE-MUC1) on the coated nanoparticles 65
1.4.12 The ratio of DPPE-MUC1 and DSPE-PEG coated on each nanoparticle determined by Malachite Green phosphate assay 65
1.4.13 Elemental analysis for estimation of the number of DPPE-MUC1 molecules coated on a single nanoparticle 65
1.4.14 Bone marrow derived dendritic cell culture 66
1.4.15 Flow cytometry of dendritic cellular marker expression 66
1.4.16 Histology of the NPs in the targeted lymph node 67
1.4.17 Mouse immunization 67
1.4.18 ELISA 67
1.4.19 Cell culture 68
1.4.20 Flow cytometry analysis 68
1.4.21 Complement dependent cytotoxicity 69
APPENDICES 70
APPENDIX A: Quantification of the lipopeptide (DSPE-MUC1) on the coated nanoparticles 71
APPENDIX B: NMR spectra 75
REFERENCES 81

CHAPTER 2 : Engineered Virus-Like Particle Qβ as a Novel Carrier for TACA-Based Anticancer Vaccines 96
2.1 Introduction 96
2.1.1 Virus-like particle as a vaccine carrier 96
2.1.2 Bacteriophages 97
2.1.3 Bacteriophage Qβ 97
2.1.4 Bacteriophage Qβ VLP in vaccine applications 100
2.1.5 Qβ VLP as a carrier for TACA-based anti-cancer vaccines. 108
2.1.6 Carrier-Induced Epitopic Suppression (CIES) in Qβ 116
2.2 Results and discussion 119
2.2.1 B cell epitope prediction 119
2.2.2 Improve stability of Qβ VLP 129
2.2.3 Immunization study 138
2.2.4 Binding of the elicited antibody against tumor cells 142
2.2.5 Tumor challenge 145
2.3 Conclusions 150
2.4 Future perspective 151
2.5 Materials and methods 155
2.5.1 Site-directed mutagenesis of Qβ VLPs 155
2.5.2 Qβ viral capsid protein expression and purification 157
2.5.3 Synthesis and characterization of Qβ or mQβ conjugates[36] 159

2.5.4 Size exclusion chromatography (SEC) 159
2.5.5 Non-denaturing agarose gel 160
2.5.6 Thermal stability measurement of viral capsid by temperature varied UV-Vis spectroscopy 160
2.5.7 Dynamic light scattering (DLS) and transmission electron microscopy (TEM) 161
2.5.8 Immunization studies[36] 161
2.5.9 Enzyme-linked immunosorbent assay (ELISA) 162
2.5.10 Cell cultures 163
2.5.11 Flow cytometry experiment 163
2.5.12 Anti-tumor immunoprotection (Tumor challenge) 163
2.5.13 Liquid chromatography–mass spectrometry (LCMS) 164
2.5.14 Transmission electron microscopy (TEM) Images 164
2.5.15 Synthesis of Tn1 and Tn2 165
2.5.16 Synthesis procedure 166
APPENDICES 171
APPENDIX A: Size Exclusion Chromatograms 172
APPENDIX B: Liquid chromatography–mass spectra 177
APPENDIX C: NMR spectra 184
REFERENCES 219

LIST OF TABLES

Table 1.1: Hydrodynamic diameters and zeta potentials of the NP vaccines in PBS.....32

Table 2.1: Sequences of Qβ specific peptides used for re-stimulation of splenocytes from the vaccinated mice.[22] 103

Table 2.2: Qβ mutants reported that assemble to form the capsid. 123

Table 2.3: Qβ mutants that fail to assemble into the VLP. 125

Table 2.4: Physical characteristics of Qβ mutants. 126

Table 2.5: The average number of Tn1 conjugated on each capsid of Qβ particle and yield of Qβ-Tn1 conjugate. [% add^n Tn = ($Tn1/subunit_{mQβ}$ − $Tn1/subunit_{wtQβ}$) × 100 / $Tn1/subunit_{wtQβ}$] 136

Table 2.6: Physical characteristics of Qβ-Tn1 conjugates. 137

Table 2.7: Primers used in the construction of mutant Qβ VLPs 156

LIST OF FIGURES

Figure 1.1: A cartoon showing two types of humoral immune activation by a tumor antigen.*Upper panel* – T cell-independent B-cell activation: the multivalent antigen crosslinks B cell receptors without the help from T cells leading to IgM secretion. *Lower panel* – T cell-dependent B-cell activation: In addition to B-cell activation by direct antigen recognition, the antigen can be taken up by antigen presenting cells such as dendritic cells, which subsequently present the antigen fragment to activate helper T cell (Th cell). The activated Th cell releases cytokines to induce B cells to undergo Ig-isotype switching from IgM to IgG. The figure is adapted and reproduced from reference[14]. 4

Figure 1.2: Illustration showing the process of cell-mediated immunity. a) The antigen-presenting cell uptakes and processes an antigen into a short fragment ($CD8^+$ T-cell epitope). The digested fragment is loaded onto MHC class I and presented to a $CD8^+$ T cell. The activated $CD8^+$ T cell then proliferates and becomes cytotoxic T cells, which will be able to kill the corresponding pathogens or cancer cells. b) The processed antigen fragments that are loaded onto MHC class II will be presented to $CD4^+$ T cell. The activated $CD4^+$ T cells will release cytokines in T-cell dependent B cell activation resulting in IgM-to-IgG isotype switching and the generation of IgG secreting plasma cells and memory B cells. The figure is reproduced with permission from reference[17].....6

Figure 1.3: a) C-terminal (MUC1-C) and N-terminal subunit (MUC1-N) are connected by non-covalent interaction after auto-proteolytic cleavage. b) C-terminal MUC1 (MUC1-C) are composed of a cytoplasmic domain (CD), a transmembrane domain (TM), and an extracellular N-terminal domain (ED). N-glycan on Asp-36 can cis-bind to receptor tyrosine kinases (RTKs) after loss of polarity. c) The N-terminal subunit (MUC1-N) will dissociate and leave the C-terminal subunit (MUC1-C) due to tumorigenesis on cancer cells. d) Cellular alteration due to tumorigenesis causes loss of polarity or delocalization of the remaining C-terminal subunit to entire cell surface, instead of specific presentation on the apical side. The C-terminal subunits form cis-interactions with receptor tyrosine kinases (RTKs) causing amplification of the aberrantly overexpression of MUC1 on cancer cells. This figure is adapted and reproduced with permission from reference[25]. 9

Figure 1.4: Variable number tandem repeats (VNTR) of twenty amino acids in N-terminal subunit (MUC1-N). 5 potential amino acids (red letters) are potentially subjected to O-glycosylation. This figure is adapted and reproduced with permissions from references[21, 25]. 10

Figure 1.5: The process of *O*-glycosylation begins with the addition of a GalNAc moiety onto a serine or threonine residue in a polypeptide. The glycosylation will then be extended from the starting GalNAc unit by T-synthase to core 1 – core 4 structures. This figure is adapted and reproduced with permission from reference[34b]. 12

Figure 1.6: The glycosylation enzyme T-synthase in cancer cells is malfunctioning due to improper enzyme folding caused by the absent of *Cosmc* chaperon in the endoplasmic reticulum in cancer cells. The malfunctioning T-synthase in cancer cells leads to the aberrant glycosylation in glycopeptide MUC1. This figure is adapted and reproduced with permission from reference[34b]. 13

Figure 1.7: The structure of TACAs; Tn, T and their sialiated products; α(2-3)ST, α(2-6)STn.....14

Figure 1.8: Representative structures of fully synthetic three-component compounds composed of B cell epitope from MUC1, Th epitope from polio virus (PV) and TLR1 and 2 agonist, Pam3CysSK4, or TLR2 and 6 agonist, Pam2CysSK4. This figure is adapted and reproduced with permission from reference[75].....23

Figure 1.9: Synthesis of the hydrophobic OA-IONPs by the thermal decomposition method, and monolayer self-assembly coating of the NPs by phospholipid functionalized MUC1 or MUC1(Tn) glycopeptide. 31

Figure 1.10: TEM images and hydrodynamic diameters from DLS a, c) OA-IONPs; b, d) **NP-5**.....31

Figure 1.11: a) MALDI-TOF mass spectrum of **NP-5** coated with lipopeptide **5** ($[M+H]^+$ = 2662) and DSPE-PEG (top spectrum); and **NP-9** coated with DSPE-PEG only (bottom spectrum). b) SDS-PAGE of DPPE-MUC1, NP-PEG (**NP-9**), and NP-MUC1 (**NP-5**). The gel was visualized through silver staining. 33

Figure 1.12: a) Flow cytometry results showing the expression of cellular markers of activation state (CD40, CD80, CD86 and MHCII) of BMDC after incubation with NP-PEG (**NP-9**) (red line), or NP-PEG (**NP-9**) + MPLA (blue line). Confocal images of BMDC incubated with b) PBS and c) **NP-9** (FITC) + MPLA. Histology of sections from d) axillary (local) lymph nodes, and e) inguins (distant) lymph node, stained by Prussian blue.....35

Figure 1.13: Microscopic images of Prussian blue staining of BMDC after incubation with **NP-9**. *Left*) only dendritic cells; *Middle*) dendritic cells incubated with NP-9 (50 μg) in PBS 12 hrs.; *Right*) dendritic cells incubated with NP-9 (50 μg) and MPLA (2 μg/mL) in PBS 12 h. 36

Figure 1.14: a) Anti-MUC1 and anti-Tn-MUC1 antibody titers from individual mouse (n=5), collected on day 35 after immunization with NP-MUC1 (**NP-5**) and NP-MUC1(Tn) (**NP-6**, **NP-7** and **NP-8**) vaccines, compared with soluble MUC1 peptide **1** and lipo-MUC1-peptide **5**. The anti-MUC1 antibody titers were determined by ELISA coated with corresponding (glyco)peptides **1-4**. b) IgG antibody titer from individual mouse, collected on day 35 after immunization with NP-MUC1 (**NP-5**), against MUC1 peptide **1** and **NP-9** c) IgM/IgG antibody response determined by ELISA at 3200-fold dilution of serum from mice immunized with different vaccines. d) IgG isotypes of antibody response determined by ELISA from mice immunized with various vaccines. 38

Figure 1.15: Cross-recognition of various MUC1 glycoforms by sera from mice immunized with **NP-5** – **NP-8**. 39

Figure 1.16: Flow cytometric analysis of the binding of antibodies induced by various constructs to a) MUC1-Ag104 cells and c) MCF-7. MTS assay analysis of complement-dependent cytotoxicity of antibodies induced by various vaccines on b) MUC1-Ag104 cells and d) MCF-7. (** $P < 0.05$, *** $P < 0.005$,).....40

Figure 1.17: Flow cytometry showing the specific binding of anti-MUC1 antibody from immunized mice a) against wild type Ag104 (Ag104(wt)) and MUC1 transfected Ag104 cells (Ag104(MUC1)); b) against MUC1 transfected Ag104 cells (Ag104(MUC1)) and endothelial cells (EA.hy926). 41

Figure 1.18: Synthesis of **Fmoc-*p*Tn-Thr-OH**. 46

Figure 1.19: HPLC chromatogram and MALDI-TOF mass spectrum of the MUC1 peptide **1**, and the MUC1 glycopeptide **2**, **3** and **4**. 52

Figure 1.20: HPLC chromatogram and MALDI-TOF mass spectrum of the lipopeptide **5**, and lipo-glycopeptide **6**, **7** and **8**. 57

Figure 1.21: TGA curve of OA-IONP. 62

Figure 1.22: MALDI-TOF mass spectrum of glyco-lipopeptide coated OAIONP; **NP-6**, **NP-7**, **NP-8** indicate the present of the glyco-lipopeptide on each nanoparticle. The clustered peaks in the base line represent the coating DSPE-PEG. 63

Figure 1.23: Quantification of the lipo(glyco)peptide on the coated nanoparticles. 71

Figure 1.24: ^{1}H NMR spectrum of **SI-3**. 75

Figure 1:25: ^{1}H NMR spectrum of **SI-4**. 76

Figure 1.26: ^{1}H NMR spectrum of **SI-5**. 77

Figure 1.27: ^{1}H NMR spectrum of **SI-7**. 78

Figure 1.28: ^{1}H NMR spectrum of **SI-8**. 79

Figure 1.29: ^{1}H NMR spectrum of **Fmoc-*p*Tn-Thr-OH**. 80

Figure 2.1: Qβ protein structure (PDB-ID: 1QBE), a.) Qβ subunit protein with secondary structure domains; b,c) The alignment of the dimer subunit and all lysine residues; d) The organization of fivefold- and quasi-sixfold units to form icosahedral shape with triangulation number (T) = 3. The green residues are cysteines at position 74 and 80, which form an intra-subunit disulfide bond.....99

Figure 2.2: Qβ specific T cell responses were measured from level of cytokines secreted from splenocytes of HA conjugated Qβ immunized mice with peptide pools spanning Qβ capsid protein regions. Each bar represents the total cytokine response to each peptide pool and the colored boxes represent level of each specific cytokine. Each peptide pool is composed of 5 peptides fragments that have the overlap sequences as listed in **Table 2.1**. The figure is reproduced from reference[22].....102

Figure 2.3: X-ray crystal structure of Qβ subunit (1qbe). The red and blue colored regions display the most probable Th epitopes. Red region = $Q\beta_{41-71}$, Blue region = $Q\beta_{101-132}$.....104

Figure 2.4: *Top panel*: Branched oligomannose glycans were conjugated via CuAAC reaction on the wild-type Qβ, mutant QβK16M or QβHPG, where the most reactive lysine at position 16 was replaced by an unnatural amino acid homopropargyl glycine. *Bottom panel*: Synthesis of QβHPG glycoconjugates QβHPG-Man8 (**11**) and QβHPG-Man8/Man9 (**12**). The figure is reproduced with permission from reference[22]. 106

Figure 2.5: Synthesis of Qβ-triazole-Tn via CuAAC reaction. The reaction condition can be adjusted to provide a variable number of Tns (78, 150 and 340 Tns) attached on the viral capsid. This figure is adapted and reproduced with permission from reference[35].....112

Figure 2.6: a) a table showing characteristic details of the vaccine compound with varied Tn density used in 6 groups to investigate the effect of antigen density on the viral capsid. b) ELISA results of IgG and c) IgM antibodies from 6 groups of immunized mice at 1/6400 dilution. This figure is adapted and reproduced with permission from reference[35].....113

Figure 2.7: a) Vaccine constructs Qβ-Tn **4** and Qβ-Tn **5**. b,c) IgG titers elicited from the vaccine constructs against Tn or triazole. The increased number of attached Tn induced lower anti-Tn antibody titers due to suppression from increased anti-triazole immune response. d) Specific recognition against Tn-expressing cancer cells of the elicited antibodies from Qβ-Tn **1** and Qβ-Tn **6**. e) Vaccine constructs Qβ-Tn **6** where the triazole linker was replaced with low immunogenic alkyl linker. f) anti-Tn antibody titers elicited from Qβ-Tn6. The IgG titers became higher compared with those from Qβ-Tn **4** and Qβ-Tn **5**. This figure is adapted and reproduced with permission from reference[36].....115

Figure 2.8: Antibody titers against D2 peptide (attached antigen) and Qβ VLP (carrier) elicited from Qβ primed- or naïve mice after 1st, 2nd and 3rd vaccination. The result suggests that the higher density of D2 on the Qβ helped reduce the suppression from CIES. This figure is adapted and reproduced with permission from reference[37].....118

Figure 2.9: a) Eight of synthetic 30-amino-acid peptides that overlapped sequence by 15 amino acids covering the entire amino acid sequence of Qβ capsid protein. b) ELISA result of peptide scanning experiment showing the binding of the peptides fragments with the anti-wtQβ IgG antibodies. The synthetic peptides were coated on the ELISA plate. The dilution of serum (1/64000 dilution) from wtQβ-immunized mice was added to test recognition towards each peptide fragments. Group (-) is a negative control group where only PBS was used in coating process.....120

Figure 2.10: Discontinuous B cell epitope prediction by DiscoTope 2.0 server[40] showing in electron cloud surface is overlaid over 3D structure of Qβ capsid protein. The red areas represent protein fragments that obtain high scores from the prediction.....122

Figure 2.11: A graph showing solvent accessible surface area (SASA) of each amino acid residue in representative chain B of Qβ capsid protein (1qbe). The figure and data were obtained from VIPERdb (http://viperdb.scripps.edu).[41] 122

Figure 2.12: Electrophoretic mobility of Qβ whole capsids by native agarose gel. The samples (~30 μg of each capsid protein) were loaded into 0.7% agarose gel in PBS with SYBR Safe DNA gel strain as a straining reagent for the encapsulated RNA. The electrophoresis was performed in TEA buffer at 4°C for 4 hours. *Top panel*) The encapsulated RNA strained in the capsids was detected by UV light. *Middle panel*) The capsid proteins were detected by Coomassie staining. *Bottom panel*) Overlaying the two panels confirms the presence of the encapsulated RNA in the mQβs. 128

Figure 2.13: X-ray crystal structure of wtQβ showing a) distances between β-carbon of residues involving disulfide formation; b) disulfide bond networks from native disulfide bonds between C74 and C80 (green residues) in wtQβ and expected non-native disulfide bonds in mQβ A40C/D102C (yellow residues). 131

Figure 2.14: a) Size exclusion chromatograms of wtQβ (red) and mQβs, A38K(yellow), A38K/A40C/A102C (green), A40C/D102C (blue); b) TEM images of wtQβ and mQβs. 131

Figure 2.15: a) SDS-PAGE of the viral capsids in non-reductive (oxidative) condition (Left) and reductive condition (right). 133

Figure 2.16: Thermal stability of mQβs determined by UV absorption at λ = 310 nm at increasing temperature. 134

Figure 2.17: Conjugation reaction between **NHS-Tn1** with the various mQβs. 136

Figure 2.18: X-ray crystal structure of wtQβ showing the hydrogen bond interaction (solid blue line) between the carboxyl group on the side chain of D102 and the amino group on the side chain of K13(distance = 3.145 Å). 138

Figure 2.19: ELISA results of post-immunized sera (day 35) from groups of mice (n=5) vaccinated with variant mQβ-Tn1. a and b) Anti-Tn1 titers of the post-immunized sera presented in linear and log scale, respectively. The statistical significance of differences between a mQβ and wtQβ was determined by the Student t test (** $p < 0.01$; *** $p < 0.001$; **** $p < 0.0001$) c) OD_{450} from the ELISA result of the post-immunized sera at 1/819200 dilution against BSA-Tn1. d) OD_{450} from the ELISA result of the post-immunized sera at 1/1638400 against the corresponding carrier capsids. The statistical significance of differences between a mQβ and wtQβ was determined by the Student t test. e) OD_{450} from ELISA result at 1/819200 sera dilution of IgG subtypes antibodies (IgG1, IgG2b, IgG2c and IgG3) elicited by wtQβ-Tn1, mQβ(A38K/A40C/D102C)-Tn1 and mQβ(A40C/D102C)-Tn1 immunization against BSA-Tn1. 140

Figure 2.20: Competitive ELISA showing reduced anti-wtQβ antibody recognition of mQβ-Tn conjugates.....142

Figure 2.21: Flow cytometry showing binding of elicited IgG antibodies by Qβ conjugates; a and b) Histogram showing binding recognition of the elicited antibodies against Jurkat cells and TA3Ha cells, respectively, c and d) Graph of median fluorescent intensities of the binding recognition of the elicited antibodies towards Jurkat cells and TA3Ha cells, respectively. 144

Figure 2.22: a) Chemical structures of **Tn1** and **Tn2**. b) MFI of cellular binding against Jurkat cells of the serum from mice immunized with wtQβ-Tn2 and mQβ(A38K/A40C/D102C)-Tn2 compared with those from wtQβ-Tn1 and mQβ(A38K/A40C/D102C)-Tn1. 145

Figure 2.23: OD_{450} from the ELISA result of the post-immunized sera at 1/819200 dilution against BSA-Tn2 from mice immunized with wtQβ-Tn2 and mQβ(A38K/A40C/D102C)-Tn2. The statistical significance of differences was determined by the Student t test. 147

Figure 2.24: Flow cytometry showing binding of elicited IgG antibodies by wtQβ-Tn2 and mQβ(A38K/A40C/D102C)-Tn2 a) Histogram showing binding recognition of the elicited antibodies against TA3Ha cells, respectively, b) Graph comparing median fluorescent intensities of the binding recognition of the elicited antibodies towards TA3Ha cells. 149

Figure 2.25: Kaplan-Meier survival curves comparing the protective effect of wtQβ-Tn2 and mQβ(A38K/A40C/D102C)-Tn2: a) after 1st tumor challenge with treatment of CP (n=10), b) after 2nd tumor challenge without any further treatment (n=5). Statistical analysis of survival is determined by using the log-rank test in GraphPad Prism software. Note: Control experiments have been done in reference[36]. 150

Figure 2.26: Chemical structure of tolerogenic CD22 ligand.....153

Figure 2.27: UV-visible absorption of wtQβ at varied temperature from 25 to 90°C. The estimated wavelength that provides the most different absorption is 310 nm (dashed line). 161

Figure 2.28: TEM images of wild-type Qβ and various Qβ mutants. 164

Figure 2.29: Size-exclusion chromatography of wild-type Qβ, varied Qβ mutants and their Tn1 derivatives.....172

Figure 2.30: Mass spectra of wild-type Qβ-Tn1 and varied Qβ mutant-Tn1 after applying MaxEnd1 algorithm. 177

Figure 2.31: ^{1}H NMR spectrum of compound **SI-11** 184

Figure 2.32: ^{13}C NMR spectrum of compound **SI-11** 185

Figure 2.33: ^{1}H-^{1}H COSY NMR spectrum of compound **SI-11** 186

Figure 2.34: gHMQC NMR spectrum of compound **SI-11**.....187

Figure 2.35: gHMBC NMR spectrum of compound **SI-11**.....188

Figure 2.36: ^{1}H NMR spectrum of compound **SI-12**.....189

Figure 2.37: ^{13}C NMR spectrum of compound **SI-12**.....190

Figure 2.38: ^{1}H-^{1}H COSY NMR spectrum of compound **SI-12**.....191

Figure 2.39: gHMQC NMR spectrum of compound **SI-12**.....192

Figure 2.40: gHMBC NMR spectrum of compound **SI-12**.....193

Figure 2.41: ^{1}H NMR spectrum of compound **SI-14**.....194

Figure 2.42: ^{13}C NMR spectrum of compound **SI-14**.....195

Figure 2.43: ^{1}H-^{1}H COSY NMR spectrum of compound **SI-14**.....196

Figure 2.44: gHMQC NMR spectrum of compound **SI-14**.....197

Figure 2.45: gHMBC NMR spectrum of compound **SI-14**.....198

Figure 2.46: ^{1}H NMR spectrum of compound **Tn1**.....199

Figure 2.47: ^{13}C NMR spectrum of compound **Tn1**.....200

Figure 2.48: ^{1}H-^{1}H COSY NMR spectrum of compound **Tn1**.....201

Figure 2.49: gHMQC NMR spectrum of compound **Tn1**.....202

Figure 2.50: gHMBC NMR spectrum of compound **Tn1**.....203

Figure 2.51: ^{1}H NMR spectrum of compound **Tn2**.....204

Figure 2.52: ^{13}C NMR spectrum of compound **Tn2**.....205

Figure 2.53: ^{1}H-^{1}H COSY NMR spectrum of compound **Tn2**.....206

Figure 2.54: gHMQC NMR spectrum of compound **Tn2**.....207

Figure 2.55: gHMBC NMR spectrum of compound **Tn2**.....208

Figure 2.56: ^{1}H NMR spectrum of compound **Tn1-NHS**.....209

Figure 2.57: ^{13}C NMR spectrum of compound **Tn1-NHS**.....210

Figure 2.58: ^{1}H-^{1}H COSY NMR spectrum of compound **Tn1-NHS**.....211

Figure 2.59: gHMQC NMR spectrum of compound **Tn1-NHS** 212

Figure 2.60: gHMBC NMR spectrum of compound **Tn1-NHS**.....213

Figure 2.61: ^{1}H NMR spectrum of compound **Tn2-NHS** 214

Figure 2.62: ^{13}C NMR spectrum of compound **Tn2-NHS** 215

Figure 2.63: ^{1}H-^{1}H COSY NMR spectrum of compound **Tn2-NHS** 216

Figure 2.64: gHMQC NMR spectrum of compound **Tn2-NHS** 217

Figure 2.65: gHMBC NMR spectrum of compound **Tn2-NHS**.....218

LIST OF SCHEMES

Scheme 1.1: Synthesis of MUC1 lipo-(glyco)peptides. The (Tn-)MUC1 peptides **1-4** were synthesized by solid phase peptide synthesis followed by coupling with the activated phospholipid **DPPE-SUC-NHS** to yield MUC1 lipo-(glyco)peptides **5-8**. 29

Scheme 2.1: Synthesis of **Tn1-NHS** and **Tn2-NHS**.....166

KEY TO ABBREVIATIONS

ADCC	antibody-dependent-cell-mediated cytotoxicity
APC	antigen presenting cell
BCR	B-cell receptor
BLI	Bio-Layer Interferometry
BMDC	bone-marrow derived dendritic cells
BSA	Bovine Serum Albumin
CAR	chimeric antigen receptor
CCL-19	chemokine (C-C motif) ligand 19
CCL-21	chemokine (C-C motif) ligand 21
CCR7	C-C chemokine receptor type 7
CD80	cluster of differentiation 80
CD86	cluster of differentiation 86
CDC	complement-dependent cytotoxicity
CFA	complete Freund’s adjuvant
CIES	carrier-induced epitopic suppression
CP	cyclophosphamide
CPMV	Cowpea mosaic virus
CTL	cytotoxic T cell
CTLA-4	cytotoxic T-lymphocyte-associated protein 4
CuAAC	copper(I)-catalyzed alkyne-azide cycloaddition
DC	dendritic cell

DCM	dichloromethane
DIPEA	diisopropylethylamine
DLS	dynamic light scattering
DMAP	4-Dimethylaminopyridine
DMEM	Dulbecco's Modified Eagle Medium
DMF	dimethylformamide
DMSO	dimethyl sulfoxide
DMSO	dimethyl sulfoxide
DNA	deoxyribonucleic acid
EGFR	epidermal growth factor receptor
ELISA	enzyme-linked immunosorbent assay
ErbB2	receptor tyrosine-protein kinase erbB-2
FACS	fluorescence-activated cell sorting
FBS	fetal bovine serum
FDA	Food and Drug Administration
FITC	fluorescein isothiocyanate
Fmoc	fluorenylmethyloxycarbonyl
GalNAc	N-acetylgalactosamine
GM-CSF	granulocyte-macrophage colony-stimulating factor
HA	hemagglutinin
HATU	1-[Bis(dimethylamino)methylene]-1H-1,2,3-triazolo[4,5-b]pyridinium 3-oxid hexafluorophosphate
HBTU	O-(benzotriazol-1-yl)-N,N,N’,N’-tetramethyluronium hexafluorophosphate
HMFG	human milk fat globulin

HOAT	1-hydroxy-7-azabenzotriazole
HOBt	1-hydroxybenzotriazole
HPG	homopropargyl glycine
HPLC	high performance liquid chromatography
HRP	horseradish peroxidase
ICP	inductively coupled plasma analysis
IFA	incomplete Freund’s adjuvant
IFN-γ	interferon gamma
IgG	Immunoglobulin G
IgM	Immunoglobulin M
IL-12	Interleukin 12
IL-6	Interleukin 6
imDC	immature dendritic cell
IONP	iron oxide nanoparticle
KLH	Keyhole limpet hemocyanin
LCMS	Liquid chromatography–mass spectrometry
LDL-C	low-density lipoprotein cholesterol
mAb	monoclonal antibody
MALDI-TOF	matrix assisted laser desorption ionization-time of flight
MAPK	mitogen-activated protein kinase
MHC	major histocompatibility complex
MHC-I	major histocompatibility complex class 1
MHC-II	major histocompatibility complex class 2

MPLA	monophosphoryl lipid A
mQβ	mutant Qβ
MRI	magnetic resonance imaging
MS	mass spectrometry
MUC1	glycoprotein Mucin 1
MW	molecular weight
NHS	N-hydroxysuccinimide
NK	natural killer cell
NMR	nuclear magnetic resonance spectroscopy
NP	nanoparticle
OA-IONP	oleic acid coated iron oxide nanoparticle
OD	optical density
PAMP	pathogen-associated molecular pattern
PBS	phosphate-buffered saline
PBST	phosphate-buffered saline tween
PCSK9	protein converstase subtillisin/kexin type 9
PD-1	Programmed cell death protein 1
PDI	polydispersity index
PDI	polydispersity index
PD-L1	programmed death-ligand 1
PEG	polyethylene glycol
PLGA	Poly(d,l-lactic-co-glycolic acid)
Qβ	bacteriophage Qbeta

RNA	ribonucleic acid
RTK	receptor tyrosine kinases
SASA	solvent accessible surface area
SDS-PAGE	sodium dodecyl sulfate polyacrylamide gel electrophoresis
SEC	Size-exclusion chromatography
SPION	superparamagnetic iron oxide nanoparticle
SPR	Surface plasmon resonance
ssRNA	single-stranded RNA
ST	sialiated Thomsen-Friedenreich antigen
STn	sialiated Thomsen-nouveau antigen
T antigen	Thomsen-Friedenreich antigen
TACA	tumor-associated carbohydrate antigen
TCR	T cell receptor
TEM	Transmission electron microscopy
TFA	trifluoroacetic acid
TGA	thermogravimetric analysis
Th	Helper T cell
THF	tetrahydrofuran
TIPS	triisopropylsilyl ether
TLC	thin layer chromatography
TLR	Toll-like receptor
Tm	melting temperature
TMSOTf	trimethylsilyl trifluoromethanesulfonate

TMV	tobacco mosaic virus
Tn antigen	Thomsen-nouveau antigen
TNF-a	tumor necrosis factor alpha
TSTU	N,N,N’,N’-tetramethyl-O-(N-succinimidyl)uronium tetrafluoroborate
TT	Tetanus toxoid
VLP	virus-like particle
VNTR	variable number tandem repeat
wtQβ	wild-type Qβ

CHAPTER 1: Lipopeptide-Coated Iron Oxide Nanoparticles as Potential Glycoconjugate-Based Synthetic Anticancer Vaccines[1]

1.1 Introduction

1.1.1 Cancer immunotherapy

Cancer is a leading cause of death and one of the most serious public health concerns. According to the American Cancer Society, it was estimated that, there were 1.7 million new cancer cases and about 590,000 people died from cancer in 2015 in US. In terms of total deaths in the United States recorded in 2014, cancer is ranked as the second leading cause of death (22.5% of the total of deaths) following heart diseases (23.4% of the total of deaths).[2] Although being ranked in the second place, with such a small gap of the difference and difficulty of finding an effective cure, cancer is expected to become the number one leading cause of death within the next few years. Worldwide, cancer causes 15% of mortality, with estimated 14 million of new cases each year.[3] The death rate worldwide is projected to reach 10 million by 2020, which may cost healthcare systems up to one trillion dollars.[4]

Until now, cancer treatment strategies still generally rely on conventional approaches of surgical resection, chemotherapy and radiation. However, chemotherapy has the limitation of severe side effects. Although surgery and radiotherapy procedures are standard treatment options for local cancers, they increase risk to generate metastasis[5] (cancer cells spread from a primary site through circulatory system to regenerate and grow in distant vital organs), which is even more lethal and harder to cure.

A promising alternative to the classical treatment strategies is *immunotherapy*.[6] By harnessing the effective immune system to specifically kill cancer cells and maintain protective

responses against cancer recurrence, immunotherapy is heralded as a revolutionary treatment being more efficacious with more cancer types and posing fewer potential side effects.

The idea of immunotherapy started back in 1884 when Anton Chekhov found strong evidence of the correlation between immune response to pathogen infection and tumor reduction.[7] Afterward in 1893, surgical oncologist William Coley tested the Chekhov's finding by using a mixture of attenuated bacteria from *Streptococcus pyogenes* and *Serratia marcescens,* called Coley's toxins, as an immune activating agent to treat cancer patients, and he found some beneficial results.[8] This evidence implied the potential of activating the immune system to control tumor growth.

Although there are many hurdles in developing successful cancer immunotherapy, cancer immunology research remains highly active and has made huge progress in understanding how the immune system deals with cancer cells. This has led to promising clinical translation of immune checkpoint therapies (such as PD-1 and CTLA-4) and chimeric antigen receptor (CAR) T-cell therapy. A lot of promises shown by recent successes in clinical trials,[9] excited the scientific community to mark "cancer immunotherapy" as a Breakthrough of the Year by *Science* journal in 2013.[10] Very recently, the PD-L1 monoclonal antibody, Pembrolizumab (Keytruda®), has been approved by FDA as a primary treatment, instead of chemotherapy, for metastatic non-small cell lung cancer.[9e] This approval further highlights the role of immunotherapy in revolution of cancer treatment.

Besides immune checkpoint therapy and CARs, another type of cancer treatment that researchers have been trying to demonstrate efficacy is an anti-cancer vaccine. When combined with other treatments, a cancer vaccine is expected to not only maximize the therapeutic effect, but also provide long lasting protection, which could potentially prevent reoccurrence of cancers

in cancer patients. A cancer vaccine is conceptualized from vaccination against pathogen infection. In a conventional pathogen vaccine, live or inactivated microbes are utilized to induce immune responses to elicite antibodies that specifically neutralize the corresponding microbes. The induced immunity will maintain the immunological memory to elicit more potent protection for future attack from the same microbe, providing long-term protection against the pathogen. To be able to further understand how the concept of pathogenic vaccine can be applied to cancer vaccines, thorough understanding of how immunity works is necessary.

1.1.2 Mechanism behind immunity

Two kinds of adaptive immune processes, humoral and cell-mediated immunity, are cooperatively responsible for defending against pathogens in the immune system. The humoral immune system is the first line of defense. It involves antibody secretion from activated B cells after they recognize B-cell epitopes. The simplest B-cell activation is induced by a T cell-independent process, from which the low affinity and short lived IgM antibodies are secreted (**Figure 1.1**).[11] The other process, known as a T cell-dependent process, relies on participation of T helper-cell activation generating cytokines to induce Ig-isotype switching from IgM to the long lasting and higher affinity antibody IgG. Moreover, T cell-dependent humoral immunity also generates memory cells, which are capable of inducing even more potent responses against subsequent encounters with the same antigen.[12] IgG has the potential to recognize and bind to pathogen-associated antigens, marking the target. The antibody-bound pathogens can be eradicated by either complement-dependent cytotoxicity (CDC) or antibody-dependent-cell-mediated cytotoxicity (ADCC), in which macrophages, neutrophils or natural killer cells will be recruited to inactivate or kill the targeted pathogen.[13]

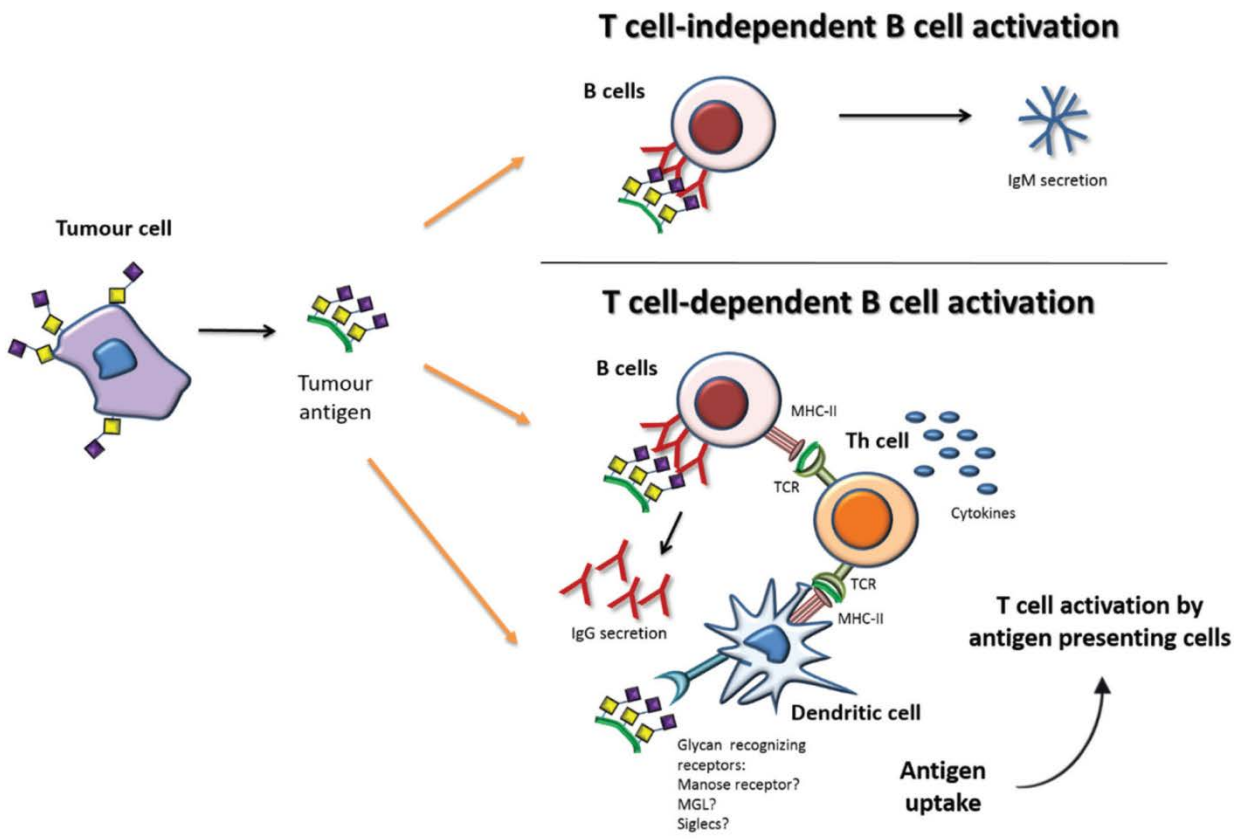

Figure 1.1: A cartoon showing two types of humoral immune activation by a tumor antigen. *Upper panel* – T cell-independent B-cell activation: the multivalent antigen crosslinks B cell receptors without the help from T cells leading to IgM secretion. *Lower panel* – T cell-dependent B-cell activation: In addition to B-cell activation by direct antigen recognition, the antigen can be taken up by antigen presenting cells such as dendritic cells, which subsequently present the antigen fragment to activate helper T cell (Th cell). The activated Th cell releases cytokines to induce B cells to undergo Ig-isotype switching from IgM to IgG. The figure is adapted and reproduced from reference[14].

Cell-mediated immunity, involves the synchronized action of a variety of immune cells, including antigen presenting cells (APCs), macrophages, natural killer cells (NKs), helper T cells, and cytotoxic T cells. These cells interact with each other through cytokine signaling and cellular surface molecules to induce effective immune protection. Among all antigen presenting cells, dendritic cells (DCs) play a key role in inducing immune responses.[15] DCs are located in peripheral tissues, such as skin, which continuously seek out invading pathogens. Once the pathogens encounter the body, DCs will internalize the foreign substances, or antigens, which are

subsequently processed into short peptides. Meanwhile, DCs undergo maturation expressing a variety of cellular surface molecules, including co-stimulatory molecules CD80, CD86, and a homing receptor, CCR7. This alteration allows DCs to migrate toward the secondary lymphatic organs in response to a high concentration of chemokines CCL-19 and CCL-21, and present the antigens to T cells residing there. To present the antigen to T-cell receptor (TCR) on the T cells, the processed peptides need to be loaded into either the major histocompatibility complex (MHC) class I or class II molecules, depending on the source of the antigens (**Figure 1.2**). Endogenous antigens, which are derived from intracellular proteins in the APCs themselves, are typically loaded on MHC class I molecules (MHC-I). In contrast, exogenous antigens, which are derived from foreign substances and taken up by DCs, are normally loaded on MHC class II molecules (MHC-II). Antigenic peptides loaded on MHC-II are presented to $CD4^+$ helper T cells, which are involved in cytokine secretion to promote B cell activation, resulting in IgM-to-IgG class switching in humoral immunity described above. However, exogenous antigens can possibly be transported into MHC-class-I presentation route via a process known as cross-presentation. The processed exogenous peptides loaded on MHC-I are presented to $CD8^+$ T cells or cytotoxic T lymphocytes (CTLs). Once presentation by MHC-I occurs, CTLs become activated and leave the lymphatic organs, seeking for the same antigenic peptide presented by MHC-I on the surface of infected cells. When CTLs recognizes the antigen, they bind to the target cells and release cytotoxic granules to kill the infected cells.[16]

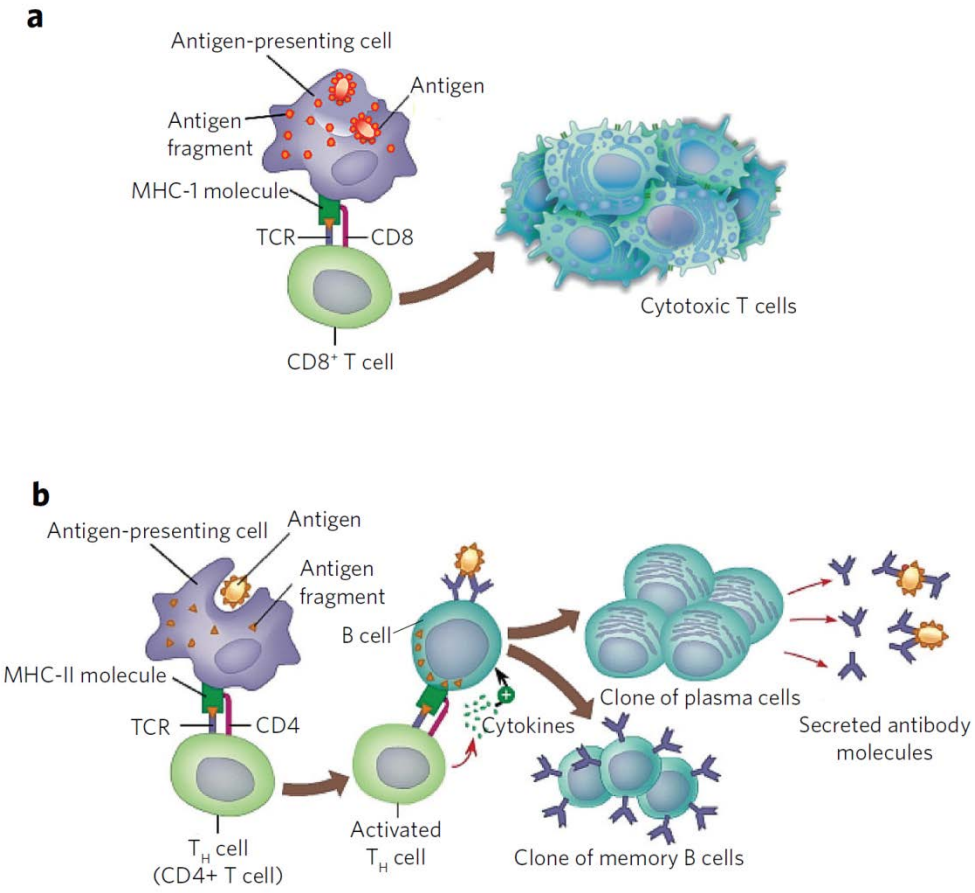

Figure 1.2: Illustration showing the process of cell-mediated immunity. a) The antigen-presenting cell uptakes and processes an antigen into a short fragment ($CD8^+$ T-cell epitope). The digested fragment is loaded onto MHC class I and presented to a $CD8^+$ T cell. The activated $CD8^+$ T cell then proliferates and becomes cytotoxic T cells, which will be able to kill the corresponding pathogens or cancer cells. b) The processed antigen fragments that are loaded onto MHC class II will be presented to $CD4^+$ T cell. The activated $CD4^+$ T cells will release cytokines in T-cell dependent B cell activation resulting in IgM-to-IgG isotype switching and the generation of IgG secreting plasma cells and memory B cells. The figure is reproduced with permission from reference[17].

By analogy with B cell epitopes as pathogen's signatures, to which the immune system targets, the key towards making a successful cancer vaccine is to generate unique/overexpressed cellular marker(s) that can differentiate cancer cells from normal cells. This differential marker can be used to educate the immune system to target and selectively eradicate cancer cells. Due to genetic- or epi-genetic mutations, human cancers either overexpress common markers or induce

unique aberrant self-derived molecules on their surface. Advances in high-throughput technologies in genomic, proteomic and glycomic research help accelerate elucidation of potential novel markers from tumor cell or tumor-associated microenvironment, leading to a variety of targets to selectively fight different type of cancers (For a review see [18]). One type of important signatures discovered in all states of tumor progression, including transformation, metastasis, angiogenesis and immune escape, is changes in glycosylation pattern.

1.1.3 Protein post-translation modification by glycosylation

After human genome sequencing was completed, it was surprising to find that functional diversity of proteins in eukaryotes far exceeds the coding capacity of the genome. Beyond the variety of amino acid translation and folding/refolding of the protein complexes, post-translational modification plays a tremendous role to diversify the complexity of proteins that regulate protein activity, cellular physiological state and signal communication between cells or microenvironment.[19] One of the common post-translation modifications in eukaryotes is glycosylation.

Glycosylation involves selective addition of carbohydrate based molecules, or glycan, onto a specific amino acid by glycosyltransferase enzymes and selective trimming of glycans by cleaving its saccharide subunit by glycosidase enzymes. There are two common sites where the glycan addition occurs. Glycan that is added onto the amide group in the side chain of asparagine in peptide sequence Asn-X-Ser/Thr (where X can be any amino acid except proline) is called *N*-glycan. By contrast, *O*-glycan is referred to glycan addition to the hydroxyl group in the side chain of serine or threonine.

1.1.4 Mucin 1

One of the most common cancer associated glycoproteins is Mucin 1 (MUC1). MUC1 is a membrane-bound glycoprotein. It is originally translated as a pro-protein, and then undergoes auto-proteolytic cleavage into C-terminal (MUC1-C) and N-terminal subunits (MUC1-N) (**Figure 1.3**a). After the cleavage, both fragments link together through a stable, non-covalent interaction. In the normal state, MUC1 is found extensively on epithelial cells and exclusively on apical side of the cells (**Figure 1.3**c). The steric hindrance of heavy glycosylation on the N-terminal subunit stretches the core peptide into linear form. This linear form of MUC1 can extend the protein terminal reach to over 200nm above the apical surface[20] (general membrane proteins extend out about 30nm[21]), and altogether forming a thick mucus layer on the epithelial cells. The thick layer of MUC1 is thought to generally function as a lubricant or a protecting layer against invasive pathogens[22] and strong acidic environment (pH = 2) in the gastrointestinal track.[23] In addition to tissue protection, some investigations also suggested its role in cell differentiation and intercellular communication.[24]

The C-terminal fragment (MUC1-C) contains a cytoplasmic domain (CD), a transmembrane domain (TD), and an extracellular N-terminal domain (ED) (Note that N-terminal domain in this context is a part of the C-terminal subunit.) (**Figure 1.3**b). The cytoplasmic domain involves intracellular signaling through mitogen-activated protein kinases (MAPK) signaling pathway.[25]

Moreover, after cellular alteration due to tumorigenesis on cancer cells, the N-terminal subunit (MUC1-N) will start to dissociate and leave the C-terminal subunit (MUC1-C), which remain attached on the cell membrane (**Figure 1.3**c). The remaining C-terminal subunit (some still have the N-terminal subunit connected) will delocalize to the entire cell surface, instead of specific presentation on the apical side. This cellular morphology change is termed “loss of

polarity". Under loss of polarity, the extracellular N-terminal domain in the C-terminal subunit is responsible for interactions with receptor tyrosine kinases (RTKs), e.g., EGFR or ErbB2 through galectin-3 on Asp-36 (**Figure 1.3**d). This cis-interaction is thought to amplify the aberrant over expression of MUC1 on cancer cells. It is postulated that the loss of polarity and over-expression of MUC1 on cancer cells contributes to intercellular repulsion resulting in metastasis and immune evasion. Although targeting C-terminal subunit would regulate intracellular signaling pathway associated with tumor transformation, C-terminal MUC1 is less applicable for immune target as it is buried underneath thick layer of highly-glycosylated N-terminal subunit, making it invisible to the immune system.

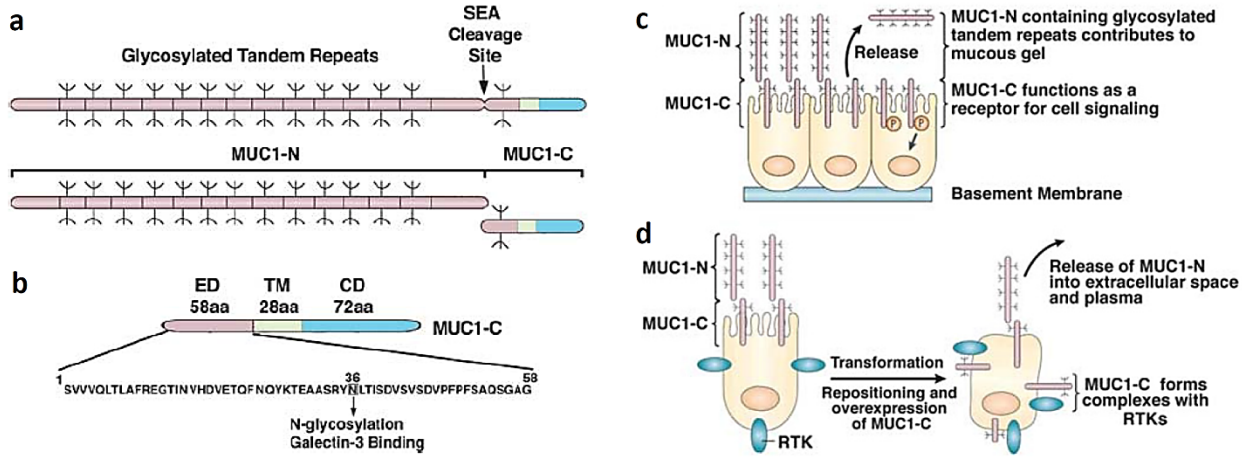

Figure 1.3: a) C-terminal (MUC1-C) and N-terminal subunit (MUC1-N) are connected by non-covalent interaction after auto-proteolytic cleavage. b) C-terminal MUC1 (MUC1-C) are composed of a cytoplasmic domain (CD), a transmembrane domain (TM), and an extracellular N-terminal domain (ED). N-glycan on Asp-36 can cis-bind to receptor tyrosine kinases (RTKs) after loss of polarity. c) The N-terminal subunit (MUC1-N) will dissociate and leave the C-terminal subunit (MUC1-C) due to tumorigenesis on cancer cells. d) Cellular alteration due to tumorigenesis causes loss of polarity or delocalization of the remaining C-terminal subunit to entire cell surface, instead of specific presentation on the apical side. The C-terminal subunits form cis-interactions with receptor tyrosine kinases (RTKs) causing amplification of the aberrantly overexpression of MUC1 on cancer cells. This figure is adapted and reproduced with permission from reference[25].

The outer layer N-terminal subunit MUC1-N contains a variable number tandem repeats (VNTR) of twenty amino acids, GVT*S*APDT*RPAPGS*T*APPAH. The number of this repeating unit varies from 20 to 125 units depending on the alleles.[26] Five amino acids, either serine or threonine (starred letters), in the VNTR can potentially be sites for *O*-glycosylation (Figure 1.4).[22, 27] The core peptide in this variable number tandem repeat domain is immunogenic and well known as a B cell epitope. The binding analysis of serum from cancer patients by ELISA[28] and microarray[29] revealed that RPAPGS, PPAHGVT and PDTRP are the minimal dominant epitopes in VNTR. The analysis also showed that sera from cancer patients bind stronger to Tn-glycosylated MUC1 than unglycosylated one. This suggested that the glycosylation in MUC1 sequence is crucial for antigenicity of the MUC1 antigen.

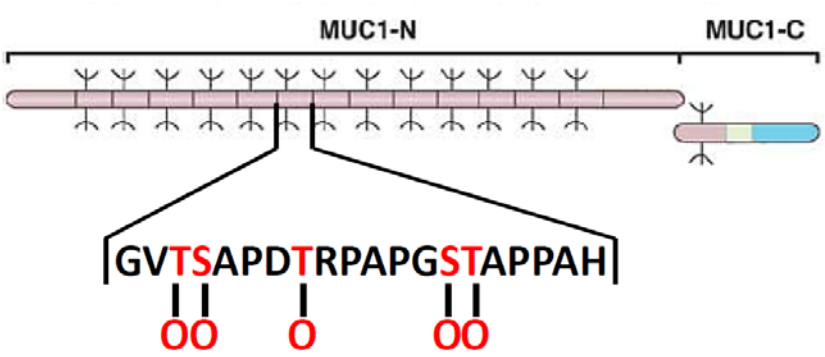

Figure 1.4: Variable number tandem repeats (VNTR) of twenty amino acids in N-terminal subunit (MUC1-N). 5 potential amino acids (red letters) are potentially subjected to O-glycosylation. This figure is adapted and reproduced with permissions from references[21, 25].

NMR assisted structure analysis of VNTR in MUC1 revealed that the secondary structure of the MUC1 forms an ordered structure of rod shape. Five rigid amino acids of proline in MUC1 sequence are thought to lead to this rod shape structure. The VNTR is composed of 2 β-turn regions at APDTRP and PGST sequences.[30] However, only the hydrophobic β-turn region of APDTRP sequence forms protruding knob out of the rod shape structure.[31] This protruding region is believed to expose the immunodominant epitope of MUC1, which is correlated with the

dominant epitopes of vaccinate induced anti-MUC1 antibodies[28] and many MUC1-specific monoclonal antibodies, such as SM3 (PDTRP), BC2 (APDTR), HMFG1 (PDTR), HMFG2 (DTR).[21, 32]

1.1.5 Aberrant glycosylation in cancer cells

Although MUC1 is also found on normal epithelial tissues, MUC1 expressed on tumor cells differs from those on normal cells in many ways. First, due to alteration in *MUC1* gene regulation, MUC1 is over-expressed (100 times compared with those expressed on normal cells) on many types of cancer cells, including lung, pancreas, prostate cancers and especially breast cancers (90% of breast carcinomas).[33] This over-expression together with the loss of polarity in the cell surface expression would, therefore, significantly increase the chance of immune recognition towards cancer cells.

Secondly, in normal cells, the post-translational modification of *O*-glycosylation will begin with the addition of an *N*-acetyl galactosamine residue (GalNAc) onto serine or threonine in the VNTR domain in MUC1. The glycosylation will then be extended from the starting GalNAc unit to core 1 – core 4 structures (**Figure 1.5**). Unlike genetic code derived cellular products such as DNA, RNA and protein, where the sequence of subunits is encoded from their templates, the occurrence of glycosyl elongation process depends on available substrates and activity of glycosyltransferase enzymes (T-synthase) on the site where the glycosylation is taking place. In cancer cells, however, the glycosylation enzyme, specifically Core-1 synthase (C1GalT1), is improperly folded due to the absence of *Cosmc* chaperon in Endoplasmic Reticulum caused by genetic/epigenetic mutation in the cancer cells (**Figure 1.6**).[34]

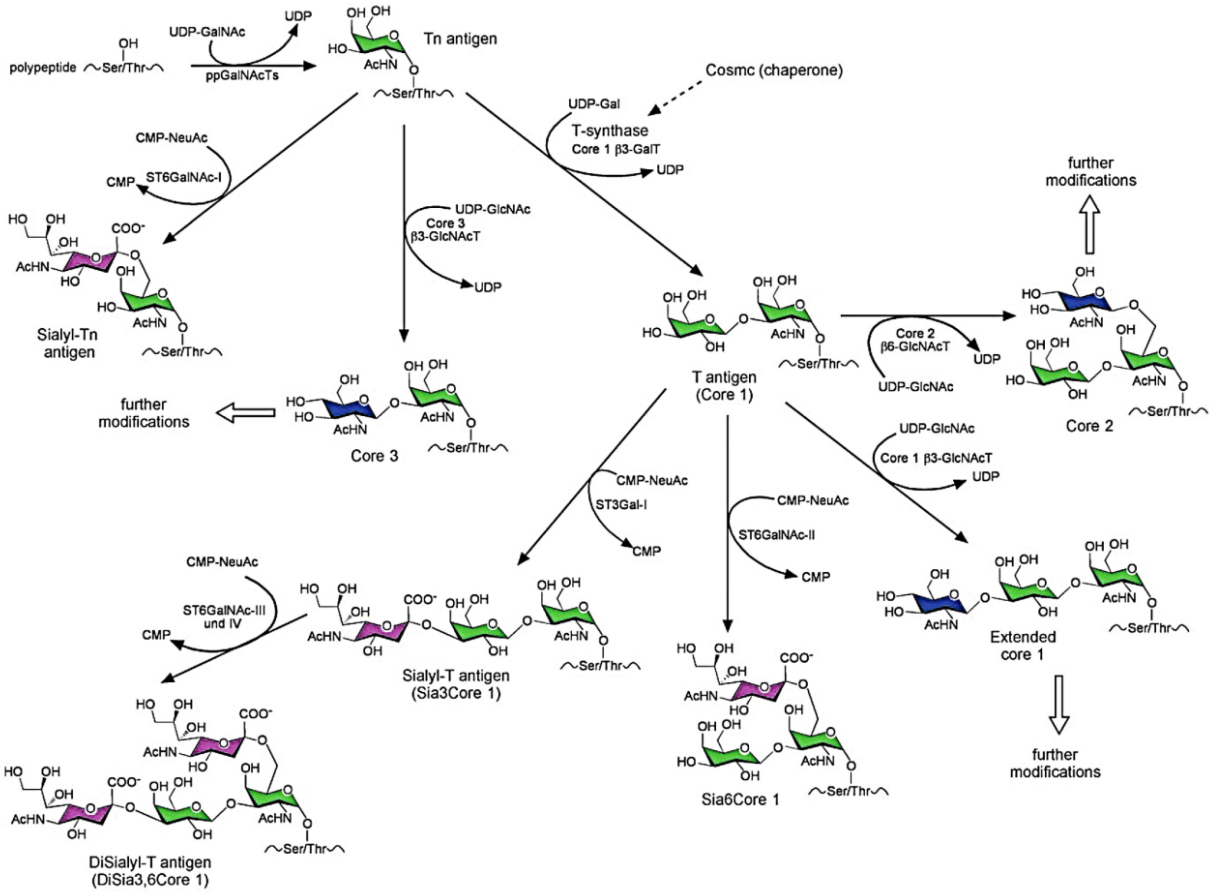

Figure 1.5: The process of *O*-glycosylation begins with the addition of a GalNAc moiety onto a serine or threonine residue in a polypeptide. The glycosylation will then be extended from the starting GalNAc unit by T-synthase to core 1 – core 4 structures. This figure is adapted and reproduced with permission from reference[34b].

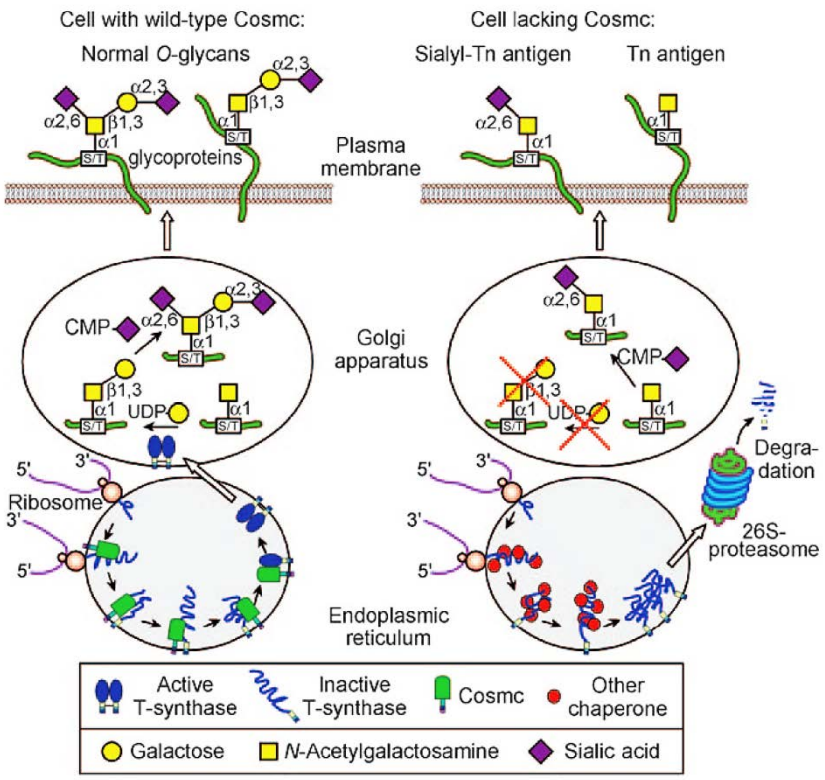

Figure 1.6: The glycosylation enzyme T-synthase in cancer cells is malfunctioning due to improper enzyme folding caused by the absent of *Cosmc* chaperon in the endoplasmic reticulum in cancer cells. The malfunctioning T-synthase in cancer cells leads to the aberrant glycosylation in glycopeptide MUC1. This figure is adapted and reproduced with permission from reference[34b].

As a result, the glycosylation patterns found on cancer-associated MUC1 are more truncated and sialylated.[35] As a consequence of the shorter glycosylation, the core peptide epitopes are more exposed and susceptible to be accessible and recognized by immune cells, while MUC1 expressed on normal cells are more protected by the unaltered glycosylation patterns.[36] Moreover, the aberrant glycosylation generates distinct carbohydrate antigens, which include Thomsen-Friedenreich (T) antigen (Galβ1-3GalNAc-α1-*O*-Ser/Thr), Thomsen-nouveau (Tn) antigen (GalNAc-α1-*O*-Ser/Thr) or their sialylated product; STn and ST antigens (**Figure 1.7**). The presence of these antigens on cancer cells are well correlated with cancer prognosis as they promote the tumorigenesis, progression and metastasis in the cancer cells.[37] However, T and

ST antigens are also found in normal tissues[38] while Tn and STn antigens are more exclusively expressed on the cancer cells. Immunohistochemistry of a variety of cancer patients samples indicated high expression level of Tn over 80% (85% in breast, 90% in ovary and 83% in endometrium cancers) compared to normal tissues.[39] The distinctly high expression of Tn or STn antigens make them more attractive as targets for anti-cancer vaccine.[40] Therefore, it is envisioned that, in addition to MUC1 antigen, inducing immune response against these tumor-associated carbohydrate antigens (TACAs) would possibly selectively eradicate cancers.

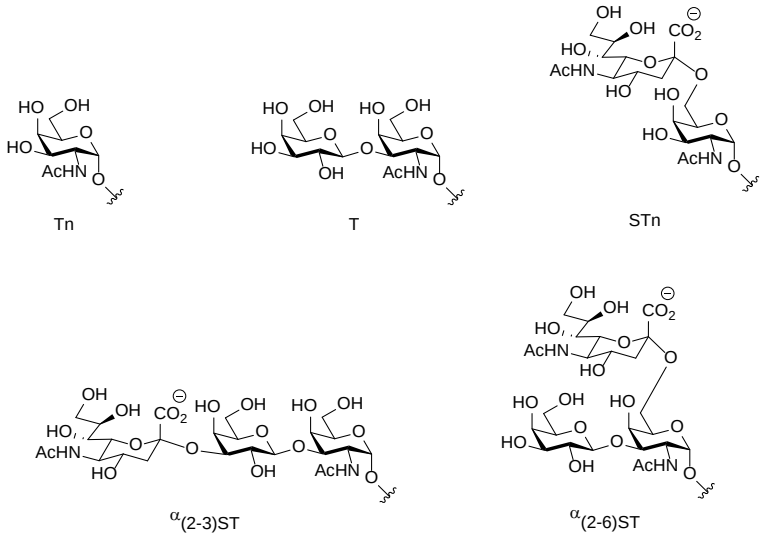

Figure 1.7: The structure of TACAs; Tn, T and their sialiated products; α(2-3)ST, α(2-6)STn.

All of these different features make MUC1 glycoprotein a promising candidate of antigens for anti-cancer vaccine. Moreover, a recent research ranked MUC1 as the second most potential cancer associated antigen, according to the total score regarding therapeutic prospect criteria such as therapeutic function, immunogenicity, specificity, and level of expression.[41]

1.1.6 Evidences supporting MUC1 based vaccine

There has been enthusiasm of finding and developing therapeutic monoclonal antibodies that target selectively against TACAs or glycopeptide MUC1 on cancer cells.[14] The discovery of

monoclonal antibody SM-3 that preferentially bound MUC1 on many types of cancer cells relative to that on normal cells led to the development of novel monoclonal antibodies that exhibited high selectivity towards tumors. Monoclonal antibody AS1402 is an example exhibiting antibody-dependent cellular cytotoxicity towards cancer-associated MUC1 expressing tumor cells. The promising efficacy of AS1402 made it enter clinical trials in phase I and II. However, no significant difference in efficacy was observed when compared with conventional approach based on chemotherapy. This unanticipated result in clinical evaluation is attributed to the excess amount of the soluble MUC1-N released from cancer cells sequestering the administrated monoclonal antibody subsequently diminishing the amount of the antibody available to access the tumor-bound MUC1. Similarly, this situation would also happen with a drug-conjugated monoclonal antibody against MUC1. Therefore, most of the anti-MUC1 monoclonal antibodies developed are still limited to diagnostic purposes, rather than for therapy.

Unlike passive immunotherapy using monoclonal antibodies, inducing immune response against the cancer-associated MUC1 would be more attractive since the active immune response can continuously generate the specific antibody to reduce the pool of secreted MUC1. In addition to targeting local cancer, the antibodies generated can eliminate circulating cancer cells in the blood, hence, preventing lethal metastases from developing. In addition to the high cost of monoclonal antibody based therapies, the efficacy of the monoclonal antibody tends to decline overtime due to the induced neutralizing antibodies against the repeatedly administered proteins.

Besides antibody responses, vaccination with MUC1 glycopeptide can also activate cytotoxic T cells. It was believed that the antigen fragment, presented by the MHC molecule to the T-cell receptor is limited to peptides and cell-mediated immunity, plays an indirect role in immune activation against non-peptidic antigen such as carbohydrates. There were multiple

reports that T cell receptors can also recognize glycopeptide fragment bound on the MHC class I molecule.[42] Cytotoxic T cells isolated from pancreatic, ovarian and breast cancer patients were found to recognize MUC1 glycopeptides and induce cytotoxicity to cancer cells *in vitro*.[43] Epitope mapping studies have identified peptide STAPPHGV and glycopeptide SAPDT(GalNAc)RPAPG, located in VNTR of MUC1 as CD8 T cell epitopes that bind to MHC class I allele HLA-A2.[44] Although these examples indicate the presence of MUC1 specific cytotoxic T cells in cancer patients, they are not sufficiently effective to overcome tumor growth. This is probably due to self-tolerance related immunosuppression due to overexpression of MUC1[45] as well as aberrant glycosylation[46] on cancer cells that inhibit the effector T cells to eliminate the targeted cancer cells. Therefore, it is envisioned that the cooperation of humoral and cell-mediate immune responses, together with immune check point therapy, would empower the immune system to efficiently eliminate cancer as well as to prevent cancer recurrence.

1.1.7 Anti-MUC1 vaccine development

Anti-MUC1 vaccine has been under study for a while. In 1994, Apostolopoulos and coworkers immunized mice with MUC1 containing a synthetic peptide, fusion protein, or natural MUC1 isolated from human milk fat globulin (HMFG).[47] Although these compounds generated high antibody responses, they failed to protect mice from tumor challenge. In the same study, the authors showed that immunizing mice with MUC1 transfected cancer cells can protect mice from tumor challenge, despite the low antibody response. The protective response of the latter case was contributed to Th1 type response, which is associated with activation of cytotoxic T cells. Antibody responses were attributed mainly to Th2 response. This finding leads to the utilization of carriers to bias immune response towards Th1 rather than Th2 for stronger protective effect of the vaccine.[47] Polysaccharide mannan is another example used to direct the type of the immune

response towards Th1 by modification of the polysaccharide carrier by oxidation.[48] In addition, the mannan carrier can enhance antigen uptake through C-type lectin receptor on antigen presenting cell resulting in more efficient immune induction event and protection of human MUC1 transgenic mouse model from tumor challenge.

Due to low immunogenicity of MUC1, immunogenic proteins have been used as MUC1 antigen carrier to enhance the immunogenicity of MUC1. Keyhole limpet hemocyanin (KLH)[49] and tetanus toxoid (TT)[50] are common protein carriers utilized for anti-MUC1 or anti-TACA vaccines. Although these immunogenic proteins can strongly boost the immune response against such low immunogenic antigens, the high immune response against the carrier itself, or linker in some cases, was also found and thought to suppress the desired immunity against the MUC1 or TACAs.[51] This suppressive effect from the vaccine carrier is known as carrier-induced epitopic suppression (CIES).[52] This issue leads to increasing interest in investigating other vaccine carrier candidates that have potential to preferentially focus immune response specific to MUC1 antigen, rather than the carrier.[22]

Over the past decade, when the concern of vaccine safety has become the top priority in a clinical trial, the paradigm of vaccinology is to replace the undefined whole-microorganism or extracted natural product derived vaccines with subunit vaccines, where their constructs are well characterized, reproducible, stable and low in undesired side effects. In addition to using immunogenic proteins as vaccine carriers, which usually suffer from carrier-induced epitopic suppression (CIES) mentioned above, fully synthetic vaccines have become a main stream of MUC1 vaccine development which is proposed to mitigate the carrier induced immune suppression due to non-essential components incorporated.[53] The well characterized synthetic MUC1 vaccines can be not only easier to manufacture, but also more homogeneous, than

compounds isolated from natural sources. Moreover, the synthetic strategies allow the glycosylation pattern on the MUC1 glycoprotein to be tuned to best represent the tumor associated antigens. This tunable and uniformly defined compound provided insight about structural factors of the vaccine, which enhance the knowledge for antigen design in vaccine development.

The concept of fully synthetic vaccine relies on minimizing vaccine components down to a construct containing only essential specific immune stimulating components, generally including tumor associated antigen(s), Th epitope(s), and agonist of Toll-like receptor(s) (For more detail about the fully synthetic vaccine, readers are directed to an intensive review[53]).

1.1.8 Particulate Vaccine

The immune system is normally prevented from responding against self- or self-derived antigens and is tolerant to those antigens. Since tumor antigens are derived from self-antigens, they are generally poorly immunogenic. Therefore, it is more challenging to develop anti-cancer vaccines compared with classical vaccines against infectious diseases.

A number of strategies have been proposed for effective induction of immune responses to break the immune tolerance. Those strategies include selection of suitable tumor associated antigens as well as mean to deliver such antigens to activate the immune system, which can be critical for the outcome of the vaccination.[54]

One proposed way to guarantee that the antigen is delivered to APC is *ex-vivo* manipulation of DC by directly incubating the antigens with isolated DCs. The loaded DCs are then re-infused back into the patients, allowing them to present the antigen and stimulate the immune system to kill cancer cells. This approach was approved by Food and Drug Administration (FDA) in 2010 with the trade name of *Provenge* for prostate cancer treatment.[55]

However, this approach relies on individual treatment, in which only DCs from the same patient can be used, as cells from other patients can potentially cause immune rejection. Therefore, this exclusive healthcare process is costly and may be impractical for most cancer patients. This complication highlights the need for better vaccine formulation that can deliver the antigen to DCs *in vivo* to circumvent expensive *ex-vivo* DC manipulation.

Another promising approach to improve the efficacy of antigen delivery to DCs *in vivo* is by employing particulate vaccines based on nanoparticles. Several studies showed that particulate materials can enhance delivery of antigenic molecules to APCs and elicit more potent immune responses compared with administration of the molecules in soluble forms.[56] Many reasons are accounted for such effective antigen delivery by particulate vaccines.[57] First, due to the nanoscale size of particulate materials that resemble small pathogens like bacteria or virus, they could be recognized by the immune cells in a similar manner as those invading foreign substances.[58] Second, particulate vaccines act as carrier vehicles protecting the antigenic materials from degradation by enzymes or harsh conditions. This characteristic can increase the amount of an intact antigen taken up into targeted cells, resulting in higher chances to activate immune response with less material.[59] Third, surface engineering on particulate particles by conjugation with targeting molecules helps improve specificity towards the target cells, and could reduce potential side effects.[60] Moreover, highly organized presentation and repetitiveness of antigenic epitopes on particulate nanomaterials can offer clustering effect for antigen presentation on B cell receptors, which helps promote B cell activation generating high antibody titers.[61] Last, adjuvant or co-stimulatory signal molecules that help immune activation can be co-delivered along with antigenic epitopes to activate the same targeted cells, which was shown to be beneficial by many studies.[62] Besides the incorporation of adjuvant, biocompatible probes,

such as fluorophore, quantum dot or MRI contrast agent, can be introduced to monitor the fate of the particulate vaccine and cellular activity. The combination of therapeutic and imaging functionalities in a single platform is a highly active research area termed "Theranostics".[63]

1.1.9 Physical properties of a particulate vaccine determine the immune response profile.

The physical characteristics of particulate system, such as size, hydrophobicity, surface charge, have dramatic impacts on circulation time, bio-compatibility, bio-distribution and cellular interaction of the particles. Size of particulate vaccine is one of the factors that plays an important role in how the vaccine is delivered to interact with and activate immune system. Particles with larger sizes (0.5–5 μm) are preferentially taken up by macrophages, while smaller particles in range of viruses (20–200 nm) can dominantly target DC.[64] Although particles up to 200 nm are able to get internalized by DC, only small particles 5–100 nm in size were purported to contribute to effective DC mediated immune activation.[65] Despite the fact that the DC in skin can uptake particles larger than 100nm, these DCs are less capable of transporting the antigen to present to B or T cells in lymph node. The *in vivo* imaging experiment by superparamagnetic iron oxide nanoparticles[66] showed that only less than 5% of DC population in lymph nodes migrated from peripheral tissues. Moreover, the DCs that arrived the draining lymph nodes could become exhausted or dead.[67] In some cases, the skin-derived DCs have to pass the captured antigen to LN-resident DCs. This transferring process could reduce the chance of maintaining sufficient amount of the antigen to be present to the T cells.[68] Therefore, direct trafficking of antigen to the dendritic cells residing in lymph node is envisaged to be more efficient in inducing immune activation. The crucial effect of size for particulate vaccines has also been emphasized by the study from Reddy and coworkers.[69] They found that NPs with 25nm in diameters can target lymph node residing dendritic cells, while 100 nm NPs are less likely to drain into the

lymph nodes. However, too small particle (< 5 nm) is not efficient in delivery antigen into the lymph node either, as it is more likely to diffuse out of lymph nodes into blood circulation.[65] Altogether, these findings suggested that the proper size of particulate vaccine is crucial for successful particulate vaccine.

1.1.10 Anti-MUC1 particulate vaccines

Several studies have applied a particulate vaccine for a MUC1 based vaccine. In 1998, Kimberley and coworker used poly(*d,l*-lactic-*co*-glycolic acid) (PLGA) as a carrier for synthetic MUC1 peptide.[70] In that study, the PLGA was used to encapsulate the MUC1 peptide together with adjuvant MPLA. The PLGA-MUC1 induced Th1 response with no MUC1 specific IgM and low IgG titer. The large size of the PLGA micro-particle (500-900 nm in diameter) may contribute to the low anti-MUC1 IgG response. In the same year, the same group also reported the utilization of liposome based particle for MUC1 vaccine.[71] It was shown that the encapsulated MUC1 inside liposomes can induce only T cell response while the antigen displayed on the surface of the particle can both elicit antibody and induce T cell response. The results from this study demonstrated the effect of how antigen is incorporated in a particulate vaccine on immune response profile. Although the liposomes bearing surface antigens were able to induce IgM and IgG, the antibody titers resulting from the vaccine were not high. The size of liposome base MUC1 vaccine in this case is around 800-900 nm. In another study, the diameters were even bigger (1.7-2.1 μm),[72] which are bigger than the suitable range for effective DC targeting in lymph nodes.

Liposome formulation is another platform widely used as a weakly immunogenic carrier for multicomponent fully synthetic MUC1 vaccine. The hydrophobic chains of the amphiphilic component are substituted by adjuvant such as TLR agonist Pam3CysSK4, in which the lipid

chains facilitate the incorporation of the synthetic compound into the liposome.[73] Several works from Boons and colleagues demonstrated excellent examples of using liposome as a platform for MUC1 vaccine.[73-74] In 2005, Boons group first reported the investigation of liposomal vaccine of fully synthetic three-component of lipidated glycopeptide containing TLR-2 agonist Pam3Cys, Th epitope YAF peptide and Tn antigen in the same molecule. The synthetic compound was incorporated onto the surface of liposome. Based on the method of preparation and negative-stain TEM analysis, the size of the liposome is about 100 nm in diameter.[74b] The liposome vaccine can induce IgG antibody from the vaccinated mice. This work pointed out the importance of appending Th epitope in the construct as it was shown previously that the Pam3Cys conjugated to Tn antigen induced low IgG response. Following this finding, the group continued to apply the same construct to MUC1 glycopeptide, instead of Tn antigen.[75] In this work, they used fully synthetic three-component compound composed of B cell epitope from MUC1, Th epitope from polio virus (PV) and TLR1 and 2 agonist Pam3CysSK4 or TLR2 and 6 agonist Pam2CysSK4 (**Figure 1.8**). It was found that Pam3CysSK4 has higher potency in inducing strong IgG response more than Pam2CysSK4. The vaccines did not elicit antibody against Th epitope, which highlight the minimal immunogenicity of this construct. This work also showed that the covalent conjugation of the three components is important in inducing high titer of the antibody response. In addition, the liposome formation containing of the three components in the same particles can elicit much higher antibody than the mixture of all components in saline solution which emphasizes the importance of particulate platform in antigen delivery to the immune system. Further study in later publication indicated the importance of Tn antigen in the construct for higher efficacy of the vaccine compared with non-glycosylated MUC1.[76] It was proposed that the glycosylation on MUC1 peptide helps conserve

the conformation of the peptide as in native form, hence, induces immune response more specific to the cancer related MUC1. The study showed high efficacy of the vaccine in inducing not only humoral immune response to lyse the cancer cells via antibody dependent cellular cytotoxicity (ADCC), but also cell-mediated immune response through the activation of MUC1 specific CTL to kill MUC1 expressing cancer cells. The resulting cooperation of both immune protection arms is believed to help reduce tumor size in a tumor challenge study.

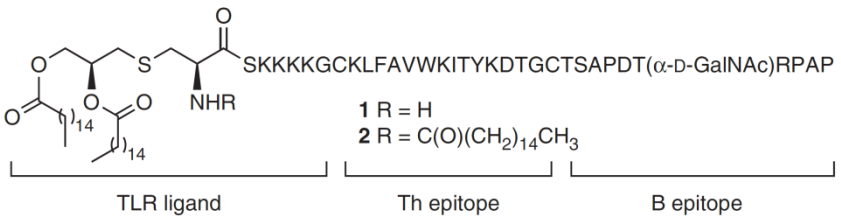

Figure 1.8: Representative structures of fully synthetic three-component compounds composed of B cell epitope from MUC1, Th epitope from polio virus (PV) and TLR1 and 2 agonist, Pam3CysSK4, or TLR2 and 6 agonist, Pam2CysSK4. This figure is adapted and reproduced with permission from reference[75].

Self-assembled subunit MUC1 has been investigated by Payne and coworkers in 2012.[77] The subunit MUC1 vaccine is composed of VNTR (glyco-) MUC1 peptide, T helper epitope PADRE and build-in adjuvant Pam3CysSer. Although, the construct is similar to other liposomal-based fully synthetic subunit MUC1 vaccine, they found that this compound can form a nanoparticle by itself without the help from liposomal formulation additives such as Egg phosphatidylcholine, phosphatidylglycerol and cholesterol.[75] The size of the particle measured by TEM is around 17-25nm. The self-assembled nanoparticle can induce IgM and IgG1, but low titer of IgG2, which suggests Th2 type response. The elicited antibodies can recognize MCF7 and B16 cancer cells. More recently in 2015, Li and colleagues developed multilayer self-assembled subunit MUC1 vaccine based on interaction of electrostatic components.[78] The Th epitope conjugated with poly-lysine can form the core of particle with positive surface charge.

Adjuvant poly-glutamic with negative charge was coated onto the core particle as a second layer, followed by third layer of positively charged poly-lysine, which was conjugated to MUC1 glycopeptide. The size of resulting particles is about 350nm. The particles were shown to be taken up by APCs RAW264.6 and induce secretion of pro-inflammatory IL-6 and IL-12. The titer of IgG induced by the multilayer particles was similar to glycopeptide MUC1 covalently linked to Th epitope. The multilayer particle vaccine induced more IgM than IgG. Nevertheless, sera from immunized mice showed binding to MCF-7 cells and induce a complement-dependent cytotoxicity to kill cancer cells.

A particulate vaccine is not limited to a particle-based platform. Nanofiber construct has also been applied to particulate MUC1 vaccine. Li and coworkers utilized peptide Q11, which can self-assemble to form β-sheet construct and has adjuvant property, as a carrier with built-in adjuvant for MUC1 antigen.[79] The conjugated peptide mixture aggregated to form nanofibers longer than 200nm. The study showed that putting Tn antigen on PDT*RP can elicit higher antibody response than putting Tn on GST*AP or both positions. This finding indicated the crucial position of glycosylation in MUC1 vaccine design. The self-assembly peptide Q11 did not induce antibody response to itself which highlight minimal immunogenicity against the carrier. The vaccine elicited predominantly IgG2a and IgM, which was possibly due to the lack of Th epitope for antibody isotype switching.[80] The elicited antibody showed binding to MFC-7 and induced complement dependent cytotoxicity to lyse the cells.

Very recently, gold nanoparticles were used as a carrier for MUC1 vaccine. MUC1 peptide together with T cell epitope P30 were conjugated on gold nanoparticles (20-30 nm).[81] The resulting nanoparticle based vaccine can mediated both Th1 and Th2 immune responses. The generated antisera from immunized mice showed binding to MCF-7 cells.

Although these studies pointed out the beneficial effects from particulate platforms and the factor of size in inducing effective immune response against MUC1, most of the results are still far from a practical candidate to overcome the tremendous challenge of anti-cancer vaccine development. Therefore, new carrier platform is still needed in order to find a successful anti-MUC1 vaccine to cure cancer.

1.1.11 Superparamagnetic iron oxide nanoparticle: SPION

Superparamagnetic Fe_3O_4 nanoparticles have been utilized extensively in drug delivery and non-invasive *in vivo* imaging applications.[82] This class of nanoparticle is shown to be biocompatible with low safety concern when used as targeting carriers for therapeutic agents.[83] Some iron oxide nanoparticles, such as Feridex I.V. (ferumoxides), Combidex (ferumoxtran-10), Feraheme (ferumoxytol), have been approved by the FDA for use in human.[84]

With regards to immunotherapy applications, iron oxide nanoparticles have become a promising antigen carrier to elicit immune response *via* peripheral dendritic cells. Mou, *et al.* demonstrated that iron oxide nanoparticles could be internalized by both mature and immature dendritic cells, and the internalization could induce initial maturation in which the essential cellular surface markers related to maturation states, including co-stimulation marker CD80, CD86 and MHC-II, were upregulated. The study also showed that the iron oxide nanoparticles did not pose significant effects on maturation phenotype and viability of the labeled dendritic cells, yet maintained the ability to activate T cells.[85] In a very recent work, iron oxide nanoparticles were evaluated as a safe, stable and built-in adjuvant vaccine delivery vehicle for a recombinant malaria vaccine antigen. There was evidence supporting the efficient internalization (> 90%) of iron oxide nanoparticle by dendritic cells. The iron oxide nanoparticles also showed their abilities to activate dendritic cells to express co-stimulatory ligand CD86, and secrete

necessary cytokines for immune response (IL-6, TNF-α, IL1-β, IFN-γ, and IL-12). Mice immunized with the iron oxide nanoparticle based malaria vaccine showed significant higher antibody response compared with the vaccine formulated with a clinically acceptable adjuvant, Montanide ISA51. Moreover, the nanoparticle based vaccine tested in nonhuman primates was able to induce high immune response and high levels of parasite inhibition.[86] Moreover, the size of iron oxide nanoparticles can be tuned by a variety of preparation method. This advantage of controllable size would allow preparation of the proper size of particulate vaccine more flexible.

Besides their tendency to activate dendritic cells, IONPs are well known as magnetic resonance imaging (MRI) contrast agent[83b], which could be used to monitor the migration of labeled DCs *in vivo* after vaccine administration by a non-invasive method based on MRI.[87] This advantage could aid us in deciphering mechanism of the immune responses. Accordingly, it could be hypothesized that iron oxide nanoparticles could have a potential as antigen carriers with intrinsic immunomodulating properties, yet low immunogenicity against the carrier itself, for immunotherapy based vaccine.

1.1.12 Self-assembly of amphiphilic-molecule coated iron oxide nanoparticles

As mentioned earlier, surface engineering on nanoparticles play an important role on physical and biological properties of the nanoparticles in vaccine design.[88] Iron oxide nanoparticles can be generated by several methods including co-precipitation, thermal decomposition, microemulsion, and hydrothermal synthesis.[89] Among these methods, the thermal decomposition method has been widely used to yield large quantities, tunable size and high-quality monodispersed iron oxide nanoparticles.[87a] However, the nanoparticles made by this method are coated by a hydrophobic layer of oleic acid or oleic amine, which are not soluble in highly polar solvents. Hence, they are not suitable for bio-applications which require good

solubility in water. In order to apply the hydrophobic nanoparticle in vaccine delivery platform, surface modifications on the nanoparticles is required.

Surface modification by covalent conjugation of ligand onto the nanoparticle surface involves multi-step chemical synthesis. For example, a catechol group can coat iron oxide nanoparticles well due to strong chelation of catechol with iron. However, the catechol group is easily oxidized, which requires an additional protection step before coating process.[90] An alternative approach for surface modification relies on self-assembled hydrophobic-hydrophobic interaction between the hydrophobic layer on iron oxide surface and hydrophobic groups on amphiphilic ligands.[91] This approach is simple and does not involve chemical conjugation. Moreover, multicomponent coating layer for multi-functional nano-vaccine can be obtained by mixing the coating components during the coating process.

Combining the promising tumor associated antigen MUC1 with the powerful antigen carrier of iron oxide nanoparticle, the goal of the study in this chapter was to evaluate the amphiphilically coated iron oxide nanoparticle as a MUC1 antigen carrier platform for anti-cancer vaccine.

1.2 Results and discussion

1.2.1 Synthesis of magnetic NPs coated with MUC1 lipopeptides and lipo-glycopeptides

We utilized the thermal decomposition method[92] to prepare high-quality monodispersed iron oxide nanocrystals in large scale and with excellent control of particle diameters. Homogeneity in size is important in NP based vaccine design, as NP diameters can significantly impact their interactions with the immune system as well as their trafficking.[69, 93] Covalent derivatization of NPs can be tedious. The NPs synthesized through the thermal decomposition

method are coated with a hydrophobic layer of oleic acid or oleic amine. This provides a platform for amphiphilic TACA to self-assemble on the NPs through hydrophobic-hydrophobic interactions without the need to covalently functionalize NPs. This approach is operationally simple, and an additional advantage is that multiple components can be readily introduced onto the NPs through self-assembly to boost immune responses.

In order to attach MUC1 onto the NPs, MUC1 peptide and glycopeptide were synthesized and conjugated with a phospholipid chain. The MUC1 peptide bearing 20 amino acid residues AHGVTSAPDTRPAPGSTAPP corresponding to one full length tandem repeat region was produced using solid phase peptide synthesis through Fmoc chemistry, using 2-chlorotrityl resin as a solid support and *O*-(benzotriazol-1-yl)-*N*,*N*,*N*',*N*'-tetramethyluronium hexafluorophosphate (HBTU) and 1-hydroxybenzotriazole (HOBt) as coupling agents (**Scheme 1.1**). Upon completion of the synthesis, the MUC1 peptide **1** was cleaved off the solid phase under an acidic condition (95:2.5:2.5, TFA:TIPS:H_2O), and purified by HPLC on a C18 reverse phase column. In order to conjugate the peptide with the lipid chain, phosphatidylethanolamine was treated with succinic anhydride to introduce a carboxylic group to the lipid part. The carboxylic group was then activated with *N*,*N*,*N'*,*N'*-tetramethyl-*O*-(*N*-succinimidyl)uronium tetrafluoroborate (TSTU) to form an NHS ester (**DPPE-SUC-NHS**). **DPPE-SUC-NHS** was incubated with MUC1 peptide **1** producing lipopeptide **5**, which was purified through HPLC on a reverse phase C4 column.

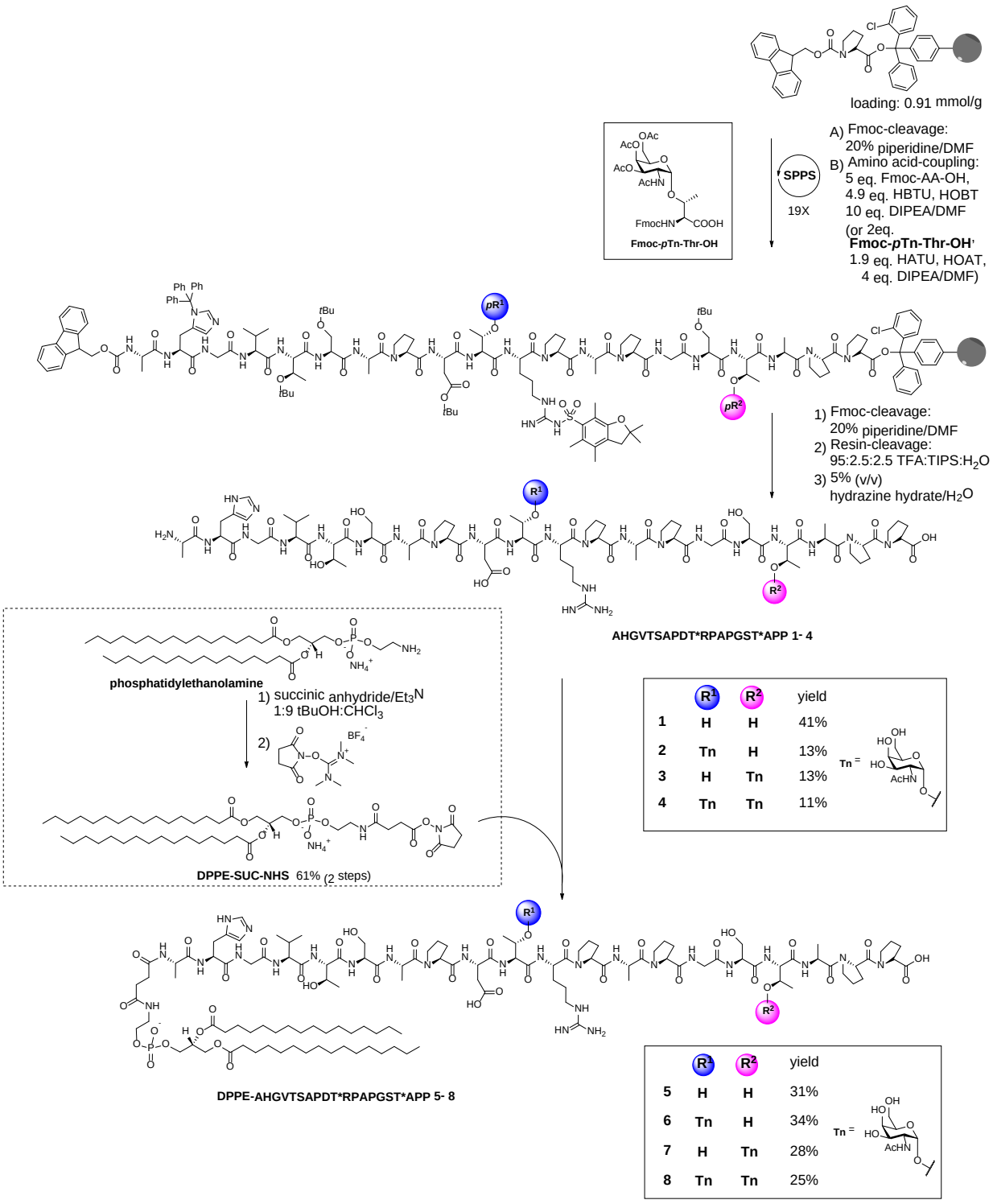

	R1	R2	yield
1	H	H	41%
2	Tn	H	13%
3	H	Tn	13%
4	Tn	Tn	11%

	R1	R2	yield
5	H	H	31%
6	Tn	H	34%
7	H	Tn	28%
8	Tn	Tn	25%

Scheme 1.1: Synthesis of MUC1 lipo-(glyco)peptides. The (Tn-)MUC1 peptides **1-4** were synthesized by solid phase peptide synthesis followed by coupling with the activated phospholipid **DPPE-SUC-NHS** to yield MUC1 lipo-(glyco)peptides **5-8**.

In addition to the unglycosylated MUC1 peptide **5**, three MUC1 lipo-glycopeptides **6**-**8** were synthesized using Tn substituted threonine **(Fmoc-*p*Tn-Thr-OH)** (For synthesis, see **section 1.4.2**) to replace the corresponding threonine building block in solid phase peptide synthesis (**Scheme 1.1**). Lipo-glycopeptide **6** contains a Tn antigen in the PDT*R region only and lipo-glycopeptide **7** bears Tn as part of the GST*A sequence, while lipo-glycopeptide **8** has the Tn in both locations. 1-[Bis(dimethylamino)methylene]-1*H*-1,2,3-triazolo[4,5-b]pyridinium 3-oxid hexafluorophosphate (HATU) and 1-hydroxy-7-azabenzotriazole (HOAT) were used as coupling agents for adding **Fmoc-*p*Tn-Thr-OH** to the peptide chain. After released from the resin, the glycopeptides **6-8** were obtained by deprotection with 5% (v/v) hydrazine hydrate followed by HPLC purification. These lipo(glyco)peptides are useful to probe the impact of the number and the location of Tn on immune responses.

With the lipopeptides in hand, antigen coated magnetic NPs were prepared. The oleic acid coated iron oxide NPs (OA-IONPs) were obtained by thermal decomposition of iron(III) acetylacetonate ($Fe(acac)_3$) in the presence of oleic acid and oleylamine at an elevated temperature (**Figure 1.9**).[94] The OA-IONPs produced have a mean size of 9 nm and a narrow polydispersity index (PDI) of 0.079 when measured as a solution in chloroform. The highly hydrophobic surface of the OA-IONPs rendered them insoluble in water (**Figure 1.10**). To facilitate the surface polarity changes and reduce NP aggregation in water, a dual solvent exchange method[95] was utilized for antigen coating (**Figure 1.9**). A mixture of the lipopeptide (DPPE-MUC1) and lipopolymer (DSPE-PEG2000) was added to a solution of OA-IONPs in chloroform. This was followed by slow addition of DMSO. Chloroform was then slowly evaporated under vacuum to induce the assembly of the amphiphilic DPPE-MUC1 and DSPE-PEG on NPs. Subsequently, DMSO was replaced with water through dialysis. Using this

procedure, the solvent polarity gradually increased to strengthen the hydrophobic interactions and assemble the lipopeptide and lipo-glycopeptide onto the NP. The NPs produced were well dispersed in water (**Figure 1.10**). The control particle NP-PEG without any (glyco)peptide (**NP-9**) was also prepared using DSPE-PEG2000 coating only.

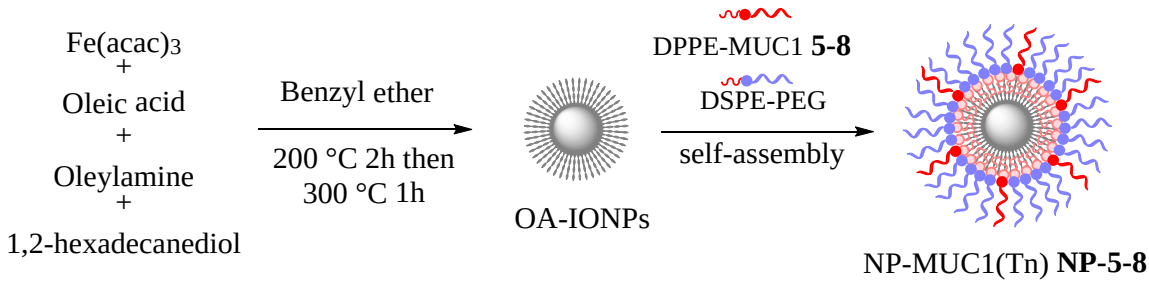

Figure 1.9: Synthesis of the hydrophobic OA-IONPs by the thermal decomposition method, and monolayer self-assembly coating of the NPs by phospholipid functionalized MUC1 or MUC1(Tn) glycopeptide.

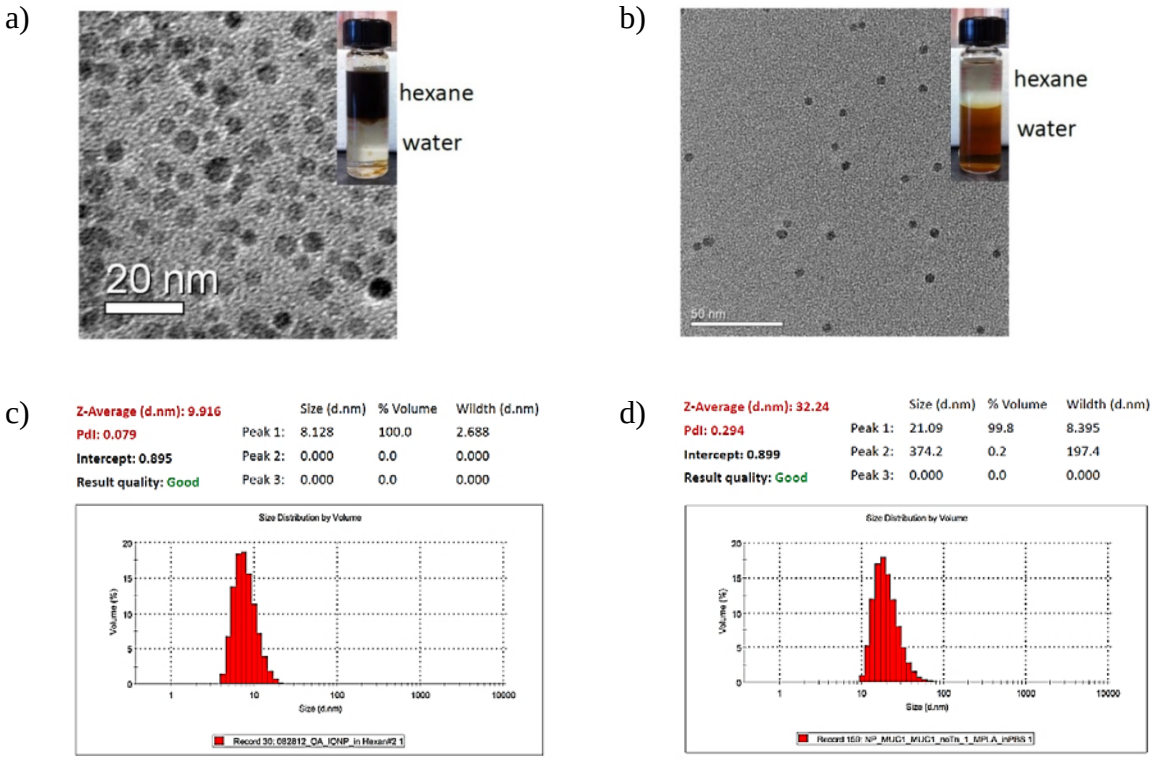

Figure 1.10: TEM images and hydrodynamic diameters from DLS a, c) OA-IONPs; b, d) **NP-5**.

The magnetic NPs were characterized. Dynamic light scattering (DLS) indicated the hydrodynamic diameters in water were around 35 nm (**Table 1.1** and **Figure 1.10**). The incorporation of the glycopeptides slightly increased the sizes of the coated NPs compared with the control **NP-9** with PEG only. The zeta-potentials of all NPs are slightly negative presumably due to the phosphate groups present.

Table 1.1: Hydrodynamic diameters and zeta potentials of the NP vaccines in PBS

NP	**Diameter (nm)**	**PDI**	**Zeta(mV)**
NP-PEG (NP-9)	31.8	0.257	-2.53
NP-5	32.2	0.294	-2.86
NP-6	37.6	0.288	-1.83
NP-7	38.1	0.265	-2.94
NP-8	38.4	0.269	-2.37

To ascertain the successful immobilization of the lipopeptides, the NPs were subjected to mass spectrometry (MS) analysis. Since lipopeptides were attached through non-covalent interactions, the coating of the NP could be readily ionized by matrix assisted laser desorption ionization (MALDI). The MALDI-TOF mass spectrum of **NP-5** showed the desired *m/z* ratio of the lipopeptide **5** (MW=2661), which was not found in that of **NP-9** coated with DSPE-PEG only (**Figure 1.11a,** and **Figure 1.22** for **NP-6, NP-7 and NP-8**). For lipopeptide quantification, the NPs were loaded onto a SDS-PAGE gel for electrophoresis, which was then visualized through silver staining (**Figure 1.11b**). The intensities of the bands were compared with a calibration curve generated based on bands from known amounts of free lipopeptides. From this analysis, it was determined that there was an average of 23 molecules of MUC1 per NP (see **section 1.4.13** and **Appendix A**).

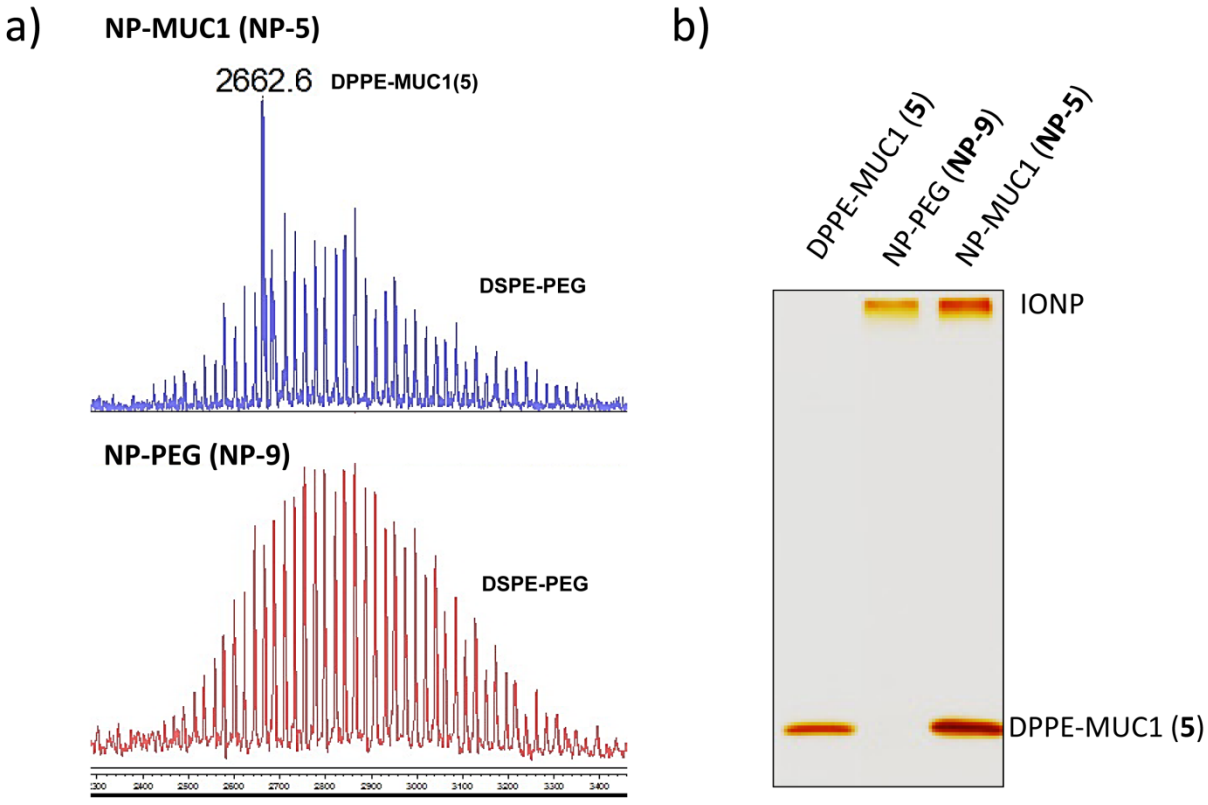

Figure 1.11: a) MALDI-TOF mass spectrum of **NP-5** coated with lipopeptide **5** ($[M+H]^+$ = 2662) and DSPE-PEG (top spectrum); and **NP-9** coated with DSPE-PEG only (bottom spectrum). b) SDS-PAGE of DPPE-MUC1, NP-PEG (**NP-9**), and NP-MUC1 (**NP-5**). The gel was visualized through silver staining.

1.2.2 *In vitro* activation of dendritic cells and detection of NP draining into local lymph nodes *in vivo*.

Dendritic cells are important antigen presenting cells, which modulate the immune responses.[96] To test DC interactions, **NP-9** was incubated with bone-marrow derived dendritic cells (BMDC). The NPs do not directly induce maturation of DCs as the expression levels of co-stimulatory molecules and activation markers on dendritic cells were unchanged upon NP incubation suggesting good biocompatibility of the NPs (**Figure 1.12a**).

The immune-potentiating activities of the NP construct can be bestowed by adding an agonist of Toll-like receptor 4 (TLR4), monophospholipid A (MPLA).[97] MPLA can elicit T cell responses and antibody isotype class switching from IgM to IgG.[98] With its amphiphilic nature, MPLA could also be immobilized onto the NPs through hydrophobic interactions.[99] The addition of MPLA to **NP-9** led to enhancement of the expression of co-stimulatory molecules, such as CD40, CD80, CD86 and MHC class II on DC as indicated by FACS analysis (**Figure 1.12a**). The expressions of these co-stimulatory molecules on APC are indication of immune activation. To confirm NP interactions with cells, **NP-9** was labeled with a fluorophore fluorescein isothiocyanate (FITC). Upon incubation with BMDC, fluorescence microscopy showed extensive green fluorescence inside the cells indicating NP uptake (**Figure 1.12b** vs **Figure 1.12c**). Similar NP uptake by BMDC was observed with or without MPLA (**Figure 1.13**).

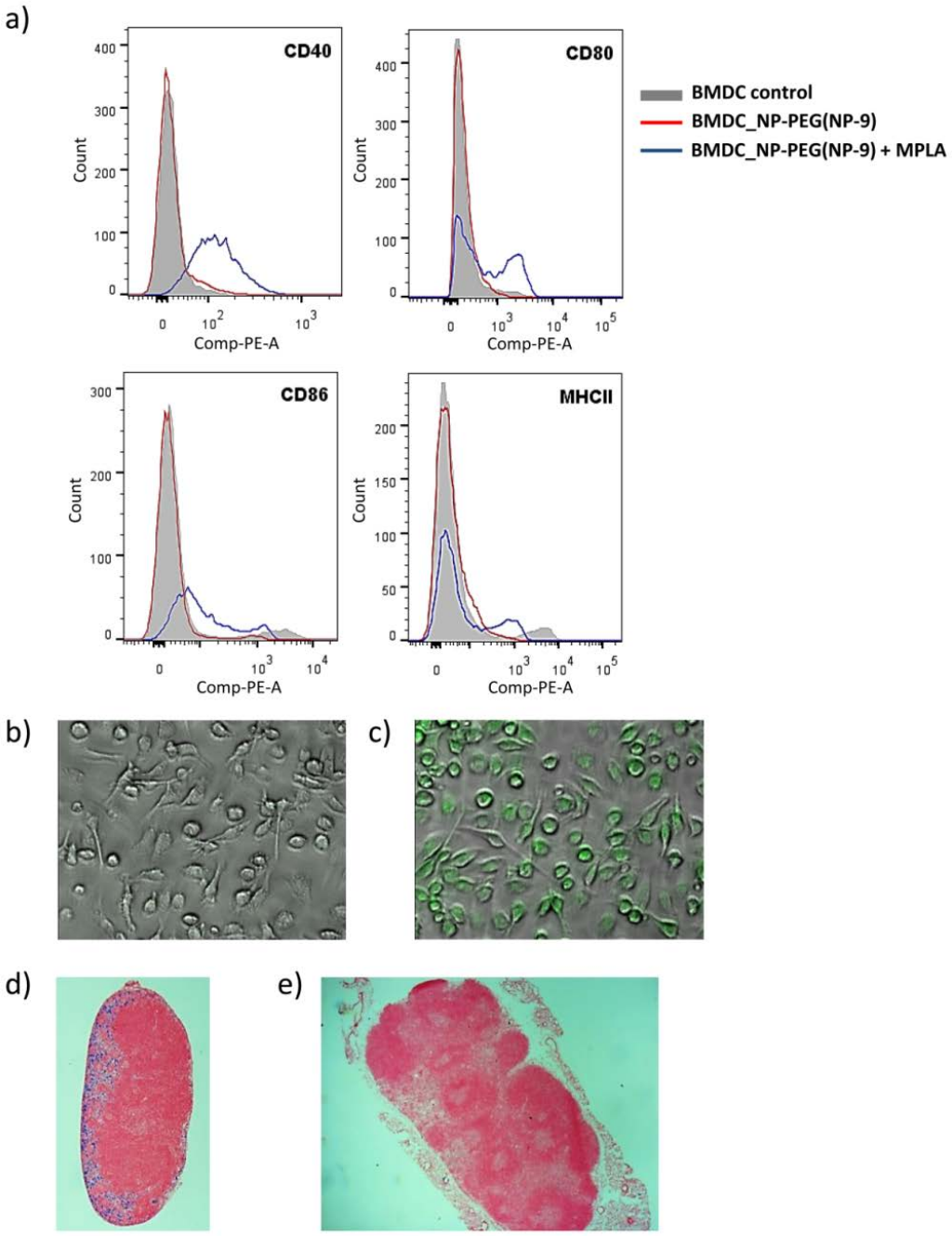

Figure 1.12: a) Flow cytometry results showing the expression of cellular markers of activation state (CD40, CD80, CD86 and MHCII) of BMDC after incubation with NP-PEG (**NP-9**) (red line), or NP-PEG (**NP-9**) + MPLA (blue line). Confocal images of BMDC incubated with b) PBS and c) **NP-9** (FITC) + MPLA. Histology of sections from d) axillary (local) lymph nodes, and e) inguins (distant) lymph node, stained by Prussian blue.

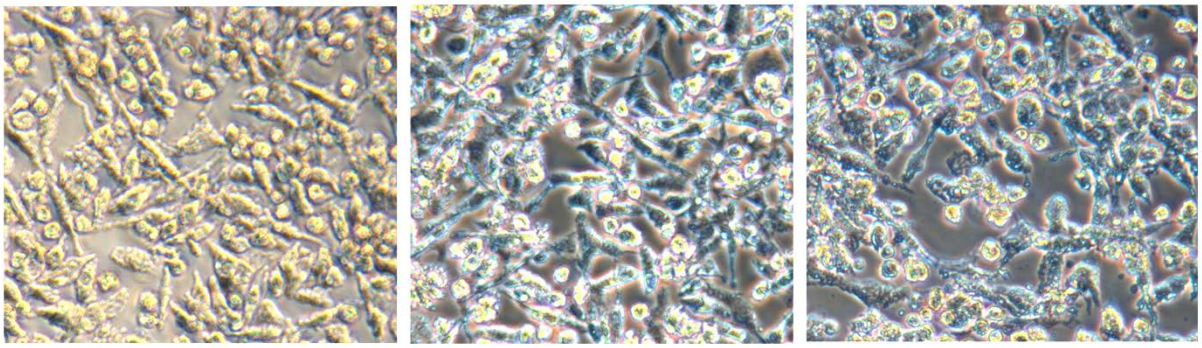

Figure 1.13: Microscopic images of Prussian blue staining of BMDC after incubation with **NP-9**. *Left*) only dendritic cells; *Middle*) dendritic cells incubated with NP-9 (50 μg) in PBS 12 hrs.; *Right*) dendritic cells incubated with NP-9 (50 μg) and MPLA (2 μg/mL) in PBS 12 h.

An important feature of our NP is that their hydrodynamic diameters are around 35 nm, which are within the size range for ready trafficking to lymph nodes for interactions with resident immunological cells.[69] To test transport to lymph nodes, NPs were injected subcutaneously into mice under their scruff. After 24 h, mice were sacrificed and their lymph nodes were removed and stained with Prussian blue, a dye sensitive to the presence of ferric ions. Histological analysis showed that the axillary (local) lymph nodes close to the injection sites exhibited extensive blue color in the B cell follicle region (**Figure 1.12d**), while there was much less blue staining in inguins (distant) lymph nodes (**Figure 1.12e**). This result suggested that the NPs could drain into local lymph nodes to interact with immunological cells.

1.2.3 Immunization with MUC1 coated NPs elicited strong anti-MUC1 IgG responses.

To evaluate the abilities of NP vaccines to induce immune responses *in vivo*, C57BL/6 mice were injected with NP-MUC1 (**NP-5**, **NP-6**, **NP-7**, **NP-8**) (corresponding to 20 μg of MUC1 peptide or glycopeptide) mixed with MPLA. Booster injections were performed on days 14 and 28. To decipher the importance of various vaccine components, control groups of mice received NP-PEG (**NP-9**)/MPLA, MUC1 peptide **1**/MPLA or MUC1 lipopeptide **5**/MPLA at the

same doses of NP and MUC1 respectively. Sera were collected from all mice a week after the final immunization.

The levels of antibody elicited were analyzed by enzyme-linked immunosorbent assay (ELISA) coated with the corresponding MUC1 or MUC1(Tn) glycopeptide. Mice (n=5) immunized with MUC1 NP vaccines elicited both IgG and IgM antibodies (**Figure 1.14a,c**) with higher IgG titers. In contrast, MUC1 peptide **1** failed to generate any appreciable amounts of anti-MUC1 antibodies. Interestingly, immunization with MUC1 lipopeptide **5** produced some anti-MUC1 IgG antibodies (mean titer ~ 5,032), although the titers were significantly lower than those induced by **NP-5** (mean IgG titer ~ 36,603, **Figure 1.14a**). This has also been supported by a study from Boons group[74a] where they found that mixture of lipidated MUC1 and MPLA can induce IgG antibody response against MUC1. The ability of lipopeptide MUC1 to generate antibodies may be due to the effect of lipid rendering MUC1 amphiphilic. The endogenous mouse serum albumin could absorb the amphiphilic lipopeptide and deliver the antigen into the lymph node for B cell activation.[100] The higher potency of the MUC1 NP construct to induce antibodies could be partly attributed to the efficient trafficking of NPs into the lymph nodes due to the suitable size regime of the NPs.[69] In addition, the NPs can present the glycopeptides in a multivalent manner rendering more efficient crosslinking of B-cell receptors and potent cellular activation.[101]

The availability of NPs bearing various MUC1 glycoforms enabled us to investigate the effects of glycosylation on antibody titers. PDT*R-MUC1 **NP-6** gave the highest IgG titers (mean titers ~ 81,402) compared to the GST*A-MUC1 **NP-7** (mean titers ~ 45,526) and the unglycosylated MUC1 **NP-5** (mean titers ~ 36,603) (**Figure 1.14a**). Interestingly, the

diglycosylated MUC1 **NP-8** gave significantly lower IgG titers (mean titers ~ 7,530) than **NP-6** and **NP-7**.

The anti-carrier responses were tested next. ELISA analysis showed that significantly lower titers (~ 200) of antibodies were generated against the NP carrier by **NP-5** than those against MUC1 (**Figure 1.14b**). This suggests that the immune responses were primarily focused on MUC1.

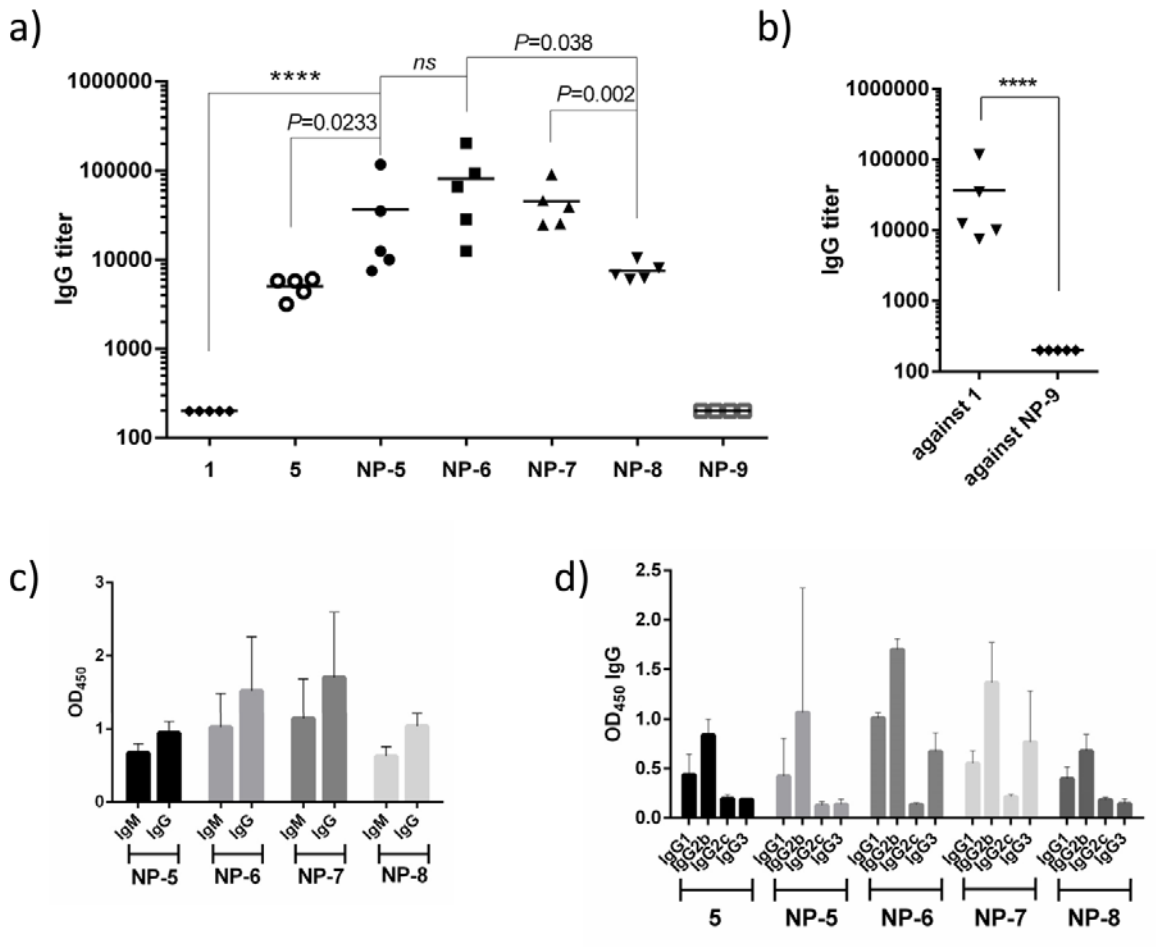

Figure 1.14: a) Anti-MUC1 and anti-Tn-MUC1 antibody titers from individual mouse (n=5), collected on day 35 after immunization with NP-MUC1 (**NP-5**) and NP-MUC1(Tn) (**NP-6**, **NP-7** and **NP-8**) vaccines, compared with soluble MUC1 peptide **1** and lipo-MUC1-peptide **5**. The anti-MUC1 antibody titers were determined by ELISA coated with corresponding (glyco)peptides **1-4**. b) IgG antibody titer from individual mouse, collected on day 35 after immunization with NP-MUC1 (**NP-5**), against MUC1 peptide **1** and **NP-9** c) IgM/IgG antibody

response determined by ELISA at 3200-fold dilution of serum from mice immunized with different vaccines. d) IgG isotypes of antibody response determined by ELISA from mice immunized with various vaccines.

The subtypes and cross-recognition of IgG antibodies elicited against MUC1 were analyzed. Higher levels of IgG2b over IgG1 were observed in all MUC1 vaccinated groups (**Figure 1.14d**), which suggested type 1 T helper cell (Th1)-skewed immune response and the generation of cell mediated immunity.[79, 102] The elicited antibodies from mice immunized with all NP vaccines could recognize other Tn-MUC1 glycopeptides (**Figure 1.15**).

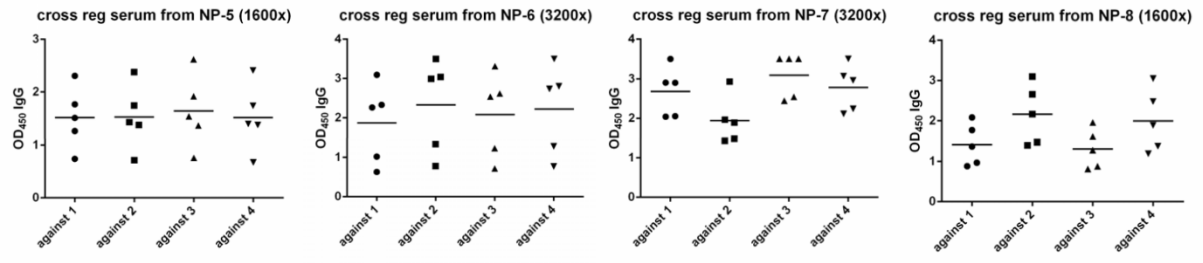

Figure 1.15: Cross-recognition of various MUC1 glycoforms by sera from mice immunized with **NP-5** – **NP-8**.

1.2.4 The antibodies from immunized mice showed binding and complement dependent cytotoxicity against MUC1-expressing tumor cells.

As ELISA tests binding to synthetic MUC1 (glyco)peptides, it is important that antibodies generated can recognize MUC1 on cancer cells. This was first tested with MUC1 transfected Ag104 cells, which express MUC1 containing exclusively Tn due to the dysfunction of Cosmc, a molecular chaperone.[103]

MUC1-Ag104 cells were incubated with sera from immunized mice followed by FITC labeled anti-mouse IgG secondary antibody. FACS analysis of the tumor cells indicated that the serum from mice immunized with MUC1 peptide **1** did not bind with the cells much (**Figure 1.16**a). In contrast, the MUC1 NPs induced antibodies capable of recognizing MUC1-Ag104

strongly. The recognition was MUC1 dependent as antibody binding to MUC1-Ag104 was much stronger than that to Ag104 cells without MUC1 transfection (**Figure 1.17**a). Moreover, the induced antibodies showed high selectivities towards MUC1-Ag104 with little binding to normal epithelial cells (**Figure 1.17**b). Consistent with the ELISA results, sera from mice immunized MUC1 **NP-6** exhibited strongest binding with MUC1-Ag104 cells. When these cells were incubated with the rabbit complement as well as the sera from MUC1 NP immunized mice, the majority of cancer cells were killed suggesting that the anti-MUC1 antibodies induced complement dependent cytotoxicities to cancer cells (**Figure 1.16**b).

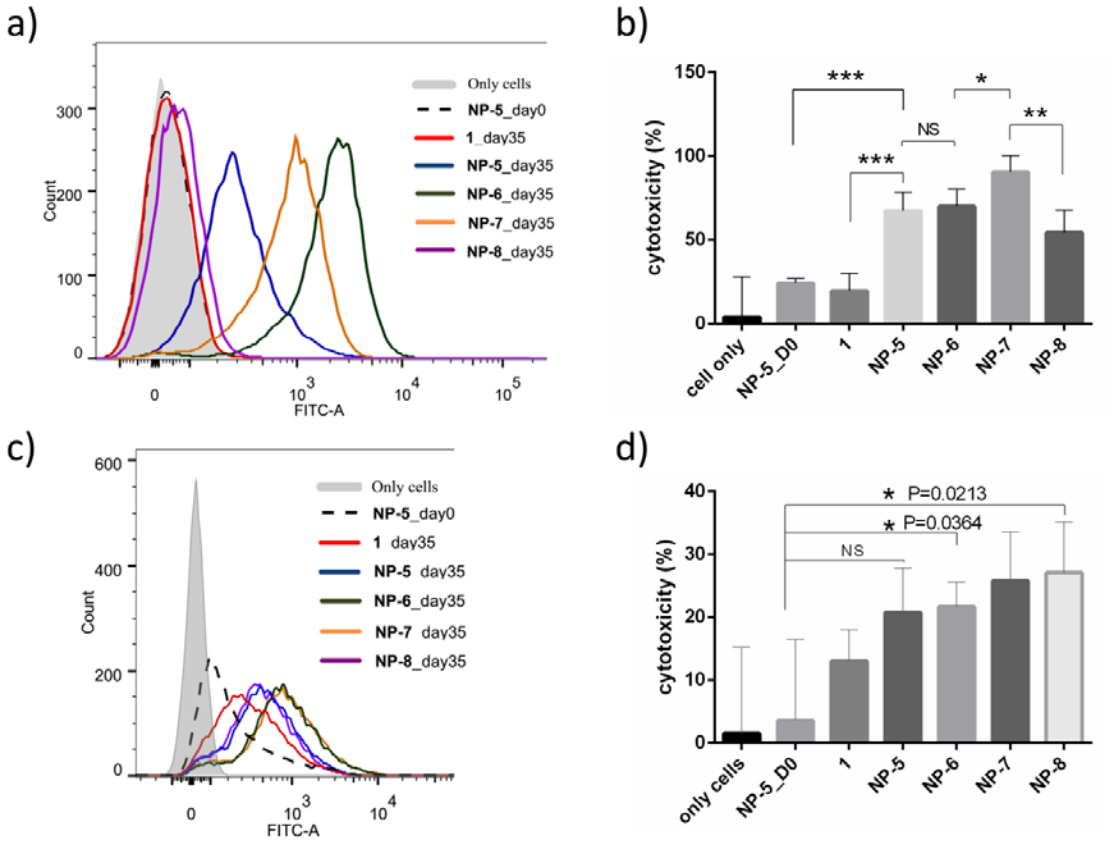

Figure 1.16: Flow cytometric analysis of the binding of antibodies induced by various constructs to a) MUC1-Ag104 cells and c) MCF-7. MTS assay analysis of complement-dependent cytotoxicity of antibodies induced by various vaccines on b) MUC1-Ag104 cells and d) MCF-7. (** $P < 0.05$, *** $P < 0.005$,)

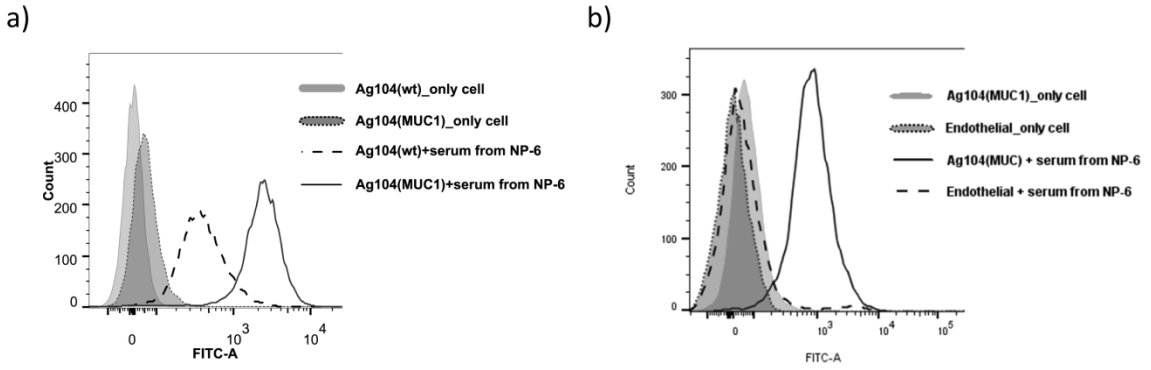

Figure 1.17: Flow cytometry showing the specific binding of anti-MUC1 antibody from immunized mice a) against wild type Ag104 (Ag104(wt)) and MUC1 transfected Ag104 cells (Ag104(MUC1)); b) against MUC1 transfected Ag104 cells (Ag104(MUC1)) and endothelial cells (EA.hy926).

Next, the interactions of post-immune sera with human breast cancer cell MCF-7 were studied. MCF-7 naturally expresses MUC1 on cell surface. Antibodies elicited by MUC1 NP vaccines were also capable of binding with MCF-7 cells (**Figure 1.16c**). The binding of antibody from mice immunized with **NP-6** and **NP-7** showed similar affinities and higher than those immunized with unglycosylated MUC1 **NP-5** and di-Tn MUC1 **NP-8** vaccines. The MUC1 NP vaccines were also capable of inducing complement dependent cytotoxicities against MCF-7 (**Figure 1.16d**).

1.2.5 Discussion

While magentic NPs have seen wide biomedical applications, they have not been utilized as TACA carriers in vaccine development. With the MUC1-magentic NP vaccines, significantly higher IgG antibody responses were observed compared to mice immunized with MUC1 peptide or lipopeptide. The study from Hubbell and coworkers[69] emphasized the crucial effect of size for vaccines. NPs with 25nm diameters can target lymph node residing dendritic cells, which are more efficient in immune activation than dendritic cells in skin, but 100nm NPs are less likely to

drain into the lymph nodes. The size of our NPs (30-40 nm) is likely a contributing factor to high antibody responses. The fact that anti-MUC1 IgG antibodies were induced suggests that magnetic NP vaccines can activate helper T cells and elicit antibody isotype switching without the need for a traditional immunogenic protein carrier or additional helper T cell epitopes. Furthermore, the magnetic NP itself is almost non-immunogenic inducing little anti-carrier antibodies. These attributes combined suggest that magnetic NPs can be a useful platform for glyco-conjugate based anti-cancer vaccines joining other types of NP such as gold NPs, polymer NPs and virus like particles.[70, 104]

Compared to MUC1 expressed on normal cells, MUC1 on cancer cells bear shortened *O*-glycans as represented by the Tn antigen. Glycosylation of MUC1 leads to conformational changes of the peptides.[105] As a result, MUC1 glycopeptides become more immunogenic.[106] This is supported by our results that lipo-glycopeptide coated NPs induced higher antibody titers and stronger binding with MUC1 positive tumor cells than unglycosylated MUC1 coated **NP-5**.

As each of the tandem repeats of MUC1 proteins contains five potential glycosylation sites, MUC1 proteins on tumor cells are hetereogenously glycosylated. How the glycan structure can influence the humoral responses is an active area of research.[107] Within our NP constructs, addition of Tn onto the peptide sequence PDT*R showed higher antibody responses than that with the Tn on GST*A sequence. This suggests glycosylation in PDT*R region more potently boosted the humoral response in our NP constructs.[79, 107g] On the other hand, further increase of the number of glycans on the protein may not lead to improved antibody titers as indicated from the reduced anti-MUC1 titers elicited by **NP-8** bearing two Tns. So far, whether fully glycosylation on MUC1 enhances immunogenicity of the vaccine is still unclear.[53] Our results

can provide guidance to selection of glycopeptide structure for future MUC1 based vaccine studies.

The cancer cell MUC1-Ag104 exclusively expresses Tn rather than longer *O*-glycans.[103] As a result, its MUC1 proteins are expected to be solely glycosylated with Tn. The antibodies from immunized mice bound more strongly and exhibited higher cytotoxicity with MUC1-Ag104 as compared to heterogenously glycosylated MCF-7 cells.[107e, 108] This suggests a potential approach to improve recognition of MCF-7 cells is to incorporate MUC1 glycopeptides bearing multiple types of glycan structures.

1.3 Conclusions

Iron oxide magnetic NPs were investigated as a new antigen carrier platform for MUC1-based cancer vaccine. A simple procedure was developed to immobilize lipo(glyco)peptides onto the NPs through self-assembly without the need for covalent NP functionalization. Good MUC1 specific IgG antibody responses were produced. Besides MUC1, this strategy can be readily applied to vaccines targeting other glycopeptides. In addition, glycolipids such as gangliosides are another class of important TACAs. The magnetic NP approach can be potentially useful for vaccines targeting the amphiphilic glycolipids as well.

With the large surface area of the NPs, multiple lipopeptides were incorporated. The resulting lipopeptide NPs could drain into local lymph nodes of mice upon vaccination and activate the immune sytem to elicit MUC1 specific antibodies. Compared to the antigen in soluble forms, the nano-vaccine induced higher antibody titers presumbly due to the suitable sizes of NPs and the multivalent display of antigens on particle surface. Combined with the low antibody titers against the carrier, this highlights the advantages of the magentic NP platform.

Immunological evaluations of MUC1 NPs demonstrated that the number and position of Tn in the glycopeptide chain can impact antibody titers. A single Tn in the PDT*R region gave the highest anti-MUC1 IgG titers. The antibodies generated not only selectively recognized MUC1 expressing tumor cells, but also mediated complement dependent cytotoxicity for tumor cell killing. Therefore, the magnetic NPs represent a new and effective platform for the development of TACA based synthetic anti-cancer vaccines.

1.4 Materials and methods

1.4.1 Materials and instrumentation

All chemicals were reagent grade and used as received from the manufacturer, otherwise noted. ^{1}H NMR spectra were recorded on an Agilent-500M spectrometer and processed by software MestReNova Version 10.0.2. Peptide or lipopeptide were purified on Shimadzu (LC-8A Liquid Chromatograph Pump, DGU-14A Degasser and SPD-10A UV-Vis Detector. TEM images were collected on a JEM-2200FS operating at 200 kV using Gatan multiscan CCD camera with Digital Micrograph imaging software. Ultrathin-carbon type A, 400 mesh copper grids for TEM were purchased form Ted Pella, Inc. Thermogravimetric analysis (TGA) was carried on a Thermal Advantage (TA Instruments-Waters LLC) TGA-Q500 series and the samples were burned under nitrogen. The hydrodynamic diameter and zeta potential were assessed on Malvern Zetasizer Nano zs instrument. FACS experiments were conducted on LSR II flow cytometer.

1.4.2 Synthesis of Fmoc-*p*Tn-Thr-OH

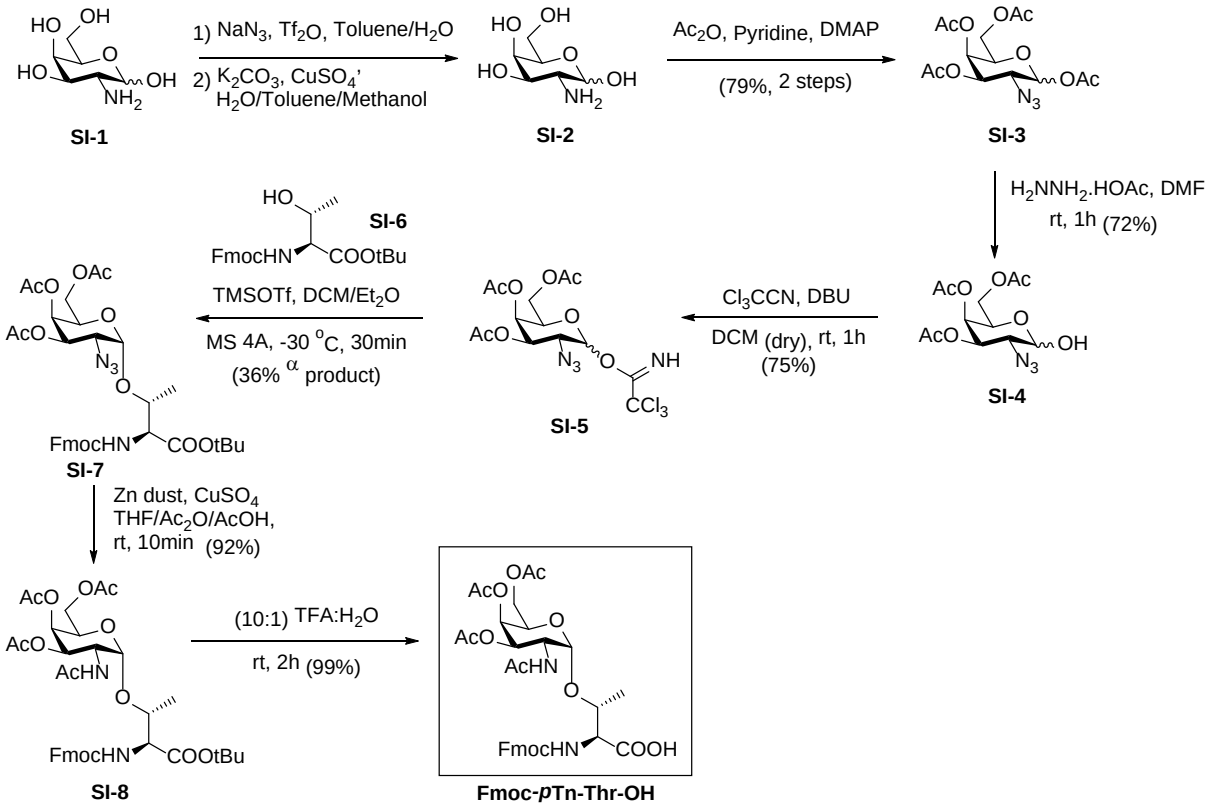

Figure 1.18: Synthesis of Fmoc-*p*Tn-Thr-OH.

*1,3,4,6-Tetra-O-acetyl-2-azido-2-deoxy-D-galactopyranoside (**SI-3**):*

The synthesis procedure was modified from reported literature.[109] A solution of NaN_3 (8.9 g, 136.7 mmol) in water (22.5 mL) was cooled down to 0°C. Toluene (22.5 mL) was added into the solution. The solution was stirred vigorously while adding Tf_2O (4.7 mL) over a period of 5 minutes. The reaction was left stirred for 2 hours at 0°C. Saturated $NaHCO_3$ solution was added until the evolution of gas stopped. The organic phase was separated and the aqueous layer was washed with toluene twice. The combined organic phase containing TfN_3 was dried over anhydrous Na_2SO_4. The solution of TfN_3 was used in the next step without further purification. Galactosamine hydrochloride (3.0 g, 13.9 mmol) was dissolved in water (45 mL). K_2CO_3 (2.89

g, 20.9 mmol) and $CuSO_4$ (20.1 mg, 0.13 mmol) were added into the reaction flask followed by MeOH (30 mL). The TfN_3 solution was added into the reaction, followed by adding MeOH until the mixture solution became homogeneous. The reaction was left stirred at room temperature for 18 hours. The reaction residue was then co-evaporated with toluene until almost dry. The resulting syrup was dissolved in pyridine (15 mL) followed by cooling down to 0°C. A catalytic amount of DMAP was added into the reaction. Ac_2O (45 mL) was added dropwise, and the reaction was left stirred for 2-3 hours. The excess Ac_2O was neutralized by slow addition of MeOH. The mixture was concentrated under vacuum, diluted with DCM and washed with 1M HCl, Na_2CO_3 and H_2O. The organic layer was dried over anhydrous $NaSO_4$ and then concentrated. The crude reaction mixture was purified by column chromatography (silica gel; 1:1, EtOAc:Hexanes) to yield compound **SI-3** as a white solid (4.12 g, 79% from 2 steps). The identity of the product was confirmed by comparison with reported literature.[110] ^{1}H NMR (500 MHz, $CDCl_3$) 5.52 (d, *J* = 8.5 Hz, 1H), 5.36 (dd, *J* = 3.3, 1.0 Hz, 1H), 4.87 (dd, *J* = 10.8, 3.3 Hz, 1H), 4.11 (qd, *J* = 11.3, 6.6 Hz, 2H), 3.98 (td, *J* = 6.7, 1.1 Hz, 1H), 3.82 (dd, *J* = 10.8, 8.5 Hz, 1H), 2.18 (s, 3H), 2.15 (s, 3H), 2.05 (s, 3H), 2.02 (s, 3H).

*2-Azido-2-deoxy-3,4,6-tri-O-acetyl-α,β-D-galactopyranose (**SI-4**):*[111]

Hydrazine acetate (66.6 mg, 0.723 mmol) in the reaction flask was flushed with nitrogen gas for 10 min. Compound **SI-3** (270.0 mg, 0.723 mmol) dissolved in DMF was added slowly into the reaction flask. The reaction was left stirred for an hour. Upon completion, the reaction mixture was diluted with EtOAc, washed with water, and dried over Na_2SO_4. The residue was purified by column chromatography (silica gel; 3:2 Hexanes:EtOAc) to obtain **SI-4** (mixture of α and β product as colorless oil (170 mg, 72%, α : β = 3:2 estimated based on NMR spectrum). Spectral analysis of the product compared with reported literature[111] confirmed the identity of the

product. ^{1}H NMR (500 MHz, $CDCl_3$) The NMR spectrum is of the mixture of α and β product. δ 5.44 (dd, *J* = 3.2, 1.3 Hz, 1H (α)), 5.42 – 5.36 (m, 2H (α)), 5.32 (dd, *J* = 3.3, 1.0 Hz, 1H (β)), 5.27 (s, 1H), 4.80 (dd, *J* = 10.8, 3.3 Hz, 1H (β)), 4.68 (dd, *J* = 7.9, 4.2 Hz, 1H (β)), 4.44 (td, *J* = 6.5, 0.9 Hz, 3H (α)), 4.15 – 4.01 (m, 2H (α/β)), 3.89 (td, *J* = 6.5, 1.1 Hz, 1H (β)), 3.73 (dd, *J* = 11.0, 3.4 Hz, 1H (α)), 3.64 (dd, *J* = 10.9, 7.9 Hz, 1H (β)), 3.23 (d, *J* = 2.6 Hz, 1H (α)), 2.15 – 2.13 (m, 3H (β)), 2.13 (d, *J* = 3.0 Hz, 3H (α)), 2.04 (dd, *J* = 3.9, 1.1 Hz, 12H (α/β).

*O-(3,4,6-Tri-O-acetyl-2-azido-2-deoxy-D-galactopyranoside) trichloroacetimi-date (**SI-5**):*

Compound **SI-4** (5.0 g, 15.1 mmol) and 1,8-diazabicyclo[5.4.0]undec-7-ene (DBU) were dissolved in dry DCM under nitrogen atmosphere. Trichloroacetonitrile (15.1 mL, 150.93 mmol) was added drop wise into the reaction flask. The reaction was stirred at room temperature for an hour. The reaction mixture was concentrated and purified by flash column chromatography (silica gel; 4:1 to 2:1 Hexane:EtOAc) to obtain compound **SI-5** as colorless oil (5.36 g, 75%). Spectral analysis of the product compared with reported literature[111] confirmed the identity of the product. ^{1}H NMR (500 MHz, $CDCl_3$) δ 8.79 (s, 1H), 6.49 (d, *J* = 3.6 Hz, 1H), 5.52 (dd, *J* = 3.2, 1.3 Hz, 1H), 5.35 (dt, *J* = 8.6, 4.3 Hz, 1H), 4.40 (td, *J* = 6.6, 0.9 Hz, 1H), 4.19 – 3.94 (m, 3H), 2.15 (s, 3H), 2.05 (s, 3H), 1.98 (s, 3H).

*N-(Fluoren-9-ylmethoxycarbonyl)-O-(3,4,6-tri-O-acetyl-2-azido-2-deoxy-α-D-galactopyranosyl-L- threonine tert-butyl ester (**SI-7**):*

The synthesis procedure was modified from reported literature[112]. Trichloroacetimidate **SI-5** (5.36 g, 11.27 mmol) and *N*-Fmoc-*O*-*t*Bu-threonine **SI-6**[113] (3.6 g, 9.39 mmol) were mixed in the reaction flask with freshly activated molecular sieves 4A (10 g) under nitrogen gas. Anhydrous DCM:Et_2O (1:1, 120 mL) was added to dissolved the mixture, and the solution was

left stirred at -30°C for 30 min. TMSOTf (0.297 mL, 1.925 mmol) was added dropwise into the reaction. The reaction was left stirred at 30°C for an hour. Upon monitoring the reaction, if there was some starting material **SI-6** left, 0.1 more eq. of TMSOTf was further added and the reaction was allowed to proceed for another hour. The temperature of the reaction was then carefully increased up to –10°C. Upon completion, diisopropylethylamine (DIPEA) was added to quench the reaction. The reaction was diluted with DCM and washed with 0.1 M HCl and then water. The organic layer was dried over Na_2SO_4 and then concentrated. The crude product was purified by column chromatography (silica gel; 3:1 EtOAc:Hexane) to yield **SI-7** (2.6 g, 36%). Spectral analysis of the product compared with reported literature[114] confirmed the identity of the product. ^{1}H NMR (500 MHz, $CDCl_3$) δ 7.77 (d, *J* = 7.5 Hz, 2H), 7.63 (d, *J* = 7.2 Hz, 2H), 7.40 (td, *J* = 7.5, 2.4 Hz, 2H), 7.35 – 7.28 (m, 2H), 5.64 (d, *J* = 9.4 Hz, 1H), 5.47 (d, *J* = 2.6 Hz, 1H), 5.34 (dd, *J* = 11.2, 3.2 Hz, 1H), 5.11 (d, *J* = 3.6 Hz, 1H), 4.35 (dddd, *J* = 23.3, 15.5, 13.1, 6.9 Hz, 6H), 4.16 – 4.04 (m, 3H), 2.16 (d, *J* = 7.1 Hz, 3H), 2.07 (d, *J* = 9.2 Hz, 3H), 2.06 – 2.02 (m, 3H), 1.52 (d, *J* = 17.3 Hz, 9H), 1.37 (t, *J* = 13.7 Hz, 3H), 1.29 – 1.22 (m, 1H).

*N-(Fluoren-9-ylmethoxycarbonyl)-O-(3,4,6-tri-O-acetyl-2-acetamido-2-deoxy-α-D-galactopyranosyl-L-threonine tert-butyl ester (**SI-8**):*[114]

Compound **SI-7** (5 g, 7.15 mmol) was dissolved in 3:2:1 of THF:Ac_2O: AcOH (120 mL). Zinc dust (5.9 g, 89.35 mmol) was added and then 11 mL of saturated aq. $CuSO_4$ was added to activate zinc. The reaction was stirred at rt for about half an hour. After completion as monitored by TLC, the zinc dust was removed by filtering the reaction mixture through Celite®. The filtrate was coevaporated with toluene to concentrate the crude product. The crude product was purified by column chromatography (silica gel; 1:1 EtOAc:Hexanes) to yield **SI-8** (4.68 g, 92%). Spectral analysis of the product compared with reported literature[114] confirmed the identity of the product.

^{1}H NMR (500 MHz, $CDCl_3$) δ 7.78 (d, *J* = 7.5 Hz, 2H), 7.64 (d, *J* = 6.9 Hz, 2H), 7.41 (td, *J* = 7.4, 2.9 Hz, 2H), 7.34 (dt, *J* = 11.9, 6.0 Hz, 2H), 5.89 (d, *J* = 9.6 Hz, 1H), 5.41 (d, *J* = 10.2 Hz, 2H), 5.09 (d, *J* = 8.8 Hz, 1H), 4.90 (d, *J* = 3.2 Hz, 1H), 4.63 (t, *J* = 8.9 Hz, 1H), 4.52 – 4.38 (m, 2H), 4.31 – 4.02 (m, 6H), 2.17 (s, 3H), 2.04 (s, 3H), 2.00 (s, 6H), 1.53 – 1.41 (m, 9H), 1.33 (d, *J* = 6.3 Hz, 3H).

*N-(Fluoren-9-ylmethoxycarbonyl)-O-(3,4,6-tri-O-acetyl-2-acetamido-2-deoxy-α-D-galactopyranosyl-L- threonine (**Fmoc-pTn-Thr-OH**):*

The synthesis procedure was modified from reported literature[112]. 10:1 TFA:H_2O (10 mL) was added dropwise into compound **SI-8** (4.7 g, 6.44 mmol) at rt. The reaction was stirred for 2 hours. The mixture was coevaporated with toluene to remove the excess TFA and water. The crude product was purified by column chromatography (silica gel, 5:1 DCM:MeOH) to yield the product **Fmoc-*p*Tn-Thr-OH** (4.27 g, 99%). Spectral analysis of the product compared with reported literature[112] confirmed the identity of the product. ^{1}H NMR (500 MHz, CD_3OD) δ 7.85 (d, *J* = 7.5 Hz, 2H), 7.72 (t, *J* = 8.1 Hz, 2H), 7.46 – 7.39 (m, 2H), 7.35 (tdd, *J* = 7.4, 4.7, 0.9 Hz, 2H), 5.42 (t, *J* = 6.6 Hz, 1H), 5.10 (dd, *J* = 11.5, 3.2 Hz, 1H), 4.96 (t, *J* = 8.0 Hz, 1H), 4.62 (dt, *J* = 13.8, 6.9 Hz, 1H), 4.54 – 4.47 (m, 1H), 4.46 – 4.37 (m, 2H), 4.34 – 4.24 (m, 3H), 4.18 – 4.08 (m, 2H), 3.98 (d, *J* = 27.1 Hz, 1H), 2.16 (d, *J* = 6.3 Hz, 3H), 2.10 – 2.03 (m, 3H), 2.03 – 1.91 (m, 6H), 1.33 – 1.22 (m, 3H).

1.4.3 Synthesis of MUC1 1 and Tn-MUC1 2-4

The MUC1 lipopeptide was derived from conjugation of phospholipid (DSPE-SUC-NHS) and the tandem repeat MUC1 peptide. The MUC1 peptide was synthesized using Fmoc-chemistry based solid phase support peptide synthesis, starting from a 2-chlorotrityl resin preloaded with Fmoc-proline. The N-terminal protecting group, Fmoc-, was de-protected by 20%

piperidine in DMF. The amino acid coupling was carried out with Fmoc amino acids (5 eq.) using HBTU/HOBt (4.9 eq.) and DIPEA (10 eq.), or Fmoc-Tn building block Fmoc-*p*Tn-Thr-OH (2eq.) using HATU/HOAT (1.9 eq.) and DIPEA (4 eq.). The peptide was cleaved from resin by TFA/TIS/H_2O=95/2.5/2.5 for 30 min. The excess TFA was evaporated out, peptide was precipitated by diethyl ether and centrifuged to pallet the peptide precipitation. The peptide was further reprecipitated three times. To remove the acetyl protecting group of the Tn, the crude peptide was treated with 5% (v/v) hydrazine acetate for 2 hours. The crude reaction was neutralized to pH 7. The deprotected peptide was then purified by HPLC, using reverse phase column SUPERCOSIL LC18, 25cm x10 mm 5 µm with gradient solvent CH_3CN and H_2O (0.1% TFA) gradient 0-22% in 25min and to 100% in 10min. The product was identified by MALDI-TOF.

1.4.4 Purification and characterization of (glyco)-peptides 1–4

1: HRMS: *m/z* calc. for $C_{80}H_{127}N_{25}O_{28}$: 1887.0430; found: 1887.9166 $[M+H]^+$.

2: HRMS: *m/z* calc. for $C_{88}H_{140}N_{26}O_{33}$: 2090.2370; found: 2091.6226 $[M+H]^+$.

3: HRMS: *m/z* calc. for $C_{88}H_{140}N_{26}O_{33}$: 2090.2370; found: 2091.4449 $[M+H]^+$.

4: HRMS: *m/z* calc. for $C_{96}H_{153}N_{27}O_{38}$: 2293.4310; found: 2293.9621 $[M+H]^+$.

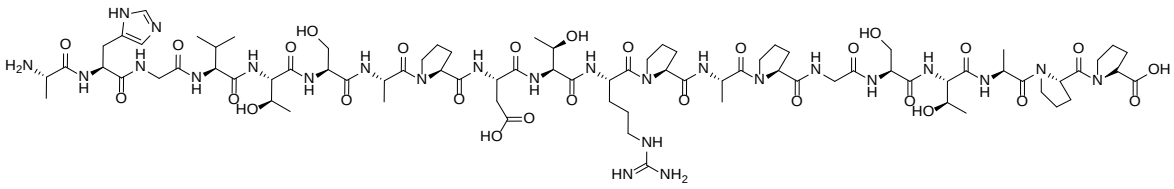

1 (Molecular Weight: 1887.0430)

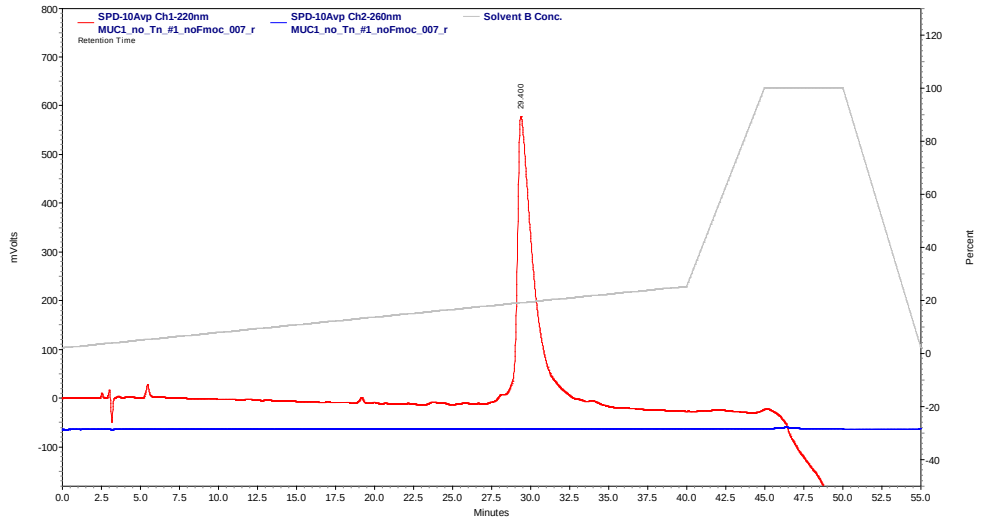

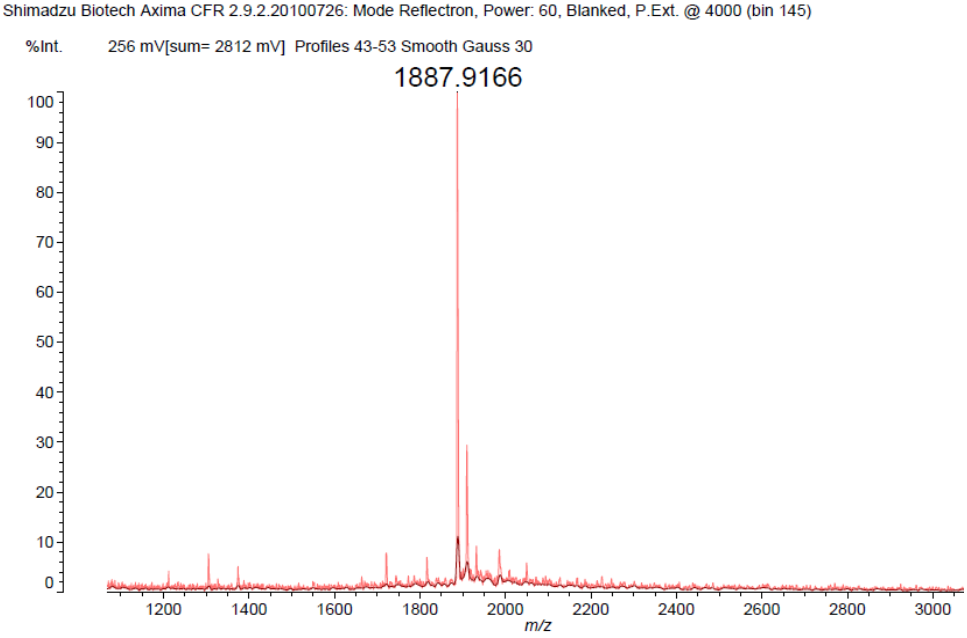

Figure 1.19: HPLC chromatogram and MALDI-TOF mass spectrum of the MUC1 peptide **1**, and the MUC1 glycopeptide **2**, **3** and **4**.

Figure 1.19: (Cont'd)

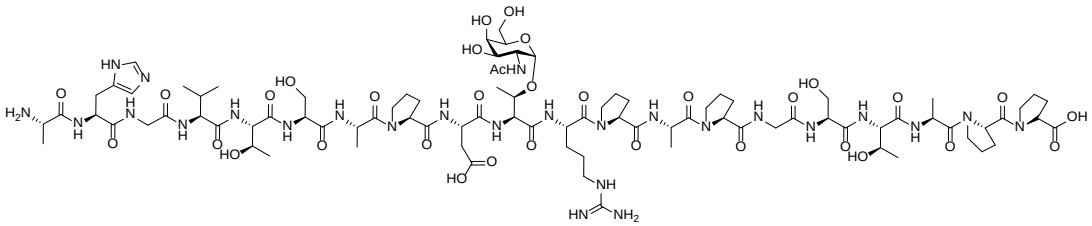

2 (Molecular Weight: 2090.2370)

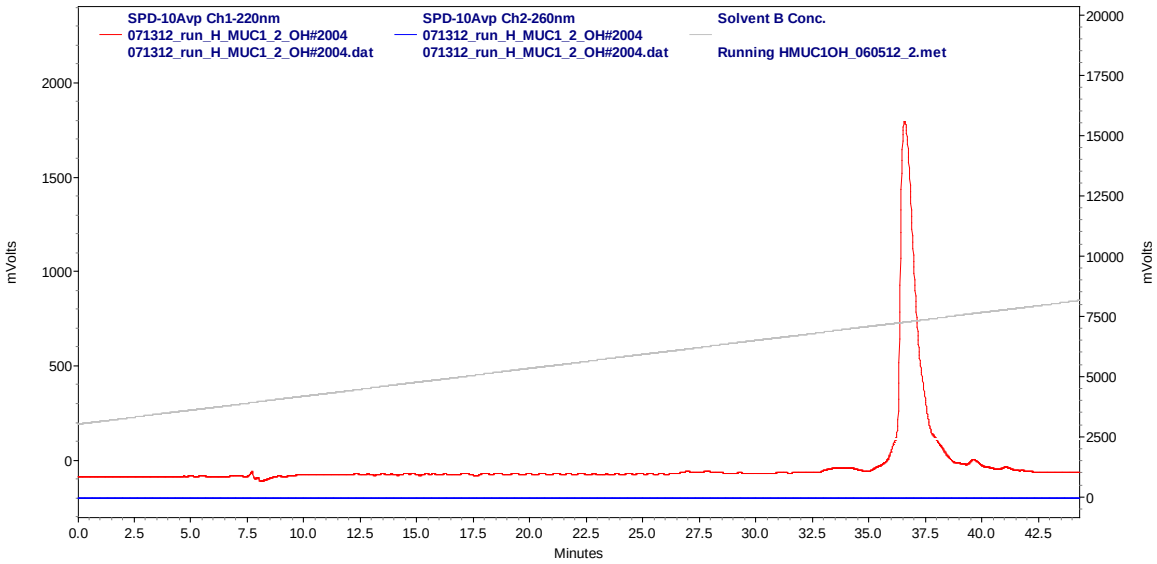

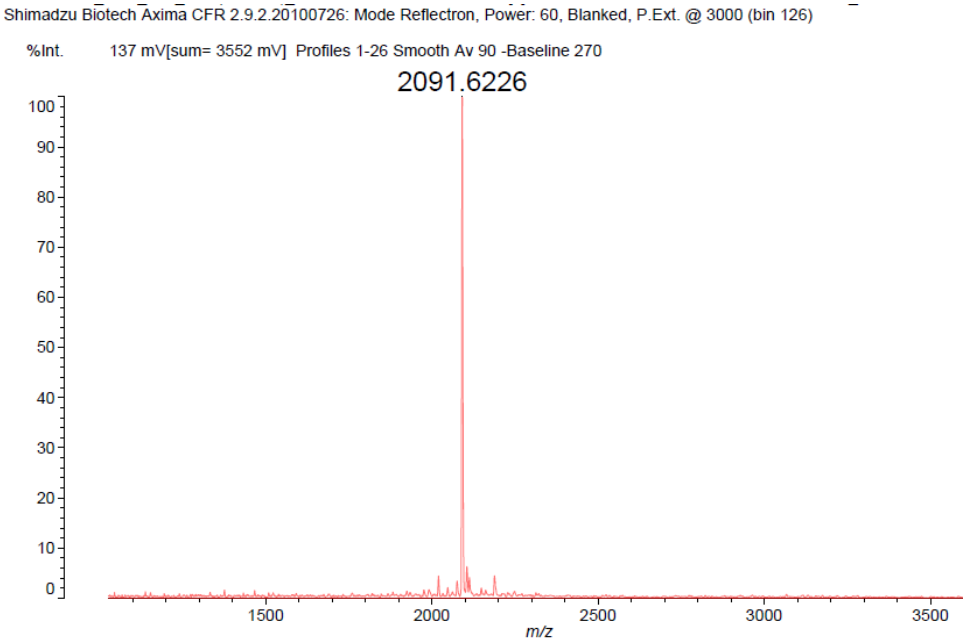

Figure 1.19: (Cont'd)

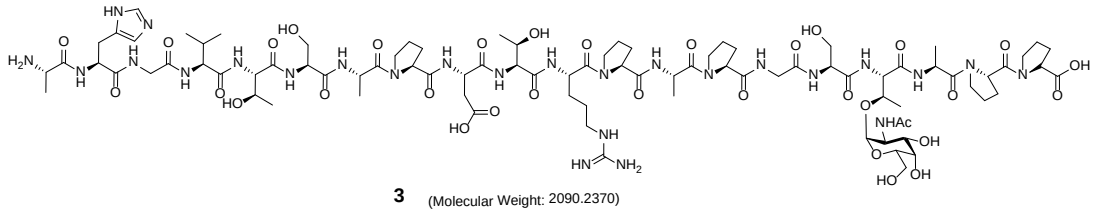

3 (Molecular Weight: 2090.2370)

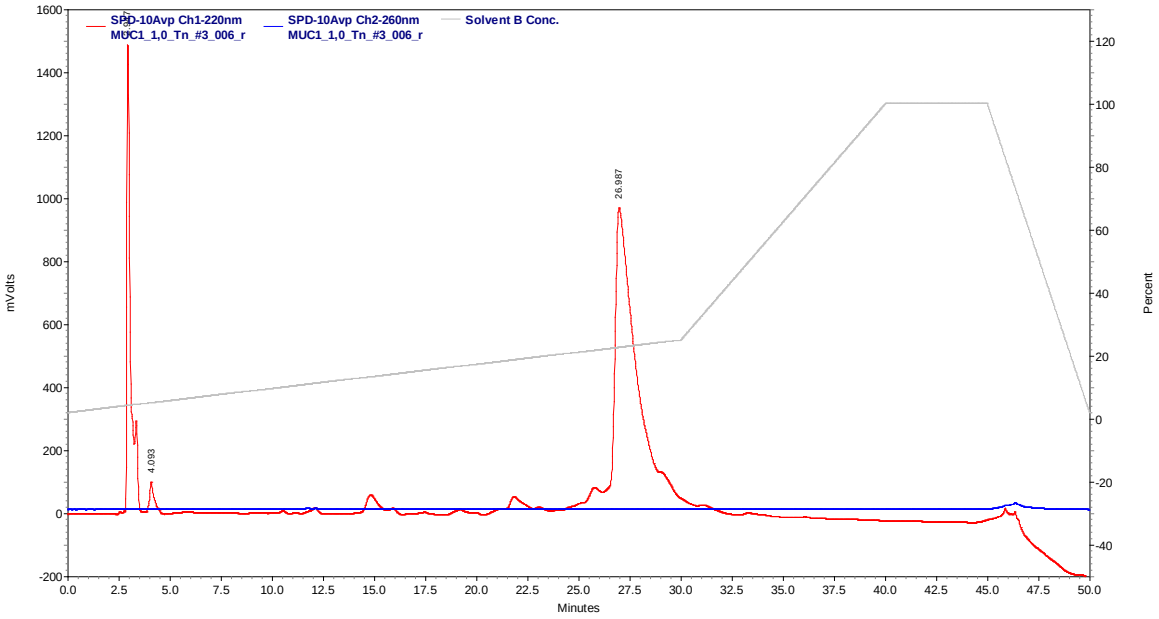

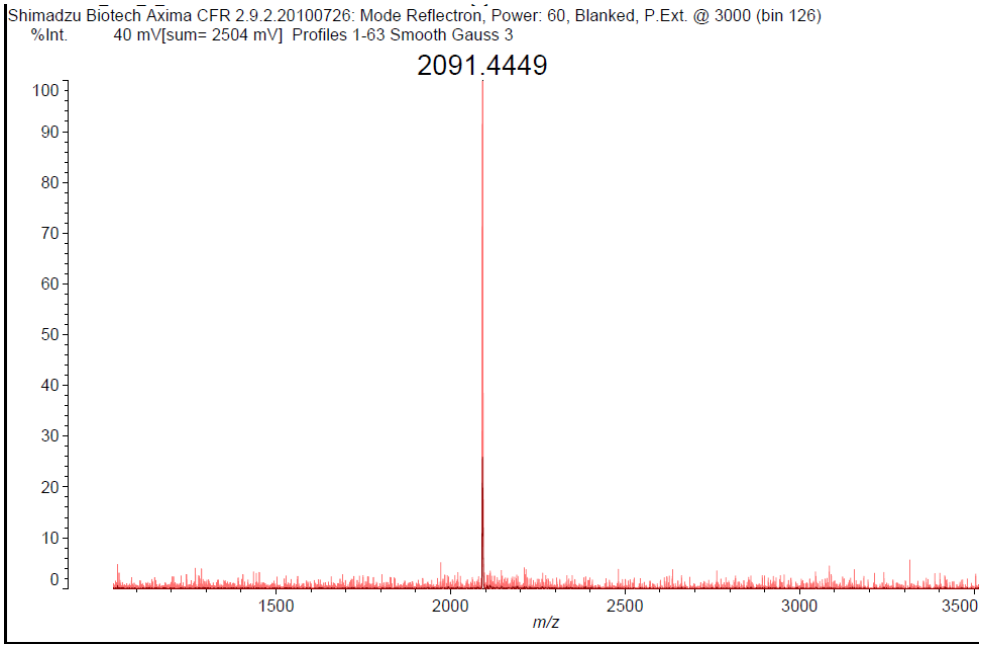

Figure 1.19: (Cont'd)

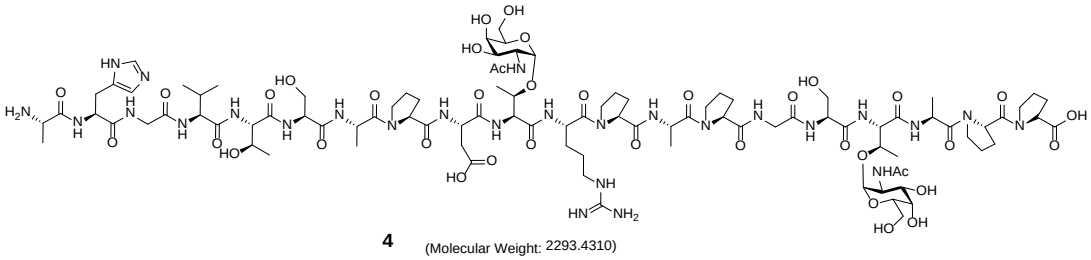

4 (Molecular Weight: 2293.4310)

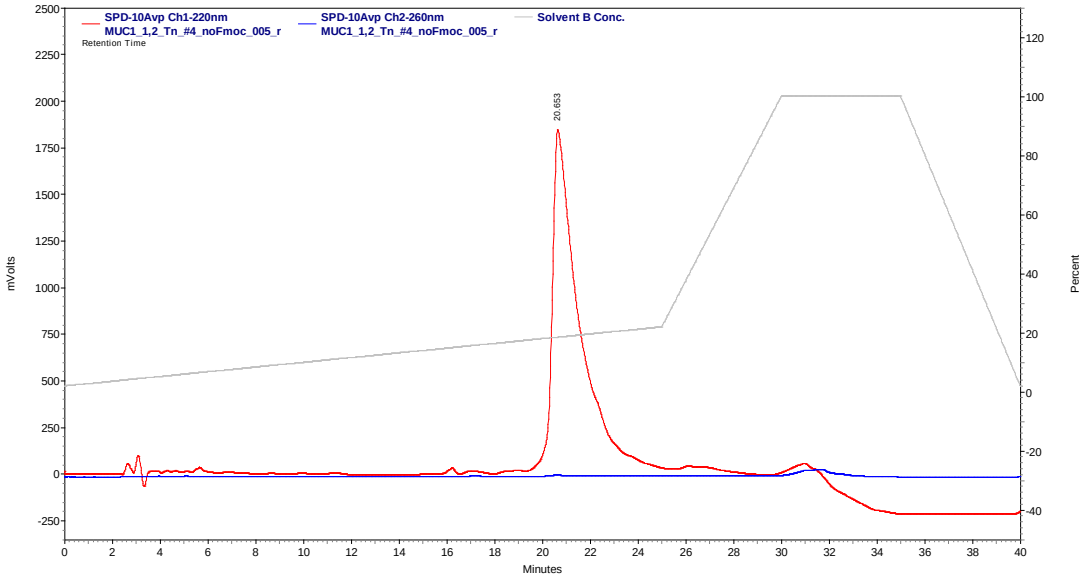

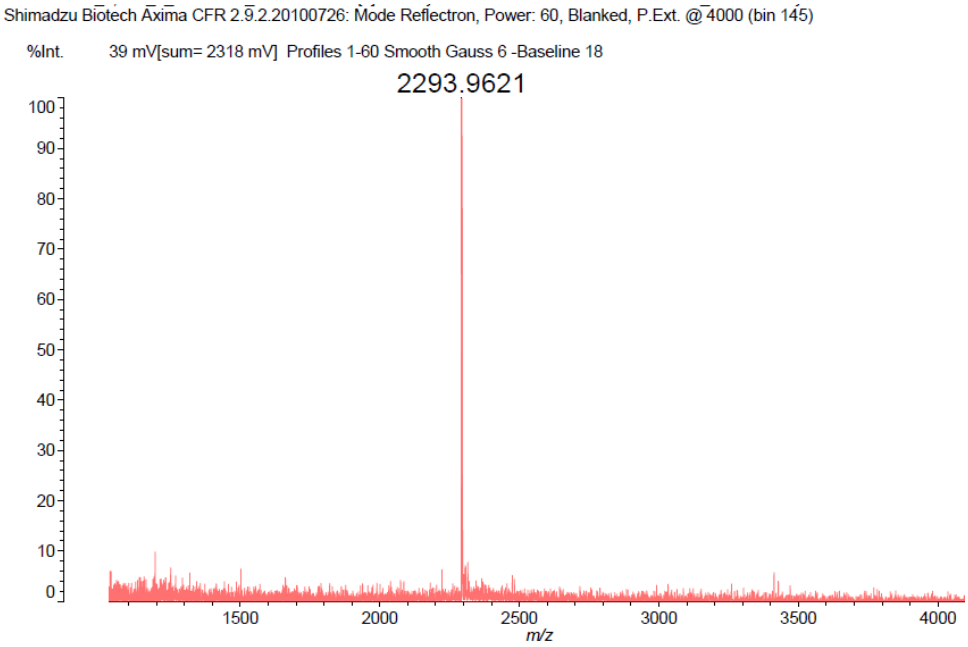

1.4.5 Synthesis of lipo-(Tn)-peptide (DPPE-MUC1 5 and DPPE-Tn-MUC1 6-8

The phospholipid was linked to succinic acid linker by reaction of DPPE with succinic anhydride and 2 eq. of Et_3N. The carboxylic acid group of the succinic linker was then activated by TSTU (*N,N,N′,N′*-tetramethyl-*O*-(*N*-succinimidyl)uranium tetrafluoroborate) to provide compound **DSPE-SUC-NHS**. The activated phospholipid was coupled to *N*-terminal of the purified (glyco)peptide **1-4**. The lipopeptide was purified by HPLC, using C_4-column (Kromasil; 5μm, 4.6x150 mm 5 μm; part # PSL847277), with gradient 30% isopropanol in H_2O (0.1% TFA) to 100% in 40 minutes.

1.4.6 Purification and characterization of lipo-(glyco)-peptide 5–8

5: HRMS: *m/z* calc. for $C_{121}H_{202}N_{26}O_{38}P$: 2660.0653; found:2661.2769 $[M+H]^+$.

6: HRMS: *m/z* calc. for $C_{129}H_{215}N_{27}O_{43}P$: 2863.2593; found:2864.1654 $[M+H]^+$.

7: HRMS: *m/z* calc. for $C_{129}H_{215}N_{27}O_{43}P$: 2863.2593; found:2864.2926 $[M+H]^+$.

8: HRMS: *m/z* calc. for $C_{137}H_{228}N_{28}O_{48}P$: 3066.4533; found:3067.2689 $[M+H]^+$.

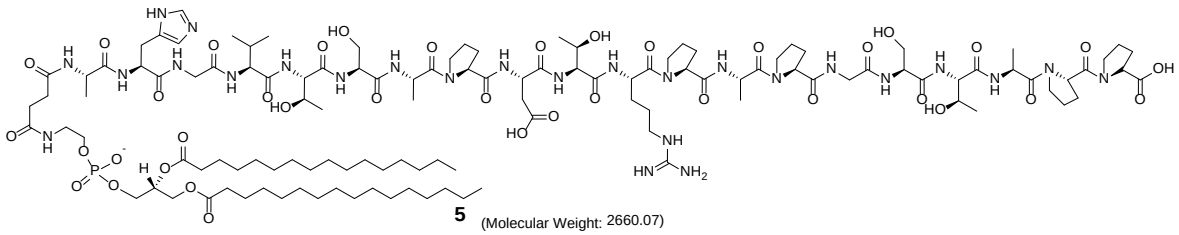

5 (Molecular Weight: 2660.07)

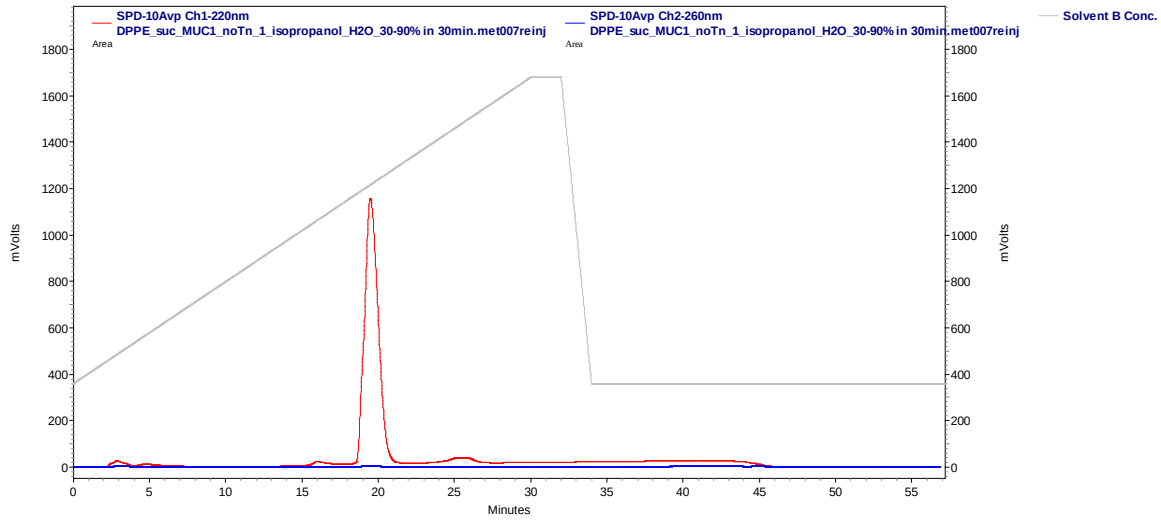

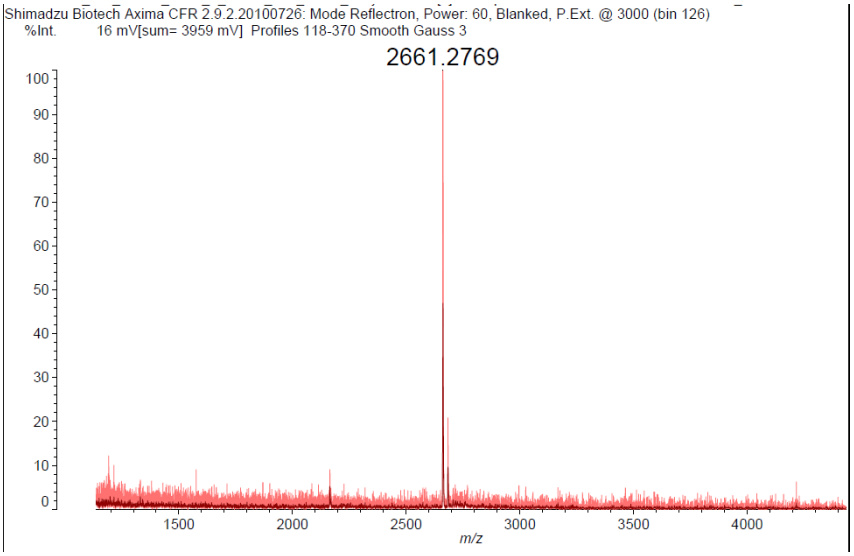

Figure 1.20: HPLC chromatogram and MALDI-TOF mass spectrum of the lipopeptide **5**, and lipo-glycopeptide **6**, **7** and **8**.

Figure 1.20: (Cont'd)

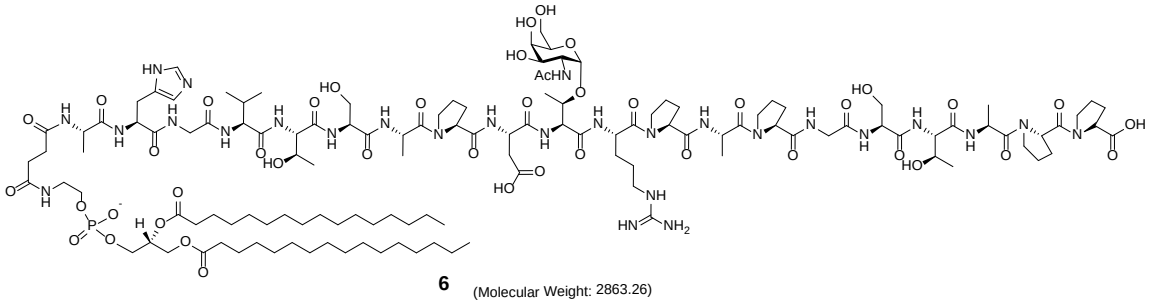

6 (Molecular Weight: 2863.26)

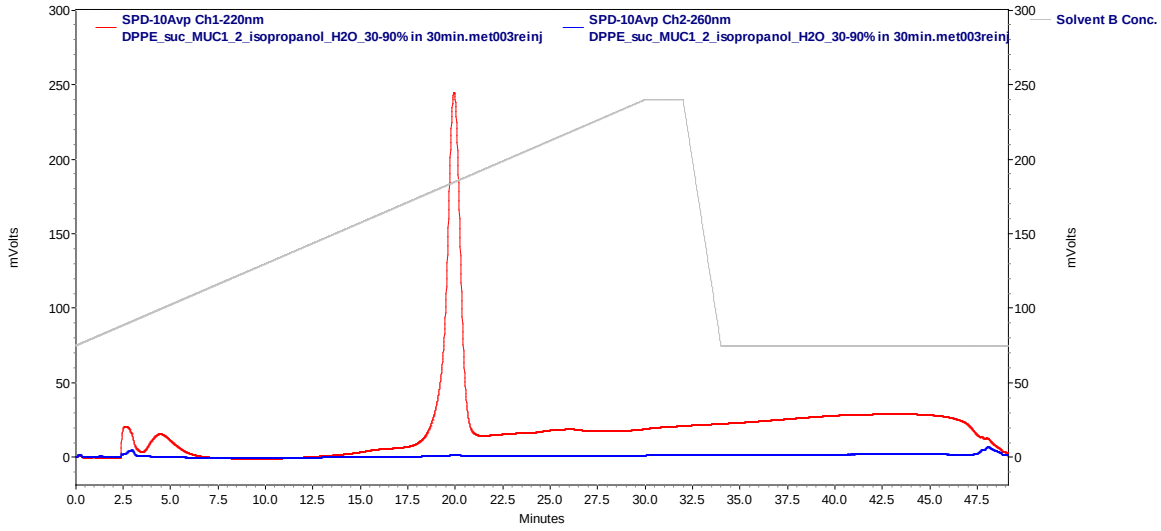

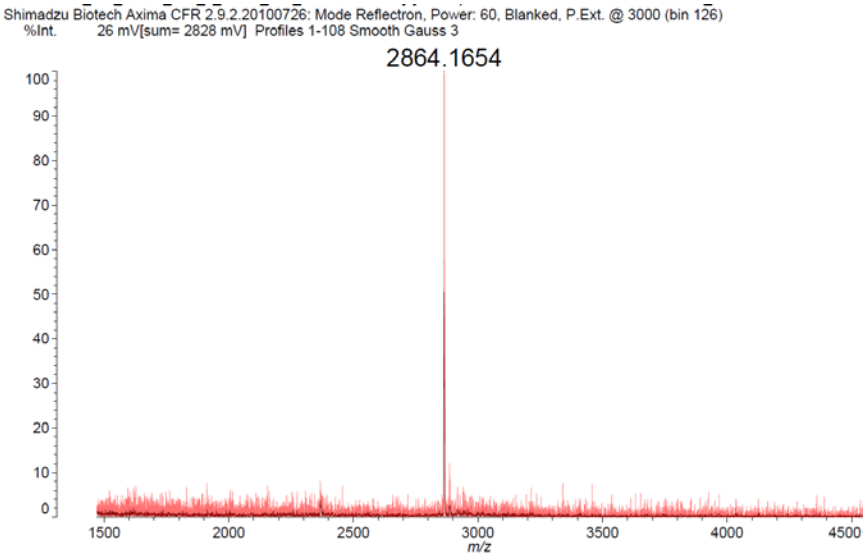

Figure 1.20: (Cont'd)

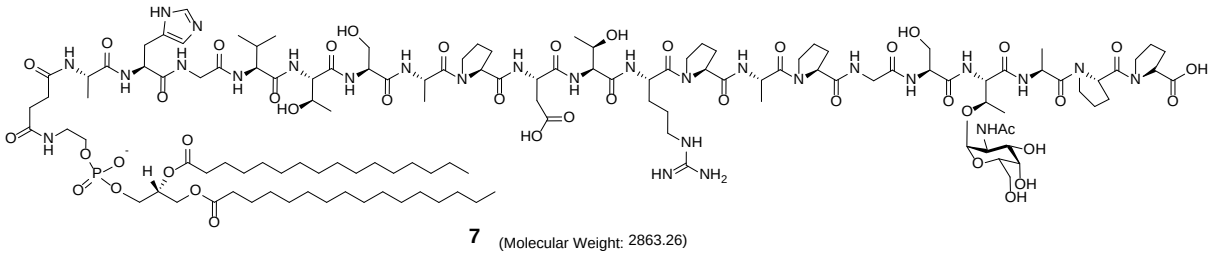

7 (Molecular Weight: 2863.26)

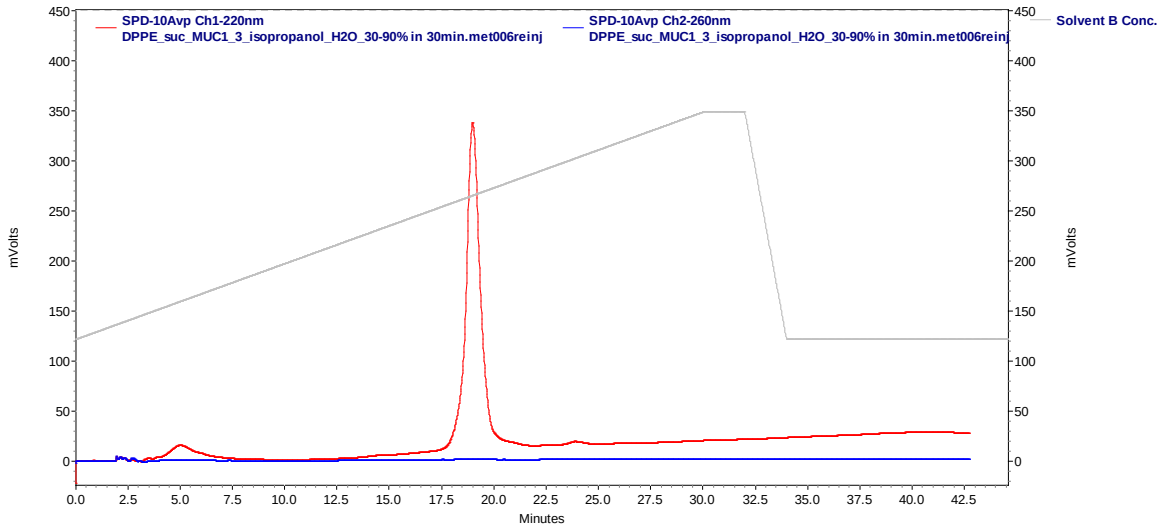

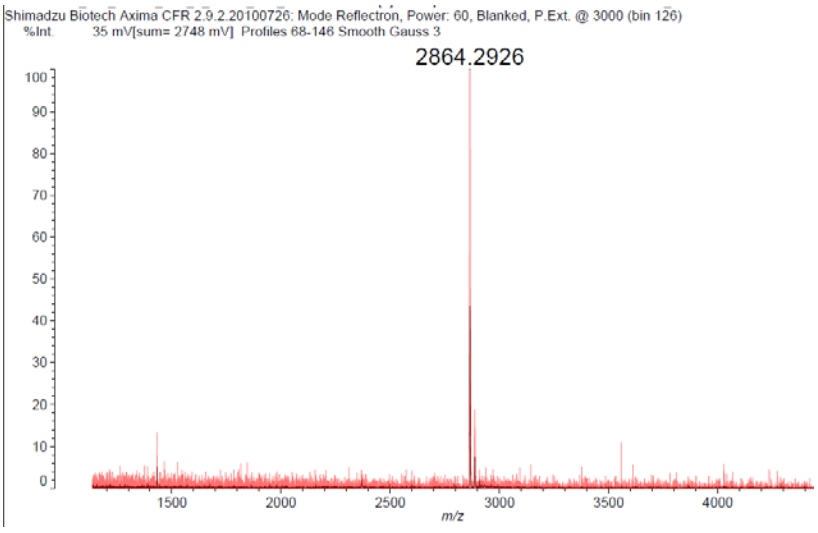

Figure 1.20: (Cont'd)

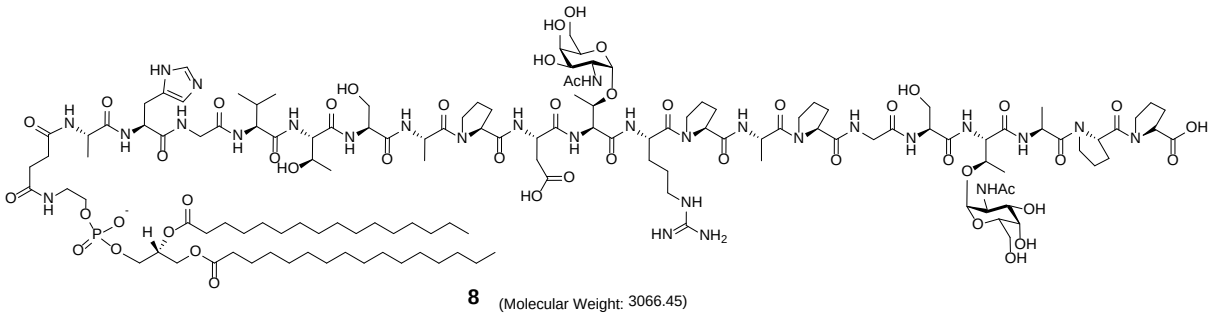

8 (Molecular Weight: 3066.45)

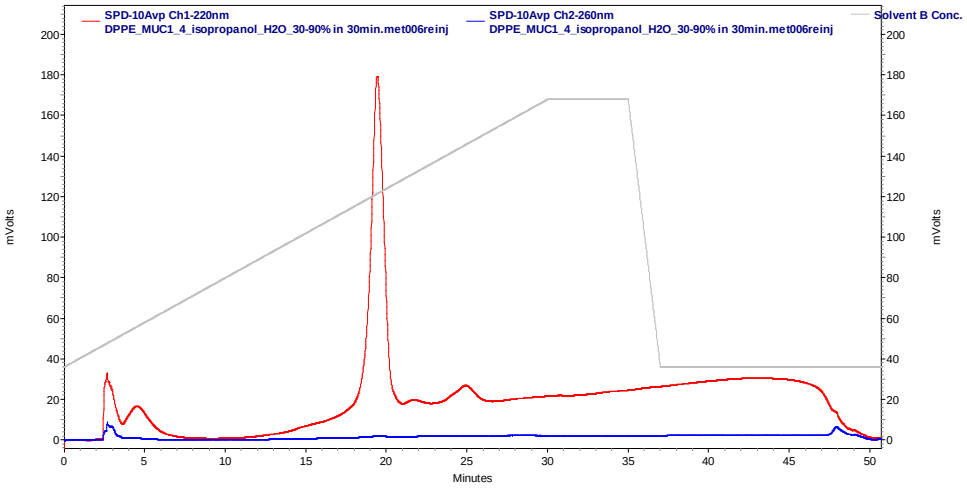

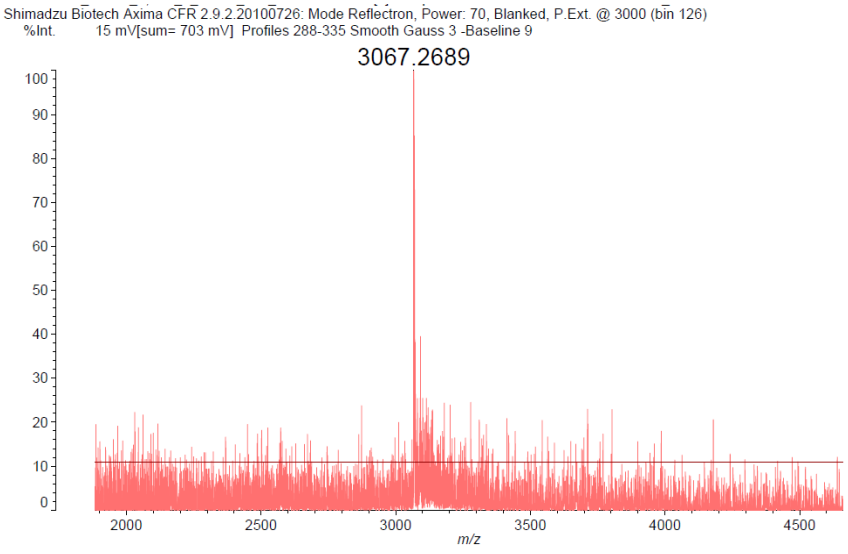

1.4.7 Preparation of iron oxide NPs (OA-IONPs)

A mixture of iron (III) acetylacetonate [$Fe(acac)_3$], 1,2-hexadecanediol, oleic acid, oleyl amine in benzyl ether were stirred under a flow of nitrogen. The mixture was heated to 200°C for 2 hours, followed by refluxing (300 °C) for 1 hour. The black mixture was allowed to cool down to room temperature, and the excess starting materials were washed out by adding ethanol into the mixture followed by external magnetic separation. The iron oxide NPs dispersed in toluene were centrifuged at 6,000 rpm to further remove the large particulates, and the supernatant containing **OA-IONPs** were collected (5 mg/mL).

1.4.8 The number of OA-IONP nanoparticle was estimated by TEM and TGA analysis.

The lattice volume of magnetite is 592 $Å^3$ and each lattice composes of 8 Fe_3O_4 molecules. The average diameter of OAIONP determined from TEM is 8.16 nm. Assuming the OAIONP is a sphere, the number of lattices in one OAIONP particle is 153 and each OAIONP particle contains 1,222 molecules of Fe_3O_4 (MW = 232). Therefore, 1 particle has the mass of 3.24×10^{-19} g. From thermogravimetric analysis (TGA) measurements, OAIONPs have 33.17 % weight change (Figure S6), implying that the metal core (Fe_3O_4) weight accounted for 66.8% of total weight. Therefore, on average, there are $(0.6683/3.24\times10^{-19}) = 2.06 \times 10^{18}$ particles in 1 g sample.

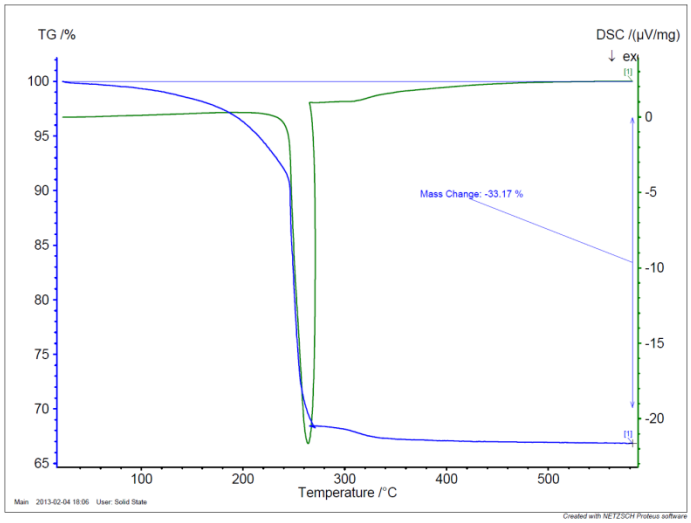

Figure 1.21: TGA curve of OA-IONP.

1.4.9 Preparation of NP5-9

The lipopolymer (DSPE-PEG, 2 mg) dispersed in 100 µl chloroform was mixed with **OA-IONPs** (1 mg), which were pre-dissolved in THF. The lipopeptide or lipoglycopeptide (1 mg) dissolved in DMSO (50 µl) was added into the mixture. DMSO (4 mL) was slowly added into the mixture while shaking. The incubated mixture was left sonicated for 30 min, then, all low boiling point solvents, chloroform and THF, were completely evaporated under vacuum for 2 hours. Water (20 mL) was slowly added into the vial while shaking. DMSO and excess starting materials were removed by centrifugal filter (100 kD cut off), and washed with water 5 times. The solution of NPs was finally filtered through 0.22 µm filter to remove any large particles. The NPs coated only with lipopolymer (NP-PEG, NP-9), used as a control, were synthesized by the same procedure. For NP-PEG-FITC used in dendritic cell uptake experiment, the NPs were coated with the same procedure as NP-PEG, but DSPE-PEG(2000)-NH_2 was used instead. The coated NPs was subsequently reacted with FITC in water. The excess FITC was washed

extensively by centrifugal filter (100 kD cut off). The FITC conjugated NPs were then re-suspended in PBS.

1.4.10 Verification of the glyco-lipopeptide (DSPE-MUC1(Tn) 6, 7 and 8 on the coated nanoparticles

The existence of glyco-lipopeptide on the coated nanoparticles was determined by MALDI-TOF.

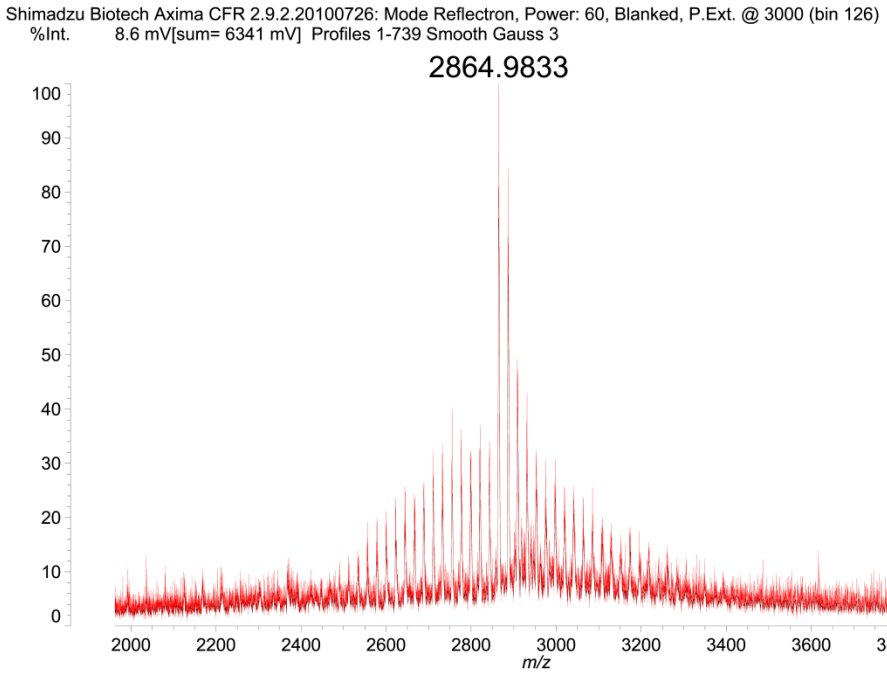

Figure 1.22: MALDI-TOF mass spectrum of glyco-lipopeptide coated OAIONP; **NP-6**, **NP-7**, **NP-8** indicate the present of the glyco-lipopeptide on each nanoparticle. The clustered peaks in the base line represent the coating DSPE-PEG.

Figure 1.22: (Cont'd)

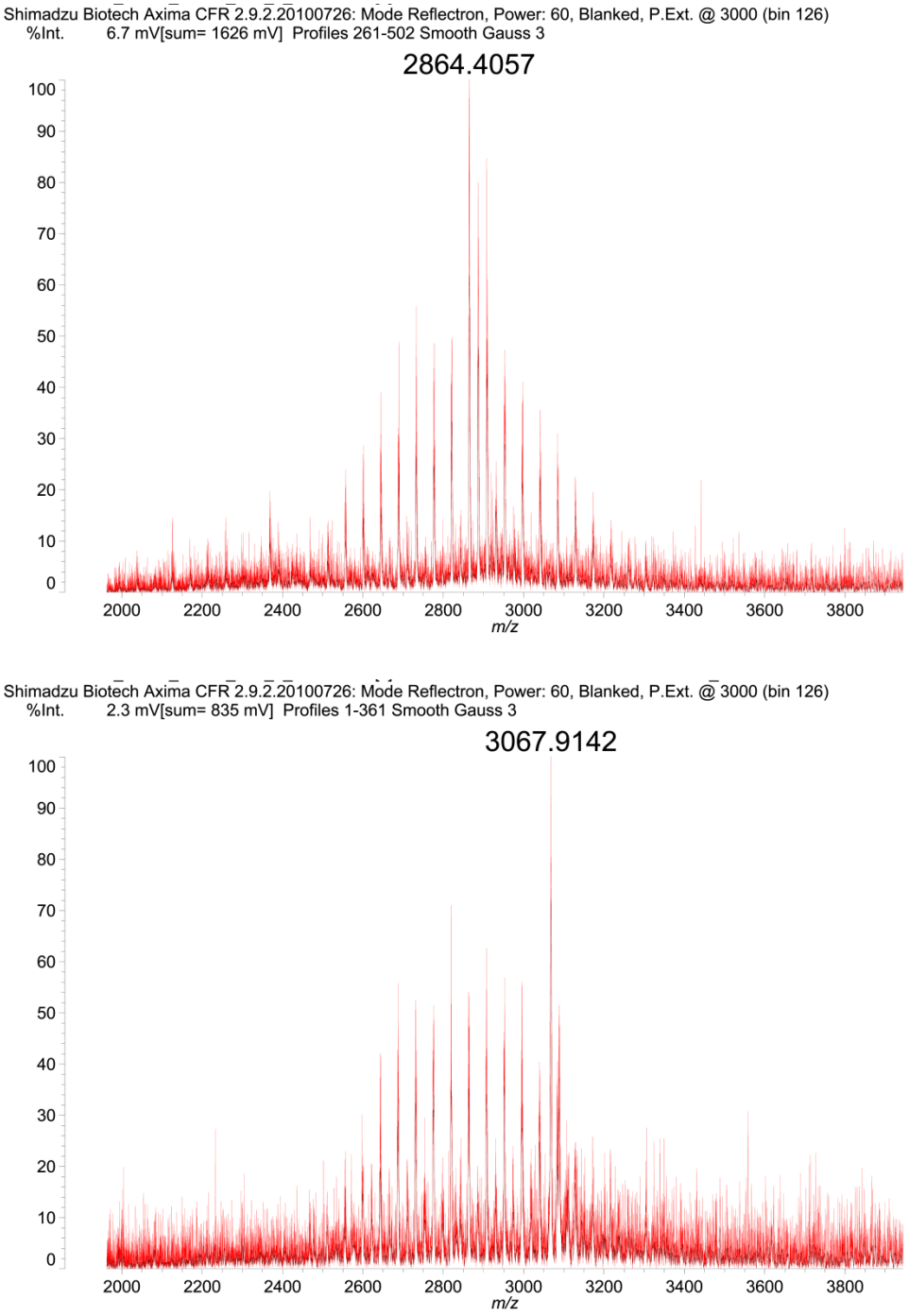

1.4.11 Quantification of the lipopeptide (DSPE-MUC1) on the coated nanoparticles

The quantification of lipopeptide on the nanoparticles was determined by the intensity of silver staining on SDS-PAGE from image analysis by ImageJ software. (Data are shown in APPENDIX A)

1.4.12 The ratio of DPPE-MUC1 and DSPE-PEG coated on each nanoparticle determined by Malachite Green phosphate assay

Since each of all coating materials is composed of a phosphate group, the amount of phosphate, determined by Malachite Green phosphate assay kit, could refer to the amount of the coating molecules. Malachite green phosphate detection kit (Sciencell Research Lab) was used to quantify the phosphate concentration in solution.[91] To prepare phosphate solution, 500 μg of nanoparticle sample was dissolved in 500 μL of 70% perchloric acid. The solution was heated at 160 °C for 20 minutes. 10M NaOH was added into the solution up to 2 mL to neutralize perchloric acid. The prepared solution was analyzed by the assay kit following the manufacturer instruction. It was determined that 1 g of nanoparticles have 0.2 mmol of phosphate. Since 1 g nanoparticles have 0.08 mmol of DPPE-MUC1 (determined by silver staining), the amount of DSPE-PEG on the nanoparticles was determined to be 0.12 mmol. Therefore, the estimated ratio of DPPE-MUC1 and DSPE-PEG coating on each nanoparticle was about 2:3.

1.4.13 Elemental analysis for estimation of the number of DPPE-MUC1 molecules coated on a single nanoparticle

Assuming that iron atom content in metal core of the nanoparticle is not changed after coating, the iron content of OAIONP after coating, analyzed by Inductively Coupled Plasma Analysis (ICP), was compared with that of uncoated nanoparticles, of which the number of particles had been determined by TGA analysis. The normalized iron content was calculated to estimate the number of nanoparticle after coating. The number of DSPE-MUC1 molecules

(estimated by SDS-PAGE method) divided by a number of iron oxide nanoparticles (estimated by ICP) gave the number of DPPE-MUC1 molecules coated on a single nanoparticle.

1.4.14 Bone marrow derived dendritic cell culture

Dendritic cells (DCs) were derived from bone marrow cells of C57BL/6 mice as described by Lutz.[115] Briefly, bone marrow was collected from the tibias and femurs. Red blood cells were depleted by ACK lysing buffer (Life Technologies). The bone marrow cells (2.5×10^6 cells) were collected and cultured in 100-mm Petri dishes containing RPMI 1640 medium (10 mL) supplemented with 10% heat-inactivated FBS, 50 μM 2-mercaptoethanol, 1% antibiotic-antimicotic, and 20 ng/mL mouse recombinant granulocyte-macrophage colony-stimulating factor (GM-CSF, Peprotech). After 9 days, non-adherent and loosely adherent cells (imDCs) were harvested, washed, and used for *in vitro* experiments. To determine the NP uptaken by dendritic cells, DCs were incubated with 50 μg/mL NP-PEG-FITC, MPLA 2 μg/mL in a 8-well plate culture at a density of 2×10^4 cells per well at 37 °C for 12 h. After washing, the cells were fixed with 4% paraformaldehyde for 20 min at room temperature. The fixed cells were observed under fluorescent microscope. The NP uptaken by dendritic cells was also confirmed by Prussian blue staining after incubation of DCs with **NP-9** (50 μg) with or without MPLA (2 μg/mL). (**Figure 1.13**)

1.4.15 Flow cytometry of dendritic cellular marker expression

After incubation of NP-PEG (50 μg) with 2 μg/mL MPLA, DCs were stained with allophycocyanin (APC)-conjugated anti-mouse CD11c monoclonal antibody for 30min on ice to label the cell membrane. After washing twice with FACs buffer (1% BSA + 0.1% NaN_3/PBS), DCs were further stained with R-phycoerythrin (PE)-conjugated anti-mouse CD40, or CD80, or CD86, or I-A^b monoclonal antibodies 30min on ice. The cells were washed again twice with

FACS buffer, re-suspended in FACS buffer, and detected with a LSR II instrument. Data analysis was done with Flowjo software. (All monoclonal antibodies in this experiment are from BD Pharmingen, San Diego, CA, USA)

1.4.16 Histology of the NPs in the targeted lymph node

8 week- C57BL/6 mice were injected subcutaneously under scruff with **NP-9** (500 μg) and MPLA (20 μg) in PBS (100 μl). Approximately 24 hour post-injection, the axillary and inguins lymph nodes were excised. The lymph nodes tissue was sent to Investigative HistoPathology Laboratory (Michigan State University, MI, USA) where histologic slides were prepared and analyzed by Prussian blue iron stain on a nuclear fast red background.

1.4.17 Mouse immunization

Pathogen-free female C57BL/6 mice age 7-9 weeks were obtained from breeding and cared for in the University Laboratory Animal Resources facility of Michigan State University. All animal care procedures and experimental protocols have been approved by the Institutional Animal Care and Use Committee (IACUC) of Michigan State University. Mice (5 mice each group) were immunized subcutaneously under scruff with NP or soluble vaccine in 100μl PBS on days 0, 14 and 28. Serum samples were collected on day 0 (before immunization) and day 35.

1.4.18 ELISA

A 96-well nunc microtiter plate was coated with 10 μg/mL, 100 μl/well of purified MUC1 or glyco MUC1 peptides in 0.05 M carbonate buffer (pH 9.6) and incubated at 4°C overnight. The plate was then washed four times with PBS/0.5% Tween-20 (PBST), followed by blocking with 1% (v/v) BSA in PBS at room temperature for 1 hour. Subsequently, the plates were washed four times with PBST. Then, the plates were incubated with 100 μl of diluted

mouse antisera in 0.1% BSA/PBS at 37°C for 2 hours, followed by washing four times with PBST. Bound antibodies were detected with 1:2000 diluted horseradish peroxidase (HRP) conjugated goat-anti-mouse IgG, or IgG1, or IgG2b, or IgG2c, or IgG3 at 37 °C for 1 hour, followed by washing four times with PBST. Then, plates were incubated with TMB substrate for 15 min. The reaction was stopped with 2M H_2SO_4 (50 µL), and the absorbances were measured at 450 nm using a microplate autoreader (BioRad). The titer was determined by regression analysis with log10 dilution plotted with optical density. The titer was calculated as the highest dilution that gave OD = 0.3.

1.4.19 Cell culture

MUC1-Ag104: a kind gift from Prof. Dapeng Zhou (University of Texas MD Anderson Cancer Center): culture medium: DMEM, 10% FBS, 100 U/mL/100 ug/mL Pen/Step (All from Sigma Aldrich); MCF-7: a kind gift from Prof. Olivera J. Finn (University of Pittsburgh) Eagle's minimum essential medium with L-glutamine (2 mM), non-essential amino acids and sodium pyruvate, bovine insulin (10 µg/mL), and FBS (10%), 100 U/mL/100 µg/mL Pen/Step. EA.hy926(Endothelial cell): culture medium: DMEM, 10% FBS, 100 U/mL/100 ug/mL Pen/Step (All from Sigma Aldrich)

1.4.20 Flow cytometry analysis

wt-Ag104, EA.hy926, MUC1-Ag104 or MCF-7 cells (3×10^5 cells) were incubated with 1/20 dilution antisera in PBS from different groups of immunized mice for 30 minutes on ice. The cells were washed twice with FACS buffer (1% BSA + 0.1% NaN_3/PBS) and incubated with a 1:50 diluted goat anti-mouse IgG labelled with FITC (BioLegend, 405305) for 30 min on ice. The cells were washed again twice with FACS buffer, re-suspended in FACS buffer, and detected with a LSR II instrument. Data analysis was performed with Flowjo software.

1.4.21 Complement dependent cytotoxicity

Complement dependent cytotoxicity on MUC1-Ag104 and MCF-7 tumor cells was determined by MTS assay. MUC1-Ag104 or MCF-7 7000 cells/well were incubated on ice with 1/20 dilution in 100μl PBS of antisera from different groups of immunized mice. After removing the unbound antisera through washing, rabbit sera 1/5 dilution in 100 μl culture medium were added, then incubated at 37°C for 8 hours. MTS (CellTiter 96® AQueous One Solution Cell Proliferation Assay; Promega, 20 μl) was added into each well and further incubated at 37°C for 4 hours. The optical absorption of the MTS assay was measured at 490nm. Only cells cultured in medium were used as positive control (maximum OD) and culture medium as a negative control (minimum OD). All data were done in four repeats. The cytotoxicity were calculated by the formula: cytotoxicity (%) = (OD positive control – OD experimental)/(OD positive control – OD negative control) x 100.

APPENDICES

APPENDIX A

Quantification of the lipopeptide (DSPE-MUC1) on the coated nanoparticles

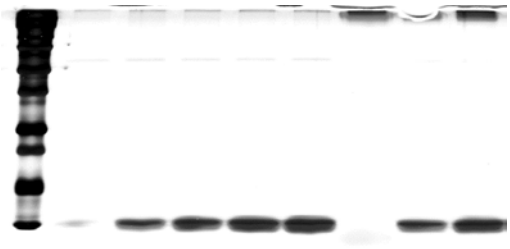

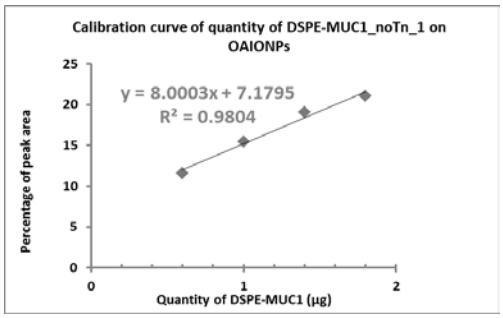

Lane	sample	load (µL)	quantity (µg)	peak area	percent	**5** µg/µL
2	**5** (0.1g/L)	2	0.2	1331.184	1.008	
3	**5** (0.1g/L)	6	0.6	15279.246	11.57	
4	**5** (0.1g/L)	10	1	20401.439	15.448	
5	**5** (0.1g/L)	14	1.4	25187.095	19.072	
6	**5** (0.1g/L)	18	1.8	27770.924	21.029	
7	NP-9	18	-	-	-	
8	NP-5	4	0.72	17062.489	12.92	0.18
9	NP-5	8	1.47	25030.217	18.953	0.18

Figure 1.23: Quantification of the lipo(glyco)peptide on the coated nanoparticles.

Figure 1.23: (Cont'd)

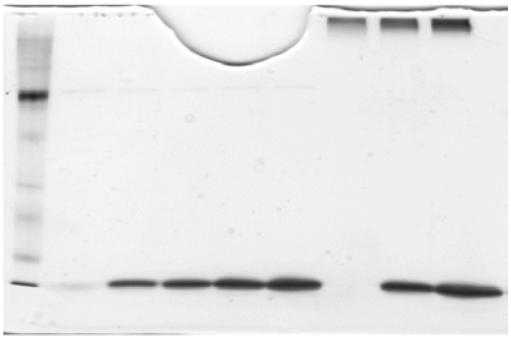

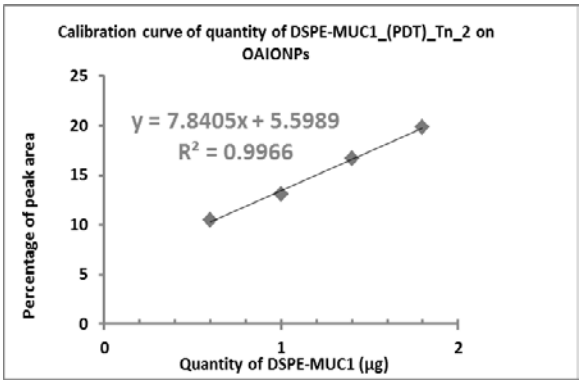

Lane	sample	load (µL)	Quantity (µg)	peak area	percent	**6** µg/µL	**6** µg/µL(Avg)
2	**6** (0.1g/L)	2	0.2	1727.205	1.713		
3	**6** (0.1g/L)	6	0.6	10593.903	10.506		
4	**6** (0.1g/L)	10	1	13205.974	13.097		
5	**6** (0.1g/L)	14	1.4	16790.823	16.652		
6	**6** (0.1g/L)	18	1.8	19940.087	19.775		
7	NP-9	18	-	-	-		
8	NP-6	4	1.42	16889.409	16.749	0.36	0.30
9	NP-6	8	2.03	21688.258	21.509	0.25	

Figure 1.23: (Cont'd)

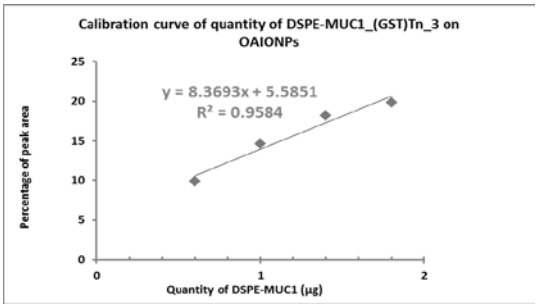

Lane	sample	load (µL)	Quantity (µg)	peak area	percent	**7** µg/µL	**7** µg/µL (Avg)
2	**7** (0.1g/L)	2	0.2	602.335	0.841		
3	**7** (0.1g/L)	6	0.6	7075.205	9.881		
4	**7** (0.1g/L)	10	1	10443.861	14.586		
5	**7** (0.1g/L)	14	1.4	13043.518	18.216		
6	**7** (0.1g/L)	18	1.8	14198.589	19.83		
7	NP-9	18	-	-	-		
8	NP-7	2	1.26	11530.811	16.104	0.63	0.54
9	NP-7	4	1.79	14708.882	20.542	0.45	

Figure 1.23: (Cont'd)

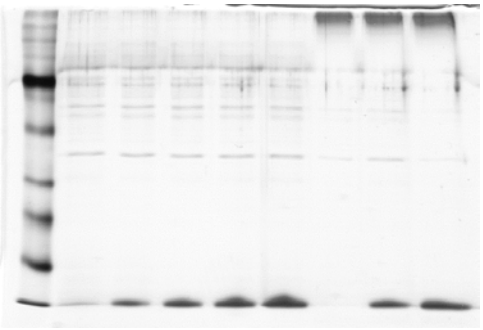

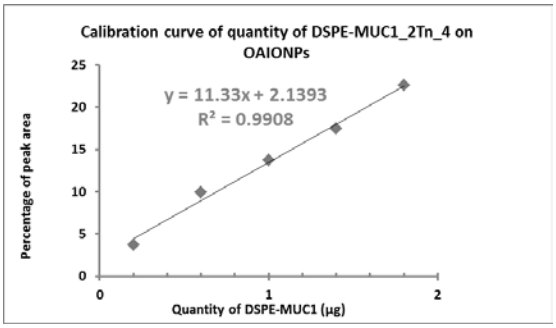

Lane	sample	load (µL)	Quantity (µg)	peak area	percent	8 µg/µL	8 µg/µL (Avg)
2	8 (0.1g/L)	2	0.2	2762.033	3.685		
3	8 (0.1g/L)	6	0.6	7449.004	9.939		
4	8 (0.1g/L)	10	1	10266.075	13.697		
5	8 (0.1g/L)	14	1.4	13059.146	17.424		
6	8 (0.1g/L)	18	1.8	16940.995	22.603		
7	NP-9	18	-	-	-		
8	NP-8	2	1.00	10066.953	13.432	0.50	0.44
9	NP-8	4	1.51	14405.903	19.221	0.38	

APPENDIX B

NMR spectra

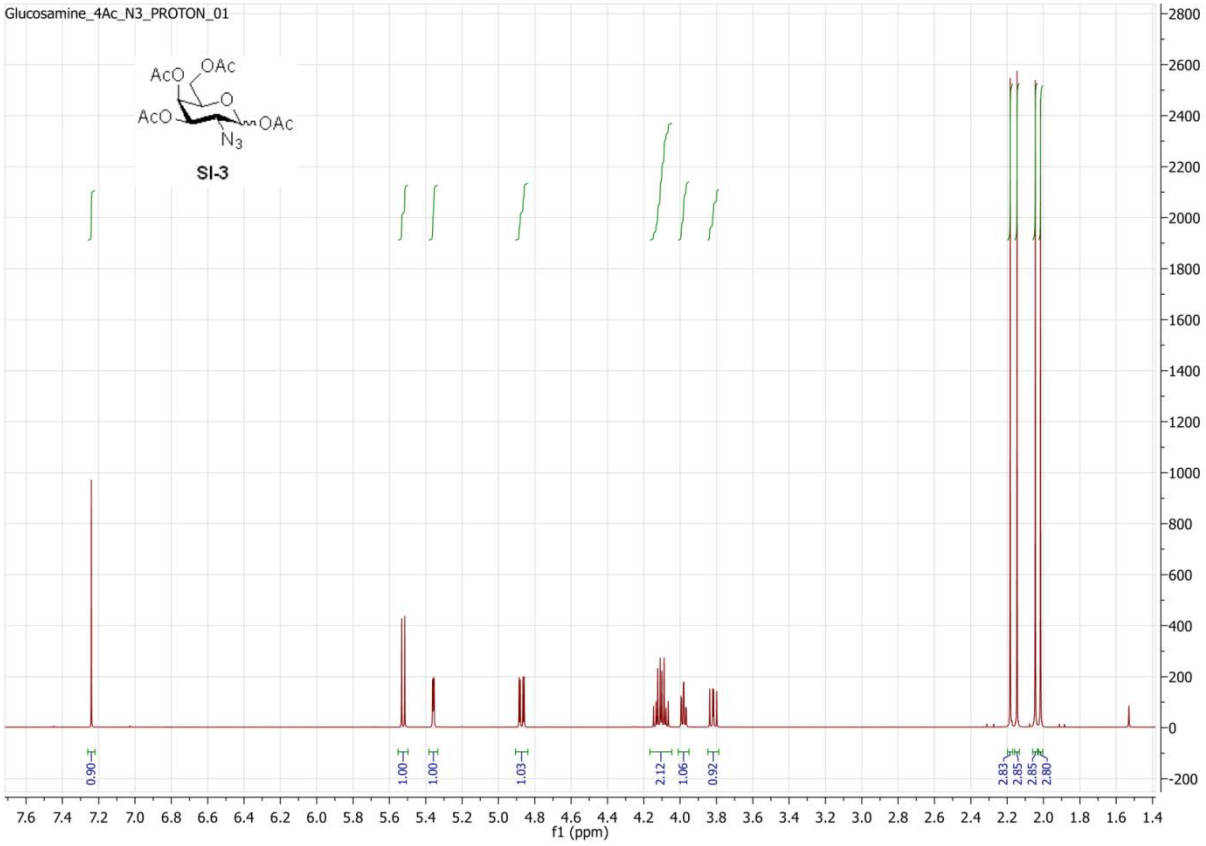

Figure 1.24: ^{1}H NMR spectrum of **SI-3**.

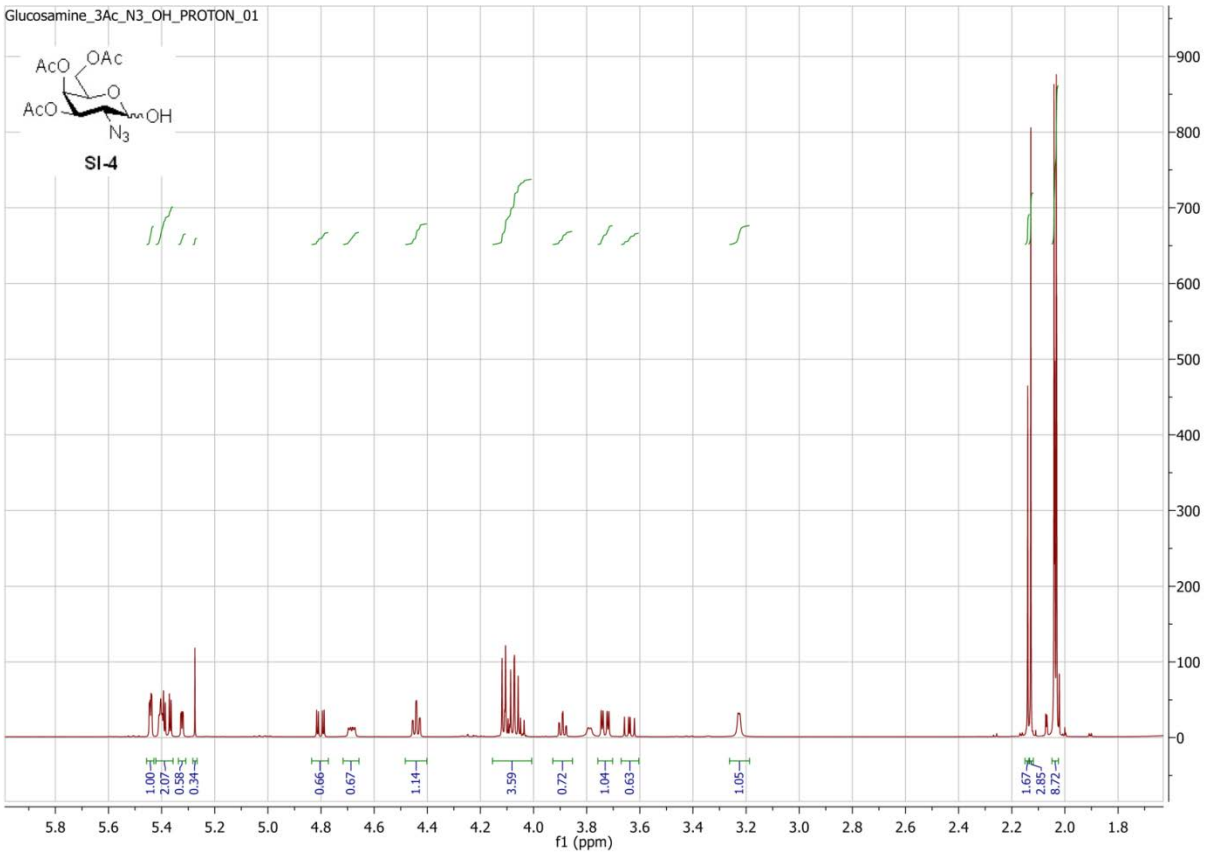

Figure 1:25: ^{1}H NMR spectrum of **SI-4**.

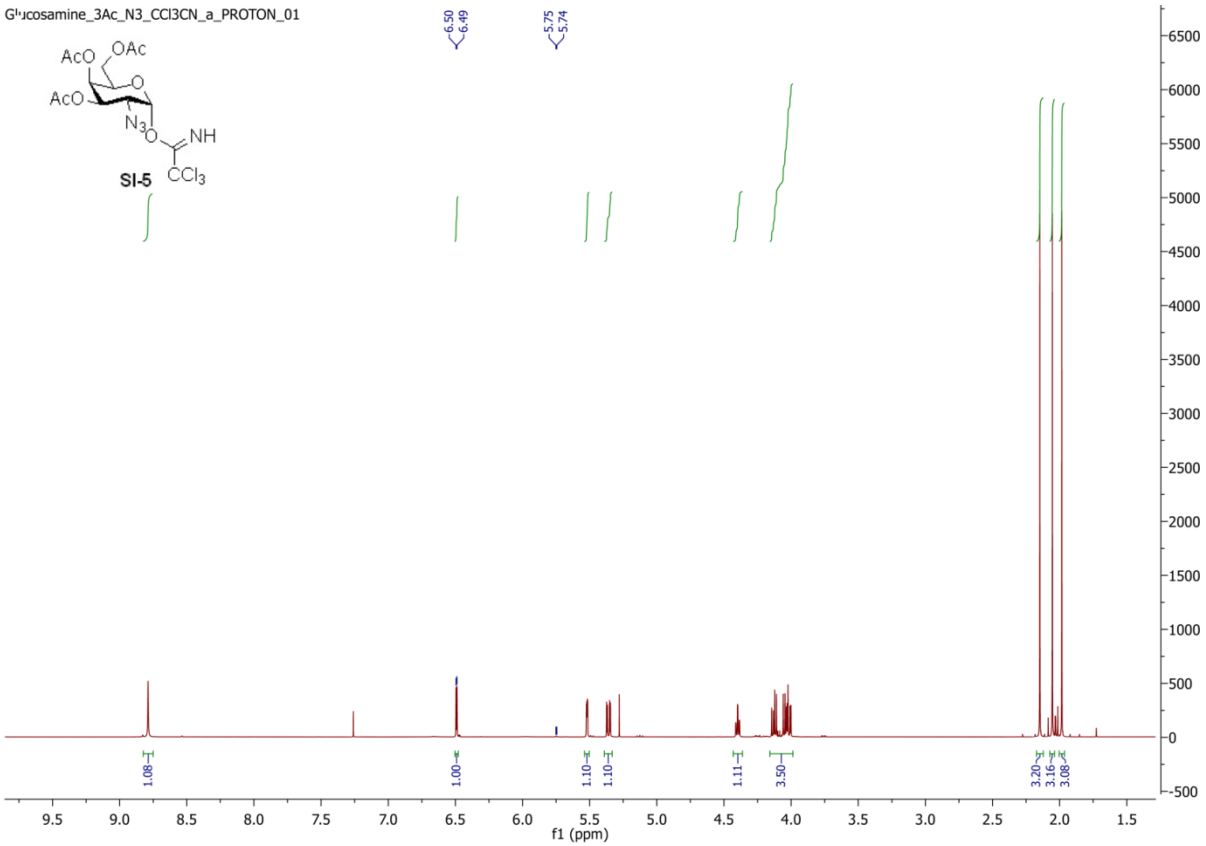

Figure 1.26: ^{1}H NMR spectrum of **SI-5**.

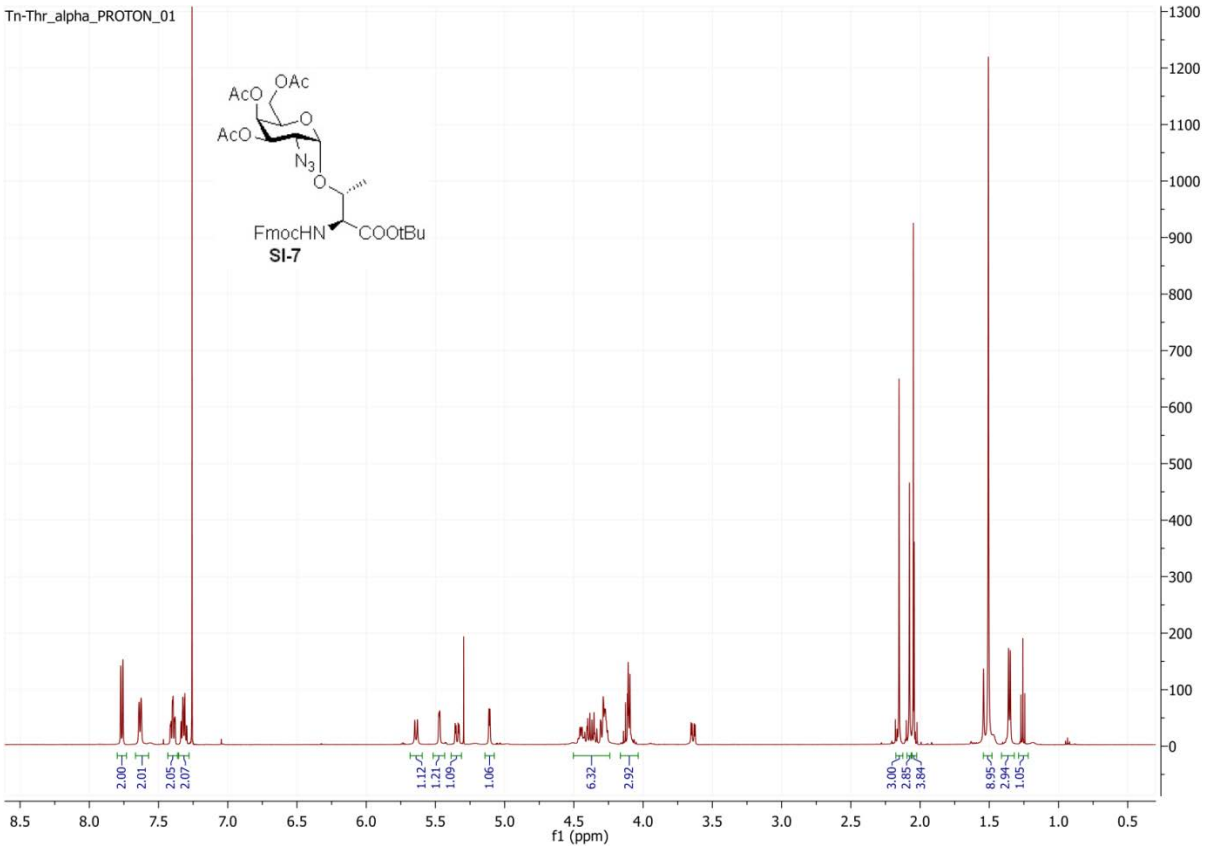

Figure 1.27: ^{1}H NMR spectrum of **SI-7**.

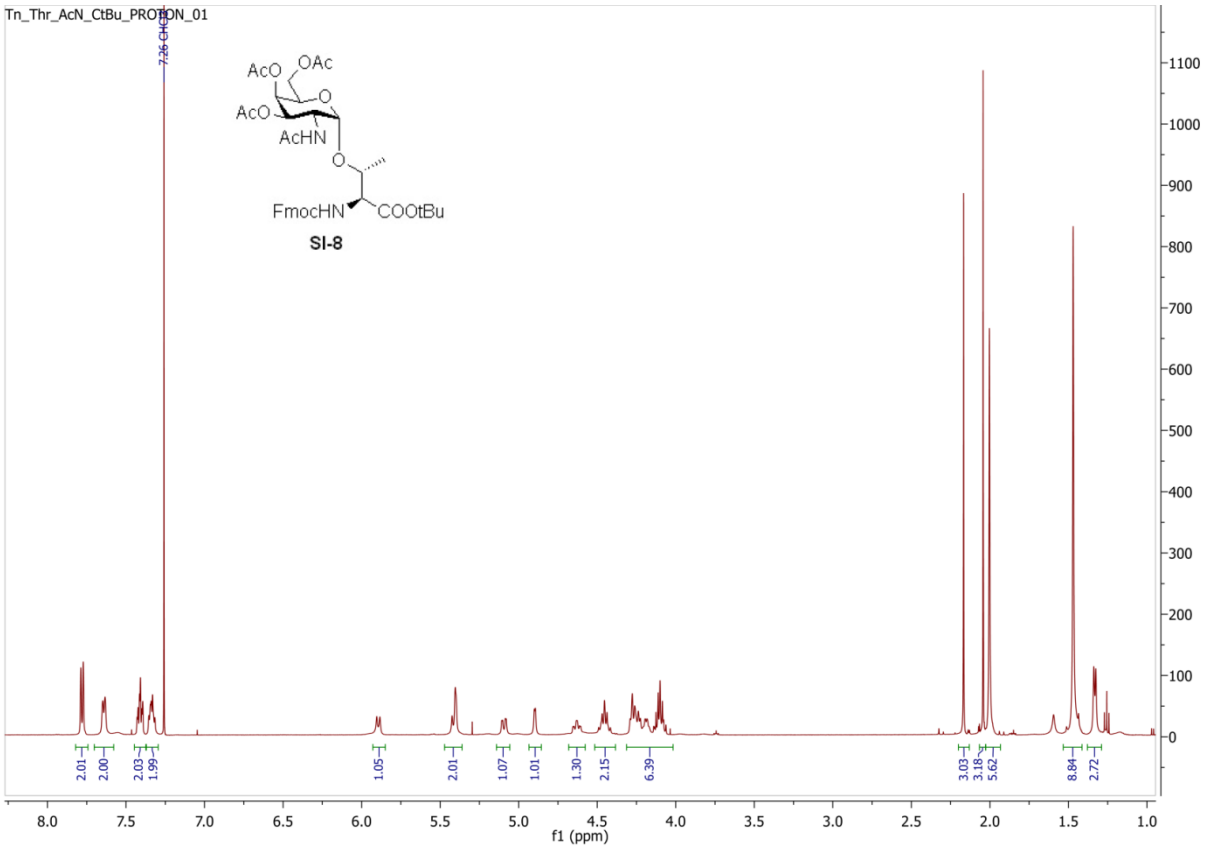

Figure 1.28: ^{1}H NMR spectrum of **SI-8**.

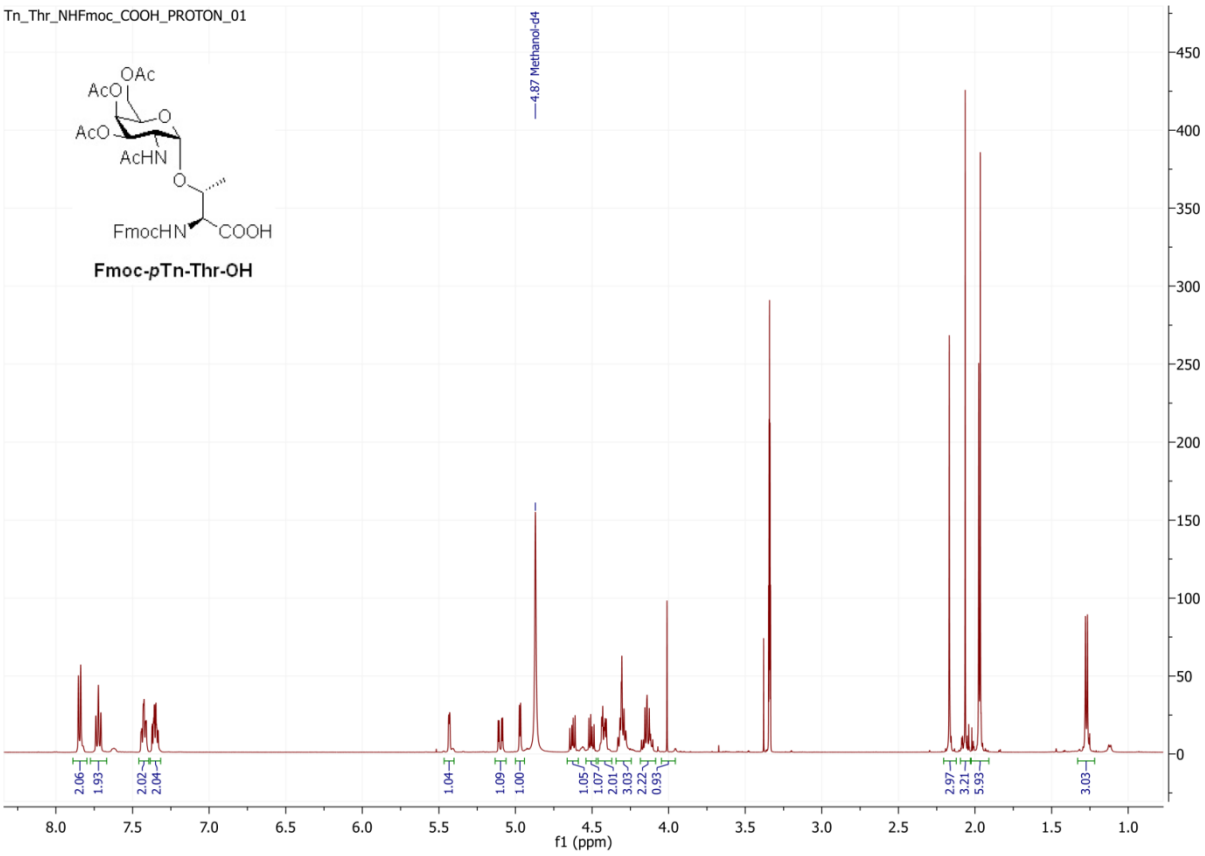

Figure 1.29: ^{1}H NMR spectrum of **Fmoc-*p*Tn-Thr-OH**.

REFERENCES

REFERENCES

1. Sungsuwan, S.; Yin, Z.; Huang, X., Lipopeptide-coated iron oxide nanoparticles as potential glycoconjugate-based synthetic anticancer vaccines. *ACS Applied Materials & Interfaces* **2015,** *7* (31), 17535-17544.

2. Heron, M., Deaths: Leading causes for 2014. *National Vital Statistics Reports* **2016,** *65* (5), 1.

3. McGuire, S., World cancer report 2014. Geneva, Switzerland: World Health Organization, International Agency for Research on Cancer, WHO Press, 2015. *Advance in Nutrition* **2016,** *7* (2), 418-9.

4. Grodzinski, P., Themed issue on cancer nanotechnology. *Integrative Biology : Quantitative Biosciences from Nano to Macro* **2012,** *5* (1), 17-18.

5. Hamidreza, B.; Jagdish, R.; Kevin, L., Minimizing metastatic risk in radiotherapy fractionation schedules. *Physics in Medicine and Biology* **2015,** *60* (22), N405.

6. Apostolopoulos, V.; Weiner, D.; Gong, J., Cancer vaccines: methods for inducing immunity. *Expert Review of Vaccines* **2008,** *7* (7), 861-862.

7. Gresser, I., A. Chekhov, M.D., and Coley's Toxins. *New England Journal of Medicine* **1987,** *317* (7), 457-457.

8. Nauts, H. C., Bacteria and cancer--antagonisms and benefits. *Cancer Surveys* **1989,** *8* (4), 713-23.

9. (a) Drake, C. G.; Lipson, E. J.; Brahmer, J. R., Breathing new life into immunotherapy: review of melanoma, lung and kidney cancer. *Nature Review Clinical Oncology* **2014,** *11* (1), 24-37; (b) Melero, I.; Gaudernack, G.; Gerritsen, W.; Huber, C.; Parmiani, G.; Scholl, S.; Thatcher, N.; Wagstaff, J.; Zielinski, C.; Faulkner, I.; Mellstedt, H., Therapeutic vaccines for cancer: an overview of clinical trials. *Nature Review Clinical Oncology* **2014,** *11* (9), 509-524; (c) Hamid , O.; Robert , C.; Daud , A.; Hodi , F. S.; Hwu , W.-J.; Kefford , R.; Wolchok , J. D.; Hersey , P.; Joseph , R. W.; Weber , J. S.; Dronca , R.; Gangadhar , T. C.; Patnaik , A.; Zarour , H.; Joshua , A. M.; Gergich , K.; Elassaiss-Schaap , J.; Algazi , A.; Mateus , C.; Boasberg , P.; Tumeh , P. C.; Chmielowski , B.; Ebbinghaus , S. W.; Li , X. N.; Kang , S. P.; Ribas , A., Safety and tumor responses with Lambrolizumab (Anti–PD-1) in melanoma. *New England Journal of Medicine* **2013,** *369* (2), 134-144; (d) Wolchok , J. D.; Kluger , H.; Callahan , M. K.; Postow , M. A.; Rizvi , N. A.; Lesokhin , A. M.; Segal , N. H.; Ariyan , C. E.; Gordon , R.-A.; Reed , K.; Burke , M. M.; Caldwell , A.; Kronenberg , S. A.; Agunwamba , B. U.; Zhang , X.; Lowy , I.; Inzunza , H. D.; Feely , W.; Horak , C. E.; Hong , Q.; Korman , A. J.; Wigginton , J. M.; Gupta , A.; Sznol , M., Nivolumab plus Ipilimumab in advanced melanoma. *New England Journal of Medicine* **2013,** *369* (2), 122-133; (e) Reck, M.; Rodríguez-Abreu, D.; Robinson, A.

G.; Hui, R.; Csőszi, T.; Fülöp, A.; Gottfried, M.; Peled, N.; Tafreshi, A.; Cuffe, S.; O'Brien, M.; Rao, S.; Hotta, K.; Leiby, M. A.; Lubiniecki, G. M.; Shentu, Y.; Rangwala, R.; Brahmer, J. R., Pembrolizumab versus chemotherapy for PD-L1–positive non–small-cell lung cancer. *New England Journal of Medicine* **2016,** *375* (19), 1823-1833.

10. McNutt, M., Cancer immunotherapy. *Science* **2013,** *342* (6165), 1417-1417.

11. DeFranco, A., B-cell activation 2000. *Immunological Reviews* **2000,** *176*, 5-9.

12. Stavnezer, J., Immunoglobulin class switching. *Current Opinion in Immunology* **1996,** *8* (2), 199-205.

13. Buskas, T.; Thompson, P.; Boons, G.-J., Immunotherapy for cancer: synthetic carbohydrate-based vaccines. *Chemical Communications* **2009,** (36), 5335-5349.

14. Loureiro, L.; Carrascal, M.; Barbas, A.; Ramalho, J.; Novo, C.; Delannoy, P.; Videira, P., Challenges in antibody development against Tn and Sialyl-Tn antigens. *Biomolecules* **2015,** *5* (3), 1783.

15. Palucka, K.; Banchereau, J., Cancer immunotherapy via dendritic cells. *Nature Reviews. Cancer* **2012,** *12* (4), 265-277.

16. Kim, J.; Mooney, D., *In vivo* modulation of dendritic cells by engineered materials: Towards new cancer vaccines. *Nano Today* **2011,** *6* (5), 466-477.

17. Wolfert, M. A.; Boons, G.-J., Adaptive immune activation: glycosylation does matter. *Nature Chemical Biology* **2013,** *9* (12), 776-784.

18. Kessler, J. H.; Melief, C. J. M., Identification of T-cell epitopes for cancer immunotherapy. *Leukemia* **2007,** *21* (9), 1859-1874.

19. (a) Karve, T. M.; Cheema, A. K., Small changes huge impact: The role of protein posttranslational modifications in cellular homeostasis and disease. *Journal of Amino Acids* **2011,** *2011*; (b) Wang, Y.-C.; Peterson, S. E.; Loring, J. F., Protein post-translational modifications and regulation of pluripotency in human stem cells. *Cell Research* **2014,** *24* (2), 143-160.

20. (a) Bramwell, M. E.; Wiseman, G.; Shotton, D. M., Electron-microscopic studies of the CA antigen, epitectin. *Journal of Cell Science* **1986,** *86* (1), 249-261; (b) Hilkens, J.; Ligtenberg, M. J. L.; Vos, H. L.; Litvinov, S. V., Cell membrane-associated mucins and their adhesion-modulating property. *Trends in Biochemical Sciences 17* (9), 359-363.

21. Singh, R.; Bandyopadhyay, D., MUC1: a target molecule for cancer therapy. *Cancer Biology & Therapy* **2007,** *6* (4), 481-6.

22. Tang, C.-K.; Apostolopoulos, V., Strategies used for MUC1 immunotherapy: preclinical studies. *Expert Review of Vaccines* **2008,** *7* (7), 951-962 and references cited therein.

23. Richardson, P. J.; Macmillan, D., Mucin-based vaccines. In *Glycoscience: Chemistry and Chemical Biology*, Fraser-Reid, B. O.; Tatsuta, K.; Thiem, J., Eds. Springer Berlin Heidelberg: Berlin, Heidelberg, 2008; pp 2645-2698.

24. (a) Singh, P. K.; Hollingsworth, M. A., Cell surface-associated mucins in signal transduction. *Trends in Cell Biology* **2006,** *16* (9), 467-476; (b) Hollingsworth, M. A.; Swanson, B. J., Mucins in cancer: protection and control of the cell surface. *Nature Reviews: Cancer* **2004,** *4* (1), 45-60.

25. Kufe, D. W., MUC1-C oncoprotein as a target in breast cancer: activation of signaling pathways and therapeutic approaches. *Oncogene* **2013,** *32* (9), 1073-1081.

26. Hanisch, F.-G.; Müller, S., MUC1: the polymorphic appearance of a human mucin. *Glycobiology* **2000,** *10* (5), 439-449.

27. Kufe, D., Mucins in cancer: function, prognosis and therapy. *Nature Reviews. Cancer* **2009,** *9* (12), 874-885.

28. von Mensdorff-Pouilly, S.; Petrakou, E.; Kenemans, P.; van Uffelen, K.; Verstraeten, A. A.; Snijdewint, F. G. M.; van Kamp, G. J.; Schol, D. J.; Reis, C. A.; Price, M. R.; Livingston, P. O.; Hilgers, J., Reactivity of natural and induced human antibodies to MUC1 mucin with MUC1 peptides and N-acetylgalactosamine (GalNAc) peptides. *International Journal of Cancer* **2000,** *86* (5), 702-712.

29. Blixt, O.; Bueti, D.; Burford, B.; Allen, D.; Julien, S.; Hollingsworth, M.; Gammerman, A.; Fentiman, I.; Taylor-Papadimitriou, J.; Burchell, J. M., Autoantibodies to aberrantly glycosylated MUC1 in early stage breast cancer are associated with a better prognosis. *Breast Cancer Research* **2011,** *13* (2), 1-16.

30. Engelmann, K.; Baldus, S. E.; Hanisch, F.-G., Identification and topology of variant sequences within individual repeat domains of the human epithelial tumor mucin MUC1. *Journal of Biological Chemistry* **2001,** *276* (30), 27764-27769.

31. Fontenot, J. D.; Tjandra, N.; Bu, D.; Ho, C.; Montelaro, R. C.; Finn, O. J., Biophysical characterization of one-, two-, and three-tandem repeats of human mucin (MUC-1) protein core. *Cancer Research* **1993,** *53* (22), 5386-5394.

32. MacLean, G. D.; Bowen-Yacyshyn, M. B.; Samuel, J.; Meikle, A.; Stuart, G.; Nation, J.; Poppema, S.; Jerry, M.; Koganty, R.; Wong, T.; et al., Active immunization of human ovarian cancer patients against a common carcinoma (Thomsen-Friedenreich) determinant using a synthetic carbohydrate antigen. *Journal of Immunotherapy (1991)* **1992,** *11* (4), 292-305.

33. Tang, C.-K.; Katsara, M.; Apostolopoulos, V., Strategies used for MUC1 immunotherapy: human clinical studies. *Expert Review of Vaccines* **2008,** *7* (7), 963-975.

34. (a) Ju, T.; Lanneau, G. S.; Gautam, T.; Wang, Y.; Xia, B.; Stowell, S. R.; Willard, M. T.; Wang, W.; Xia, J. Y.; Zuna, R. E.; Laszik, Z.; Benbrook, D. M.; Hanigan, M. H.; Cummings, R. D., Human tumor antigens Tn and Sialyl Tn arise from mutations in Cosmc. *Cancer Research* **2008,** *68* (6), 1636-1646; (b) Ju, T.; Otto, V. I.; Cummings, R. D., The Tn antigen—structural simplicity and biological complexity. *Angewandte Chemie International Edition* **2011,** *50* (8), 1770-1791; (c) Ju, T.; Aryal, R. P.; Kudelka, M. R.; Wang, Y.; Cummings, R. D., The Cosmc connection to the Tn antigen in cancer. *Cancer Biomark* **2014,** *14* (1), 63-81.

35. Ju, T.; Cummings, R., A unique molecular chaperone Cosmc required for activity of the mammalian core 1 beta 3-galactosyltransferase. *Proceedings of the National Academy of Sciences of the United States of America* **2002,** *99* (26), 16613-16618.

36. Hull, S.; Bright, A.; Carraway, K.; Abe, M.; Hayes, D.; Kufe, D., Oligosaccharide differences in the DF3 sialomucin antigen from normal human milk and the BT-20 human breast carcinoma cell line. *Cancer Communications* **1989,** *1* (4), 261-267.

37. Varki, A.; Kannagi, R.; Toole, B. P., *Glycosylation Changes in Cancer*. 2 ed.; Cold Spring Harbor Laboratory Press: La Jolla, CA, USA, 2009; Vol. 2.

38. (a) Kudelka, M. R.; Ju, T.; Heimburg-Molinaro, J.; Cummings, R. D., Chapter three - simple sugars to complex disease—Mucin-type *O*-glycans in cancer. In *Advances in Cancer Research*, Richard, R. D.; Lauren, E. B., Eds. Academic Press: 2015; Vol. Volume 126, pp 53-135; (b) Wang, P.-H.; Lee, W.-L.; Juang, C.-M.; Yang, Y.-H.; Lo, W.-H.; Lai, C.-R.; Hsieh, S.-L.; Yuan, C.-C., Altered mRNA expressions of sialyltransferases in ovarian cancers. *Gynecologic Oncology* **2005,** *99* (3), 631-639; (c) Videira, P. A.; Correia, M.; Malagolini, N.; Crespo, H. J.; Ligeiro, D.; Calais, F. M.; Trindade, H.; Dall'Olio, F., ST3Gal.I sialyltransferase relevance in bladder cancer tissues and cell lines. *BMC Cancer* **2009,** *9* (1), 357; (d) Schneider, F.; Kemmner, W.; Haensch, W.; Franke, G.; Gretschel, S.; Karsten, U.; Schlag, P. M., Overexpression of sialyltransferase CMP-sialic acid:Galβ1,3GalNAc-R α6-sialyltransferase is related to poor patient survival in human colorectal carcinomas. *Cancer Research* **2001,** *61* (11), 4605-4611.

39. Sedlik, C.; Heitzmann, A.; Viel, S.; Ait Sarkouh, R.; Batisse, C.; Schmidt, F.; De La Rochere, P.; Amzallag, N.; Osinaga, E.; Oppezzo, P.; Pritsch, O.; Sastre-Garau, X.; Hubert, P.; Amigorena, S.; Piaggio, E., Effective antitumor therapy based on a novel antibody-drug conjugate targeting the Tn carbohydrate antigen. *OncoImmunology* **2016,** *5* (7), e1171434.

40. (a) Osako, M.; Yonezawa, S.; Siddiki, B.; Huang, J.; Ho, J. J. L.; Kim, Y. S.; Sato, E., Immunohistochemical study of mucin carbohydrates and core proteins in human pancreatic tumors. *Cancer* **1993,** *71* (7), 2191-2199; (b) Cao, Y.; Karsten, U. R.; Liebrich, W.; Haensch, W.; Springer, G. F.; Schlag, P. M., Expression of thomsen-friedenreich-related antigens in primary and metastatic colorectal carcinomas. A reevaluation. *Cancer* **1995,** *76* (10), 1700-1708; (c) David, L.; Nesland, J. M.; Clausen, H.; Carneiro, F.; Sobrinho-Simoes, M.,

Simple mucin-type carbohydrate antigens (Tn, sialosyl-Tn and T) in gastric mucosa, carcinomas and metastases. *APMIS. Supplementum* **1992,** *27*, 162-72.

41. Cheever, M.; Allison, J.; Ferris, A.; Finn, O.; Hastings, B.; Hecht, T.; Mellman, I.; Prindiville, S.; Viner, J.; Weiner, L.; Matrisian, L., The prioritization of cancer antigens: A national cancer institute pilot project for the acceleration of translational research. *Clinical Cancer Research : An Official Journal of the American Association for Cancer Research* **2009,** *15* (17), 5323-5337.

42. (a) Galli-Stampino, L.; Meinjohanns, E.; Frische, K.; Meldal, M.; Jensen, T.; Werdelin, O.; Mouritsen, S. o., T-cell recognition of tumor-associated carbohydrates: The nature of the glycan moiety plays a decisive role in determining glycopeptide immunogenicity. *Cancer Research* **1997,** *57* (15), 3214-3222; (b) Glithero, A.; Tormo, J.; Haurum, J. S.; Arsequell, G.; Valencia, G.; Edwards, J.; Springer, S.; Townsend, A.; Pao, Y.-L.; Wormald, M.; Dwek, R. A.; Jones, E. Y.; Elliott, T., Crystal structures of two H-2Db/glycopeptide complexes suggest a molecular basis for CTL cross-reactivity. *Immunity* **1999,** *10* (1), 63-74; (c) Haurum, J. S.; Arsequell, G.; Lellouch, A. C.; Wong, S. Y.; Dwek, R. A.; McMichael, A. J.; Elliott, T., Recognition of carbohydrate by major histocompatibility complex class I-restricted, glycopeptide-specific cytotoxic T lymphocytes. *The Journal of Experimental Medicine* **1994,** *180* (2), 739-744; (d) Haurum, J. S.; Tan, L.; Arsequell, G.; Frodsham, P.; Lellouch, A. C.; Moss, P. A. H.; Dwek, R. A.; McMichael, A. J.; Elliott, T., Peptide anchor residue glycosylation: effect on class I major histocompatibility complex binding and cytotoxic T lymphocyte recognition. *European Journal of Immunology* **1995,** *25* (12), 3270-3276; (e) Jensen, T.; Galli-Stampino, L.; Mouritsen, S.; Frische, K.; Peters, S.; Meldal, M.; Werdelin, O., T cell recognition of Tn-glycosylated peptide antigens. *European Journal of Immunology* **1996,** *26* (6), 1342-1349.

43. (a) Vlad, A. M.; Muller, S.; Cudic, M.; Paulsen, H.; Otvos, L.; Hanisch, F.-G.; Finn, O. J., Complex carbohydrates are not removed during processing of glycoproteins by dendritic cells: Processing of tumor antigen MUC1 glycopeptides for presentation to major histocompatibility complex class II–restricted T cells. *The Journal of Experimental Medicine* **2002,** *196* (11), 1435-1446; (b) Ioannides, C. G.; Fisk, B.; Jerome, K. R.; Irimura, T.; Wharton, J. T.; Finn, O. J., Cytotoxic T cells from ovarian malignant tumors can recognize polymorphic epithelial mucin core peptides. *The Journal of Immunology* **1993,** *151* (7), 3693-703.

44. (a) Doménech, N.; Henderson, R. A.; Finn, O. J., Identification of an HLA-A11-restricted epitope from the tandem repeat domain of the epithelial tumor antigen mucin. *The Journal of Immunology* **1995,** *155* (10), 4766-74; (b) Brossart, P.; Heinrich, K. S.; Stuhler, G.; Behnke, L.; Reichardt, V. L.; Stevanovic, S.; Muhm, A.; Rammensee, H.-G.; Kanz, L.; Brugger, W., Identification of HLA-A2–restricted T-cell epitopes derived from the MUC1 tumor antigen for broadly applicable vaccine therapies. *Blood* **1999,** *93* (12), 4309-4317; (c) Ninkovic, T.; Kinarsky, L.; Engelmann, K.; Pisarev, V.; Sherman, S.; Finn, O. J.; Hanisch, F.-G., Identification of *O*-glycosylated decapeptides within the MUC1 repeat domain as potential MHC class I (A2) binding epitopes. *Molecular Immunology* **2009,** *47* (1), 131-140.

45. Agrawal, B.; Krantz, M. J.; Reddish, M. A.; Longenecker, B. M., Rapid induction of primary human CD4+ and CD8+ T cell responses against cancer-associated MUC1 peptide epitopes. *International Immunology* **1998,** *10* (12), 1907-16.

46. Perdicchio, M.; Ilarregui, J. M.; Verstege, M. I.; Cornelissen, L. A. M.; Schetters, S. T. T.; Engels, S.; Ambrosini, M.; Kalay, H.; Veninga, H.; den Haan, J. M. M.; van Berkel, L. A.; Samsom, J. N.; Crocker, P. R.; Sparwasser, T.; Berod, L.; Garcia-Vallejo, J. J.; van Kooyk, Y.; Unger, W. W. J., Sialic acid-modified antigens impose tolerance via inhibition of T-cell proliferation and de novo induction of regulatory T cells. *Proceedings of the National Academy of Sciences* **2016,** *113* (12), 3329-3334.

47. Apostolopoulos, V.; Xing, P. X.; McKenzie, I. F., Murine immune response to cells transfected with human MUC1: immunization with cellular and synthetic antigens. *Cancer Research* **1994,** *54* (19), 5186-93.

48. Apostolopoulos, V.; Pietersz, G. A.; Gordon, S.; Martinez-Pomares, L.; McKenzie, I. F., Aldehyde-mannan antigen complexes target the MHC class I antigen-presentation pathway. *European Journal of Immunology* **2000,** *30* (6), 1714-23.

49. (a) Danishefsky, S. J.; Allen, J. R., From the laboratory to the clinic: A retrospective on fully synthetic carbohydrate-based anticancer vaccines. *Angewandte Chemie, International Edition in English* **2000,** *39*, 836-863; (b) Sabbatini, P. J.; Ragupathi, G.; Hood, C.; Aghajanian, C. A.; Juretzka, M.; Iasonos, A.; Hensley, M. L.; Spassova, M. K.; Ouerfelli, O.; Spriggs, D. R.; Tew, W. P.; Konner, J.; Clausen, H.; Abu Rustum, N.; Dansihefsky, S. J.; Livingston, P. O., Pilot study of a heptavalent vaccine-Keyhole Limpet Hemocyanin conjugate plus QS21 in patients with epithelial ovarian, fallopian tube, or peritoneal Cancer. *Clinical Cancer Research* **2007,** *13* (14), 4170-4177.

50. (a) Hoffmann-Roder, A.; Kaiser, A.; Wagner, S.; Gaidzik, N.; Kowalczyk, D.; Westerlind, U.; Gerlitzki, B.; Schmitt, E.; Kunz, H., Synthetic antitumor vaccines from Tetanus Toxoid conjugates of MUC1 glycopeptides with the Thomsen-Friedenreich antigen and a fluorine-substituted analogue. *Angewandte Chemie, International Edition in English* **2010,** *49* (45), 8498-8503; (b) Rich, J. R.; Wakarchuk, W. W.; Bundle, D. R., Chemical and chemoenzymatic synthesis of S-linked ganglioside analogues and their protein conjugates for use as immunogens. *Chemistry – A European Journal* **2006,** *12*, 845-858.

51. (a) Musselli, C.; Livingston, P. O.; Ragupathi, G., Keyhole limpet hemocyanin conjugate vaccines against cancer: the Memorial Sloan Kettering experience. *Journal of Cancer Research and Clinical Oncology* **2001,** *127 Suppl 2*, R20-6; (b) Buskas, T.; Li, Y.; Boons, G.-J., The immunogenicity of the tumor-associated antigen Lewis y may be suppressed by a bifunctional cross-linker required for coupling to a carrier protein. *Chemistry – A European Journal* **2004,** *10* (14), 3517-3524.

52. Jegerlehner, A.; Wiesel, M.; Dietmeier, K.; Zabel, F.; Gatto, D.; Saudan, P.; Bachmann, M. F., Carrier induced epitopic suppression of antibody responses induced by virus-

like particles is a dynamic phenomenon caused by carrier-specific antibodies. *Vaccine* **2010,** *28* (33), 5503-5512.

53. Gaidzik, N.; Westerlind, U.; Kunz, H., The development of synthetic antitumour vaccines from mucin glycopeptide antigens. *Chemical Society Reviews* **2013,** *42* (10), 4421-4442.

54. (a) Joshi, M.; Unger, W.; Storm, G.; van Kooyk, Y.; Mastrobattista, E., Targeting tumor antigens to dendritic cells using particulate carriers. *Journal of Controlled Release : Official Journal of the Controlled Release Society* **2012,** *161* (1), 25-37; (b) Zhu, G.; Zhang, F.; Ni, Q.; Niu, G.; Chen, X., Efficient nanovaccine delivery in cancer immunotherapy. *ACS Nano* **2017**.

55. Mellman, I.; Coukos, G.; Dranoff, G., Cancer immunotherapy comes of age. *Nature* **2011,** *480* (7378), 480-489.

56. Reddy, R.; Zhou, F.; Nair, S.; Huang, L.; Rouse, B. T., *In vivo* cytotoxic T lymphocyte induction with soluble proteins administered in liposomes. *The Journal of Immunology* **1992,** *148* (5), 1585-9.

57. Xiang, S.; Scalzo-Inguanti, K.; Minigo, G.; Park, A.; Hardy, C.; Plebanski, M., Promising particle-based vaccines in cancer therapy. *Expert Review of Vaccines* **2008,** *7* (7), 1103-1119.

58. (a) de Haan, A.; Haijema, B.; Voorn, P.; Meijerhof, T.; van Roosmalen, M.; Leenhouts, K., Bacterium-like particles supplemented with inactivated influenza antigen induce cross-protective influenza-specific antibody responses through intranasal administration. *Vaccine* **2012,** *30* (32), 4884-4891; (b) McKee, S.; Young, V.; Clow, F.; Hayman, C.; Baird, M.; Hermans, I.; Young, S.; Ward, V., Virus-like particles and α-galactosylceramide form a self-adjuvanting composite particle that elicits anti-tumor responses. *Journal of Controlled Release : Official Journal of the Controlled Release Society* **2012,** *159* (3), 338-345.

59. Waeckerle-Men, Y.; Allmen, E.; Gander, B.; Scandella, E.; Schlosser, E.; Schmidtke, G.; Merkle, H.; Groettrup, M., Encapsulation of proteins and peptides into biodegradable poly(D,L-lactide-co-glycolide) microspheres prolongs and enhances antigen presentation by human dendritic cells. *Vaccine* **2006,** *24* (11), 1847-1857.

60. Thomann-Harwood, L.; Kaeuper, P.; Rossi, N.; Milona, P.; Herrmann, B.; McCullough, K., Nanogel vaccines targeting dendritic cells: Contributions of the surface decoration and vaccine cargo on cell targeting and activation. *Journal of Controlled Release : Official Journal of the Controlled Release Society* **2012,** *166* (2), 95-105.

61. Bachmann, M.; Rohrer, U.; Kündig, T.; Bürki, K.; Hengartner, H.; Zinkernagel, R., The influence of antigen organization on B cell responsiveness. *Science (New York, N.Y.)* **1993,** *262* (5138), 1448-1451.

62. (a) Black, M.; Trent, A.; Tirrell, M.; Olive, C., Advances in the design and delivery of peptide subunit vaccines with a focus on toll-like receptor agonists. *Expert Review of Vaccines* **2010,** *9* (2), 157-173; (b) Wille-Reece, U.; Flynn, B. J.; Loré, K.; Koup, R. A.; Kedl, R. M.; Mattapallil, J. J.; Weiss, W. R.; Roederer, M.; Seder, R. A., HIV Gag protein conjugated to a Toll-like receptor 7/8 agonist improves the magnitude and quality of Th1 and CD8+ T cell responses in nonhuman primates. *Proceedings of the National Academy of Sciences of the United States of America* **2005,** *102* (42), 15190-15194; (c) Kastenm; xFc; ller, K.; Wille-Reece, U.; Lindsay, R. W. B.; Trager, L. R.; Darrah, P. A.; Flynn, B. J.; Becker, M. R.; Udey, M. C.; Clausen, B.; xF; rn, E.; Igyarto, B. Z.; Kaplan, D. H.; ller, W.; Germain, R. N.; Seder, R. A., Protective T cell immunity in mice following protein-TLR7/8 agonist-conjugate immunization requires aggregation, type I IFN, and multiple DC subsets. *The Journal of Clinical Investigation 121* (5), 1782-1796.

63. Lim, E.-K.; Kim, T.; Paik, S.; Haam, S.; Huh, Y.-M.; Lee, K., Nanomaterials for theranostics: Recent advances and future challenges. *Chemical Reviews* **2015,** *115* (1), 327-394.

64. (a) Xiang, S. D.; Scholzen, A.; Minigo, G.; David, C.; Apostolopoulos, V.; Mottram, P. L.; Plebanski, M., Pathogen recognition and development of particulate vaccines: Does size matter? *Methods* **2006,** *40* (1), 1-9; (b) Thiele, L.; Merkle, H. P.; Walter, E., Phagocytosis of synthetic particulate vaccine delivery systems to program dendritic cells. *Expert Review of Vaccines* **2002,** *1* (2), 215-226.

65. Moyer, T. J.; Zmolek, A. C.; Irvine, D. J., Beyond antigens and adjuvants: formulating future vaccines. *The Journal of Clinical Investigation 126* (3), 799-808.

66. Mou, Y.; Hou, Y.; Chen, B.; Hua, Z.; Zhang, Y.; Xie, H.; Xia, G.; Wang, Z.; Huang, X.; Han, W.; Ni, Y.; Hu, Q., *In vivo* migration of dendritic cells labeled with synthetic superparamagnetic iron oxide. *International Journal of Nanomedicine* **2011,** *6*, 2633-2640.

67. (a) MacPherson, G. G.; Fossum, S.; Harrison, B., Properties of lymph-borne (veiled) dendritic cells in culture. II. Expression of the IL-2 receptor: role of GM-CSF. *Immunology* **1989,** *68* (1), 108-113; (b) Matsuno, K.; Kudo, S.; Ezaki, T.; Miyakawa, K., Isolation of dendritic cells in the rat liver lymph. *Transplantation* **1995,** *60* (7), 765-8; (c) Pugh, C. W.; MacPherson, G. G.; Steer, H. W., Characterization of nonlymphoid cells derived from rat peripheral lymph. *The Journal of Experimental Medicine* **1983,** *157* (6), 1758-1779.

68. (a) Inaba, K.; Turley, S.; Yamaide, F.; Iyoda, T.; Mahnke, K.; Inaba, M.; Pack, M.; Subklewe, M.; Sauter, B.; Sheff, D.; Albert, M.; Bhardwaj, N.; Mellman, I.; Steinman, R. M., Efficient presentation of phagocytosed cellular fragments on the major histocompatibility complex class II products of dendritic cells. *The Journal of Experimental Medicine* **1998,** *188* (11), 2163-2173; (b) Allan, R. S.; Waithman, J.; Bedoui, S.; Jones, C. M.; Villadangos, J. A.; Zhan, Y.; Lew, A. M.; Shortman, K.; Heath, W. R.; Carbone, F. R., Migratory dendritic cells transfer antigen to a lymph node-resident dendritic cell population for efficient CTL priming. *Immunity* **2006,** *25* (1), 153-162; (c) Belz, G. T.; Behrens, G. M. N.; Smith, C. M.; Miller, J. F. A. P.; Jones, C.; Lejon, K.; Fathman, C. G.; Mueller, S. N.; Shortman, K.; Carbone, F. R.; Heath,

W. R., The CD8α+ dendritic cell is responsible for inducing peripheral self-tolerance to tissue-associated antigens. *The Journal of Experimental Medicine* **2002,** *196* (8), 1099-1104.

69. Reddy, S. T.; van der Vlies, A. J.; Simeoni, E.; Angeli, V.; Randolph, G. J.; O'Neil, C. P.; Lee, L. K.; Swartz, M. A.; Hubbell, J. A., Exploiting lymphatic transport and complement activation in nanoparticle Vaccines. *Nature Biotechnology* **2007,** *25*, 1159-1164.

70. Newman, K. D.; Sosnowski, D. L.; Kwon, G. S.; Samuel, J., Delivery of MUC1 mucin peptide by poly(D,L-lactic-co-glycolic acid) microspheres induces type 1 T helper immune responses. *Journal of Pharmaceutical Sciences* **1998,** *87* (11), 1421-1427.

71. Guan, H. H.; Budzynski, W.; Koganty, R. R.; Krantz, M. J.; Reddish, M. A.; Rogers, J. A.; Longenecker, B. M.; Samuel, J., Liposomal formulations of synthetic MUC1 peptides: Effects of encapsulation versus surface display of peptides on immune responses. *Bioconjugate Chemistry* **1998,** *9* (4), 451-458.

72. Samuel, J.; Budzynski, W. A.; Reddish, M. A.; Ding, L.; Zimmermann, G. L.; Krantz, M. J.; Koganty, R. R.; Longenecker, B. M., Immunogenicity and antitumor activity of a liposomal MUC1 peptide-based vaccine. *International Journal of Cancer* **1998,** *75*, 295-302.

73. Lakshminarayanan, V.; Thompson, P.; Wolfert, M. A.; Buskas, T.; Bradley, J. M.; Pathangey, L. B.; Madsen, C. S.; Cohen, P. A.; Gendler, S. J.; Boons, G.-J., Immune recognition of tumor-associated mucin MUC1 is achieved by a fully synthetic aberrantly glycosylated MUC1 tripartite vaccine. *Proceedings of the National Academy of Sciences* **2012,** *109* (1), 261-266.

74. (a) Ingale, S.; Wolfert, M. A.; Buskas, T.; Boons, G.-J., Increasing the antigenicity of synthetic tumor-associated carbohydrate antigens by targeting toll-like receptors. *ChemBioChem* **2009,** *10* (3), 455-463; (b) Buskas, T.; Ingale, S.; Boons, G.-J., Towards a fully synthetic carbohydrate-based anticancer vaccine: Synthesis and immunological evaluation of a lipidated glycopeptide containing the tumor-associated Tn antigen. *Angewandte Chemie International Edition* **2005,** *44* (37), 5985-5988.

75. Ingale, S.; Wolfert, M. A.; Gaekwad, J.; Buskas, T.; Boons, G.-J., Robust immune responses elicited by a fully synthetic three-component vaccine. *Nature Chemical Biology* **2007,** *3* (10), 663-667.

76. Lakshminarayanan, V.; Thompson, P.; Wolfert, M. A.; Buskas, T.; Bradley, J. M.; Pathangey, L. B.; Madsen, C. S.; Cohen, P. A.; Gendler, S. J.; Boons, G.-J., Immune recognition of tumor-associated mucin MUC1 is achieved by a fully synthetic aberrantly glycosylated MUC1 triparticle vaccine. *Proceedings of the National Academy of Sciences of the United States of America* **2012,** *109*, 261-266.

77. Wilkinson, B. L.; Day, S.; Chapman, R.; Perrier, S.; Apostolopoulos, V.; Payne, R. J., Synthesis and immunological evaluation of self-assembling and self-adjuvanting tricomponent glycopeptide cancer-vaccine candidates. *Chemistry – A European Journal* **2012,** *18* (51), 16540-16548.

78. Liu, Y.-F.; Sun, Z.-Y.; Chen, P.-G.; Huang, Z.-H.; Gao, Y.; Shi, L.; Zhao, Y.-F.; Chen, Y.-X.; Li, Y.-M., Glycopeptide nanoconjugates based on multilayer self-assembly as an antitumor vaccine. *Bioconjugate Chemistry* **2015,** *26* (8), 1439-1442.

79. Huang, Z.-H.; Shi, L.; Ma, J.-W.; Sun, Z.-Y.; Cai, H.; Chen, Y.-X.; Zhao, Y.-F.; Li, Y.-M., A totally synthetic, self-assembling, adjuvant-free MUC1 glycopeptide vaccine for cancer therapy. *Journal of the American Chemical Society* **2012,** *134* (21), 8730-8733.

80. Restuccia, A.; Fettis, M. M.; Hudalla, G. A., Glycomaterials for immunomodulation, immunotherapy, and infection prophylaxis. *Journal of Materials Chemistry B* **2016,** *4* (9), 1569-1585.

81. Cai, H.; Degliangeli, F.; Palitzsch, B.; Gerlitzki, B.; Kunz, H.; Schmitt, E.; Fiammengo, R.; Westerlind, U., Glycopeptide-functionalized gold nanoparticles for antibody induction against the tumor associated mucin-1 glycoprotein. *Bioorganic & Medicinal Chemistry* **2016,** *24* (5), 1132-1135.

82. Lee, N.; Yoo, D.; Ling, D.; Cho, M. H.; Hyeon, T.; Cheon, J., Iron oxide based nanoparticles for multimodal imaging and magnetoresponsive therapy. *Chemical Reviews* **2015,** *115* (19), 10637-10689.

83. (a) Tassa, C.; Shaw, S.; Weissleder, R., Dextran-coated iron oxide nanoparticles: a versatile platform for targeted molecular imaging, molecular diagnostics, and therapy. *Accounts of Chemical Research* **2011,** *44* (10), 842-852; (b) Mi Kyung, Y.; Jinho, P.; Sangyong, J., Magnetic nanoparticles and their applications in image-guided drug delivery. *Drug Delivery and Translational Research* **2011,** *2*.

84. Zhang, C.; Liu, T.; Gao, J.; Su, Y.; Shi, C., Recent development and application of magnetic nanoparticles for cell labeling and imaging. *Mini Reviews in Medicinal Chemistry* **2010,** *10* (3), 193-202.

85. Mou, Y.; Chen, B.; Zhang, Y.; Hou, Y.; Xie, H.; Xia, G.; Tang, M.; Huang, X.; Ni, Y.; Hu, Q., Influence of synthetic superparamagnetic iron oxide on dendritic cells. *International Journal of Nanomedicine* **2011,** *6*, 1779-1786.

86. Pusic, K.; Aguilar, Z.; McLoughlin, J.; Kobuch, S.; Xu, H.; Tsang, M.; Wang, A.; Hui, G., Iron oxide nanoparticles as a clinically acceptable delivery platform for a recombinant blood-stage human malaria vaccine. *FASEB Journal : Official Publication of the Federation of American Societies for Experimental Biology* **2013,** *27* (3), 1153-1166.

87. (a) Ruirui, Q.; Chunhui, Y.; Mingyuan, G., Superparamagnetic iron oxide nanoparticles: from preparations to *in vivo* MRI applications. *Journal of Materials Chemistry* **2009,** *19*; (b) Ulbrich, K.; Holá, K.; Šubr, V.; Bakandritsos, A.; Tuček, J.; Zbořil, R., Targeted drug delivery with polymers and magnetic nanoparticles: Covalent and noncovalent approaches, release control, and clinical studies. *Chemical Reviews* **2016,** *116* (9), 5338-5431.

88. Dobrovolskaia, M.; McNeil, S., Immunological properties of engineered nanomaterials. *Nature Nanotechnology* **2007,** *2* (8), 469-478.

89. Wu, W.; He, Q.; Jiang, C., Magnetic iron oxide nanoparticles: synthesis and surface functionalization strategies. *Nanoscale Research Letters* **2008,** *3* (11), 397-415.

90. (a) Amstad, E.; Gillich, T.; Bilecka, I.; Textor, M.; Reimhult, E., Ultrastable iron oxide nanoparticle colloidal suspensions using dispersants with catechol-derived anchor groups. *Nano Letters* **2009,** *9* (12), 4042-4048; (b) Jiang, S.; Eltoukhy, A. A.; Love, K. T.; Langer, R.; Anderson, D. G., Lipidoid-coated iron oxide nanoparticles for efficient DNA and siRNA delivery. *Nano Letters* **2013,** *13* (3), 1059-1064.

91. Tong, S.; Hou, S.; Ren, B.; Zheng, Z.; Bao, G., Self-assembly of phospholipid-PEG coating on nanoparticles through dual solvent exchange. *Nano Letters* **2011,** *11* (9), 3720-3726.

92. Park, J.; An, K.; Hwang, Y.; Park, J.-G.; Noh, H.-J.; Kim, J.-Y.; Park, J.-H.; Hwang, N.-M.; Hyeon, T., Ultra-large-scale syntheses of monodisperse nanocrystals. *Nature Materials* **2007,** *3*, 891-896.

93. Dobrovolskaia, M.; McNeil, S., Immunological properties of engineered nanomaterials. *Nature Nanotechnology* **2007,** *2* (8), 469-478.

94. Sun, S.; Zeng, H.; Robinson, D. B.; Raoux, S.; Rice, P. M.; Wang, S. X.; Li, G., Monodisperse MFe_2O_4 (M = Fe, Co, Mn) nanoparticles. *Journal of the American Chemical Society* **2004,** *126*, 273-279.

95. Tong, S.; Hou, S.; Ren, B.; Zheng, Z.; Bao, G., Self-assembly of phospholipid-PEG coating on nanoparticles through dual solvent exchange. *Nano Letters* **2011,** *11* (9), 3720-3726.

96. Steinman, R. M., Dendritic cells: Versatile controllers of the immune system. *Nature Medicine* **2007,** *13*, 1155-1159.

97. Iwasaki, A.; Medzhitov, R., Toll-like receptor control of the adaptive immune responses. *Nature Immunology* **2004,** *5* (10), 987-995.

98. Pihlgren, M.; Silva, A. B.; Madani, R.; Giriens, V.; Waeckerle-Men, Y.; Fettelschoss, A.; Hickman, D. T.; López-Deber, M. P.; Ndao, D. M.; Vukicevic, M.; Buccarello, A. L.; Gafner, V.; Chuard, N.; Reis, P.; Piorkowska, K.; Pfeifer, A.; Kündig, T. M.; Muhs, A.; Johansen, P., TLR4- and TRIF-dependent stimulation of B lymphocytes by peptide liposomes enables T cell–independent isotype switch in mice. *Blood* **2012,** *121* (1), 85-94.

99. Jeong, J.; Kwon, E.-K.; Cheong, T.-C.; Park, H.; Cho, N.-H.; Kim, W., Synthesis of multifunctional Fe_3O_4–CdSe/ZnS nanoclusters coated with Lipid A toward dendritic cell-based immunotherapy. *ACS Applied Materials & Interfaces* **2014,** *6* (7), 5297-5307.

100. Liu, H.; Moynihan, K. D.; Zheng, Y.; Szeto, G. L.; Li, A. V.; Huang, B.; Van Egeren, D. S.; Park, C.; Irvine, D. J., Structure-based programming of lymph-node targeting in molecular vaccines. *Nature* **2014,** *507* (7493), 519-522.

101. Bachmann, M. F.; Jennings, G. T., Vaccine delivery: A matter of size, geometry, kinetics and molecular patterns. *Nature Reviews: Immunology* **2010,** *10* (11), 787-796.

102. Steinhagen, F.; Kinjo, T.; Bode, C.; Klinman, D. M., TLR-based immune adjuvants. *Vaccine* **2011,** *29* (17), 3341-3355.

103. (a) Schietinger, A.; Philip, M.; Yoshida, B. A.; Azadi, P.; Liu, H.; Meredith, S. C.; Schreiber, H., A mutant chaperone converts a wild-type protein into a tumor-specific antigen. *Science* **2006,** *314*, 304-308; (b) Wang, Y.; Ju, T.; Ding, X.; Xia, B.; Wang, W.; Xia, L.; He, M.; Cummings, R. D., Cosmc is an essential chaperone for correct protein *O*-glycosylation. *Proceedings of the National Academy of Sciences of the United States of America* **2010,** *107*, 9228-9233.

104. (a) Peri, F., Clustered carbohydrates in synthetic vaccines. *Chemical Society Reviews* **2013,** *42*, 4543-4556; (b) Brinas, R. P.; Sundgren, A.; Sahoo, P.; Morey, S.; Rittenhouse-Olson, K.; Wilding, G. E.; Deng, W.; Barchi, J. J., Design and synthesis of multifunctional gold nanoparticles bearing tumor-associated glycopeptide antigens as potential cancer vaccines. *Bioconjugate Chemistry* **2012,** *23*, 1513-1523; (c) Yin, Z.; Comellas-Aragones, M.; Chowdhury, S.; Bentley, P.; Kaczanowska, K.; BenMohamed, L.; Gildersleeve, J. C.; Finn, M. G.; Huang, X., Boosting immunity to small tumor-associated carbohydrates with bacteriophage Qβ capsids. *ACS Chem. Biol.* **2013,** *8*, 1253-1262; (d) Parry, A. L.; Clemson, N. A.; Ellis, J.; Bernhard, S. S. R.; Davis, B. G.; Cameron, N. R., 'Mulicopy multivalent' glycopolymer-stabilized gold nanoparticles as potential synthetic cancer vaccines. *Journal of the American Chemical Society* **2013,** *135*, 9362-9365; (e) Ojeda, R.; de Paz, J. L.; Barrientos, A. G.; Martin-Lomas, M.; Penades, S., Preparation of multifunctional glyconanoparticles as a platform for potential carbohydrate-based anticancer vaccines. *Carbohydrate Research* **2007,** *342* (3-4), 448-59.

105. (a) Kinarsky, L.; Suryanarayanan, G.; Prakash, O.; Paulsen, J.; Clausen, H.; Hanisch, F. A.; Hollingsworth, M. A.; Sherman, S., Conformational studies on the MUC1 tandem repeat glycopeptides: Implication for the enzymatic *O*-glycosylation of the mucin protein core. *Glycobiology* **2003,** *13*, 929-939; (b) Karsten, U.; Serttas, N.; Paulsen, H.; Danielczyk, A.; Goletz, S., Binding patterns of DTR-specific antibodies reveal a glycosylation-conditioned tumor-specific epitope of the epithelial mucin (MUC1). *Glycobiology* **2004,** *14* (8), 681-692; (c) Matsushita, T.; Ohyabu, N.; Fujitani, N.; Naruchi, K.; Shimizu, H.; Hinou, H.; Nishimura, S., Site-specific conformational alteration induced by sialylation of MUC1 tandem repeating glycopeptides at an epitope region for the anti-KL-6 monoclonal antibody. *Biochemistry* **2013,** *52*, 402-414.

106. (a) von Mensdorff-Pouilly, S.; Moreno, M.; Verheijen, R. H. M., Natural and induced humoral responses to MUC1. *Cancers* **2011,** *3* (3), 3073-3103; (b) Ryan, S. O.; Turner, M. S.; Gariépy, J.; Finn, O. J., Tumor antigen epitopes interpreted by the immune system as self

or abnormal-self differentially affect cancer vaccine responses. *Cancer Research* **2010,** *70*, 5788-5796.

107. (a) Burford, B.; Gentry-Maharaj, A.; Graham, R.; Allen, D.; Pedersen, J. W.; Nudelman, A. S.; Blixt, O.; Foukala, E. O.; Bueti, D.; Dawnay, A.; Ford, J.; Desai, R.; David, L.; Trinder, P.; Acres, B.; Schwientek, T.; Gammerman, A.; Reis, C. A.; Silva, L.; Osorio, H.; Hallett, R.; Wandall, H. H.; Mandel, U.; Hollingsworth, M. A.; Jacobs, I.; Fentiman, I.; Clausen, H.; Taylor-Papadimitriou, J.; Menon, U.; Burchell, J. M., Autoantibodies to MUC1 glycopeptides cannot be used as a screening assay for early detection of breast, ovarian, lung or pancreatic cancer. *British Journal of Cancer* **2013,** *108*, 2045-2055; (b) Tarp, M. A.; Sorensen, A. L.; Mandel, U.; Paulsen, H.; Burchell, J.; Taylor-Papadimitriou, J.; Clausen, H., Identification of a novel cancer-specific immunodominant glycopeptide epitope in the MUC1 tandem repeat. *Glycobiology* **2007,** *17*, 197-209; (c) Sorensen, A. L.; Reis, C. A.; Tarp, M. A.; Mandel, U.; Ramachandran, K.; Sankaranarayanan, V.; Schwientek, T.; Graham, R.; Taylor-Papadimitriou, J.; Hollingsworth, M. A.; Burchell, J.; Clausen, H., Chemoenzymatically synthesized multimeric Tn/STn MUC1 glycopeptides elicit cancer-specific anti-MUC1 antibody responses and override tolerance. *Glycobiology* **2006,** *16* (2), 96-107; (d) Brockhausen, I., Mucin-type O-glycans in human colon and breast cancer: glycodynamics and functions. *EMBO Reports* **2006,** *7* (6), 599-604; (e) Muller, S.; Hanisch, F. G., Recombinant MUC1 probe authentically reflects cell-specific O-glycosylation profiles of endogenous breast cancer mucin. high density and prevalent core 2-based glycosylation. *Journal of Biological Chemistry* **2002,** *277* (29), 26103-26112; (f) Westerlind, U.; Hobel, A.; Gaidzik, N.; Schmitt, E.; Kunz, H., Synthetic vaccines consisting of tumor-associated MUC1 glycopeptide antigens and a T-cell epitope for the induction of a highly specific humoral immune response. *Angewandte Chemie, International Edition in English* **2008,** *47* (39), 7551-7556; (g) Cai, H.; Sun, Z.-Y.; Huang, Z.-H.; Shi, L.; Zhao, Y.-F.; Kunz, H.; Li, Y.-M., Fully synthetic self-adjuvanting thioether-conjugated glycopeptide-lipopeptide antitumor vaccines for the induction of complement-dependent cytotoxicity against tumor cells. *Chemistry – A European Journal* **2013,** *19* (6), 1962-1970.

108. Bäckström, M.; Link, T.; Olson, F. J.; Karlsson, H.; Graham, R.; Picco, G.; Burchell, J.; Taylor-Papadimitriou, J.; Noll, T.; Hansson, G. C., Recombinant MUC1 mucin with a breast cancer-like *O*-glycosylation produced in large amounts in chinese-hamster ovary cells. *Biochemical Journal* **2003,** *376*, 677-686.

109. Koeller, K. M.; Smith, M. E. B.; Wong, C.-H., Chemoenzymatic synthesis of PSGL-1 glycopeptides: Sulfation on tyrosine affects glycosyltransferase-catalyzed synthesis of the *O*-glycan. *Bioorganic & Medicinal Chemistry* **2000,** *8* (5), 1017-1025.

110. Vasella, A.; Witzig, C.; Chiara, J.-L.; Martin-Lomas, M., Convenient synthesis of 2-azido-2-deoxy-aldoses by diazo transfer. *Helvetica Chimica Acta* **1991,** *74* (8), 2073-2077.

111. Guazzelli, L.; Catelani, G.; D'Andrea, F.; Giannarelli, A., Stereoselective entry into the D-GalNAc series starting from the D-Gal one: A new access to N-acetyl-D-galactosamine and derivatives thereof. *Carbohydrate Research* **2009,** *344* (3), 298-303.

112. Wu, Z.; Guo, X.; Guo, Z., Chemoenzymatic synthesis of glycosylphosphatidylinositol-anchored glycopeptides. *Chemical Communications* **2010,** *46* (31), 5773-5774.

113. Schultz, M.; Kunz, H., Synthetic *O*-glycopeptides as model substrates for glycosyltransferases. *Tetrahedron: Asymmetry* **1993,** *4* (6), 1205-1220.

114. Winans, K. A.; King, D. S.; Rao, V. R.; Bertozzi, C. R., A chemically synthesized version of the insect antibacterial glycopeptide, diptericin, disrupts bacterial membrane integrity. *Biochemistry* **1999,** *38* (36), 11700-11710.

115. Lutz, M. B.; Kukutsch, N.; Ogilvie, A. L. J.; Rößner, S.; Koch, F.; Romani, N.; Schuler, G., An advanced culture method for generating large quantities of highly pure dendritic cells from mouse bone marrow. *Journal of Immunological Methods* **1999,** *223* (1), 77-92.

CHAPTER 2: Engineered Virus-Like Particle Qβ as a Novel Carrier for TACA-Based Anticancer Vaccines

2.1 Introduction

2.1.1 Virus-like particle as a vaccine carrier

The first part of this dissertation has already shown the importance of nanoparticle platform that helps direct the antigen into lymph node and multivalent display of the antigen to B cells resulting in higher immune response when compared with the soluble form. Although the combination of the nanoparticle with adjuvant MPLA can bypass the requirement of Th epitope for antibody isotype switching, the IgG titers of the generated antibodies were still inferior to those induced by immunogenic protein carriers. This is probably due to the lack of direct effect from the Th epitope. Another type of carrier platforms that our group has demonstrated its promising potential in activating the immune system to elicit strong anti-TACA immune responses is virus-like particle.

Virus-like particles (VLPs) are highly organized nano-constructs built from self-assembly of multimeric subunits of one or more proteins. This self-assembled nanoparticle resembles the structural organization of the protein in a viral capsid. VLPs differ from natural viruses in the way that VLPs are not able to infect host and they are non-replicating due to the lack of infectious viral genetic materials. Many features of VLPs render themselves a highly attractive candidate platform for vaccine application. The repetitiveness of highly ordered organization of the protein(s) in the VLPs is well recognized as pathogen-associated molecular patterns (PAMPs)[1], which is ideal for effective polyvalent display of antigen to crosslink B-cell receptors to induce intense cellular signaling for strong immune activation.[2] The distance between subunits of the capsid allows positioning B cell epitopes 5-10 nm away from each other, which was found

to optimally activate B cells.[3] Similar to the iron oxide nanoparticle, the nanostructure of the VLPs, which is in size range of 20 to 100 nm, can efficiently drain into lymph nodes to directly interact with residing immune cells, which has been demonstrated in the first chapter (For review, see[4]). During the recombinant protein expression, the nucleotide molecules (RNA) from *E. coli* cell host can be encapsulated in the empty cavity of the VLPs. These non-infectious genetic materials can act like internal adjuvants, and subsequently be released after particle dissociation during cellular uptake to stimulate internal cellular signals via TLR3/7/8/9 in the antigen presenting cells. Moreover, the production of VLPs can be done in a variety of expression systems including plant, bacterial, yeast, insect, mammalian cell and cell-free systems. These expression systems allow the production to be scaled up to manufacturing level.[5] All of these characteristics make VLPs a promising platform for vaccine development, which has been utilized in many recent vaccines including those against viruses, bacteria and chronic diseases.[6]

2.1.2 Bacteriophages

Viruses are viewed as the simplest organism that live to transfer genetic material, either DNA or RNA, into their host cells in order to replicate themselves. The hosts for viruses extend from single-cell organism to vertebrate. The specificity of the host to viruses depends on the compatibility of the cellular machinery that a certain group of viruses will take over for the replication. A group of viruses that specifically infects only bacteria is known as bacteriophages, or phages.

2.1.3 Bacteriophage Qβ

Bacteriophage Qβ belongs to genus allolevivirus, which is in *Leviviridae* family. This bacteriophage carries a single-stranded RNA genome encoding for a maturation protein (A1-

protein), a replicase enzyme and a coat protein. The production of Qβ VLP can be carried out by recombinant protein expression in *E. coli*, yeast and cell-free protein synthesis, which provide flexibility in research and capacity in large-scale production.[7] The monomer of Qβ's coat protein is composed of 132 amino acids. It can be divided into 9 domains including 2 domains of beta hairpin (βA and βB) starting from the N-terminus, followed by 5 domains of stranded beta sheets (βC, βD, βE, βF, βG), and ending with 2 domains of alpha-helixes (αA and αB) towards the C-terminus (**Figure 2.1**a). The alignment of the alpha-helixes of a subunit over beta stands F and G of another subunit results in initial dimer formation (**Figure 2.1**b,c). The beta-sheet domains are located in the internal side of the capsid, which is involved the binding to the hairpin sequence of the encapsulated RNA.[8] The single-stranded RNA is believed to facilitate the self-assembly of the viral capsid by forming an initial complex with a few dimers first. This intermediate complex will attract each other to assemble to form fivefold- and quasi-sixfold units. These multifold-units will finally assemble to form a well-organized icosahedral construct. Each Qβ viral capsid is composed of 180 units of the monomer per capsid with triangulation number (T) = 3.[9] The Qβ viral capsid has diameter approximately 27 nm.[10] In vaccine applications, this single-stranded RNA (ssRNA) is an agonist of TLR7,[11] where their interaction helps enhance immune activation via Th1 type response[12] and presentation of Th epitopes on MHC class II.[13] In contrast to recombinantly expressed coat protein from *E. coli*, the native viral capsid contains 3-5 subunits of maturation protein or A1 protein, in which the amino acid sequence is extended C-terminally to 196 amino acids as a result of natural read-through of the stop codon UGA in the gene of the coat protein.[14] This extended domain of A1 protein is believed to help infect bacteria.[10, 15] The incorporation of A1 protein into the natural viral capsid suggests that extending of the C-terminal of some subunits with a short peptide does not disrupt the ability of the admixed proteins to form

the capsid. Since the C-terminally extended peptide was found to be exposed on the surface, this implication has been applied for *in situ* conjugation by genetic manipulation to link an antigen peptide for vaccine application[16] or a poly-histidine tag for ease of purification.[17] Qβ VLP is exceptionally stable compared to other viral capsids from the same family due to inter-subunit disulfide bonds between cysteine residues at positions 74 and 80 (green residues in **Figure 2.1**d) of the adjacent subunit where they form networks to hold five- and six-fold units together (**Figure 2.1**d).[8c, 18]

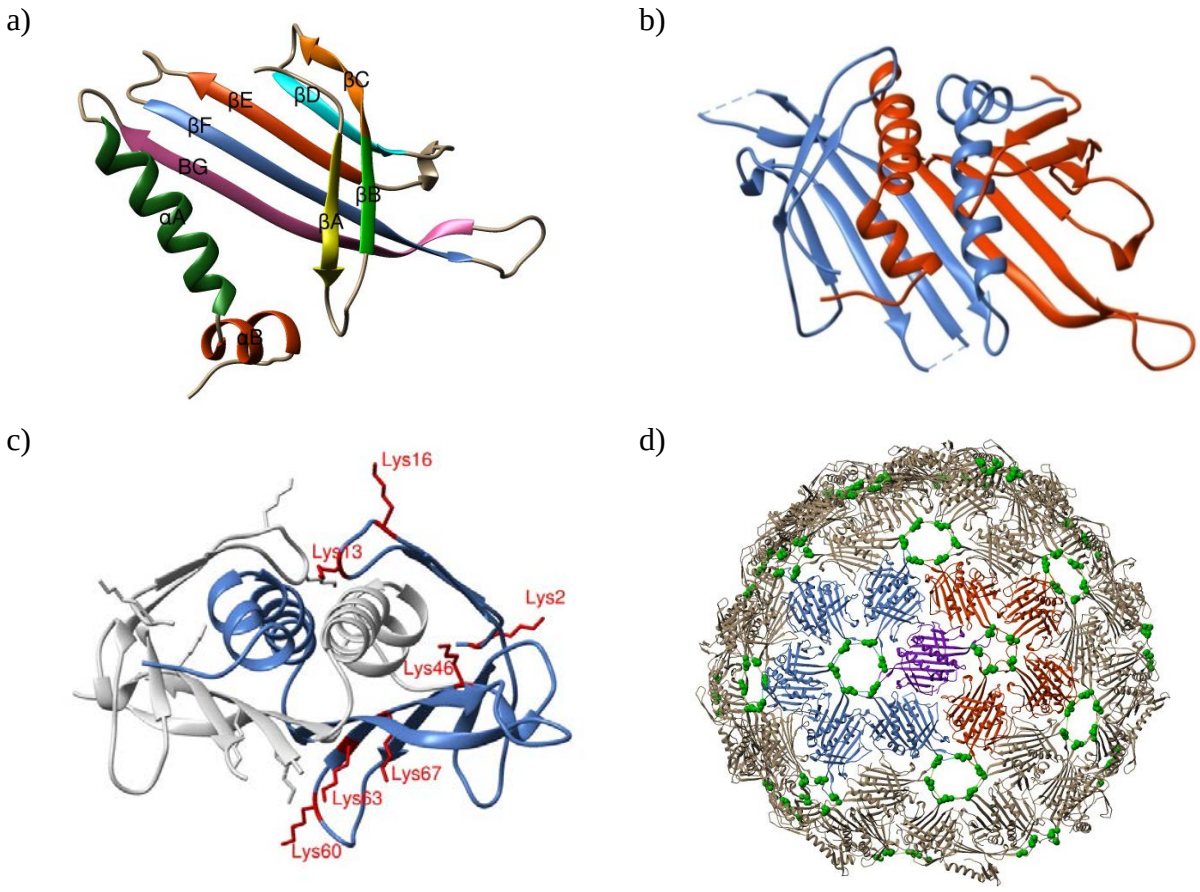

Figure 2.1: Qβ protein structure (PDB-ID: 1QBE), a.) Qβ subunit protein with secondary structure domains; b,c) The alignment of the dimer subunit and all lysine residues; d) The organization of fivefold- and quasi-sixfold units to form icosahedral shape with triangulation number (T) = 3. The green residues are cysteines at position 74 and 80, which form an intra-subunit disulfide bond.

2.1.4 Bacteriophage Qβ VLP in vaccine applications

Qβ VLP has been long investigated, both pre-clinically and clinically, as a vaccine carrier for many antigens by Martin F. Bachmann's group and Cytos Biotechnology. A vaccine against nicotine for smoking-cessation was evaluated in 2005.[19] Due to the low immunogenicity of nicotine, inducing potent immune response to neutralize and block the addictive molecule into the brain was challenging. Cytos Biotechnology has demonstrated that covalently conjugating nicotine onto Qβ VLP in high valency number (585 nicotine molecules per particle) can greatly enhance the immunogenicity of nicotine. Administering the nicotine conjugate vaccine with alum adjuvant can induce Th1 immune response in mice, rats and rabbits. The titers of the antibody response were shown to be 50-fold higher than titers from nicotine conjugated to a common carrier protein, BSA. The vaccine was shown to reduce the nicotine level in brain by approximately half in the vaccinated mice. The Qβ VLP as a carrier platform for nicotine proved safe and low in side-effect in phase I clinical trial. In phase II clinical trial, the nicotine conjugated vaccine was safe and able to induce the immune response in all immunized patients. However, only a group of the subjects that showed sufficiently high antibody response achieved statistically significant difference in smoking-cessation.

In 2006, Bachmann's group reported using Qβ VLP to induce antibodies against a house dust mite allergen Der p1 in human subjects (phase I clinical trial).[20] The study indicated that the repetitive pattern display of otherwise non-immunogenic peptide allergen on VLP can enhance immunogenicity of the antigen. The vaccine was capable of inducing IgM and IgG response without the help from adjuvant. The immune response was found to be dose-dependent.

In 2007, Qβ based vaccine has been investigated to generate antibody against a self-antigen, angiotensin II, for hypertension treatment.[21] The short peptide of angiotensin II (angiotensin$_{1\text{-}8}$) covalently linked to Qβ VLP was found to induce strong antibody response with

high affinity against the whole angiotensin II in mice and rats without using an adjuvant. The vaccinated rats were found to have significant lower blood pressure compared with a control group. However, the antibody response subsided over time after the last injection. Phase I clinical trial of this vaccine was shown to be highly efficient in human subject (100% responder rate), yet well tolerated and safe. With the promising results, this angiotensin II conjugated Qβ vaccine (CYT006-AngQβ) was assessed in phase II clinical trial. Although the vaccine proved immunogenic, well tolerated and no adverse side effect, the efficacy of the vaccine was dose dependent and the antibody response was also reversible as found in phase I. Only a dose of 300 μg induced sufficient anti-angiotensin II antibody titers to significantly reduce blood pressure in patients.

The use of Qβ VLP as a carrier platform for glycoprotein hemagglutinin (HA) to induce neutralizing antibodies against H5N1 influenza virus has been evaluated in 2013.[22] *E. coli* derived globular head domain of hemagglutinin (HA) glycoprotein, which was found as a neutralizing epitope on the influenza viral capsid[23], was conjugated on Qβ VLP. Compared with a licensed anti-H5N1 influenza vaccine, Panvax, the antigen-Qβ VLP conjugate formulated with alum adjuvant induced as high neutralizing antibody titer as Panvax. Although, the Qβ-based vaccine requires approximately 5 times higher dose of the globular HA content to induce comparable titer, the Qβ-based vaccine is superior over Panvax in activating T helper cells to elicit Th1 related cytokine interferon-γ (IFN-γ), while the protecting immunity from Panvax did not involve T helper cell activation. This is due to the presence of Th epitope on both the globular protein and the Qβ VLP. Both arms of immunities were thought to synchronize in reducing virus titers in challenged mouse and ferret animal models. Moreover, in another

publication, mice immunized with the conjugate vaccine were protected from lethal infection with homologous and highly drifted viral strains.[23c]

One important inference from this work is the potential Th epitopes of Qβ VLP. EPIMAX technique was utilized to reveal the peptide regions in Qβ viral capsid that are capable of activating $CD4^+$ T cells in splenocytes from mice. Peptide regions 41-71 and 101-132 (**Table 2.1**) were found to induce $CD4^+$ T cells to release high level of cytokine IFN-γ, hence, these two regions are suspected to contain Th epitopes (Figure 2.2). The resulting peptide regions are aligned on the 3D crystal structure of Qβ subunit as shown in **Figure 2.3**.

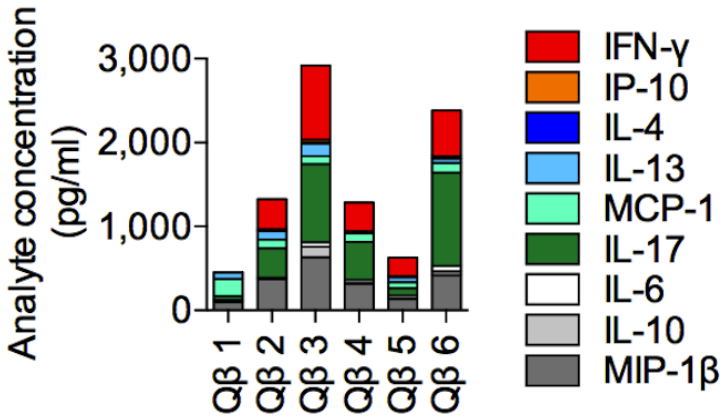

Figure 2.2: Qβ specific T cell responses were measured from level of cytokines secreted from splenocytes of HA conjugated Qβ immunized mice with peptide pools spanning Qβ capsid protein regions. Each bar represents the total cytokine response to each peptide pool and the colored boxes represent level of each specific cytokine. Each peptide pool is composed of 5 peptides fragments that have the overlap sequences as listed in **Table 2.1**. The figure is reproduced from reference[22].

Table 2.1: Sequences of Qβ specific peptides used for re-stimulation of splenocytes from the vaccinated mice.[22]

Protein	Peptide #	Peptide pools	Amino Acid Sequence
Qβ	1	Qβ 1	AKLETVTLGNIGKDG
Qβ	2	Qβ 1	TVTLGNIGKDGKQTL
Qβ	3	Qβ 1	GNIGKDGKQTLVLNP
Qβ	4	Qβ 1	KDGKQTLVLNPRGVN
Qβ	5	Qβ 1	QTLVLNPRGVNPTNG
Qβ	6	Qβ 2	LNPRGVNPTNGVASL
Qβ	7	Qβ 2	GVNPTNGVASLSQAG
Qβ	8	Qβ 2	TNGVASLSQAGAVPA
Qβ	9	Qβ 2	ASLSQAGAVPALEKR
Qβ	10	Qβ 2	QAGAVPALEKRVTVS
Qβ	11	Qβ 3	VPALEKRVTVSVSQP
Qβ	12	Qβ 3	EKRVTVSVSQPSRNR
Qβ	13	Qβ 3	TVSVSQPSRNRKNYK
Qβ	14	Qβ 3	SQPSRNRKNYKVQVK
Qβ	15	Qβ 3	RNRKNYKVQVKIQNP
Qβ	16	Qβ 4	NYKVQVKIQNPTACT
Qβ	17	Qβ 4	QVKIQNPTACTANGS
Qβ	18	Qβ 4	QNPTACTANGSCDPS
Qβ	19	Qβ 4	ACTANGSCDPSVTRQ
Qβ	20	Qβ 4	NGSCDPSVTRQAYAD
Qβ	21	Qβ 5	DPSVTRQAYADVTFS
Qβ	22	Qβ 5	TRQAYADVTFSFTQY
Qβ	23	Qβ 5	YADVTFSFTQYSTDE
Qβ	24	Qβ 5	TFSFTQYSTDEERAF
Qβ	25	Qβ 5	TQYSTDEERAFVRTE
Qβ	26	Qβ 6	TDEERAFVRTELAAL
Qβ	27	Qβ 6	RAFVRTELAALLASP
Qβ	28	Qβ 6	RTELAALLASPLLID
Qβ	29	Qβ 6	AALLASPLLIDAIDQ
Qβ	30	Qβ 6	ASPLLIDAIDQLNPAY

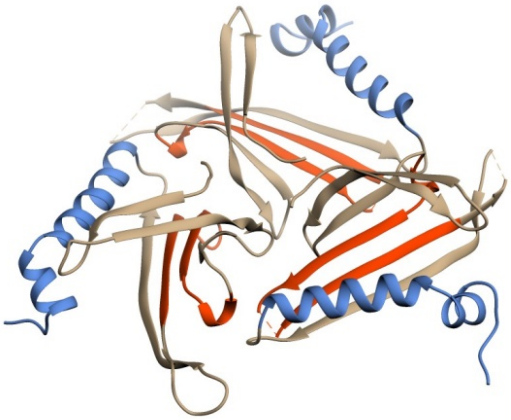

Figure 2.3: X-ray crystal structure of Qβ subunit (1qbe). The red and blue colored regions display the most probable Th epitopes. Red region = $Q\beta_{41\text{-}71}$, Blue region = $Q\beta_{101\text{-}132}$.

In this study[22], the importance of the ssRNA packaged in Qβ VLP was illustrated. The presence of the encapsulated ssRNA in Qβ enhanced the expression of IFNγ in $CD4^+$ T cell and elicited antibody titers 4 times higher than the titer from the capsid with ssRNA replaced by polyglutamic acid. Although the difference in the total titer was not statistically significant, the inclusion of the ssRNA directed the immune response towards Th1 type response as shown by higher IgG2a over IgG1 response, which was reversed in the titers from the one without the encapsulated ssRNA. Since the lack of the ssRNA does not significantly affect the total neutralizing titer when administered with alum adjuvant, directing immunity to favor Th1 or Th2 response could be controlled by Qβ VLP devoid of or containing the encapsulated ssRNA.

In 2010, Qβ VLP was assessed by Dannis R. Burton and M.G. Finn groups as an antigen carrier for inducing broadly neutralizing antibodies against a cluster of high mannose glycan, a "glycan shield" of the glycoprotein gp120 displayed on the surface spike of HIV.[24] Inducing protective humoral immunity to generate neutralizing antibodies against HIV is highly challenging as the conserved epitope on the viral envelop spike is shielded by highly variable

immunogenic epitope and clusters of glycans. The discovery of broadly neutralizing monoclonal antibody 2G12, which binds the high-mannose glycan shield and protect the viral infection, suggested an alternative target for anti-HIV vaccine development. Due to the multivalent antigen display pattern of Qβ, the attached antigens can mimic the cluster of trimeric structure of the viral envelop spike glycoprotein. Branched oligomannose glycans were conjugated via CuAAC reaction on the wild-type Qβ, mutant QβK16M or QβHPG, where the most reactive lysine at position 16 was replaced by an unnatural amino acid homopropargyl glycine (**Figure 2.1**). The mannoside Qβ conjugates were found to well represent the epitope of mAb 2G12 as shown by strong binding profile from sandwich ELISA. Although the Qβ glyco-conjugates was able to elicit high titers of antibodies specific to the synthetic high-mannose glycans, they failed to induce antibodies that have specific binding against the native glycan shield on HIV as the mAb 2G12. One important implication from this work is that the QβK16M-Man_9 elicited lower antibodies against the Qβ carrier than QβK16M-Man_4 and much lower than naked QβK16M. This suggested that the bulkier the size of antigen attached on the Qβ, the lower the titers of anti-carrier antibodies. This is probably because the immunogenic B-cell epitopes on Qβ capsid could be shielded by the attached antigen, making the carrier epitope less accessible to Qβ-specific B cells.

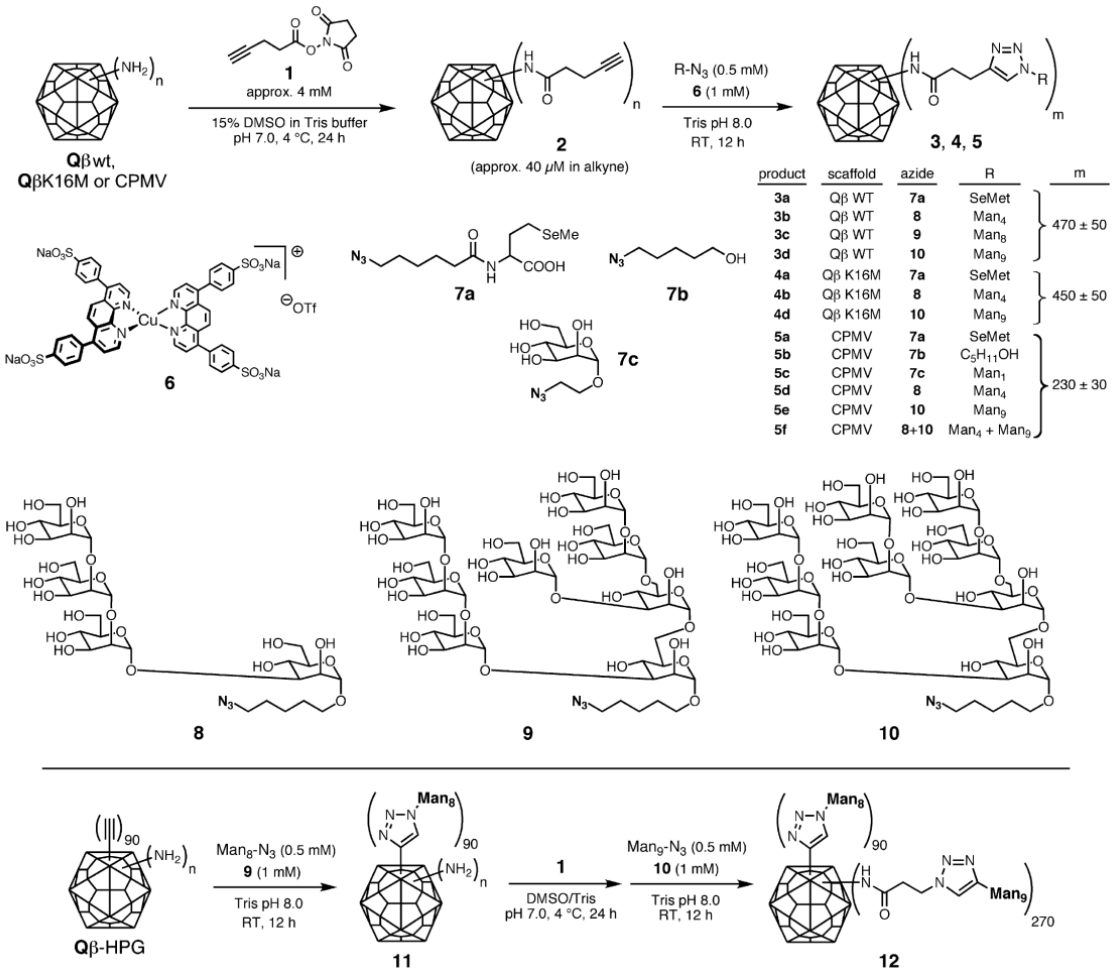

Figure 2.4: *Top panel*: Branched oligomannose glycans were conjugated via CuAAC reaction on the wild-type Qβ, mutant QβK16M or QβHPG, where the most reactive lysine at position 16 was replaced by an unnatural amino acid homopropargyl glycine. *Bottom panel*: Synthesis of QβHPG glycoconjugates QβHPG-Man8 (**11**) and QβHPG-Man8/Man9 (**12**). The figure is reproduced with permission from reference[22].

Qβ VLP has also been used as a carrier for inducing antibodies against inflammatory cytokine interleukin-1β (IL-1β) to treat type 2 diabetes.[25] In 2014, a "detoxified version" of IL-1β chemically conjugated on Qβ VLP was shown to be safe and able to mount IgG antibodies to neutralize IL-1B and improved glucose tolerance in diet-induced type 2 diabetes mouse model. This vaccine was further assessed in nonhuman primate subjects followed by phase I and II clinical trial with patients with type 2 diabetes.[26] Although the vaccine was demonstrated to be

clearly safe in both subjects in the studies, the efficacy of the vaccine is relatively low, as the titers of anti-IL-1B IgG induced were not sufficiently high compared with the results tested in mouse model. To generate the neutralizing titers of the anti-IL-1B IgG, the vaccine needed to be given in high dose (900 μg/injection) up to eight injections. Moreover, the titers elicited were decreased over time after immunization. The anti-carrier immune response against the Qβ was found to be relatively strong and this is suspected to be a factor responsible for low titers against the conjugated antigen.

In 2015, Erin Crossey and colleagues reported Qβ VLP based vaccine to induce antibodies against protein converstase subtillisin/kexin type 9 (PCSK9), which is a protein that disrupts a regulation process of low-density lipoprotein cholesterol (LDL-C) in blood circulation.[27] High level of this secretory protein leads to increasing level of LDL-C, a purported cause of hypercholesterolemia, atherosclerosis and cardiovascular disease. Even though, inducing potent immunity against this self-antigen was considered challenging due to B cell tolerance, this study is one of many cases mentioned earlier showing that conjugating the self-antigen on Qβ VLP can break B cell tolerance and generated strong neutralizing immunity against the self-antigen in mice and non-human primate macaques.[28]

In addition to Cytos Biotechnology AG, Pfizer Vaccine Immunotherapeutics has also been working on utilizing Qβ VLP in vaccine application. In 2016, there was a report of using Qβ VLP for anti-IgE vaccine aiming to treat both allergic asthma and rhinitis.[11] The main part of this study was on the importance of the encapsulated ssRNA. The role of the RNA as a TLR7 agonist was emphasized through the elicited high antibody response in wide-type mice but low in TLR7-knocked out mice. The lack of the encapsulated RNA can be compensated by adding external adjuvants including alum and CpG adjuvants.

In conclusion, many studies and clinical trials have proved the Qβ VLP as a promising immunogenic antigen carrier to break B cell tolerance and induce high antibody responses against self-antigens. The high potential of Qβ VLP in such purpose renders itself highly attractive for the development of TACA-based anticancer vaccine, where the antigens are self-antigens and weakly immunogenic. Moreover, after more than a decade, there is still no approved vaccine derived from Qβ VLP. This is probably due to the Qβ based vaccines mentioned above have not yet been optimized to be potent enough for approval. This also suggests that much improvement of this vaccine carrier construct is still needed.

2.1.5 Qβ VLP as a carrier for TACA-based anti-cancer vaccines.

The major challenge of anti-TACA vaccine is the low immunogenicity of TACAs. Two main factors are believed to contribute to their low immunogenicity. First, unlike glycopeptide MUC1, most TACAs are non-peptidic. Hence, administering TACAs alone fails to induce effective immunity due to the lack of help from T helper cells.[29] Secondly, TACAs are self-derived antigens, to which the self-tolerance mechanism suppresses their immunogenicity in order to prevent autoimmunity. Therefore, immunogenic carriers are generally required to render TACAs sufficiently immunogenic.

Keyhole limpet haemocyanin (KLH), or tetanus toxoid (TT) are traditional immunogenic proteins used for TACA based vaccine design. Despite strong immunogenicity of KLH, vaccination of KLH-Tn failed to generate IgG of anti-Tn antibodies probably due to the very low immunogenicity of the Tn antigen.[30] Another reason for the low anti-TACA response is the improper antigen display. This has been supported by studies from Danishefsky and Lo-Man groups. They showed that by putting Tn antigen together into a trimeric cluster, instead of monomeric form, the constructs can elicit more antibodies than those from the monomeric Tn

conjugated constructs.[31] As mentioned in the first chapter, the pattern of antigen display on the vaccine construct plays a crucial role to effectively cross link B cell receptor to induce strong cellular signals for B cell activation leading to IgM-to-IgG isotype switching and subsequent potent antibody response. Since KLH is amorphous where its antigen display is not highly ordered, it is not very effective for generating a strong humoral immune response. Moreover, KLH is a glycoprotein, containing native glycans,[32] which can possibly compete with conjugated TACAs for anti-glycan B cell responses.

Unlike KLH or TT, VLP is superior to those carriers for the proper size and highly organized display pattern for particulate vaccine as described above. Our group has demonstrated the utility of VLPs as a promising antigen carrier platform for TACA based anti-cancer vaccines.

In 2008, our group started to apply VLP as an immunogenic carrier for anti-TACA based vaccine. Cowpea mosaic virus (CPMV) was the first VLP that was examined for the purpose. CPMV is a plant virus, thus, non-infective and safe to humans. The viral capsid is composed of 60 subunits of a self-assembly protein to form a 30 nm icosahedral capsid. The Tn antigen (GalNAc-α-*O*-Ser/Thr) was selected as a prototypical model for TACA in this study. Maleimide linked Tn was reacted with site-specific mutagenesis derived cysteines on the exterior surface of the viral capsid. The number of Tn loaded was 60 Tn/capsid. The immunization was tested in mouse with a dose of 40 μg of Tn/mouse. The anti-Tn IgG titer elicited from the immunization was 10,500. The sera from the immunized mice showed binding to Tn expressed cancer cells MCF-7 and multidrug resistant breast cancer cell line NCI-ADR RES as determined by FACS. This work established a new type of carrier platform for presenting TACA in an organized display pattern to induce strong immune response against otherwise low immunogenic antigen of

the monomeric Tn antigen. This encouraging finding led to exploring other promising VLPs for highly effective carriers for anti-TACA vaccine.

In 2012, tobacco mosaic virus (TMV) capsid was evaluated as a carrier for Tn antigen.[33] TMV capsid derives from self-assembly protein of 2130 subunits to form a 300 nm long nano-rod.[34] Tn antigen was conjugated to genetically inserted cysteine near C-termini, which is exposed on the capsid surface. From the analysis, 410 Tn antigens were attached on each capsid. The TMV-Tn vaccine induced low level of IgG or IgM anti-Tn antibodies (titer ≈ 1,600) presumably due to the low density of Tn antigens on the viral capsid. The efficiency of conjugation was improved by robust reaction of copper(I) catalyzed azide-alkyne cycloaddition reaction (CuAAC). The number of Tn attached on TMV was increased up to 1530 Tn/TMV. However, there were little changes of IgG/IgM titers compared with the previous method of conjugation. When the conjugation site was changed to Tyr 139, which locates close to the capsid's surface, 2000 copies of Tn were linked onto a TMV capsid due to the well exposed and reactive residue at this position. Putting the antigen on such a well exposed point on the capsid could potentially get better recognition by B cells. Significantly higher antibody titers (titer ≈ 2550) were elicited from immunized mice by this formulation. Note that, the dose in this administration was 4 times (20 μg vs 4 μg Tn/mouse) higher than the previous two constructs. By extending the linker to better exposed the Tn out from the surface, the resulting IgG antibody titers increased up to about 7000 with 4μg of Tn/mouse dose. However, with 20 μg of Tn/mouse dose, the short and long linkers elicited comparable antibody titers. This suggests that increasing the linker length does not help increase the immune response. The resulting antibodies could bind to Tn or GalNAc containing antigens coated on glycan microarrays and native Tn on human leukemia Jurkat cells as determined by FACS. It is interesting that, despite the lower titer, the

serum from the dose of 20 μg of Tn can bind stronger against the cells, compared with the serum from mice receiving of 4μg Tn. This work indicated that the increased number of Tn on the construct is not responsible for the higher antibody response, but the location where the antigen is displayed, is crucial in inducing strong immune responses.

In 2013, it was the first time that Qβ VLP was reported by our group as a carrier for TACA based anti-cancer vaccine.[35] In contrast to rod shape of TMV, Qβ has icosahedral shape, which can present an antigen in an ordered manner. Although Qβ and CPMV are about the same in size, their capsid surface topologies are different. The CPMV is composed of 60 asymmetric subunits of 66 kDa protein, while Qβ is composed of 180 subunits of 14 kDa protein. By controlling reaction time and equivalence of the azide-modified Tn in the CuAAC reaction, the number of Tn loaded onto the Qβ capsid could be varied from 78, 150 to 340 Tn/Qβ (Figure 2.5). Compared with other VLPs mentioned before, Qβ is superior to CPMV or TMV in ability to induce dramatically higher IgG titers (titers ≈ 263,600) at the same antigen dose (4μg of Tn/mouse).

In addition to antibody response against Tn, it was found that the vaccine can also induce immune response against the carrier Qβ and the triazole linker (titers ≈ 35,300), which may suppress the desired immune response against the Tn. The impact of local density of the immobilized Tn on Qβ VLP has also been investigated. Qβ-Tn conjugates with varied density of Tn on each capsid (low density (78 Tn/Qβ), medium density (150 Tn/Qβ) and high density (340 Tn/Qβ)) were injected into groups of mice by either keeping amount of Qβ constant or both the total amounts of Tn and Qβ constant. The results showed that only groups that received high local density Qβ-Tn generated strong IgG antibody response. This suggests the importance of the high local density of the antigen on each particle in inducing high IgG antibody response. These

results provided another crucial factor for the design in the vaccine development. The resulting sera from the immunized mice showed specific binding to GalNAc containing glycans coated on glyco-microarray chip and native Tn expressed on human leukemia cancer cells, Jurkat cells. The higher potency of Qβ over other VLPs in inducing immunity against TACA excited us to investigate further into detail of this construct aiming to find the best formulation of this carrier for anti-TACA-based vaccine. This led to a following study by the same group of investigators.

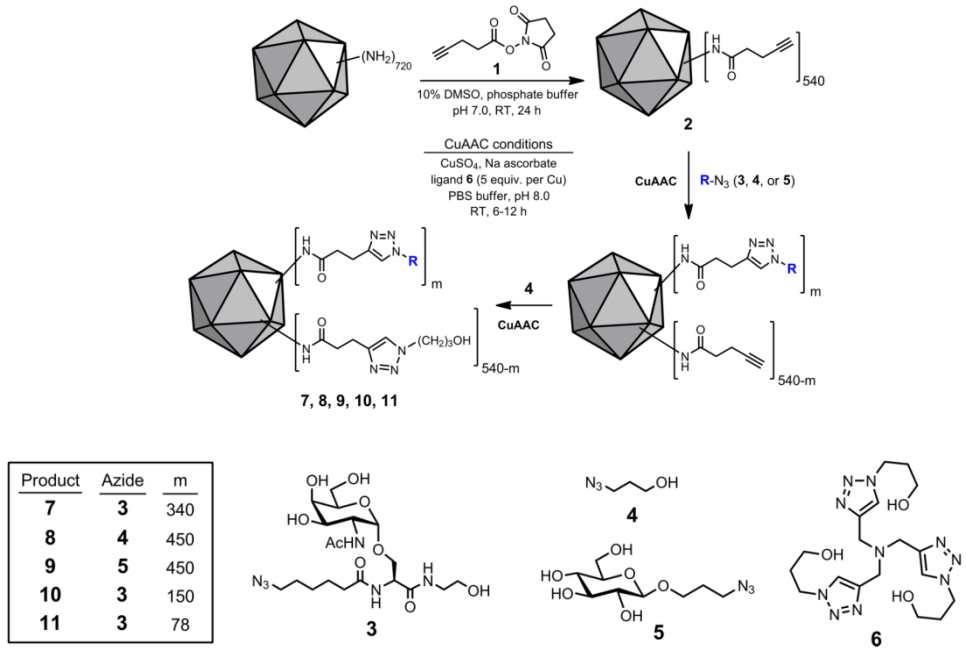

Product	Azide	m
7	**3**	340
8	**4**	450
9	**5**	450
10	**3**	150
11	**3**	78

Figure 2.5: Synthesis of Qβ-triazole-Tn via CuAAC reaction. The reaction condition can be adjusted to provide a variable number of Tns (78, 150 and 340 Tns) attached on the viral capsid. This figure is adapted and reproduced with permission from reference[35].

(a)

Group #	1	2	3	4	5	6
Tn density (particle)	L	M	H	L	M+N	H+N
Vaccine Construct	**11**	**10**	**7**	**11**	**10** + Qβ	**7** + Qβ
Tn Occupancy[a] (%)	23	44	100	23	44 + 0	100 + 0
Total Tn[b] (μg)	0.23	0.44	1	1	1	1
Total Qβ Virion[b] (μg)	18	18	18	75	75	75

[a]Tn occupancy in Qβ-Tn **7**, which displays 340 Tn antigens, was set as 100%.

[b]Amount for each injection in each mouse.

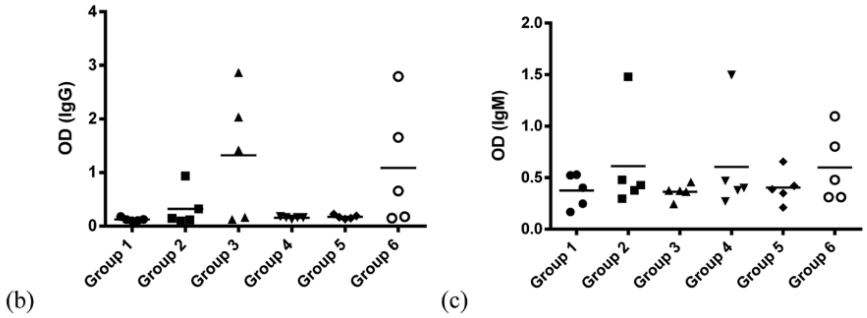

(b) (c)

Figure 2.6: a) a table showing characteristic details of the vaccine compound with varied Tn density used in 6 groups to investigate the effect of antigen density on the viral capsid. b) ELISA results of IgG and c) IgM antibodies from 6 groups of immunized mice at 1/6400 dilution. This figure is adapted and reproduced with permission from reference[35].

In 2015, our group found that the conjugation linker between the Tn and Qβ played an important role in generating of protecting antibodies against Tn expressing cancer cells.[36] The results showed that the triazole formed in the linker from CuAAC conjugation method can induce immune response against the linker. In contrast to the previous finding, increasing the density of the Tn on each capsid from 360 to 540 did not result in higher anti-Tn IgG antibody titer, but higher anti-triazole-linker IgG antibody titer was produced instead (**Figure 2.7**a-c). This suggests that there are some optimal points in increasing the number of the attached antigen on each capsid to obtain the best result, especially in this case that there are other competitive immunogenic components in the construct, such as the rigid triazole ring. The triazole immunogen can compete with Tn to dominate the immune response and suppress anti-Tn

immunity. Although the resulting sera can bind to Tn-expressing Jutkat cells, they failed to bind to Tn expressing murine breast cancer TA3Ha cells (**Figure 2.7d**).

In contrast, when removing the competing epitope in the linker by changing the linker from the rigid triazole linker to a non-rigid alkyl amide linker, the vaccine construct could not only elicit significantly higher titers of IgG antibody against Tn (1,461,000 vs 263,600) (**Figure 2.7e,f**), but the resulting sera also showed binding to both Jurkat and TA3Ha cells. The new vaccine construct significantly improved survival rate of mice in tumor challenge from 0% to 50% when combined with chemotherapy. This finding clearly supports that an immunogenic component in the vaccine construct can indeed suppress the desired immune response against TACA. The further mechanistic investigation found that it is not the triazole moiety itself that interferes the binding between the Tn and B cell receptor, rather most likely the induced anti-triazole polyclonal antibodies hindered the recognition of Tn by Tn-specific B cells. Moreover, this induced anti-triazole antibody was found to generate faster than those against the Tn. In summary, this work suggested that any potentially immunogenic components in the vaccine construct should be removed to minimize the suppressing effect towards the desired antigen caused by the induced antibodies against the interfering component.

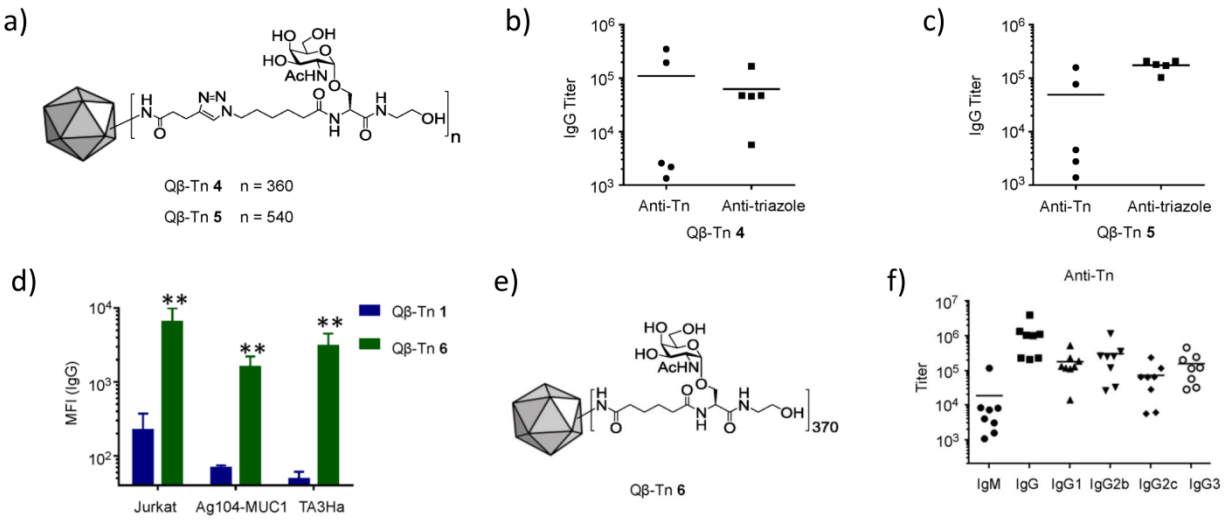

Figure 2.7: a) Vaccine constructs Qβ-Tn **4** and Qβ-Tn **5**. b,c) IgG titers elicited from the vaccine constructs against Tn or triazole. The increased number of attached Tn induced lower anti-Tn antibody titers due to suppression from increased anti-triazole immune response. d) Specific recognition against Tn-expressing cancer cells of the elicited antibodies from Qβ-Tn **1** and Qβ-Tn **6**. e) Vaccine constructs Qβ-Tn **6** where the triazole linker was replaced with low immunogenic alkyl linker. f) anti-Tn antibody titers elicited from Qβ-Tn6. The IgG titers became higher compared with those from Qβ-Tn **4** and Qβ-Tn **5**. This figure is adapted and reproduced with permission from reference[36].

Investigations described above contributed key knowledge for the design of VLP based anti-TACA vaccine as the following: 1) Qβ is, by far, the best carrier for the anti-TACA vaccine; 2) A co-adjuvant has been optimized; 3) The local density of the antigen on each capsid plays an important role for effective immune response; and 4) Unnecessary immunogenic component, such as immunogenic linker, should be excluded to maximize the desired immune response against TACA. However, another big challenge still remains, which is the robust immunogenicity of the carrier Qβ itself. Similar to the triazole linker, the strong antibody response against the carrier can cause carrier-induced epitopic suppression (CIES) resulting in reduction of the desired immune response against TACA.[37] It is envisioned that minimizing such strong immunogenicity of the carrier would re-focus the immunity towards generating higher potency of the desired immune response against TACAs. To logically address this issue, we need

to understand the mechanism of the suppressing effect for a rational approach towards carrier modification.

2.1.6 Carrier-Induced Epitopic Suppression (CIES) in Qβ

Carrier-Induced Epitopic Suppression (CIES) is referred as an effect derived from pre-existing or co-induced immunity against immunogenic carrier that suppresses immune response against any weaker immunogen attached on the related carrier. The exact mechanism of CIES is still unclear. Based on several studies, the main immune cells responsible for CIES are B cells.[38] The mechanism of CIES has been proposed by several views. The investigation from Schutze *et. al.* led to a theory of antigen/carrier specific B cells competition, where the higher rate of proliferation of carrier-specific B cells will dominate the number of haptan-specific B cells in competing for the antigen binding and stimulating cytokines for cellular activation.[38a] In contrast, Galelli *et. at.* found that the immunogenic carrier does not alter the number of haptan-specific memory B cells, but it prevents the memory B cells from turning into antibody releasing plasma cells.[38c] In addition to both theories, CIES is also generally viewed as the clearance mediated by pre-existing innate immunity against the carrier.

The effect of CIES on Qβ VLP as a vaccine carrier has been studied by the Bachmann group.[37] In this study, an 18 amino acid peptide antigen from Salmonella (D2) was used as a model antigen. The CIES effect on Qβ was evaluated by comparing the antibody titers from naive mice and pre-immunized mice with the carrier Qβ. The result showed that the antibody titers against D2 antigen from pre-immunized mice were statistically significantly lower than those from naïve mice. This result clearly indicated the suppression effect of pre-existing immunity against Qβ due to CIES. An interesting finding in this study is the effect of antigen density on the carrier on the reduction of CIES. It was found that the higher the antigen density

(142, 293 vs 13, 56, 94), the lower the suppression from pre-existing anti-carrier immunity (**Figure 2.8**). The authors gave an explanation from a mechanistic investigation that the pre-exiting carrier-specific antibodies will bind the subsequently injected vaccine. The bound antibodies sterically interfere the presentation of the antigen and the binding between the antigen and B-cell receptors. The increased antigen density can help block the anti-carrier specific antibodies, resulting in less interference and increasing B cell interaction with the desired antigen attached. This explanation resembles the finding from our group that the induced anti-triazole antibodies will bind to the Qβ-Tn vaccine and sterically blocked Tn recognition by Tn-specific B cells. It is worth noting that the pre-immunization with the carrier did not change the anti-carrier antibodies titers from the vaccination, except with highest antigen density (293 D2/Qβ), where the anti-carrier significantly reduced in the naïve mice, yet the anti-D2 antibodies titers increased in pre-immunized mice. This is because the higher density of the attached antigen better shields the B cell epitopes on the carrier, making the carrier less recognizable by carrier-specific B cells. The shielding effect caused by the attached antigen is correlated well with the finding from an investigation of Qβ based anti-HIV vaccine by Burton and Finn groups, which has already been mentioned above.[24] Besides the increased antigen density, the authors suggested repeated injections and increasing dose of the administration will also help to overcome the suppression effect from CIES, leading to higher anti-D2 antibody response.

The mechanism of CIES of Qβ was investigated further by passively transferring of antibodies or B cells or $CD4^+$ T cells from pre-immunized mice into naïve mice, which were subsequently immunized with the vaccine conjugate. The result showed that antibodies and B cells are responsible for the CIES. This study also inferred that heterogeneous prime-boost strategy for reducing CIES may not work with Qβ based vaccine as pre-immunizing the immune

system with D2 antigen conjugated with another VLP, AP205, did not significantly enhance the titers of the antibodies against D2 antigen after subsequent injection with the D2-Qβ conjugate.

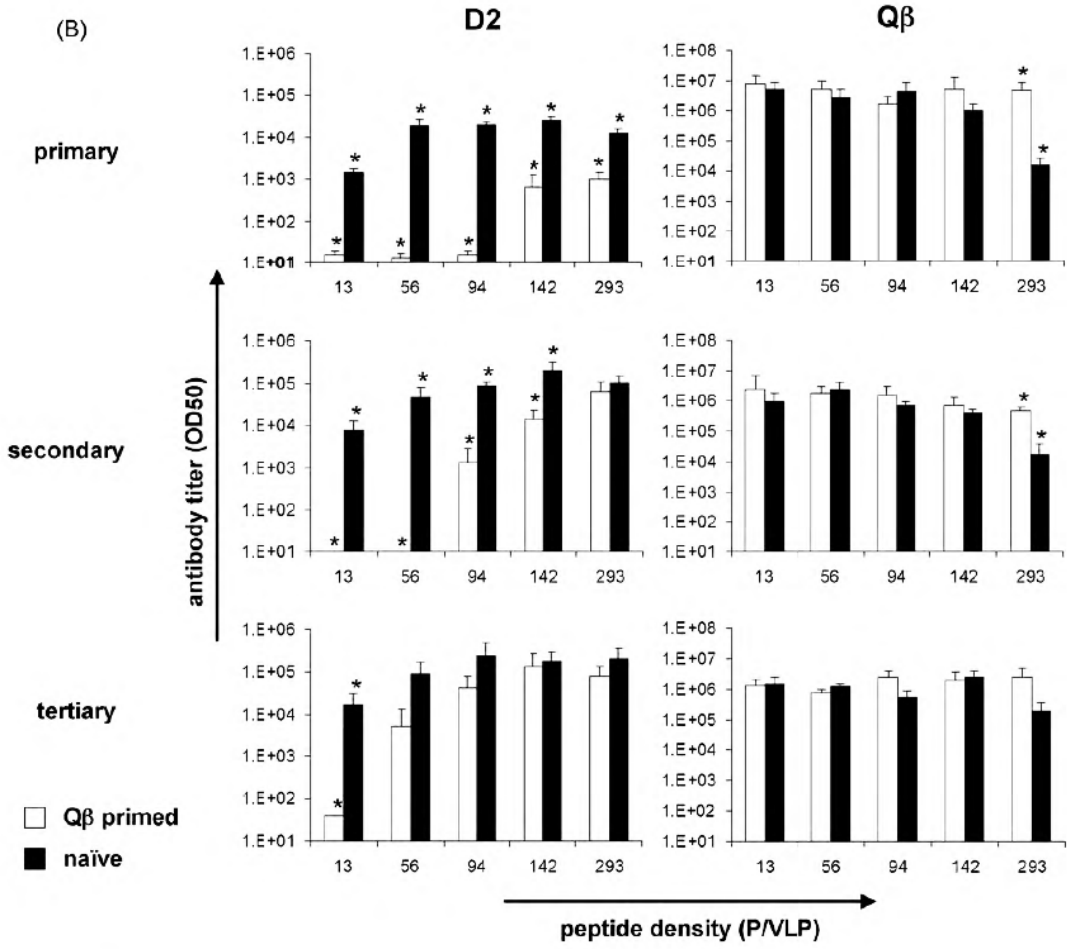

Figure 2.8: Antibody titers against D2 peptide (attached antigen) and Qβ VLP (carrier) elicited from Qβ primed- or naïve mice after 1st, 2nd and 3rd vaccination. The result suggests that the higher density of D2 on the Qβ helped reduce the suppression from CIES. This figure is adapted and reproduced with permission from reference[37].

The aforementioned studies showed clearly that VLP Qβ has the ability to cause CIES to the attached antigen. The suppression could limit the full potential of the Qβ in inducing maximum immune response against the antigen. Although the suppression effect could be partially addressed by the suggested solutions, including increasing the density of the antigen, repeated injection or increasing the dose, the improved results were still very subtle. Therefore,

an innovative strategy for reducing the CIES caused by the Qβ carrier is needed to unlock its maximum potential towards the best carrier for TACA-based anticancer vaccine.

The robust immunity against the vaccine carrier originates from B cell activation through binding with B cell epitopes in the Qβ capsid protein. In order to reduce undesired immune response, B cell epitopes on Qβ capsid protein will have to be either removed or modified to block the interactions with B cells. The strategy to achieve this was investigated as the following:

1) Firstly, the candidate fragments for B cell epitopes were searched based on computational prediction from available 3D structure, together with analysis of binding of synthetic peptide fragments by anti-capsid sera.

2) The potential B cell epitope on the viral capsid surface was subjected to site specific mutagenesis to induce structural changes and introduce a new conjugation site. The mutated Qβ capsid was then conjugated with a TACA antigen model and tested for its ability to shield the dominant epitope to further prevent recognition by B cells.

3) The Qβ VLP mutant was stabilized by additional disulfide network to make it less susceptible to disassembly after reactions to conjugate the antigen onto the new conjugation sites. In addition, the higher stability of the capsid can potentially enable longer interactions of the conjugate with immune cells leading to stronger immune activation. The best mutant Qβ was selected based on the criteria of higher stability, decreased immunogenicity against the carrier and increased antibody response towards the conjugated antigen.

2.2 Results and discussion

2.2.1 B cell epitope prediction

B cell epitopes are immunogenic fragments of a protein recognizable by B cell receptors (BCRs). The recognition of B cell epitopes occurs through complementary interactions between

binding sites of B cell receptors and the antigenic fragments on the surface of an immunogen. B cell epitopes are categorized into continuous and discontinuous types. The continuous, or linear, epitopes are simple short fragments where all recognizable residues are aligned in sequence. However, 90% of B cells epitopes are discontinuous or conformational epitopes[39], in which the fragments or residues responsible for the binding with BCR are not contiguous, but brought close together by the folding of tertiary or quaternary protein structure. The type of B cell epitopes on the Qβ capsid was tested first by peptide scanning experiment. Eight synthetic 30-amino-acid peptides with overlapping sequence by 15 amino acids covering the entire amino acid sequence of Qβ capsid protein (**Figure 2.9**a) were immobilized onto ELISA plate individually. Serum from wide-type Qβ (wtQβ)-immunized mice was used to test the peptide recognition by anti-wtQβ IgG antibodies. None of the synthetic peptides showed strong binding to the IgG anti-Qβ antibodies from the serum compared with the binding with the whole capsids coated on the ELISA plate (**Figure 2.9**b).

a)

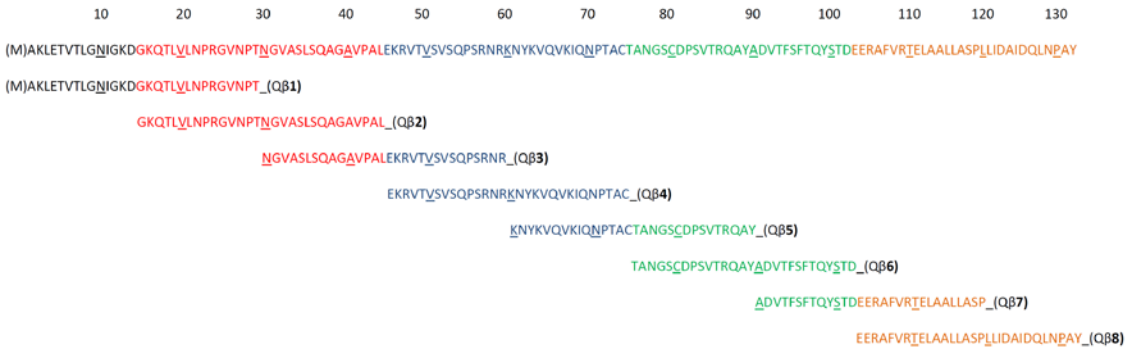

Figure 2.9: a) Eight of synthetic 30-amino-acid peptides that overlapped sequence by 15 amino acids covering the entire amino acid sequence of Qβ capsid protein. b) ELISA result of peptide scanning experiment showing the binding of the peptides fragments with the anti-wtQβ IgG antibodies. The synthetic peptides were coated on the ELISA plate. The dilution of serum (1/64000 dilution) from wtQβ-immunized mice was added to test recognition towards each peptide fragments. Group (-) is a negative control group where only PBS was used in coating process.

Figure 2.9: (Cont'd)

b)

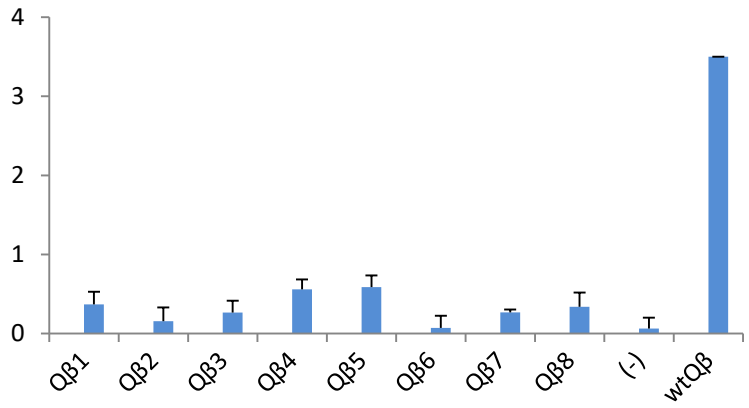

For conformational epitopes, random mutations of B cell epitope on the 132-amino acid Qβ viral capsid protein involves tedious work and high cost of mutations to the viral capsid. Due to the complex structures of the capsid, the computational prediction based on available epitope database are generally not very accurate. Nevertheless, the prediction could provide guidance for potential mutation points and rational design in engineering the viral capsid, making the B cell determination more practical with less time and cost. DiscoTope 2.0 server[40] (http://www.cbs.dtu.dk/services/DiscoTope/) is one of available prediction severs for discontinuous B cell epitopes. The prediction model is based on analysis of three-dimensional structure of an input protein structure. The prediction algorithm behind DiscoTope employs propensity scores from amino acid statistics, spatial proximity information and surface accessibility profile of the protein structure to guide the determination of potential epitope region. The prediction correlates well with available accessible surface profile from virus like particle database (http://viperdb.scripps.edu/)[41] (**Figure 2.10** and **Figure 2.11**).

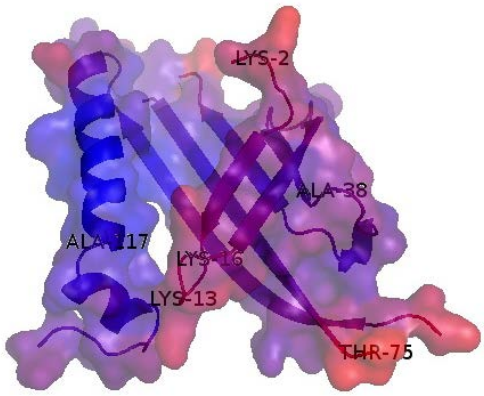

Figure 2.10: Discontinuous B cell epitope prediction by DiscoTope 2.0 server[40] showing in electron cloud surface is overlaid over 3D structure of Qβ capsid protein. The red areas represent protein fragments that obtain high scores from the prediction.

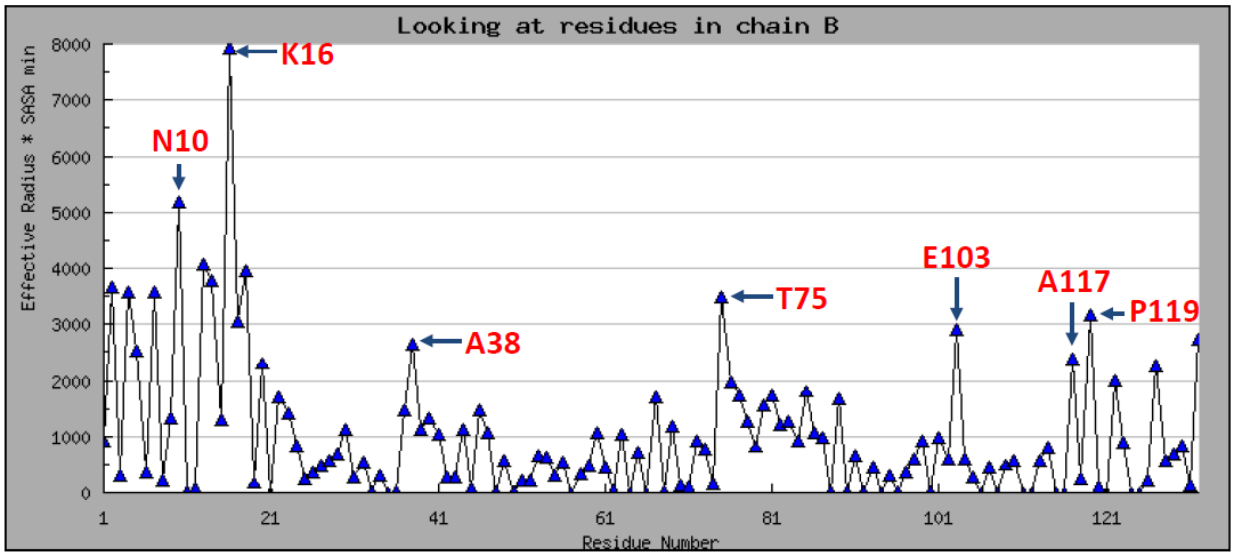

Figure 2.11: A graph showing solvent accessible surface area (SASA) of each amino acid residue in representative chain B of Qβ capsid protein (1qbe). The figure and data were obtained from VIPERdb (http://viperdb.scripps.edu).[41]

Since our strategy for reducing anti-carrier antibody response is based on structural modification to block the interactions between B cell epitopes and B cell receptors, selected amino acid residues in the protein sequence were subjected to site-specific mutations to lysine in order to introduce both structural change and new conjugation site for an antigen of interest to

additionally block the recognition by B cell receptors. In contrast to polymers or synthetic inorganic nanoparticles, a single change of the viral capsid protein by the site-specific mutation can distribute the structural change evenly over all identical 180 subunits and the display pattern can be controlled completely and precisely over the capsid surface.

In addition to the prediction, the selection of a potential amino acid for the modification is also based on following criteria: 1) the amino acid needs to be exposed well on the surface as the highly accessible residue is more likely to interact with BCR; 2) it should not be involved in inter-subunit interaction as the change may disrupt the self-assembly ability of the protein; 3) the amino acid should not be in part of Th epitopes to avoid reduction of Th activation.

Regarding the first criteria, the well-exposed residues can be determined by the solvent accessible surface area (SASA) from the available data mentioned above (**Figure 2.11**). The amino acid residues that are found to be critical for self-assembly of the capsid were collected from literature reports[7a, 42] (**Table 2.2** and **Table 2.3**). The potential Th epitopes of Qβ have been reported[22] and mentioned earlier in the introduction (**Figure 2.3**).

Table 2.2: Qβ mutants reported that assemble to form the capsid.

entry	**Mutation(s)**	**category**	**Yield(mg/L)**	**T_m (°C)**
1	WT	-	++	83.3
2[42a]	K16M	exterior charge/reactive site	na	na
3[42a]	T93M	internal reactive site	na	na
3[42b]	D14R	exterior charge	-	na
4[42b]	N10R	exterior charge	++	na
5[42b]	T18R	exterior charge	++	na
6[42b]	D14R/T18R	exterior charge	-	unstable

Table 2.2: (Cont'd)

entry	Mutation(s)	category	Yield(mg/L)	T_m (°C)
7[7a]	C74S	Remove disulfide	+	61.7
8[7a]	C74S/C80S	Remove disulfide	++	61
9[7a]	Y62F	Interdimer H-bond	+	82.8
10[7a]	D81N	Interdimer salt bridge	++	78.7
11[7a]	Q65H	RNA binding	++	78.6
12[7a]	D91N	RNA binding	+	79.4
13[7a]	Q65H/D91N	RNA binding	+	81.6
14[7a]	Y62F/C74S/C80S	combination	++	60.4
15[7a]	D81N/C74S/C80S	combination	++	62
16[7a]	Q65H/C74S	combination	+	60.7
17[7a]	D91N/C74S	combination	+	62.1
18[7a]	Q65H/D91N/C74S	combination	++	61.4
19[7a]	Y62R	interdimer H-bond	+	67.3
20[7a]	Y62W	Trp replace	+	77.0
21[7a]	Y99W	Trp replace	+	74.8
22[7a]	Y132W	*C-term.*Trp replace	+	80.9
23[7a]	L35W	Trp replace	++	72.2
24[7a]	P23A	structure	-	73.8
25[7a]	K2Q	exterior charge	++	74.5
26[7a]	K13Q/K16Q	exterior charge	++	75.6
27[7a]	A1S	conjugation handle	+	73.9
28[43]	K13E	exterior charge	na	na
29[43]	K13Q	exterior charge	na	na
30[43]	K16E	exterior charge	na	na
31[43]	K16Q	exterior charge	na	na
32[43]	K16F	exterior charge	na	na

Table 2.2: (Cont'd)

entry	Mutation(s)	category	Yield(mg/L)	T_m (°C)
33[43]	K16Y	exterior charge	na	na
34[43]	K46Q	exterior charge	na	na
35[43]	K13Q/K16Q	exterior charge	na	na

Note: Yield ++ : >80 mg/L, + : >20-80 mg/L, –: <20 mg/L, na : not applicable

Table 2.3: Qβ mutants that fail to assemble into the VLP.

Entry	Mutation(s)
1[42b]	WT_*C*-$R_{2,5,8}$
2[42b]	WT_*C*-$G_{2,5}R_{2,5,8}$
3[42b]	$D^{14}GKQT^{18}$ to R_5^{14-18}
4[a]	N10R/T18R
5[7a]	K2E
6[7a]	L8W
7[7a]	L19W
8[7a]	L35G, L35H, L35A, L35V
9[7a]	Y62E
10[7a]	C74H
11[7a]	C80H

Entry	Mutation(s)
12[7a]	R86W
13[7a]	F94H, F94L, F94W
14[7a]	F96H, F96W
15[7a]	E104Q
16[7a]	E111Q
17[7a]	L128W
18[7a]	C74S/V108I
19[43]	K46E
20[43]	K13E/K16E
21[43]	K2Q/K46Q
22[43]	K2Q/K13Q/K16Q

Note: WT_*C*-$R_{2,5,8}$ = mQβ with C terminal peptide extensions of polyarginine composed of 2, 5 and 8 arginine subunits, respectively. WT_*C*-$G_{2,5}R_{2,5,8}$ = mQβ with C terminal peptide extensions of the polyarginine with polyglycine linker composed of 2 and 5 glycine subunits, respectively. $D^{14}GKQT^{18}$ to R_5^{14-18} = mQβ, where the native peptide fragment $D^{14}GKQT^{18}$ is replaced by polyarginine of 5 arginine subunits.

Based on the prediction and the criteria mentioned above, threonine at position 7 (T7), asparagine at position 10 (N10), alanine at position 38 (A38), threonine at position at 75 (T75), glutamic acid at position 103 (E103), alanine at position 117 (A117) and proline at 119 (P119)

were assigned as potential amino acid residues for the modification. Although E103, A117 and P119 are on the region of the potential Th epitope determined by EPIMAX analysis[22] (**Figure 2.2** and **Figure 2.3**), they are expected not to disrupt the Th epitope sequence as they are located close to the end of the determined region and it would be interesting to find out if they are crucial for the immunogenicity of the carrier. (Please note that the known Th epitopes were elucidated from BALB/c mouse in which MHC class II alleles (H-2^d) in TCR differs from those in C57BL/6 mouse (H-2^b).[44] Therefore, the known Th epitopes may not necessarily represent the epitope for C57BL/6 mouse, the animal model in our study.)

The residues were modified genetically by site-specific mutagenesis. Each of the mutated plasmids was transformed into a bacteria vector for the viral capsid protein expression. All expressed mutated proteins, except E103K, were found to assemble to form viral capsids. The characteristic properties of the Qβ mutants are summarized as in **Table 2.4**.

Table 2.4: Physical characteristics of Qβ mutants.

Qβ Mutants	**Yield(**mg/L**)**	**SEC rv. (**mL**)**	**Z-Ave (**d.nm**)**	**PDI**	**Zeta potential**
WT	60	11.7	28.79	0.046	-2.89
T7K	10	11.8	29.00	0.278	-1.08
N10K	12	11.7	28.72	0.192	-1.90
A38K	16	12.7	26.58	0.083	-1.43
T75K	25	12.0	29.02	0.096	-1.64
A117K	31	12.1	29.73	0.187	-1.54
P119K	22	12.1	29.72	0.070	-2.00
A40C/D102C	38	11.8	29.06	0.031	-1.67
A38K/A40C/D102C	26	12.6	27.55	0.028	-1.55
A40S/D102S	20	12.0	27.82	0.028	-1.37
A40C/D102C/K13R	15	11.9	28.86	0.119	-1.97

Since the Qβ capsid is composed of 180 subunits, a small local change of an amino acid could dramatically alter the global charge of the capsid. The mutation of the native amino acids to lysine in all mutants makes the surface charge of the mutant capsids more positive as assessed by Zeta potential (**Table 2.4**) and non-denaturing agarose gel (Figure 2.12**:**). In non-denaturing agarose gel, all mutants moved towards the cathode indicating higher positive surface charge of the mutants compared with wtQβ, which moved towards the anode. The positive charge of the mutants is supposedly to be derived from the new lysine from the mutation as the positive charge was neutralized after the conjugation reaction of surface lysines with NHS-Tn **1**. This change in the surface charge after mutation could be another evidence to support that the amino group in the side chain of the non-native lysine is exposed on the external surface, which could provide extra conjugation site for the antigen for epitope shielding in an anticipated mutation point. Prasuhn and coworkers have investigated the effect of positive charges on Qβ on plasma clearance rate.[42a] They found that the high surface positive charge of Qβ slowed down the plasma clearance rate. The change in the surface charge in our Qβ mutants would allow longer plasma circulation time, which would increase the chance of maintaining sufficient amount of the injected vaccine for immune activation. Moreover, the longer plasma circulation time will also help minimize the dose in vaccination and in therapeutic drug delivery. It should be noted that mQβ(T7K) and mQβ(N10K) are the most positively charged mutants, probably because these residues are located in the most exposed area, which would alter the surface charge the most. However, the surface charge of mQβ(T75K) is the least altered. This may be because this lysine is only partially solvent exposed.

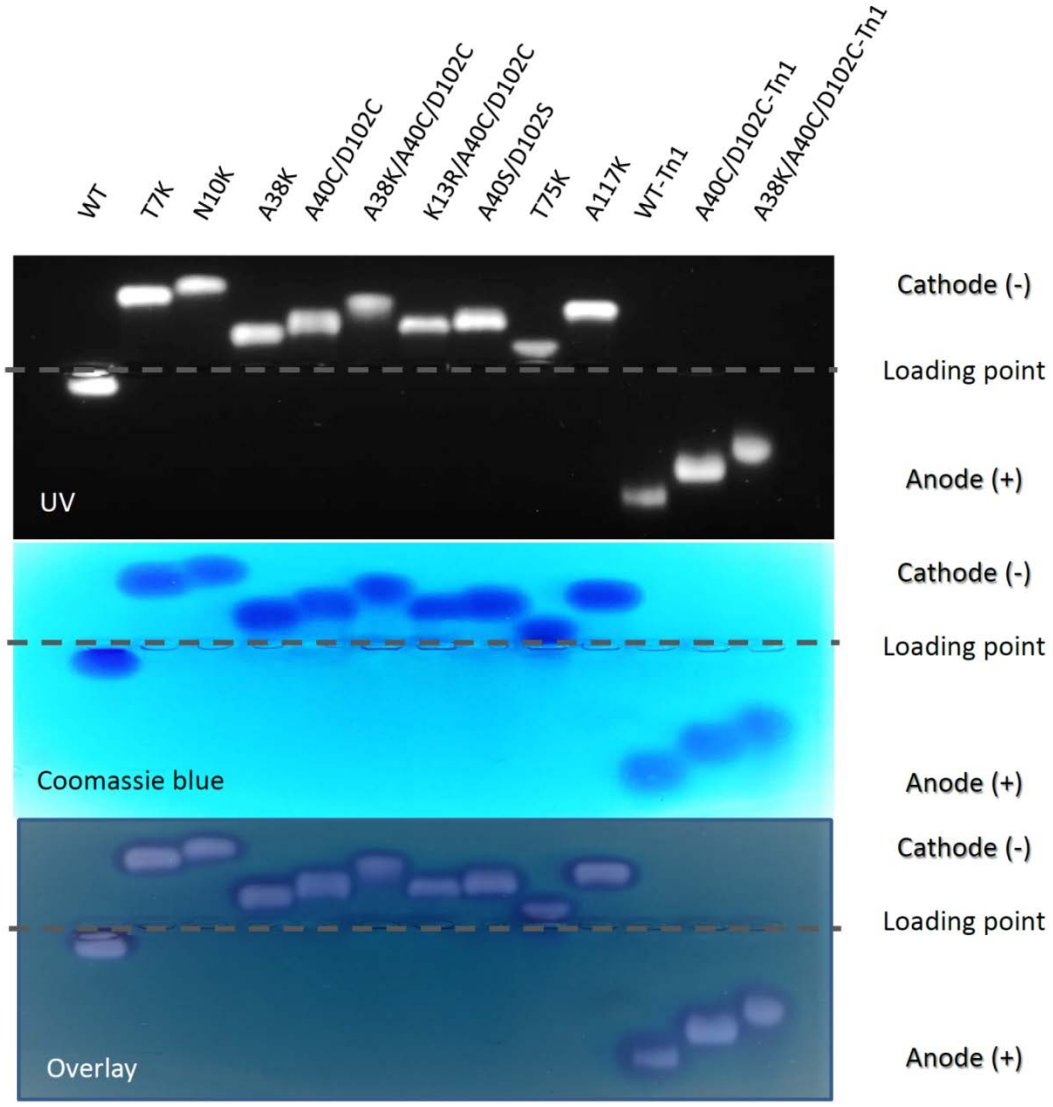

Figure 2.12: Electrophoretic mobility of Qβ whole capsids by native agarose gel. The samples (~30 μg of each capsid protein) were loaded into 0.7% agarose gel in PBS with SYBR Safe DNA gel strain as a straining reagent for the encapsulated RNA. The electrophoresis was performed in TEA buffer at 4°C for 4 hours. *Top panel*) The encapsulated RNA strained in the capsids was detected by UV light. *Middle panel*) The capsid proteins were detected by Coomassie staining. *Bottom panel*) Overlaying the two panels confirms the presence of the encapsulated RNA in the mQβs.

Although the sizes of the mutant capsids are slightly different, it should be noted that the size of A38K mutant is noticeably smaller than other mutants (**Table 2.4**, **Figure 2.14**). This is probably because A38 is located in the domain found to have an influence on the arrangement

between subunits.[7a] Therefore, a change in this residue may alter subunit organization, thus, change in the capsid size. X-ray crystallography analysis suggests the difference in space group of A38K mutant compared with wild-type Qβ. A38K mutant has space group I23 and contains 5 chains in an asymmetric unit, but the wild-type Qβ has space group R3 and contains 20 chains in an asymmetric unit. Although both structures can closely superimpose with each other, the re-construction of the full capsid from the repeating units by respective symmetry operations failed to provide the full capsid of A38K mutant. (Data is not shown) (The X-ray crystal structure analysis was done by kind help from Dr. Xiangshu Jin.) Fiedler and coworkers reported that changing nearby leucine residue at position 35 to tryptophan or phenylalanine (L35W, L35F) reduces the capsid size of Qβ from diameter of 28 nm down to 21 nm.[7a] Since L35 and A38 are located in the same domain that involves the inter-subunit organization to cause difference in the capsid size, it is of interest for study of manipulation of this domain to control the size of the viral capsid. Such controllable size of the capsid would allow us to investigate the effect of size on immunization profile and drug delivery efficiency. Moreover, the slightly change in size will also allow the fine-tuning of antigen display pattern of the VLP, which play crucial role in antigen cluttering for B cell activation.

2.2.2 Improve stability of Qβ VLP

The distinct inter-subunit disulfide bonds in Qβ viral capsid provide exceptionally high stability to the construct over other viral capsids from the same family.[7a] For example, MS2 VLP has a melting temperature (Tm) about 66°C[45], while Qβ has Tm up to 83°C[7a]. Despite its high stability, changing amino acids may alter the structural conformation of the protein folding leading to decreased stability of the capsid as shown in many cases reported in the literature (**Table 2.2**).[7a] The low stability of the capsid may not endure harsh condition in conjugation

process involving organic solvents and reagents. Moreover, the less stable carrier may alter the fate of the vaccine contents delivered into the immune system, which potentially reduce the efficiency of the vaccine.[46] For instance, the early degradation may expose inner B cell epitope(s), or lose the particulate characteristic of the particle, which is crucial for inducing strong immune responses. The self-assembled structure of the viral capsid was therefore engineered to strengthen the stability of the capsid to accommodate structural modification and rigorous condition in conjugate reaction. The rational design is based on additional disulfide bonds to reinforce the covalent network between the subunits in the capsid construct. An amino acid pair, in which each of them is from adjacent subunits but brought in spatial proximity in 3D structure to potentially form a disulfide bond after being mutated into cysteine, was searched by Disulfide by Design 2.0 web-based modeling software[47] (DbD, http://cptweb.cpt.wayne.edu/DbD2/). The algorithm of the software calculates the predicted potential of a candidate amino acid pair as B-factor, the higher B-factor, the higher the potential to form disulfide bond that can increase stability of the protein complex. From the prediction, an amino acid pair of A40 and D102 gives the highest B-factor. The proximity (≈ 4 Å) of the beta carbons in the side chain of A40 and D102 was confirmed by 3D structure (**Figure 2.13**). We, therefore, mutated these two amino acids to cysteines to determine the ability of the mutant capsid protein to form additional disulfide bonds for increased capsid stability. The result showed that the mutant A40C/D102C can assemble to form the capsid similar to wtQβ as determined by size and shape from SEC (blue line vs red line in **Figure 2.14a**, DLS (**Table 2.4**), and TEM, respectively (**Figure 2.14b**).

a)

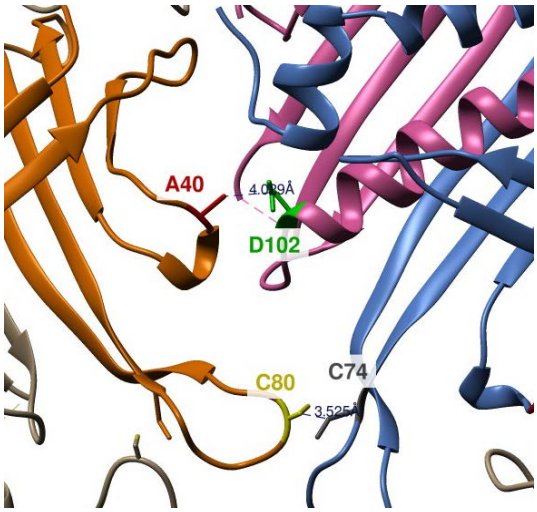

b)

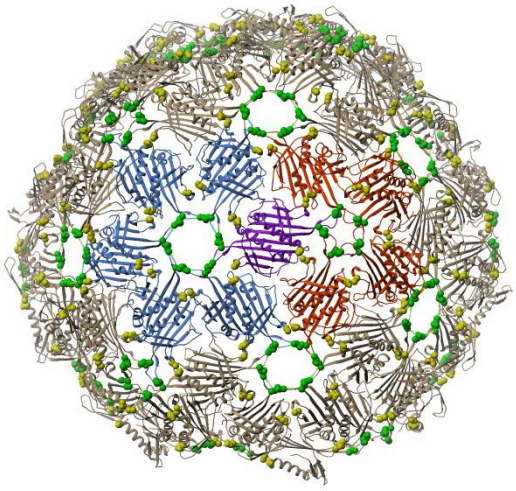

Figure 2.13: X-ray crystal structure of wtQβ showing a) distances between β-carbon of residues involving disulfide formation; b) disulfide bond networks from native disulfide bonds between C74 and C80 (green residues) in wtQβ and expected non-native disulfide bonds in mQβ A40C/D102C (yellow residues).

a)

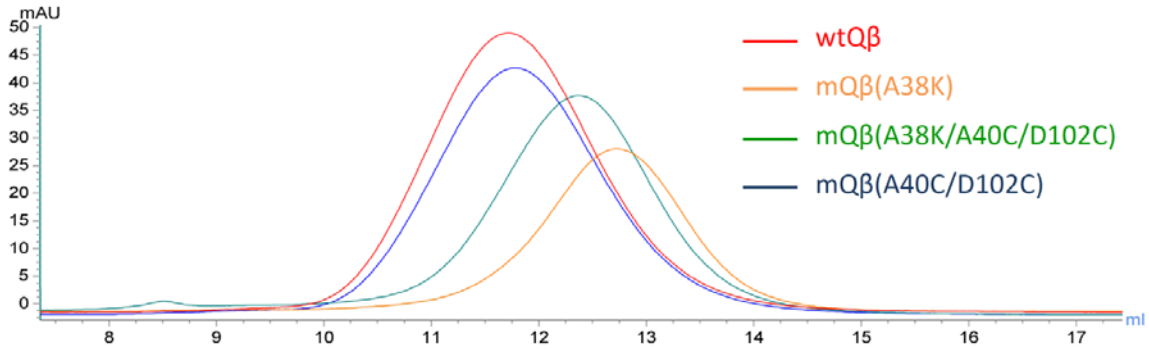

Figure 2.14: a) Size exclusion chromatograms of wtQβ (red) and mQβs, A38K(yellow), A38K/A40C/A102C (green), A40C/D102C (blue); b) TEM images of wtQβ and mQβs.

Figure 2.14: (Cont'd)

b)

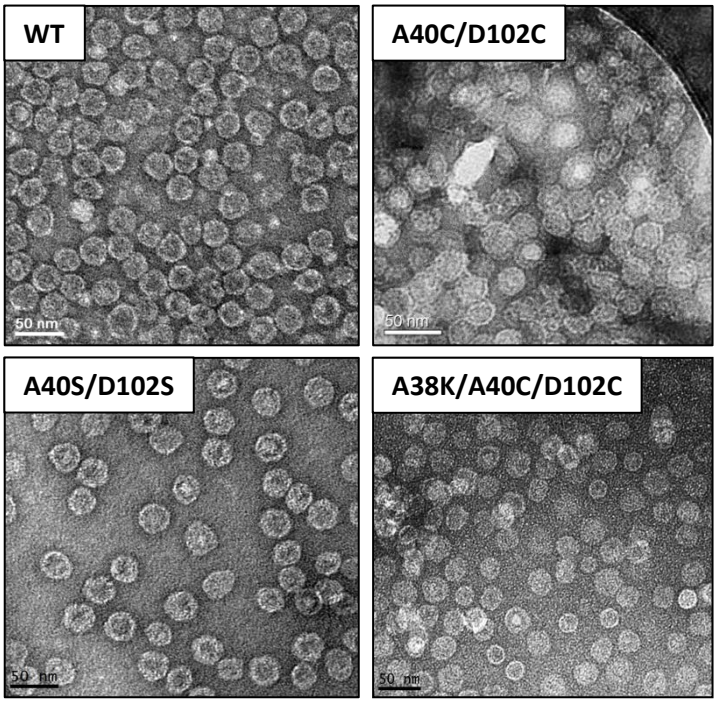

The formation of the additional disulfide bonds in mQβ(A40C/D102C) was confirmed by non-reducing SDS-PAGE (**Figure 2.15**). Any mQβs involving A40C/D102C mutation showed multimeric protein bands, while other mQβs including mQβ(A40S/D102S), which is chemically equivalent but unable to form the disulfide bonds, showed similar band pattern as wtQβ (**Figure 2.15b**).

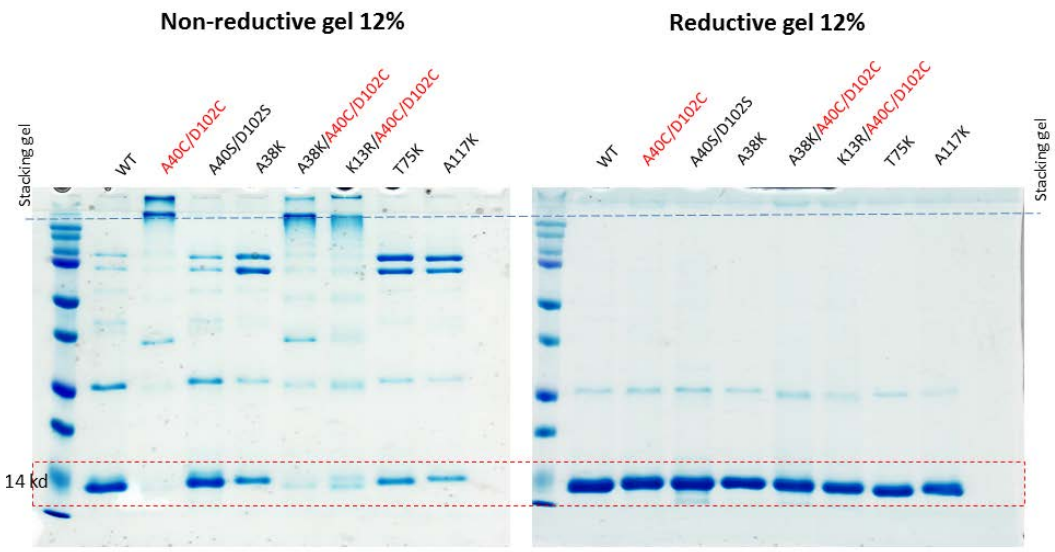

Figure 2.15: a) SDS-PAGE of the viral capsids in non-reductive (oxidative) condition (Left) and reductive condition (right).

From the thermal stability measurements, the addition of non-native disulfide bond was found to improve the stability of the capsid (**Figure 2.16**). The increased stability derived from the non-native disulfide bonds was supported by the decreased stability of mQβ(A40S/D102S) (**Figure 2.16** *middle*). The structural change in mQβ(A38K) was found to decrease the stability of the capsid. This is probably because A38K is involved in interaction between subunit as seen in the effect of the alteration of this point on the capsid size. However, the addition of non-native disulfide bonds can help strengthen the stability of the capsid up close to that of wtQβ as shown by the increased thermal stability of mQβ(A38K/A40C/D102C) (**Figure 2.16** *bottom*).

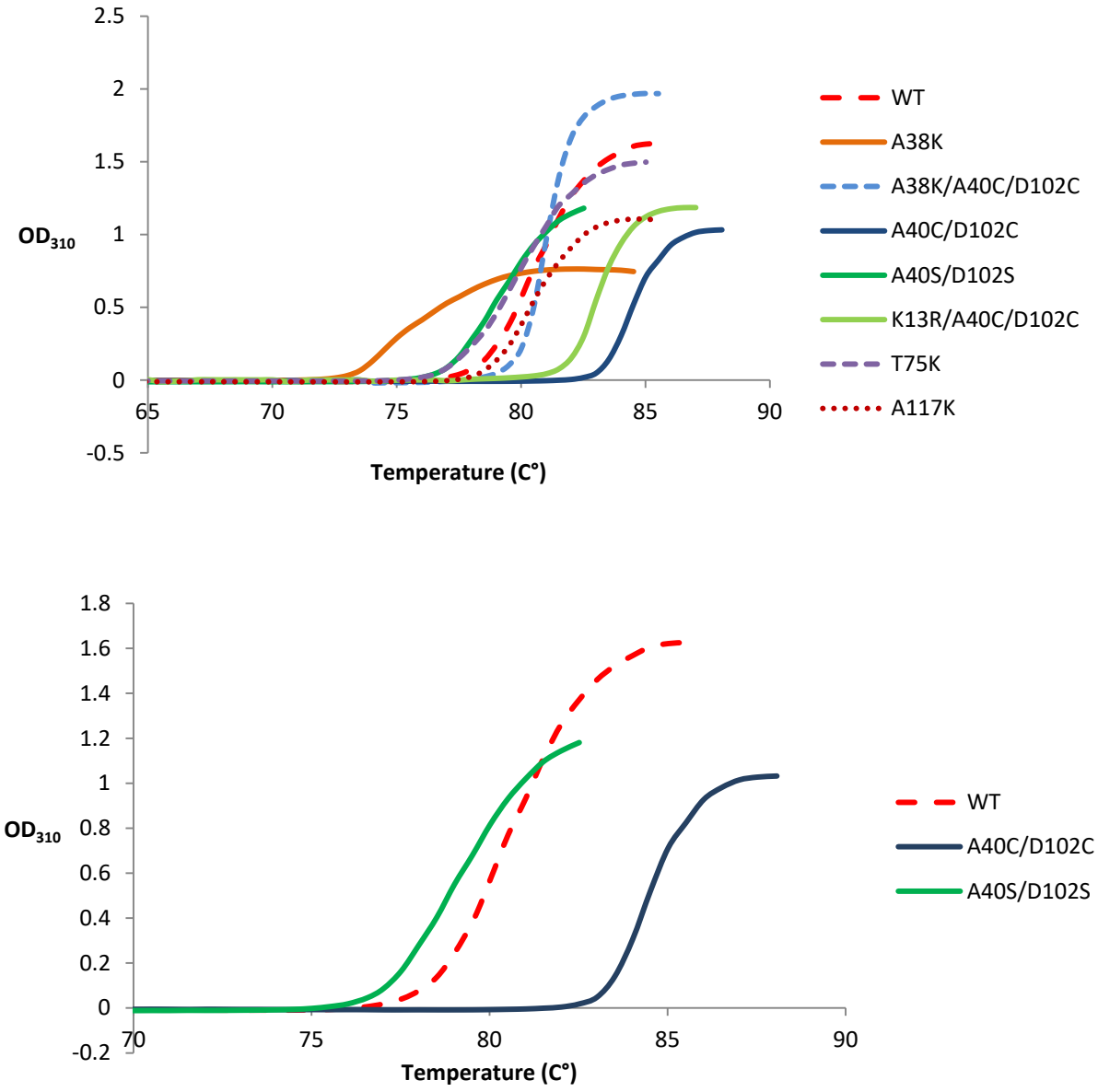

Figure 2.16: Thermal stability of mQβs determined by UV absorption at λ = 310 nm at increasing temperature.

Figure 2.16: (Cont'd)

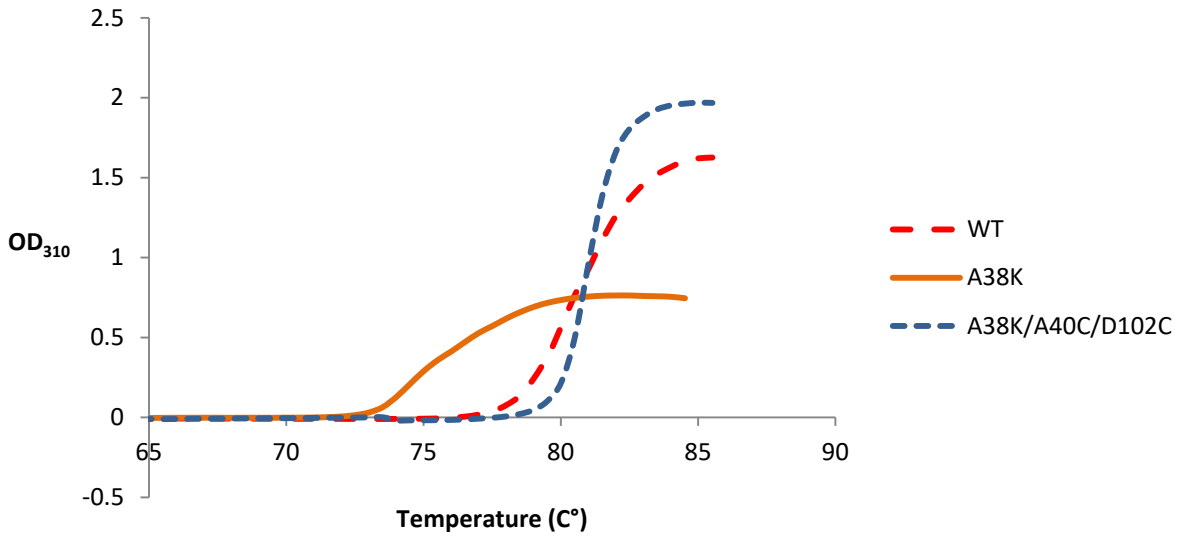

Although the impact of non-covalent interactions between the interdimer residues on the stability of Qβ VLP has been intensively studied by Fiedler and coworkers[7a], the additional stability due to non-native di-sulfide bond between subunits had not been observed before. This enhanced stability would confer flexibility in engineering and applications of this type of protein particle.

To assess the potency of mQβ in inducing immunity against either TACA or the carriers themselves, a prototypical TACA, **Tn1** (**Figure 2.17**, see experimental **section 2.5.15** for the synthesis), were immobilized on the surface of mQβs via amide formation between amino groups of exposed lysines and NHS group of **NHS-Tn1** (Figure 2.17). LCMS together with data processing with maximum entropy deconvolution algorithm (MaxEnt1)[48] was used to determine the number of **Tn1** on each capsid, as we found this method gave comparable results to Microfluidic capillary gel electrophoresis analysis[49], yet with more quantitative information and convenience (details for the method are included in experimental section).

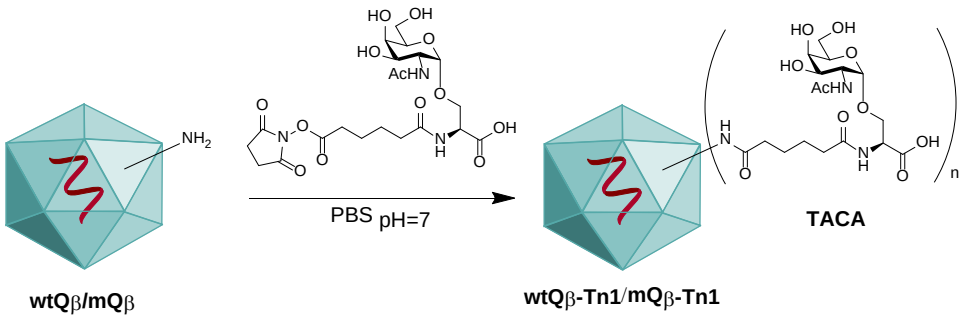

Figure 2.17: Conjugation reaction between **NHS-Tn1** with the various mQβs.

Table 2.5: The average number of Tn1 conjugated on each capsid of Qβ particle and yield of Qβ-Tn1 conjugate. [% add^{n} Tn = (Tn1/subunit$_{mQβ}$ − Tn1/subunit$_{wtQβ}$) × 100 / Tn1/subunit$_{wtQβ}$]

Qβs	**Tn1/Qβ**	**Tn1/subunit**	**%add^{n} Tn**	**Yield (%)**
WT	332	1.84	0	73
T7K	423	2.35	28	89
N10K	402	2.23	21	69
A38K	410	2.27	23	73
A38K/A40C/D102C	498	2.77	51	64
A40C/D102C	436	2.42	32	57
A40S/D102S	410	2.33	27	66
K13R/A40C/D102C	328	1.82	-1	79
A75K	447	2.48	34	72
A117K	390	2.16	17	77
P119K	394	2.19	19	73

Table 2.6: Physical characteristics of Qβ-Tn1 conjugates.

Qβ-Tn1 conjugates	**SEC rv. (**mL**)**	**Z-Ave (**d.nm**)**	**PDI**
WT-Tn1	11.7	29.62	0.086
T7K-Tn1	11.6	29.35	0.025
N10K-Tn1	11.6	28.82	0.063
A38K-Tn1	12.6	26.82	0.028
T75K-Tn1	11.8	31.66	0.110
A117K-Tn1	11.9	30.77	0.105
P119K-Tn1	11.9	31.87	0.169
A40C/D102C-Tn1	11.6	29.37	0.072
A38K/A40C/D102C-Tn1	12.4	27.61	0.024

From the average number of the conjugated Tn1 on each capsid of mQβ, it was surprising that despite no additional lysine added into the mQβ(A40C/D102C), the average number of Tn1 per Qβ is as high as other mQβs with an additional lysine. After comprehensive analysis of the structure affected by the residue changes, we found that there is non-covalent interaction, probably hydrogen bond (≈ 3 Å), between the carboxyl group on the side chain of D102 and the amino group on the side chain of K13 (solid blue line in **Figure 2.18**). This interaction may suppress the reactivity of the amino group in conjugation reaction. This explanation is also supported by another finding[50] that lysine 13 in the wtQβ is not reactive, as changing reactive lysine to arginine (mQβ(K13R)) did not reduce the number of conjugated molecules (fluorescein-NHS ester) compared with wtQβ. Therefore, when D102 is mutated to cysteine and its side chain no longer binds the K13 residue, the amino group in the side chain of K13 can possibly rotate out to the external surface and become more available to react with **NHS-Tn1**. This is also supported by the reduced average number of **Tn1** on mQβ(K13R/A40C/D102C)

(323Tn1/particle) when compared with mQβ(A40C/D102C) (436Tn1/particle) and mQβ(A40S/D102S) (410Tn1/particle) (**Table 2.5**).

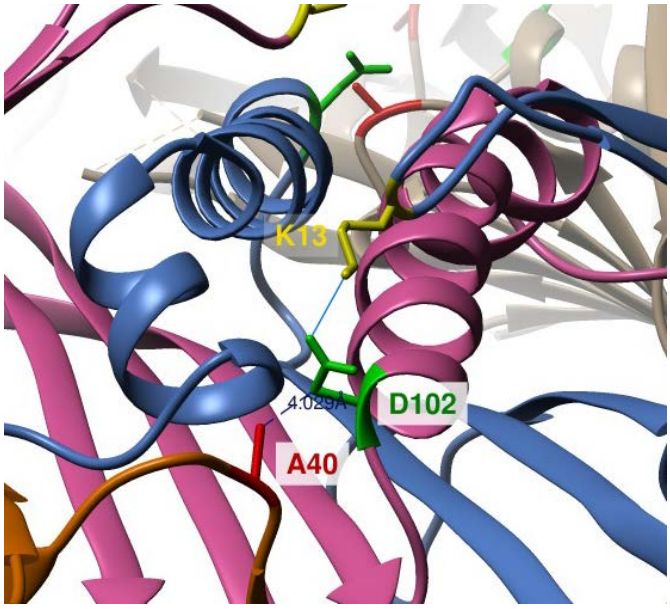

Figure 2.18: X-ray crystal structure of wtQβ showing the hydrogen bond interaction (solid blue line) between the carboxyl group on the side chain of D102 and the amino group on the side chain of K13(distance = 3.145 Å).

2.2.3 Immunization study

The ability of mQβ-Tn1 conjugates in reducing unwanted anti-carrier immune response and increasing desired anti-TACA immune response were evaluated *in vivo*. C57BL/6 female mice (n=5) were injected subcutaneously with 0.1 mL of the various mQβ-Tn1 conjugates as emulsion with complete Freund's adjuvant (CFA) for prime injection on day 0 and with incomplete Freund's adjuvant (IFA) for boost injections on days 14 and 28. The dose for each injection was 1.93μg based on the amount of the attached Tn1. The sera from immunized mice were collected on day 35 and used to determine the induced anti-Tn or anti-mQβ antibodies titers by ELISA coated with BSA-Tn1 or mQβ. ELISA results showed that all mQβs we picked for *in*

vivo study elicited higher antibodies titers against Tn1 antigen, but lower antibodies titers against self-carriers compared with wtQβ (**Figure 2.19**). The mutant that can induce highest anti-Tn1 antibody response is mQβ(A38K/A40C/D102C). To rule out variations between ELISA analysis, the amount of elicited IgG antibodies from different groups of the study were measured based on optical density (OD_{450}) in the same ELISA plate against BSA-Tn1 and corresponding carriers at sera dilution 1/819200 and 1/1638400, respectively. The result pointed out a reverse trend of the titers of antibodies against Tn1 and mQβs, that is any vaccine that elicited low anti-carrier antibodies induced inversely proportionally high anti-Tn1 antibodies (**Figure 2.19**c,d). The higher elicited IgG2 over IgG1 in mQβs suggest T-cell dependent immune response bias towards Th1 response (**Figure 2.19**e).

These results suggested that reducing CIES of the Qβ based vaccine construct can indeed result in enhanced anti-TACA antibody response. The number of **Tn1** on each capsid seemed to play a role in increasing anti-Tn antibody response similar to what have been suggested by Bachmann group.[37] However, this is not the case for T75K and A117K mutants, as mQβ(T75K) has higher Tn1/capsid (447 versus 390 Tn1/capsid) but induced lower titer of anti-Tn1 antibodies than mQβ(A117K) (**Figure 2.19**a). Interestingly, based on the antibody titers, the potency of mQβ(A38K/A40C/D102C) in inducing anti-Tn1 antibody response seems to be as a result of a combination of potency from A38K and A40C/D102C mutants (**Figure 2.19**a). This suggested that the structural changes for suppressing CIES could be combined together in order to minimize the suppression from a carrier caused by multiple B-cell epitopes.

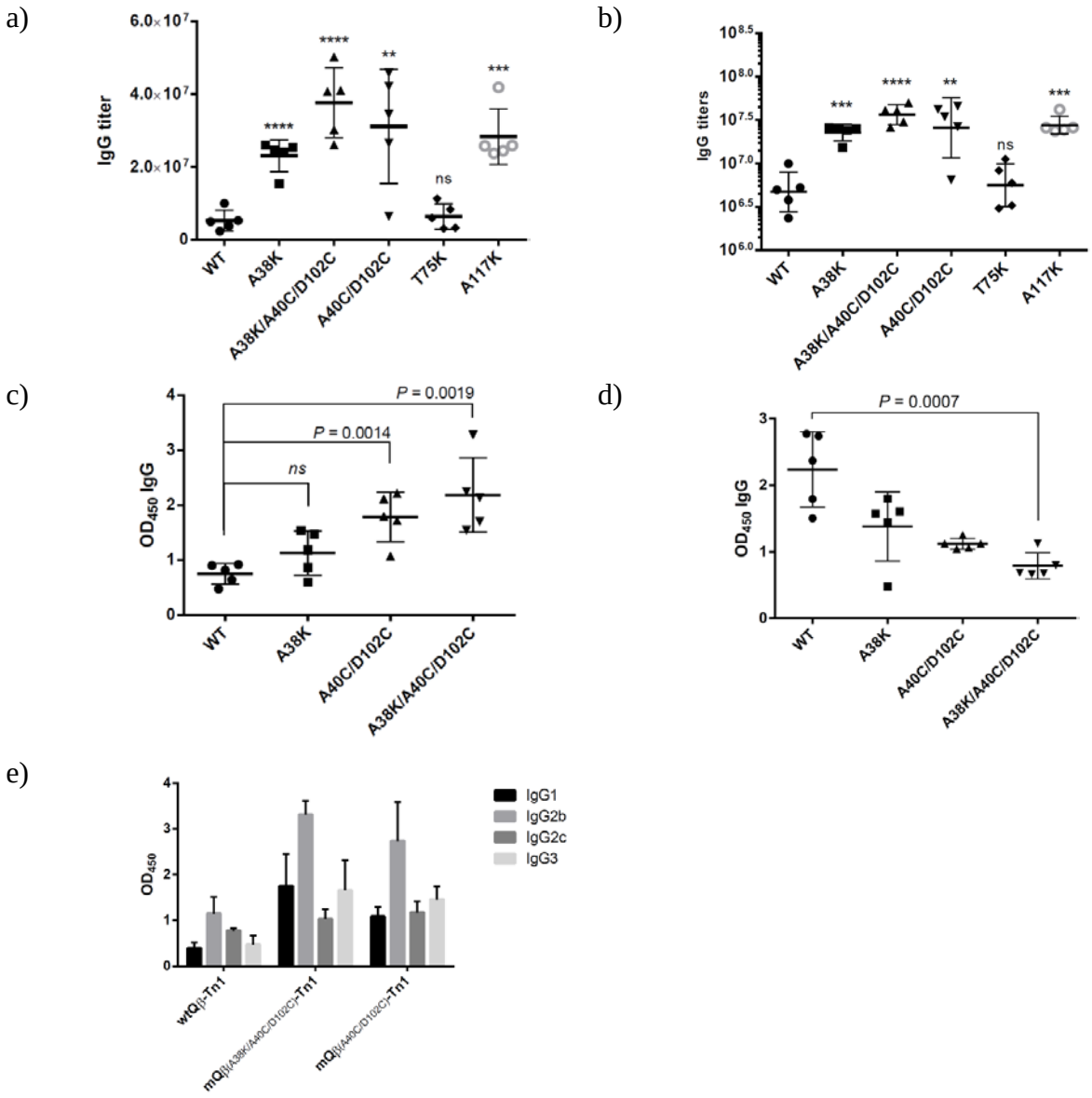

Figure 2.19: ELISA results of post-immunized sera (day 35) from groups of mice (n=5) vaccinated with variant mQβ-Tn1. a and b) Anti-Tn1 titers of the post-immunized sera presented in linear and log scale, respectively. The statistical significance of differences between a mQβ and wtQβ was determined by the Student t test (** $p < 0.01$; *** $p < 0.001$; **** $p < 0.0001$) c) OD_{450} from the ELISA result of the post-immunized sera at 1/819200 dilution against BSA-Tn1. d) OD_{450} from the ELISA result of the post-immunized sera at 1/1638400 against the corresponding carrier capsids. The statistical significance of differences between a mQβ and wtQβ was determined by the Student t test. e) OD_{450} from ELISA result at 1/819200 sera dilution of IgG subtypes antibodies (IgG1, IgG2b, IgG2c and IgG3) elicited by wtQβ-Tn1, mQβ(A38K/A40C/D102C)-Tn1 and mQβ(A40C/D102C)-Tn1 immunization against BSA-Tn1.

Since the structural change in mQβ(A40C/D102C) and mQβ(A38K/A40C/D102C) is believed to make K13 become more reactive towards **NHS-Tn1**, it is reasonable to postulate that the conjugation of **Tn1** on K13 would help together with conjugated **Tn1** on K16 to block the flexible and highly exposed loop, which is potentially a dominant B cell epitope based on the prediction. This would explain the statistically significant reduction of anti-carrier antibody response and higher anti-Tn1 antibody response in mQβ(A40C/D102C) and mQβ(A38K/A40C/D102C).

This hypothesis is also supported by analysis from a competitive ELISA. In the competitive ELISA, sera from a wtQβ-immunized mouse at dilution 1/204800 was incubated with the wtQβ, mQβ(A40C/D102C) or mQβ-Tn conjugates with different number of Tn, respectively. The mixtures of the pre-incubated sera with the corresponding Qβ were added into ELISA plate coated with wtQβ. Any viral capsid that can be recognized by anti-wtQβ antibodies will compete with the coated wtQβ for binding with the antibodies. Qβ capsids with higher binding avidity with anti-wtQβ antibodies will reduce the available antibodies binding on the plate which will result in proportionally lower OD from the analysis. Despite the fact that A40 and D102 are not highly exposed residues, the result suggested that the changes of these residues can reduce the recognition of the capsid by the antibodies, where the interaction generally involves highly exposed residues (**Figure 2.20**). The effect became more obvious with the mQβ-Tn conjugates, where the Tns could possibly conjugated to K13 and shielded the suggested B cell epitope. The lower antibody recognition of mQβ(A40C/D102C)-Tn2(560) compared with mQβ(A40C/D102C)-Tn1(436) suggested better B cell epitope shielding with higher numbers of Tn on the capsid.

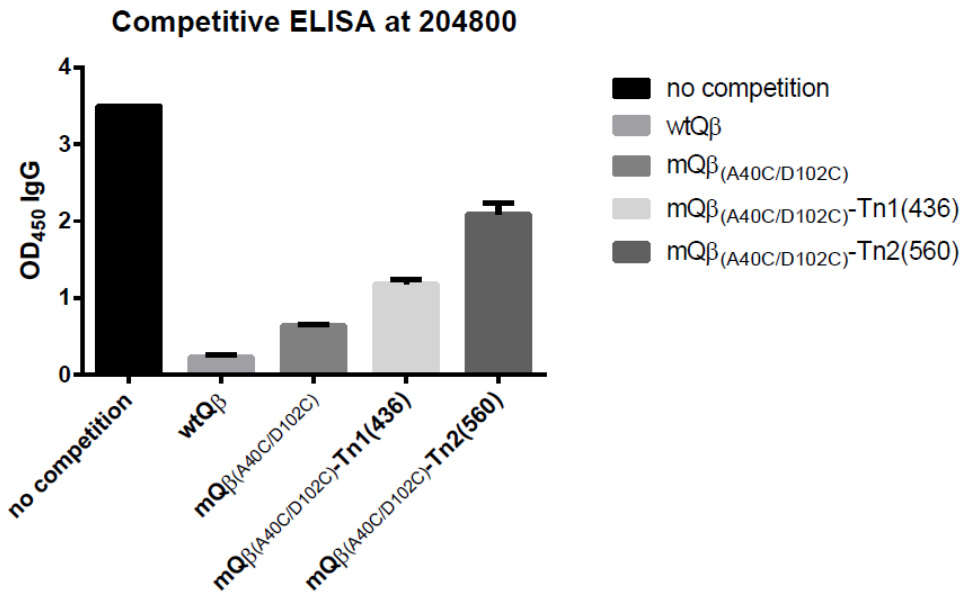

Figure 2.20: Competitive ELISA showing reduced anti-wtQβ antibody recognition of mQβ-Tn conjugates.

2.2.4 Binding of the elicited antibody against tumor cells

To test binding of sera from immunized mice against native Tn expressed on cancer cells, human lymphoma Jurkat cells were used as a model for Tn expressing cancer cells. Quantitative flow cytometry of Jurkat binding with anti-Tn mAb (Chi-Tn mAb) reportedly showed that there are average 5×10^5 Tn's expressed on each cell.[51] Although the serum from mQβ(A38K/A40C/D102C)-Tn1 immunized mice showed the highest titers, the binding of the serum on Jurkat cells was relatively weak compared with other mQβs (**Figure 2.21** left panel). This may indicate the difference in specificity or affinity of the antibodies elicited by different mQβ where the patterns of Tn display are different.

Murine mammary adenocarcinoma cell line, TA3Ha, is another Tn expressing cancer cell line commonly used in testing specific binding and *in vivo* cell growing inhibition by anti-Tn antibodies.[31c, 51-52] The flow cytometry data showed that the sera from the mQβ immunized mice

bound TA3Ha cells with affinity comparable with the binding of the sera from wtQβ immunized mice and Tn-specific mAb. The low binding of TA3Ha cells with the antibodies is probably due to the low expression level of Tn on this cell line (1.5×10^5 Tn's/cell), which was reportedly determined by quantitative flow cytometry.[51] Moreover, the loss of Tn expression during *in vitro* cell culturing could also happen as indicated by the weak binding of the anti-Tn mAb (bric111 mAb) to the cells (**Figure 2.21** right panel).

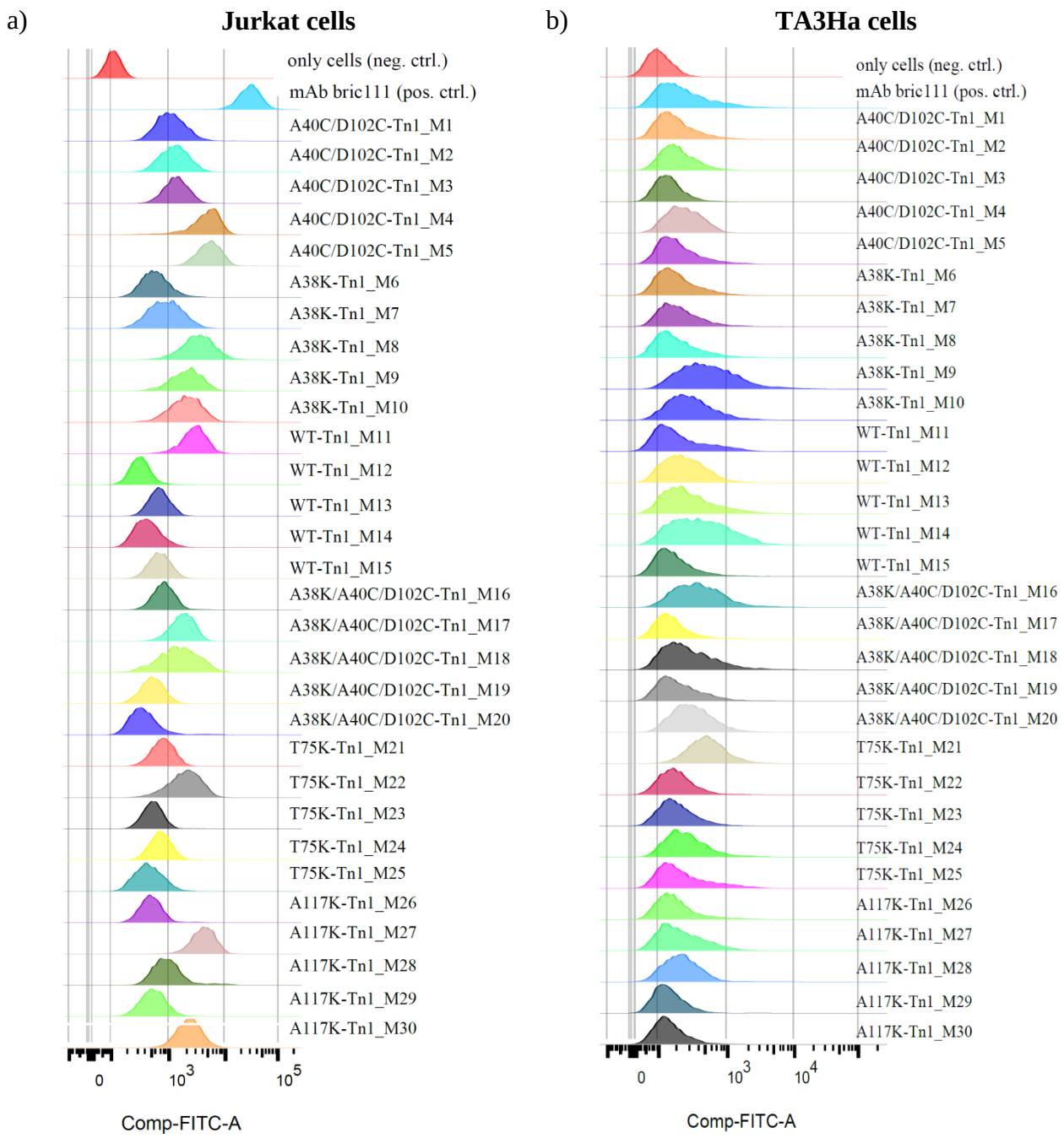

Figure 2.21: Flow cytometry showing binding of elicited IgG antibodies by Qβ conjugates; a and b) Histogram showing binding recognition of the elicited antibodies against Jurkat cells and TA3Ha cells, respectively, c and d) Graph of median fluorescent intensities of the binding recognition of the elicited antibodies towards Jurkat cells and TA3Ha cells, respectively.

Figure 2.21: (Cont'd)

c)

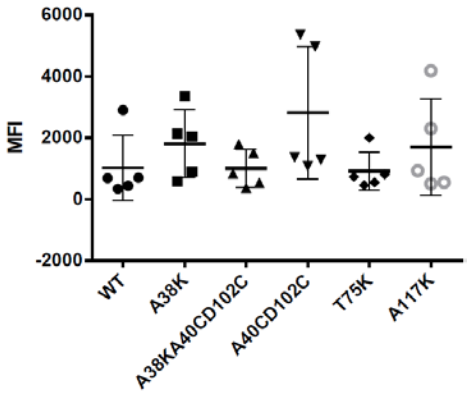

d)

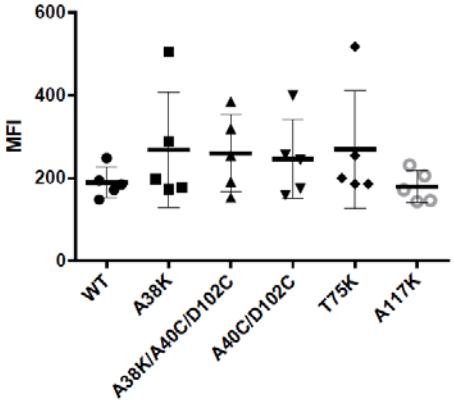

2.2.5 Tumor challenge

Due to the ease of its synthesis, **Tn1** (**Figure 2.22**a) was used as a simplest prototypical TACA in the initial immunization to find out the best mutant carrier capable of inducing highest immune response against TACA. However, in term of cancer cell binding, **Tn2** (**Figure 2.22**a) was found to be superior to **Tn1** as wtQβ-Tn2 and mQβ(A38K/A40C/D102C)-Tn2 can induce anti-TACA antibodies that bind Jurkat cells with higher affinity compared with the serum from mice immunized with wtQβ-Tn1 and mQβ(A38K/A40C/D102C)-Tn1, respectively (**Figure 2.22**b).

a)

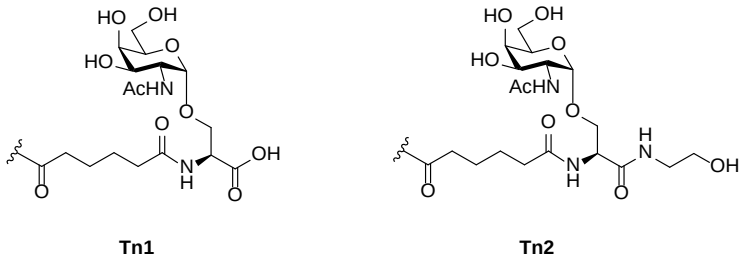

Figure 2.22: a) Chemical structures of **Tn1** and **Tn2**. b) MFI of cellular binding against Jurkat cells of the serum from mice immunized with wtQβ-Tn2 and mQβ(A38K/A40C/D102C)-Tn2 compared with those from wtQβ-Tn1 and mQβ(A38K/A40C/D102C)-Tn1.

Figure 2.22: (Cont'd)

b)

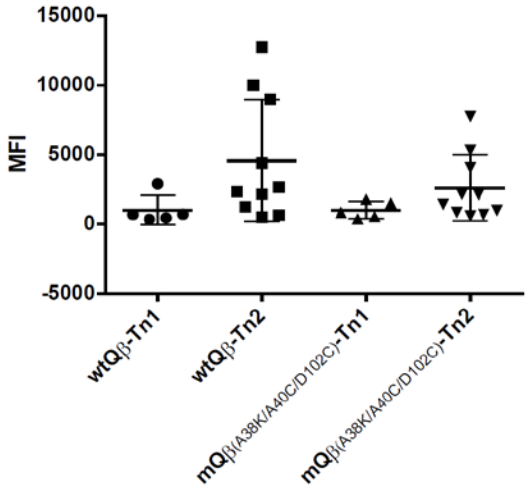

Tn2 was, therefore, chosen as a TACA in tumor challenge experiment. To rule out the factor of the antigen density on the viral capsid, the number of **Tn2** on both wtQβ and mQβ(A38K/A40C/D102C) were controlled to be equally attached on each capsid approximately 370 Tn2/particle. Groups of 10 mice were administered subcutaneously with either wtQβ-Tn2 or mQβ(A38K/A40C/D102C)-Tn2. The doses for each administration were kept constant, 1.93μg based on the amount of the attached **Tn2**. The adjuvants and schedule for vaccination were the same as those vaccinations in initial trial for mQβs. CFA and IFA were used in prime and boost injections, respectively. Mice were vaccinated in 2-week interval (day 0, 14 and 28).

Sera from the vaccinated mice were collected a week after the last injection to determine the anti-Tn antibodies titers and selective binding to the Tn-expressing tumor cells. Preliminary ELISA results showed that mQβ(A38K/A40C/D102C)-Tn2 elicited higher amount of anti-Tn IgG antibodies than the serum from mice given wtQβ-Tn2 (**Figure 2.23**). Although there was not statistical significance between groups of mice, the data suggested higher potency of the mQβ(A38K/A40C/D102C) in eliciting Tn-specific antibodies, despite the similar number of Tn attached on the viral capsid. The higher antibody response could contribute to the structural

change of the B cell epitope due to mutation. However, it is reasonable to expect that the higher density of the antigen would better shield the carrier's B cell epitope, resulting in lower CIES, hence even higher titers of anti-Tn antibodies.

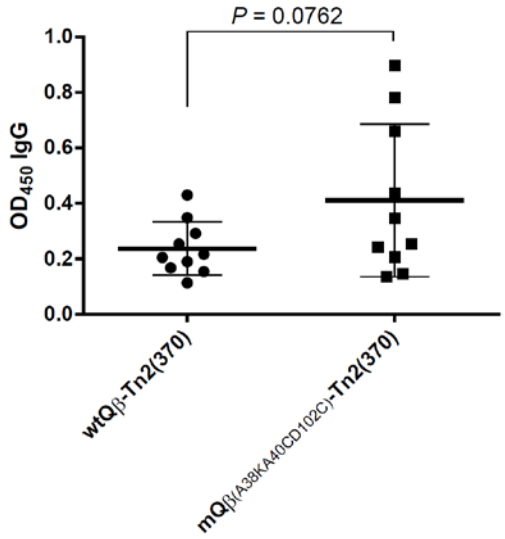

Figure 2.23: OD_{450} from the ELISA result of the post-immunized sera at 1/819200 dilution against BSA-Tn2 from mice immunized with wtQβ-Tn2 and mQβ(A38K/A40C/D102C)-Tn2. The statistical significance of differences was determined by the Student t test.

For tumor challenge, murine mammary adenocarcinoma cell line, TA3Ha, was used as a Tn expressed xenograft cancer model. The model has been used in many investigations of Tn-based cancer vaccines.[31c, 51-52, 53] This cell line was grown by passage on A/J mice to minimize the loss of Tn expression overtime caused by in vitro culture. Two groups of mice were immunized following previously described procedure with wtQβ-Tn2 and mQβ(A38K/A40C/D102C)-Tn2, respectively. The immunization was done on day -36, -22 and -8 before the tumor challenge. On day 0 (after blood collection), 5000 cells of TA3Ha cells were injected intraperitoneally into all mice. A day after (day 1), cyclophosphamide (CP) at a dose of 50 mg/kg was injected intraperitoneally. The survival of all mice was monitored from the day CP was given (day 1) till day 30. The protective efficacies of wtQβ-Tn2 and

mQβ(A38K/A40C/D102C)-Tn2 were compared by Kaplan-Meier survival curves. There was not statistically difference in the binding of the induced antibodies from both vaccines against TA3Ha cells (**Figure 2.24**). Although the difference is not statistically significant, the mQβ showed higher survival rate of the challenged mice compared with wtQβ (**Figure 2.25**) (Control experiments have been done in reference[36].) To investigate immune protection against tumor recurrence due to immune memory after tumor challenge, group of five mice surviving the first tumor challenge were rechallenged with 5,000 TA3Ha cells without further vaccination and administration of CP. All mice immunized with the mQβ-Tn2 conjugates survived from the second tumor challenge for 30 days. This suggested protection against tumor recurrence of immune memory in the immunized mice.

a) **TA3Ha cells**

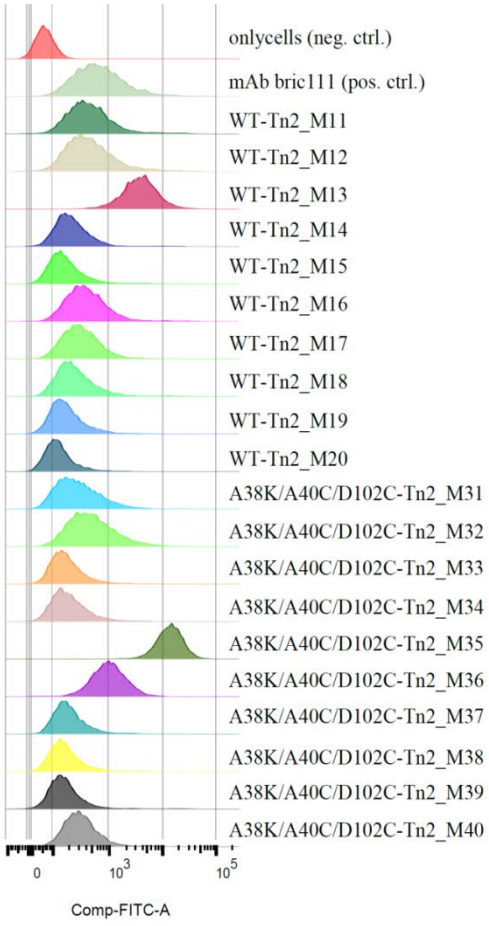

b)

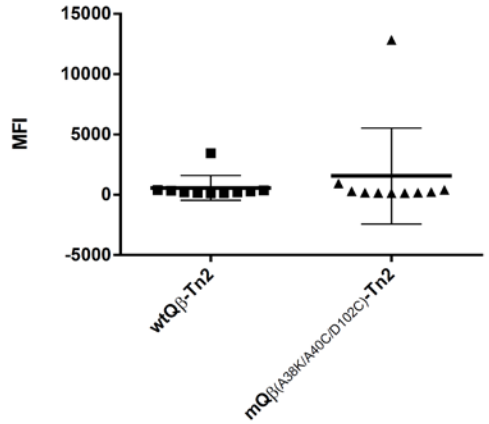

Figure 2.24: Flow cytometry showing binding of elicited IgG antibodies by wtQβ-Tn2 and mQβ(A38K/A40C/D102C)-Tn2 a) Histogram showing binding recognition of the elicited antibodies against TA3Ha cells, respectively, b) Graph comparing median fluorescent intensities of the binding recognition of the elicited antibodies towards TA3Ha cells.

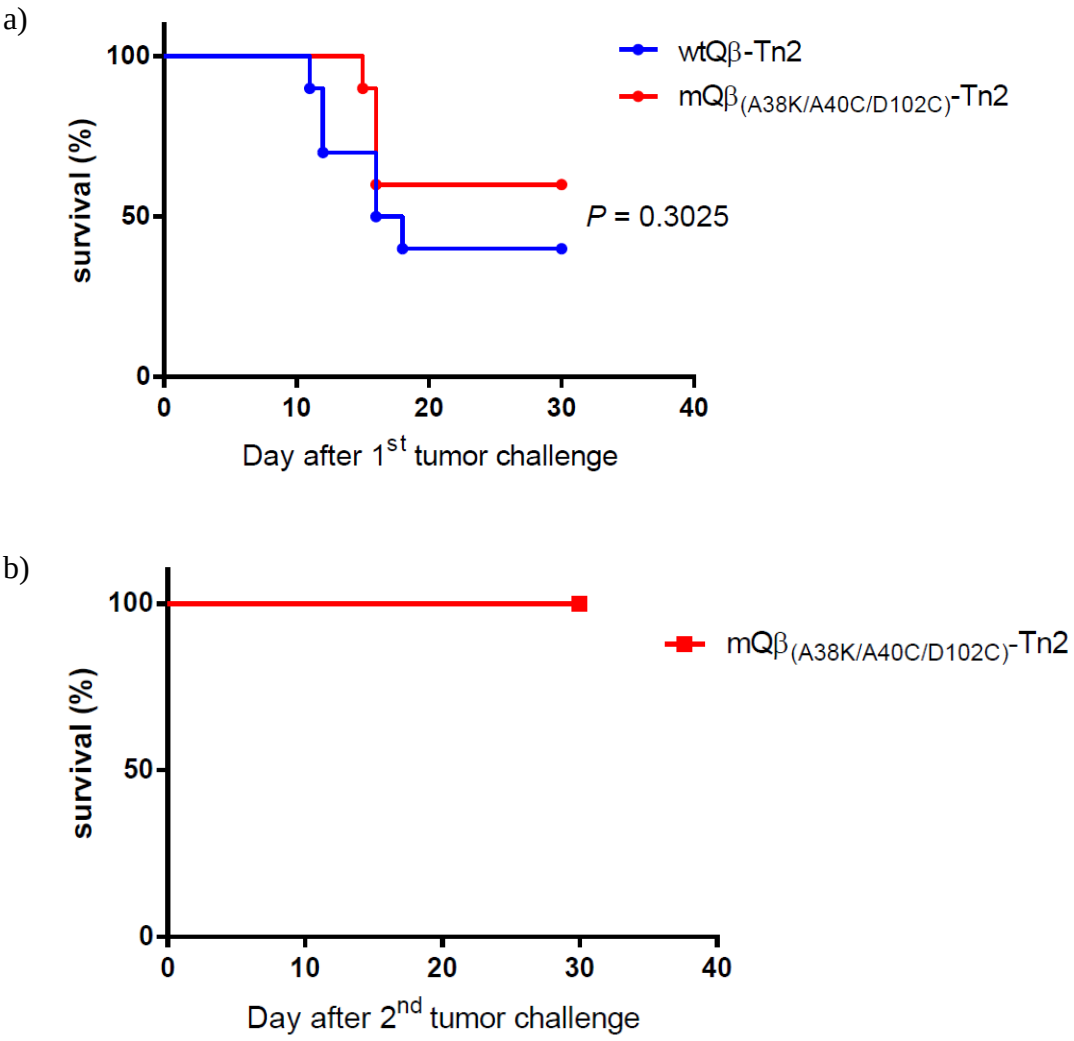

Figure 2.25: Kaplan-Meier survival curves comparing the protective effect of wtQβ-Tn2 and mQβ(A38K/A40C/D102C)-Tn2: a) after 1st tumor challenge with treatment of CP (n=10), b) after 2nd tumor challenge without any further treatment (n=5). Statistical analysis of survival is determined by using the log-rank test in GraphPad Prism software. Note: Control experiments have been done in reference[36].

2.3 Conclusions

Bacteriophage Qβ has been demonstrated as a promising immunogenic carrier able to break self-tolerance to induce strong antibody response against TACA.[35] Carrier-induced epitopic suppression (CIES) due to its strong immunogenicity is potentially problematic for VLP

based vaccine, which limits the full potential of this type of carrier in inducing maximum desired immune response against TACA.[37]

From the results presented in this study, the carrier-induced epitopic suppression (CIES) of Qβ VLP can be addressed by engineering the viral capsid to block the recognition of the B cell epitopes by B cell receptors. Non-native disulfide bonds introduced into the capsid were found to not only enhance the stability of the engineered capsids, but also induce structural change to allow the conjugated antigen to shield the B cell epitope. Our results showed that reducing the unwanted anti-carrier immune response of the mQβs can enhance the wanted titers of antibodies against TACA. The approaches presented in this study provide a fundamental implication for rational design of engineered VLP-based carrier to maximize the potency of vaccines targeting TACA expressing cancers as well as other diseases.

2.4 Future perspective

The studies shown in this work has been demonstrated the proof-of-principle of engineering VLP carrier to suppress CIES effect in order to improve the potency of the vaccine in inducing the desired immune response against TACAs. Besides, there is a lot of room for further improvement that are worth exploring in this promising platform.

In term of B cell epitope mapping, although the computational-based prediction can guide us to the potential regions of the B cell epitopes, the exact location of the epitopes could be further identified using monoclonal antibodies against the capsid. The monoclonal antibodies elicited by hybridoma B cells from immunized mice could be used for 3D epitope mapping based on cryo-electron microscopy reconstruction method[54] to pinpoint the exact location of the conformational epitopes.

Moreover, the monoclonal antibodies could be used to compare the binding against the capsid after B cell epitope editing or shielding by SPR or Bio-Layer Interferometry (BLI) techniques. In addition to the location, these techniques would provide insight about the binding affinity of the monoclonal antibodies against the modified B cell epitope(s) which will help us narrow down the targeted residues for the next experimental design.

A novel strategy of presenting vaccine carrier with tolerogenic CD22 ligand for reducing the unwanted anti-carrier immune response is also of high interest to be investigated. Sialic acid-binding immunoglobulin-like lectins 2, known as CD22, was found to have a function as B cell inhibitory co-receptor.[55] Evidence from several studies[56] suggested that B cell antigen in co-presenting with CD22 ligand (Figure 2.26) can regulate B cell activation specific to that antigen. The physical tethering of CD22 ligand with the antigen will recruit intracellular domain of CD22 towards B cell receptor. The interaction in close proximity between signaling domains of both receptors can suppress BCR mediated activating signal, leading to B cell tolerance specifically to the antigen that binds to the corresponding B cell. The effects has been confirmed by a variety of display platforms including polymer[56c, 57] and liposome.[56d] Macauley *et al.* have proved that CD22 ligand in conjugation with antigens can suppress the antigen-specific antibody production, yet preserve the immune response against unrelated antigens.[56d] Those studies also showed that the inhibitory effect is not only for T cell independent antigen, but also for T cell-dependent antigen where the antigen specific silencing comes through antigen specific B cell deletion from the polyclonal B cell repertoire. Since CD22 is thought to be conserved functionally between mouse and human,[56b] this suggests that the concept of CD22 based specific B cell tolerance could be practical in clinical trials.

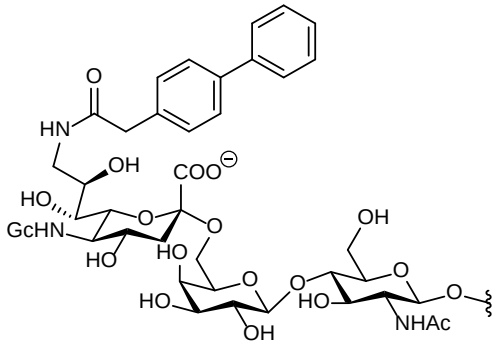

Figure 2.26: Chemical structure of tolerogenic CD22 ligand.

Therefore, it could be postulated that injecting Qβ displaying CD22 ligand prior to immunization would tolerize the Qβ specific B cells. Thus, anti-carrier immune response would be suppressed in subsequent immunization with Qβ-TACA. The synthesis procedure of CD22 ligand has been reported.[58] The synthetic CD22 ligand can be conjugated onto Qβ capsid in similar way as TACA or by using chemoenzymatic reaction to extend the oligosaccharide units from conjugated monosaccharide on VLP.[59] Alternatively, the conjugation site can be manipulated through site-specific unnatural amino acid incorporated into the capsid. This will ensure the optimized distance between the ligand and the predicted/identified capsid epitope,[59] as well as the optimized density of the ligand, in order to properly enforce the ligation between B cell receptor and CD22 to induce the most inhibitory effect.[56c] The level of antibody response against the desired antigens correlated with unwanted anti-Qβ response can be compared with immunization without prior tolerization.

As mentioned in the introductions in both chapters of this dissertation, the defined display pattern of the antigen on the capsid play a crucial role in proper B cell receptor crosslink. This work suggests the ability of genetic mutation to precisely control the TACA antigen display pattern to mimic the native one in order to induce specific antibodies recognizing the native form of TACA on cancer cells. For example, the conjugation of Tn antigen onto the reactive lysines at

position 13 and 16 together with position 10 (from N10K) would be expected to yield consecutive glycosylation that mimic the native trimeric Tn cluster in syndecan-1, of which high cellular expression was well correlated with tumor invasion and metastasis.[60] This hypothesis is also supported by the finding that a synthetic dendrimer glycopeptide MAG-Tn3, where Tn antigen is presented in trimeric cluster form, showed promising results for TACA-based anticancer vaccine,[31c] which are currently under evaluation in clinical trials.[52a] The role of patterned antigen display could also be closely investigated through site-specific orthogonal conjugation via chemical mutation[48b] or unnatural-amino-acid incorporation derived from amber codon suppression.

Moreover, the adjustable size of the VLP could be accomplished through mutation at inter-subunit domain as reported in literature,[7a] together with our finding on A38K mutant. The adjustable size of the capsid can provide an additional way to fine tune the antigen display pattern. Moreover, the understanding of the inter-subunit interaction of this domain not only helps establish models for protein self-assembly in computational design,[61] but also aid research in virology evolution field. The ability to tune the size of the VLP capsid will overcome the limitation of this construct in nanoparticle applications, such as drug delivery, *in vivo* imaging and nano-reactor.[62]

2.5 Materials and methods

2.5.1 Site-directed mutagenesis of Qβ VLPs

Primers were designed following a guildline in the manual of QuikChange® Site-Directed Mutagenesis Kit. Online based software PrimerX (http://www.bioinformatics.org/primerx/) was used to generate the primer sequence, or the sequence can be designed manually in some cases. The designed primers were further analyzed for proper %GC and Tm again by Oligoanalyzer 3.1 from IDT Inc. All primers were commercially synthesized by IDT Inc. For PCR reaction, the reagent mixture and cycling setting are prepared by adding reagents, respectively, as the following,

Reagents	**µl**
10X buffer	5
20 ng plasmid template (from 20 ng/µl)	1
125 ng Forward primer (from 100 ng/µl)	1.25
125 ng Reverse primer (from 100 ng/µl)	1.25
dNTP mix	1
BP561-1 water	39.5
Pfu turbo	1

PCR thermocycler setting

Number of cycles	Temperature	Time
1X	95 C°	30 Sec
17X	95 C°	30 Sec
	5 C° less than T_m of the primers, or using gradian	1 Min
	68 C°	6 Min
Finish	4 C°	till done

After PCR reaction, the resulting reaction was added 1µl *Dpn*I and incubated at 37°C for 1 hour to digest the template plasmid DNA. The reaction's products were verified by 0.8%

agarose gel electrophoresis with ethidium bromide as a staining reagent. The reactions were then used without purification to transform DH5α *E.coli*. The transformed DH5α *E. coli* cultures were plated onto SOB agar plate with 20μg/mL Kanamycin sulfate and incubated at 37°C overnight. 4-6 colonies were selected to inoculate 6 mL SOB with 20ug/mL Kanamycin and incubated at 37°C overnight to amplify the *E. coli*. Mutated DNA plasmid from the bacteria cultures were extracted with QIAprep Spin Miniprep Kit (QIAGEN). The extracted plasmids were submitted to GENEWIZ for sequencing. Plasmid of the mutated plasmids that provide correct DNA sequences with highest scores of sequencing quality were used for transformation into BL21(DE3)pLysS *E. coli* by the heat shock method, then plated on SOB agar plate as DH5α *E. coli*. A single colony was selected for protein expression.

Table 2.7: Primers used in the construction of mutant Qβ VLPs

Primer #	**Name**	**Sequence**
1	CP_T7K_F1	5'-ATTAGAGACTGTTA**AAG**TTAGGTAACATCGGG-3'
2	CP_T7K_R1	5'-CCCGATGTTACCTAA**CTT**AACAGTCTCTAAT-3'
3	CP_N10K_F1	5'-CTGTTACTTTAGGTA**AAG**ATCGGGAAAGATGG-3'
4	CP_N10K_R1	5'-CCATCTTTCCCGAT**CTT**ACCTAAAGTAACAG-3'
5	CP_K13R_F1	5'-GGTAACATCGGG**AGA**GATGGAAAACAA-3'
6	CP_K13R_R1	5'-TTGTTTTCCATC**TCT**CCCGATGTTACC-3'
7	CP_A38K_F1	5'-GCCTCGCTTTCACAA**AAG**GGTGCAGTTCCTGCG-3'
8	CP_A38K_R1	5'-CGCAGGAACTGCACC**CTT**TTGTGAAAGCGAGGC-3'
9	CP_A38K_[A40C]_F1	5'-CCTCGCTTTCACAA**AAG**GGTTGTGTTCCTGC-3'
10	CP_A38K_[A40C]_R1	5'-GCAGGAACACAACC**CTT**TTGTGAAAGCGAGG-3'
11	CP_A40C_F1	5'-CACAAGCGGGT**TGT**GTTCCTGCGCTGG-3'
12	CP_A40C_R1	5'-CCAGCGCAGGAAC**ACA**ACCCGCTTGTG-3'

Table 2.7: (Cont'd)

Primer #	Name	Sequence
13	CP_A40S_F1	5'-CACAAGCGGGT**TCA**GTTCCTGCGCTGG-3'
14	CP_A40S_R1	5'-CCAGCGCAGGAAC**TGA**ACCCGCTTGTG-3'
15	CP_T75K_F1	5'-CCGACCGCTTGC**AAG**GCAAACGGTTC-3'
16	CP_T75K_R1	5'-GAACCGTTTGC**CTT**GCAAGCGGTCGG-3'
17	CP_D102C_F1	5'-GCAGTATAGTACC**TGT**GAGGAACGAGC-3'
18	CP_D102C_R1	5'-GCTCGTTCCTC**ACA**GGTACTATACTGC-3'
19	CP_D102S_F1	5'-GCAGTATAGTACC**TCT**GAGGAACGAGC-3'
20	CP_D102S_R1	5'-GCTCGTTCCTC**AGA**GGTACTATACTGC-3'
21	CP_E103K_F1	5'-GTATAGTACCGAT**AAG**GAACGAGCTTTTG-3'
22	CP_E103K_R1	5'-CAAAAGCTCGTTC**CTT**ATCGGTACTATAC-3'
23	CP_A117K_F1	5'-GCTTGCTGCTCTGCTC**AAG**AGTCCTCTGCTGATCG-3'
24	CP_A117K_R1	5'-CGATCAGCAGAGGACT**CTT**GAGCAGAGCAGCAAGC-3'
25	CP_P119K_F1	5'-GCTCTGCTCGCTAGT**AAG**CTGCTGATCGATGC-3'
26	CP_P119K_R1	5'-GCATCGATCAGCAG**CTT**ACTAGCGAGCAGAGC-3'

2.5.2 Qβ viral capsid protein expression and purification

A single colony of BL21(DE3)pLysS *E. coli* with mutated plasmid was selected to be inoculated into starting culture of 50 mL SOC containing 20ug/mL Kanamycin. The starting culture was grown overnight at 37°C, 230 rpm. After overnight, the resulting cloudy culture was then transferred into 1L culture medium with the antibiotic selection. The culture was continued at the same condition until the OD_{600} was between 0.7-1.0, 1mL of 1M isopropyl β-D-1-thiogalactopyranoside (IPTG) was then added into the culture to induce protein expression (final concentration = 1mM). The culture was continued 4-5 hours. After 4-5 hours, the bacteria were pelleted at 6,000 rpm for 30min. The culture medium was discarded. The pellets were re-suspended in 0.1M PBS pH 7. The bacteria in the suspension were then lysed with a probe

sonicator in an ice bath. The sonication generator was set at power of 30% for 10 min, with interval of 5 second pulses and 5 second stops. The lysis was centrifuged at 14,000 rpm for 20 min. The supernatant containing the capsid protein was added PEG 8000 to final concentration of 10% (w/v) and put on a nutating mixer at 4°C overnight to allow complete protein precipitation. The precipitate was pelleted down at 14,000rpm for 20 min. The pellet was resuspended in 0.1M PBS pH=7. The re-suspended solution was 1:1 (v/v) mixed with 1:1 (v/v) chloroform/n-butanol till the mixture turns colloid. The colloidal mixture was centrifuged at 7,000 rpm for 1 hour to separate layer. The top (aqueous) layer was collected. Viral capsid protein in the collected aqueous layer was further purified by sucrose density gradients 10-40% (w/v). The linear (continuous) sucrose gradients was prepared following freezing-thawing method.[63] The loaded sucrose gradients were centrifuged with swing bucket rotor SW32 rotor at 28,000 rpm for 5 hours. The viral capsid band can be visualized by LED light shining through the top of the tube. The bright blue band from scattered light was collected as fractions of 1mL. The collected fraction was analyzed for purity of the capsid by size-exclusion chromatography using column Superose 6 resin 10/300 (void volume = 9mL). The fraction that shows a single peak at elution around 11-15 mL was determined as a fraction containing pure VLP. The remaining sucrose in the collected fraction was removed by filtration through Millipore 100k MWCO centrifugal filter tube, and washed thoroughly with the PBS buffer. Total protein concentration in the final solution was quantified by Pierce BCA Protein Assay Kit, using bovine serum albumin as the standard. The purified VLP was characterized by size-exclusion chromatography, Dynamic light scattering (DLS), and transmission electron microscopy (TEM) for particles' size, homogeneity, shape, and purity. The change of the amino acid(s) as a result of mutation was determined by the molecular weight difference compared with wide-type Qβ. The

molecular weight of the protein was determined by LCMS QTOF ESI mass spectroscopy and the multiple charge mass spectrums were transformed to single charge by Maximum Entropy deconvolution algorithm (MaxEnt™ 1)[48]

2.5.3 Synthesis and characterization of Qβ or mQβ conjugates[36]

13.2 mg of VLP Qβ or mQβ (5.1 nmol particle, 0.9 μmol subunit, 3.6 μmol reactive amines) suspended in potassium phosphate buffer (0.1 M, pH=7, 5.5 mL) was added into a 15-mL falcon tube. DMSO 0.35 mL was slowly dropped into the solution. **Tn1-NHS** or **Tn2-NHS** (20 mg/mL in 0.35 mL, 0.017 mmol, 4.7 eq. to the reactive amine) was added into the reaction tube. The reaction mixture was rotated on a rotating mixer at room temperature overnight. The reaction was diluted with 0.1 M PBS pH=7 to total volume 50 mL. The VLP conjugates were purified by filtration through Millipore 100k MWCO centrifugal filter tube, and washed thoroughly with the PBS buffer. The purified VLP conjugates were characterized as described above. The average number of conjugated Tn1 or Tn2 on each viral capsid subunit was estimated from the intensity of peaks in the deconvoluted mass spectra from LCMS analysis. Results are shown in **Figure 2.30**.

2.5.4 Size exclusion chromatography (SEC)

SEC analysis and purification were performed on an AKTApure 25L system, equipped with Superose 6 Increase 10/300 GL column. 0.1 M potassium phosphate buffer pH=7 was used as the eluent with a flow rate of 0.5 mL/min at 4 °C. The capsid protein was detected with a UV detector at wavelength 280nm. 0.5 mL of sample was injected. The sample was eluted with 1.5 column volume and the fractions were collected every 1mL. Results are shown in **Figure 2.29**.

2.5.5 Non-denaturing agarose gel

The viral capsid samples (30 μg of each capsid protein) were loaded into 0.7% agarose gel in PBS with SYBR Safe DNA gel stain as a staining reagent for the encapsulated RNA. The electrophoresis was performed in TEA (Tris-acetate-EDTA) buffer at 4°C for 4 hours. After visualizing the encapsulated RNA bands by UV light, the gel was later stained with Coomassie blue stain to detect the capsid protein.

2.5.6 Thermal stability measurement of viral capsid by temperature varied UV-Vis spectroscopy

1mg/mL of VLPs in potassium phosphate buffer (0.1 M, pH=7) was measured against the buffer as a standard solution. 1cm quartz cuvettes with caps were used as cells for the sample and standard buffer. The measurement was done with Varian Cary 1 Bio UV-Vis spectroscopy equipped with Cary temperature variable controller (Agilent Technologies). The wavelength was set at 310 nm as this wavelength gives the most sensitivity for detecting the denatured protein (**Figure 2.27**). The absorbances were measured every 1 °C with temperature change at a rate 5°C/min from 25°C to 60°C, then the absorbances were measured every 0.5 °C with temperature change at a rate 1°C /min from 60 °C to 90 °C.

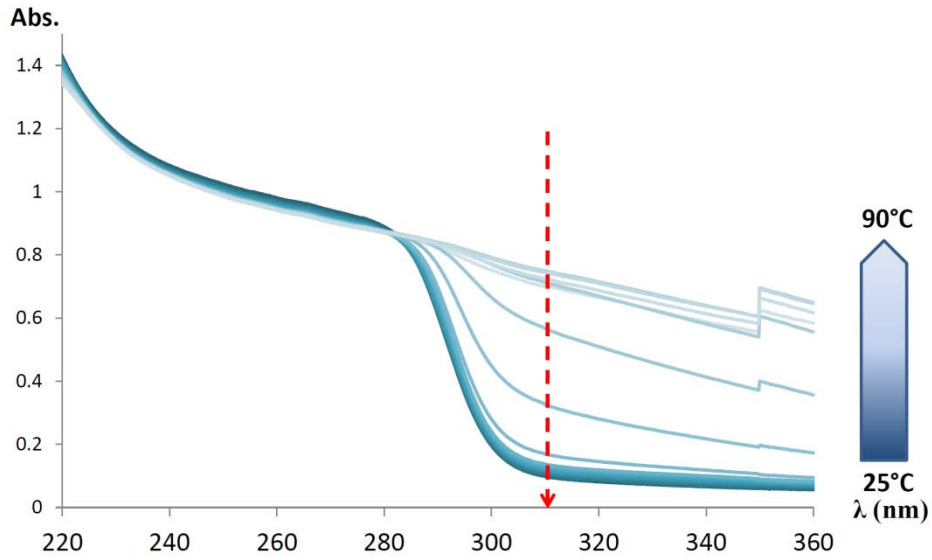

Figure 2.27: UV-visible absorption of wtQβ at varied temperature from 25 to 90°C. The estimated wavelength that provides the most different absorption is 310 nm (dashed line).

2.5.7 Dynamic light scattering (DLS) and transmission electron microscopy (TEM)

The hydrodynamic diameter and zeta potential were assessed on a Malvern Zetasizer Nano zs instrument. TEM images were collected on a JEM-2200FS operating at 200 kV using Gatan multiscan CCD camera with Digital Micrograph imaging software. Samples were prepared on ultrathin-carbon type A, 400 mesh copper grids, or ultrathin C film on holey carbon support film, 400 mesh, Cu for high resolution TEM (Ted Pella, Inc.). The viral capsids were strained by aqueous 2% uranyl acetate. Results are shown in Figure 2.28.

2.5.8 Immunization studies[36]

Pathogen-free C57BL/6 female mice age 6−10 weeks were obtained from the Jackson Laboratory and maintained in the University Laboratory Animal Resources facility of Michigan State University. All animal care procedures and experimental protocols have been approved by the Institutional Animal Care and Use Committee (IACUC) of Michigan State University. Groups of 5 mice were injected subcutaneously under the scruff on day 0 with 0.1 mL of various

Qβ constructs as emulsions in complete Freund's adjuvant (Sigma-Aldrich, F5881), and boosters were given subcutaneously under the scruff on days 14 and 28 with 0.1 mL of various Qβ constructs as emulsions in incomplete Freund's adjuvant (Sigma-Aldrich, F5506). All Tn vaccine constructs administered have the same amounts of Tn antigen (1.93 μg). Serum samples were collected on day 0 (before immunization), 7, and 35. The final bleeding was done by cardiac bleed.

2.5.9 Enzyme-linked immunosorbent assay (ELISA)

A Nunc MaxiSorp® flat-bottom 96 well plate was coated with BSA-Tn (10ug/mL) or corresponding Qβ capsids (1ug/mL) in PBS pH = 7.4, overnight at 4 °C. The coated plate was then washed 4 times with PBS/0.5% Tween-20 (PBST), followed by the addition of 1% (w/v) BSA in PBS to each well and incubation at room temperature for one hour. The plate was washed again 4 times with PBST. 100 μl of the dilution of mouse sera in 0.1% BSA/PBS were added in each well. (For competitive ELISA, the diluted sera were incubated with 50 μg of the viral capsids at 37 °C for 1 hour before adding into the plate.) The plate was incubated for two hours at 37 °C and washed. A 1:2000 diluted horseradish peroxidase (HRP)-conjugated goat anti-mouse IgG, IgG1, IgG2b, IgG2c, IgG3 or IgM antibody (Jackson ImmunoResearch Laboratory IgG #115−035−071, IgM #115−035−075) in 0.1% BSA/PBS was added to each well, respectively. The plate was incubated for one hour at 37 °C, washed, and a solution of 3,3′,5,5′-tetramethylbenzidine (TMB) was added. Color was allowed to develop for 15 min, and then a solution of 0.5 M H_2SO_4 (50 μl) was added to stop the reaction. The optical density was measured at 450 nm using a microplate autoreader (BioRad). Each experiment was repeated at least four times, and the average of the quadruplicate was used to calculate the titer. The titer was

determined by regression analysis with log10 dilution plotted with optical density. The titer was calculated as the highest dilution that gave OD = 0.3.

2.5.10 Cell cultures

Human lymphoma Jurkat cells (kindly provided by Profs. Barbara Kaplan and Norbert Kaminski, Michigan State University) were cultured in RPMI 1640 supplemented with 10% FBS, 2 mM L-glutamine, 1 mM sodium pyruvate, minimal essential medium nonessential amino acid, 100 U/mL each of penicillin G, and streptomycin.

Murine mammary adenocarcinoma cell line TA3Ha (kindly provided by Prof. John Hilkens, The Netherlands Cancer Institute) were isolated from ascites collected from passage growing on A/J mice. The cells were cultured using RPMI 1640, 10% FBS, 100 U/mL penicillin and 100 U/mL streptomycin.

2.5.11 Flow cytometry experiment

Cells were harvested from the culture. The cells suspended in FACS buffer (5% FBS, 0.1% NaN_3 in PBS) were incubated with 1:20 diluted mice sera on ice for 30 min. The cell suspension was centrifuged at 1600 rpm, 5 min at 4°C to remove the unbound antibodies. The cell-bound IgG antibodies were then labeled with goat anti-mouse IgG conjugated with FITC (BioLegend, 405305) for 30 min. The excess secondary antibody was washed out and the cells were suspended in FACS buffer. Acquisition of cells was performed with LSR II (BD), and data was analyzed with FlowJo® software (Tree Star Inc.).

2.5.12 Anti-tumor immunoprotection (Tumor challenge)

After day 35 of the immunization, 5,000 cells of TA3Ha were intraperitoneally injected into groups of C57BL/6 mice (n=10) on day 36. Mice were injected cyclophosphamide (50

mg/kg) intraperitoneally on day 37. Survival of mice was monitored for 30 days. Statistical analysis of survival was performed with GraphPad Prism using log-rank test.

2.5.13 Liquid chromatography–mass spectrometry (LCMS)

The samples for LCMS were prepared with the following procedure: 1:1 v/v of 40μg/mL of VLP stock solution and 100mM DTT was mixed and incubated in a water bath at 37°C for 30 min. One drop of 50% formic acid was added into the mixture. The samples are ready for the LCMS. LCMS was performed on Waters Xevo G2-XS quadrupole/time-of-flight UPLC/MS/MS. The liquid chromatography was done on ACQUITY UPLC® Peptide BEH C18 column, 130Å, 1.7 μm, 2.1 mm × 150 mm, using gradient eluent from 95% 0.1% formic acid in water to 95% 0.1% formic acid in ACN (0.3 mL/min flowrate) at column temperature 40°C. The multiple charge mass spectra were transformed to single charge by using algorithm MaxEnd1[48a]. The average numbers of Tn/subunit were analyzed by signal intensity of mass spectrum. Results are shown in **Figure 2.30**.

2.5.14 Transmission electron microscopy (TEM) Images

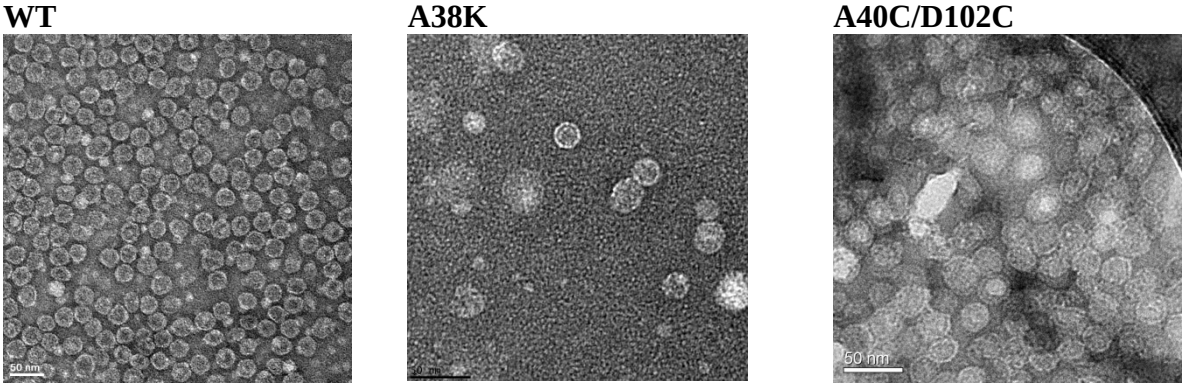

Figure 2.28: TEM images of wild-type Qβ and various Qβ mutants.

Figure 2.28: (Cont'd)

A38K/A40C/D102C

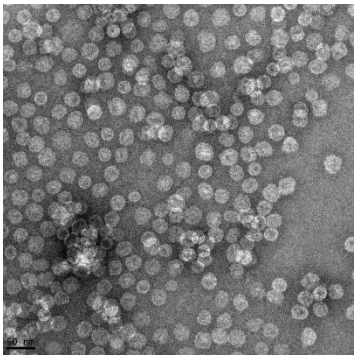

T75K

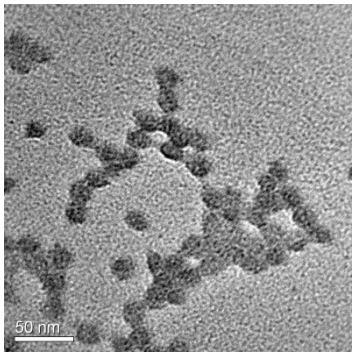

A117

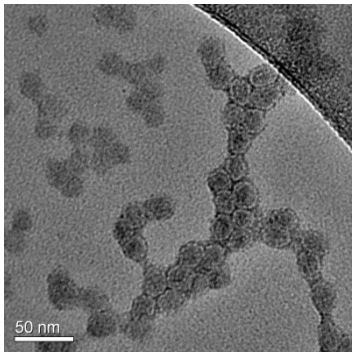

A40S/D102S

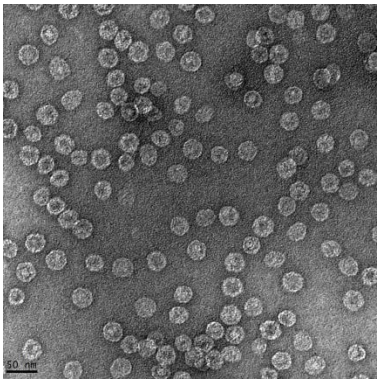

T7K

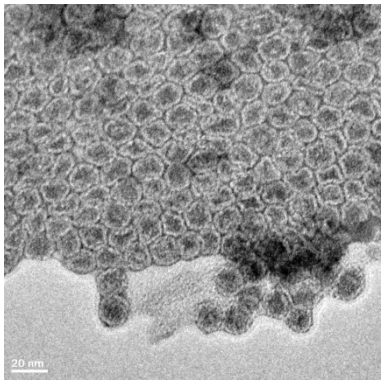

N10K

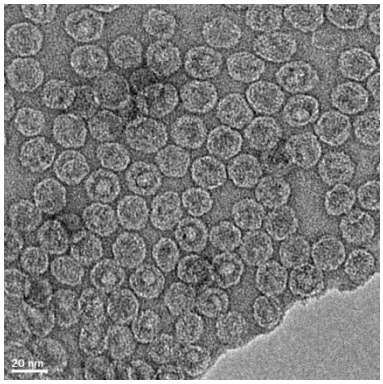

2.5.15 Synthesis of Tn1 and Tn2

All chemicals were reagent grade and used as received from the manufacturer, otherwise noted. ^{1}H NMR spectra were recorded on an Agilent-500M spectrometer and processed by MestReNova version 10.0.2.

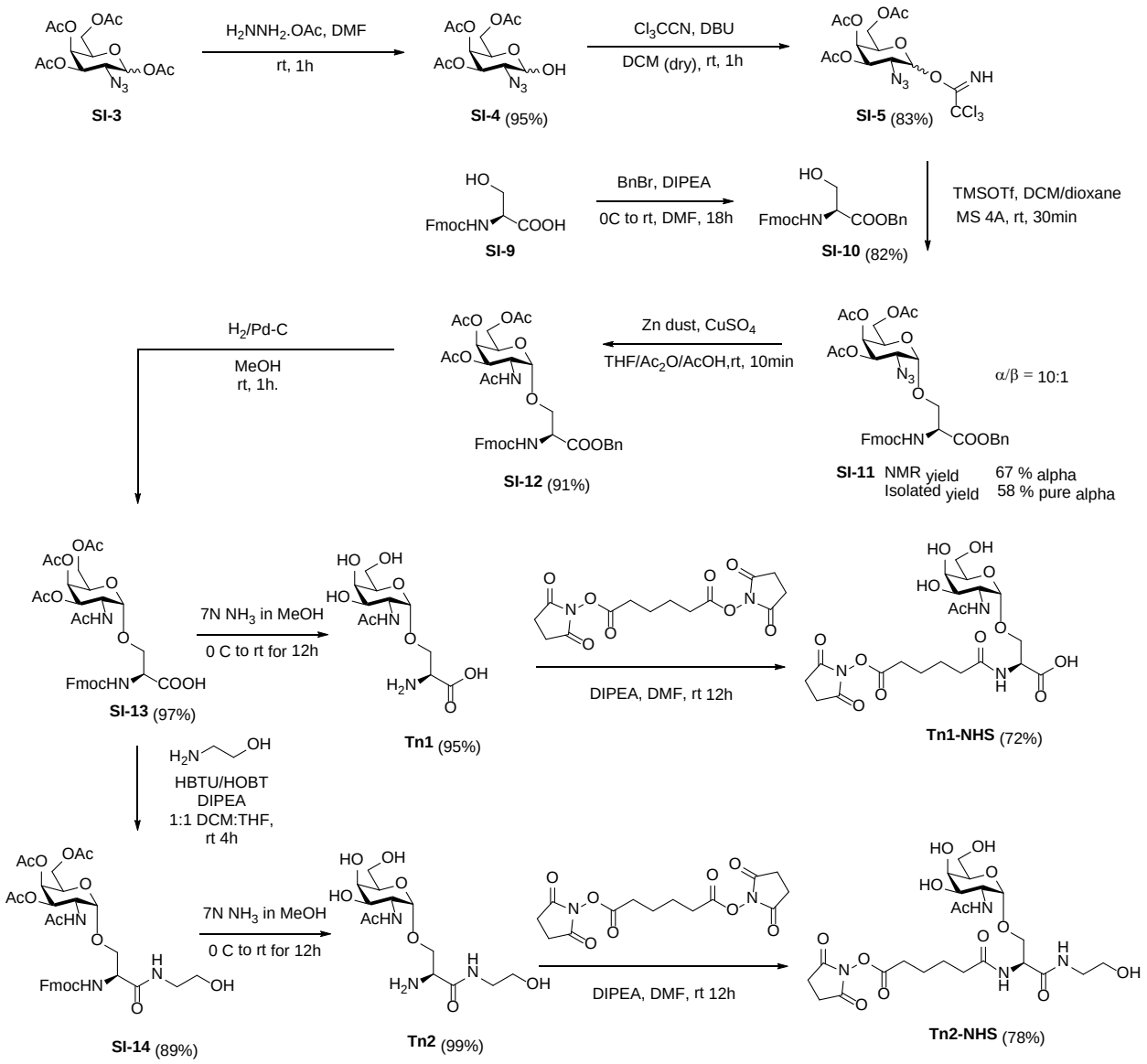

Scheme 2.1: Synthesis of **Tn1-NHS** and **Tn2-NHS**

2.5.16 Synthesis procedure

*N-(Fluoren-9-ylmethoxycarbonyl)-O-(3,4,6-tri-O-acetyl-2-azido-2-deoxy-α-D-galactopyranosyl-L- serine benzyl ester (**SI-11**)*[64]*:*

Trichloroacetimidate **SI-5**[49] (3.01 g, 6.33 mmol) and *N*-Fmoc-*O*-Bn-Serine **SI-10**[65] (2.2 g, 5.28 mmol) were mixed in the reaction flask with freshly activated molecular sieves 4A (10 g)

under nitrogen gas. Anhydrous DCM:Dioxane (1:1, 60 mL) was added to dissolve the mixture, and the solution was left stirred at rt. for 30 min. TMSOTf (0.297 mL, 1.925 mmol) was added dropwise into the reaction. The reaction was left stirred at rt. for an hour. Upon monitoring the reaction, if there was some starting material **SI-5** left, 0.1 more eq. of TMSOTf was further added and the reaction was allowed to proceed for another hour. Upon completion, diisopropylethylamine (DIPEA) was added to quench the reaction. The reaction was diluted with DCM and washed with 0.1 M HCl and then water. The organic layer was dried over Na_2SO_4 and then concentrated. The crude product was purified by column chromatography (silica gel; 3:1 EtOAc:Hexane) to yield **SI-11**(alpha) (2.23 g, 58%). Spectral analysis of the product compared with reported literature[64] confirmed the identity of the product. ^{1}H NMR (500 MHz, Chloroform-*d*) δ 7.76 (dt, *J* = 7.7, 0.9 Hz, 2H), 7.66 – 7.59 (m, 2H), 7.44 – 7.28 (m, 9H), 6.00 (d, *J* = 8.1 Hz, 1H), 5.40 (dd, *J* = 3.4, 1.2 Hz, 1H), 5.31 – 5.19 (m, 3H), 4.87 (d, *J* = 3.6 Hz, 1H), 4.62 (dt, *J* = 8.2, 3.1 Hz, 1H), 4.45 – 4.36 (m, 2H), 4.24 (t, *J* = 7.2 Hz, 1H), 4.17 (dd, *J* = 10.9, 3.2 Hz, 1H), 4.10 – 3.94 (m, 4H), 3.59 (dd, *J* = 11.2, 3.6 Hz, 1H), 2.15 (s, 3H), 2.07 (s, 3H), 1.96 (s, 3H).

*N-(Fluoren-9-ylmethoxycarbonyl)-O-(3,4,6-tri-O-acetyl-2-acetamido-2-deoxy-α-D-galactopyranosyl-L-serine benzyl ester (**SI-12**):*[66]

The synthesis procedure was modified from reported literature.[66] Compound **SI-11** (2.41 g, 3.30 mmol) was dissolved in 3:2:1 of THF:Ac_2O: AcOH (60 mL). Zinc dust (2.72 g, 41.23 mmol) was added and then 5 mL of saturated aq. $CuSO_4$ was added to activate zinc. The reaction was stirred at rt. for about half an hour. After completion as monitored by TLC, the zinc dust was removed by filtering the reaction mixture through Celite®. The filtrate was coevaporated with toluene to concentrate the crude product. The crude product was purified by column chromatography (silica gel; 1:1 EtOAc:Hexanes) to yield **SI-12** (2.24 g, 91%). Spectral analysis

of the product compared with reported literature confirmed the identity of the product. ^{1}H NMR (500 MHz, Chloroform-*d*) δ 7.77 (d, *J* = 7.5 Hz, 2H), 7.61 (d, *J* = 7.5 Hz, 2H), 7.43 – 7.28 (m, 9H), 5.88 (d, *J* = 8.3 Hz, 1H), 5.58 (d, *J* = 9.5 Hz, 1H), 5.31 (d, *J* = 3.2 Hz, 1H), 5.20 (q, *J* = 12.1 Hz, 2H), 5.04 (dd, *J* = 11.4, 3.2 Hz, 1H), 4.78 (d, *J* = 3.7 Hz, 1H), 4.66 – 4.48 (m, 2H), 4.43 (d, *J* = 7.1 Hz, 2H), 4.23 (t, *J* = 7.1 Hz, 1H), 4.16 – 3.89 (m, 5H), 2.16 (s, 3H), 2.01 (s, 3H), 1.97 (s, 3H), 1.91 (s, 3H).

*N-(Fluoren-9-ylmethoxycarbonyl)-O-(3,4,6-tri-O-acetyl-2-acetamido-2-deoxy-α-D-galactopyranosyl-L- serine (**SI-13**):*[66]

The synthesis procedure was as reported.[66] The reaction yielded the product **SI-13** (0.88 g, 98%). Spectral analysis of the product compared with reported literature[66] confirmed the identity of the product.

*N-(Fluoren-9-ylmethoxycarbonyl)-O-(3,4,6-tri-O-acetyl-2-acetamido-2-deoxy-α-D-galactopyranosyl-L-serine 2-ethanolyl amide (**SI-14**):*

Compound **SI-13** (1.90 g, 2.89 mmol) in 1:1 anhydrous THF:DCM was activated using HBTU (1.2 g, 3.18 mmol), HOBt (0.43 g, 3.18 mmol) and DIPEA (1.1 mL, 6.37 mmol) at rt. for 20 min. Ethanolamine (0.22 mL, 3.62 mmol) was added into the reaction mixture. Upon completion, the precipitate was filtered out and the crude mixture in filtrate was dried and purified by column chromatography (silica gel; 2-10% Methanol in Hexanes) to yield 1.8 g. (89%). Spectral analysis of the product compared with reported literature confirmed the identity of the product.[66] ^{1}H NMR (500 MHz, Chloroform-*d*) δ 7.75 (d, *J* = 7.6 Hz, 2H), 7.57 (d, *J* = 7.5 Hz, 2H), 7.39 (t, *J* = 7.5 Hz, 2H), 7.30 (t, *J* = 7.5 Hz, 2H), 6.87 (t, *J* = 5.7 Hz, 1H), 6.37 (d, *J* = 9.5 Hz, 1H), 5.92 (d, *J* = 7.4 Hz, 1H), 5.35 – 5.28 (m, 1H), 5.11 (dd, *J* = 11.4, 3.2 Hz, 1H), 4.89 (d, *J* = 3.3 Hz, 1H), 4.57 (ddd, *J* = 11.4, 9.5, 3.6 Hz, 1H), 4.50 – 4.31 (m, 3H), 4.17 (dt, *J* = 24.6,

6.5 Hz, 2H), 4.08 – 3.98 (m, 2H), 3.92 (d, *J* = 8.8 Hz, 1H), 3.73 (d, *J* = 17.4 Hz, 3H), 3.44 (s, 2H), 3.08 (s, 1H), 2.15 (s, 3H), 2.00 (s, 3H), 1.97 (s, 3H), 1.95 (s, 3H).

*O-2-acetamido-2-deoxy-α-D-galactopyranosyl-L-serine or O-2-acetamido-2-deoxy-α-D-galactopyranosyl-L-serine 2-ethanolyl amide (**Tn1 or Tn2**):*

The synthesis procedure was as from reported literature.[66] Compound **SI-13** (100 mg, 0.152 mmol) or **SI-14** (660 mg, 0.94 mmol) under N_2 at 0 °C was added 5mL of 7N ammonia in methanol. The reaction was warm up to rt. overnight. Upon completion, the solvent was evaporated by flowing N_2 gas. The crude reaction mixture was dissolved in MeOH and then precipitated in EtOAc. The filtrate was dried to yield **Tn1** (43.4 mg, 92 %) or **Tn2** (330 mg, 99 %), respectively. **Tn1**: ^{1}H NMR (500 MHz, Methanol-d_4) δ 4.81 (d, *J* = 3.7 Hz, 1H), 4.31 (dd, *J* = 10.9, 3.6 Hz, 1H), 4.06 (d, *J* = 17.2 Hz, 1H), 3.92 – 3.65 (m, 7H), 2.01 (s, 3H). **Tn2**: ^{1}H NMR (500 MHz, Methanol-d_4) δ 4.78 (d, *J* = 3.7 Hz, 1H), 4.28 (dd, *J* = 11.0, 3.7 Hz, 1H), 3.92 – 3.65 (m, 7H), 3.65 – 3.49 (m, 3H), 3.37 – 3.28 (m, 3H), 2.00 (s, 3H).

*N-(N-Hydroxysuccinimidyl adipoyl)-O-2-acetamido-2-deoxy-α-D-galactopyranosyl-L-serine or N-(N-Hydroxysuccinimidyl adipatyl)-O-2-acetamido-2-deoxy-α-D-galactopyranosyl-L-serine 2-ethanolyl amide (**Tn1-NHS or Tn2-NHS**):*

Disuccinimidyl adipate (5 eq.) in anhydrous DMF (0.5 mL) was added to **Tn1** (40 mg, 0.13 mmol) or **Tn2** (66 mg, 0.18 mmol) dissolved in DMF (0.5 mL). DIPEA (1 eq.) was added in the reaction mixture. The reaction was left stirred for 2-3 h. Upon completion, DMF was evaporated under vacuum until dryness. The crude product was precipitated in EtOAc twice and then washed with 10% MeOH in EtOAc 3-5 times to remove the excess diNHS-linker. The final precipitate was dried under vacuum to yield **Tn1-NHS** (50 mg, 72%). **Tn1-NHS:** ^{1}H NMR (500 MHz, Methanol-d_4) δ 4.83 (d, *J* = 3.7 Hz, 1H), 4.65 (t, *J* = 4.0 Hz, 1H), 4.25 (dd, *J* = 11.0, 3.7 Hz, 1H), 3.99 – 3.62 (m, 5H), 2.83 (s, 4H), 2.73 – 2.62 (m, 2H), 2.35 (t, *J* = 6.8 Hz, 2H), 2.00 (d,

J = 7.7 Hz, 4H), 1.77 (dt, *J* = 6.9, 3.5 Hz, 4H); **Tn2-NHS** (84.5 mg, 78 %). **Tn2-NHS:** ^{1}H NMR (500 MHz, Methanol-d_4) δ 4.82 (d, *J* = 3.8 Hz, 1H), 4.59 (t, *J* = 5.2 Hz, 1H), 4.26 (dd, *J* = 11.0, 3.7 Hz, 1H), 3.92 – 3.65 (m, 8H), 3.60 (td, *J* = 5.8, 1.8 Hz, 2H), 3.37 – 3.26 (m, 6H), 2.83 (s, 4H), 2.73 – 2.63 (m, 2H), 2.42 – 2.27 (m, 2H), 2.01 (d, *J* = 2.0 Hz, 4H), 1.82 – 1.70 (m, 3H).

APPENDICES

APPENDIX A

Size Exclusion Chromatograms

Qβ(WT) and Qβ(WT)-Tn1

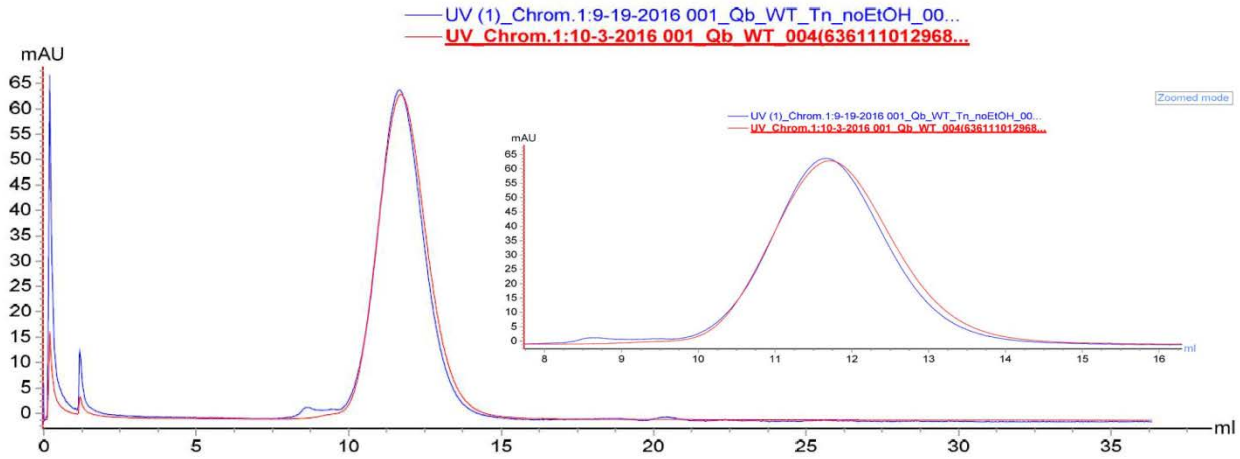

Qβ(T7K) and Qβ(T7K)-Tn1

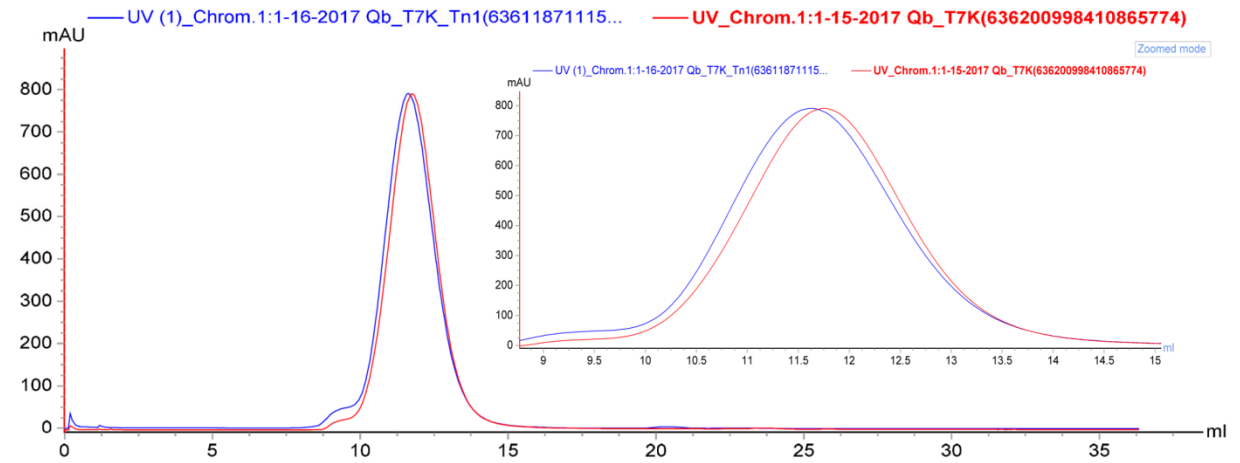

Figure 2.29: Size-exclusion chromatography of wild-type Qβ, varied Qβ mutants and their Tn1 derivatives.

Figure 2.29: (Cont'd)

Qβ(N10K) and Qβ(N10K)-Tn1

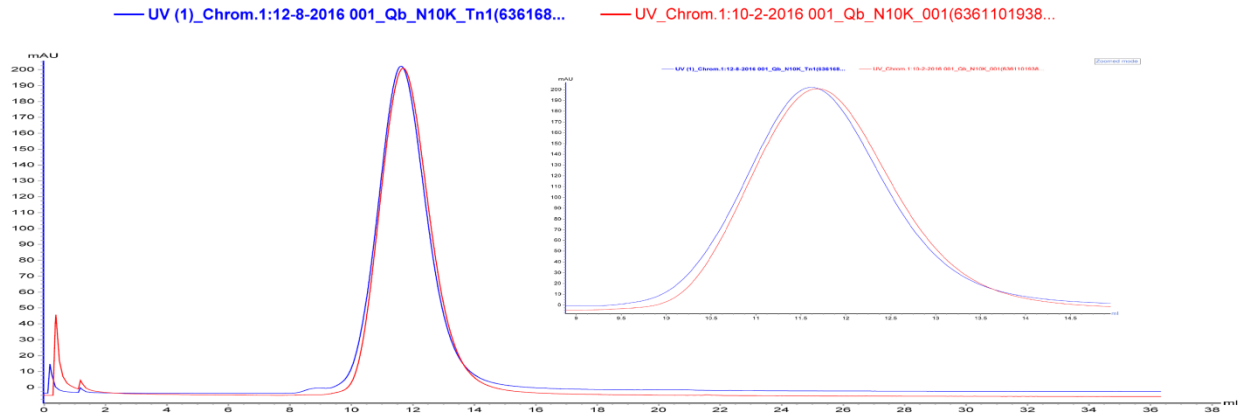

Qβ(A38K) and Qβ(A38K)-Tn1

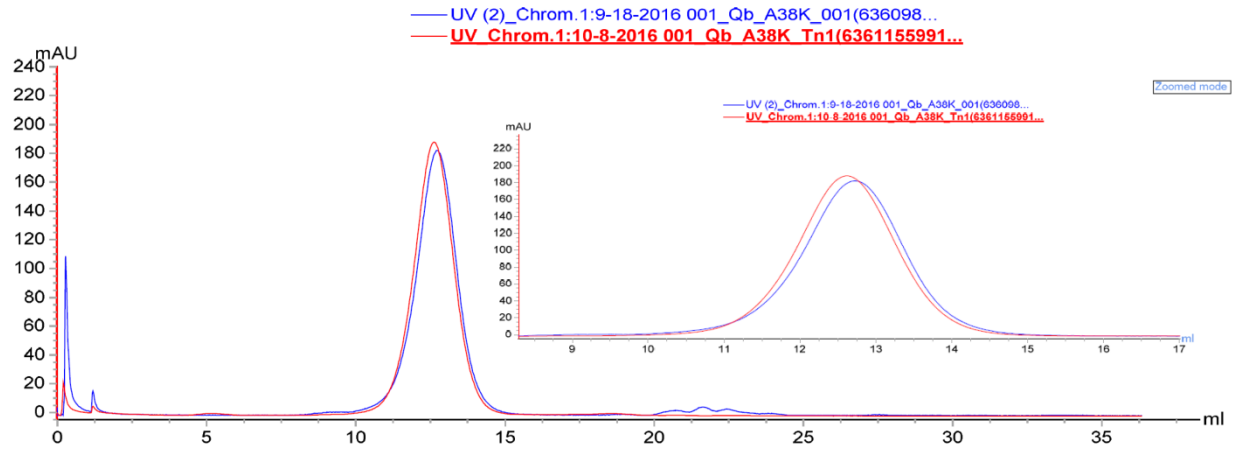

Figure 2.29: (Cont'd)

Qβ(A38K/A40C/D102C) and Qβ(A38K/A40C/D102C)-Tn1

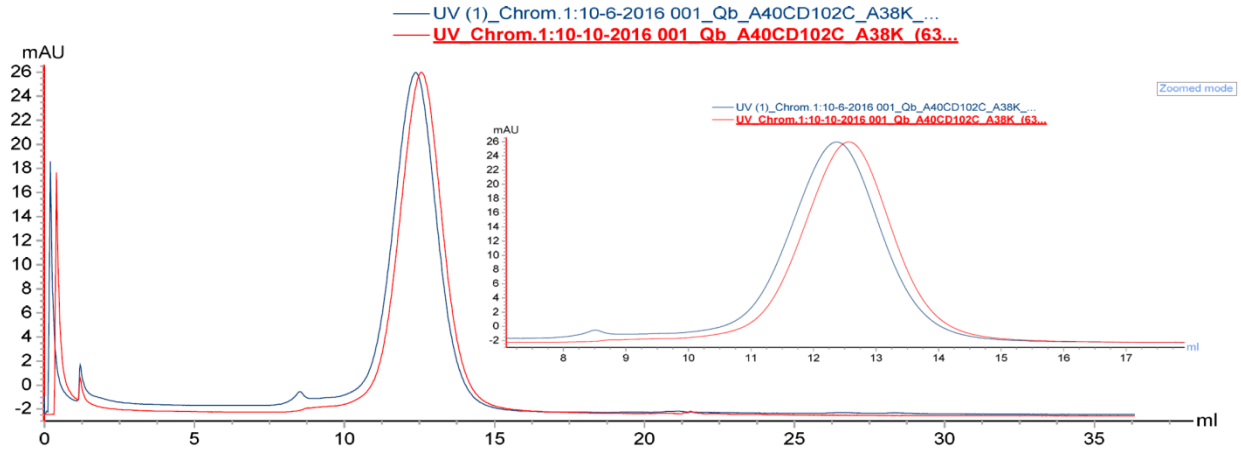

Qβ(A40C/D102C) and Qβ(A40C/D102C)-Tn1

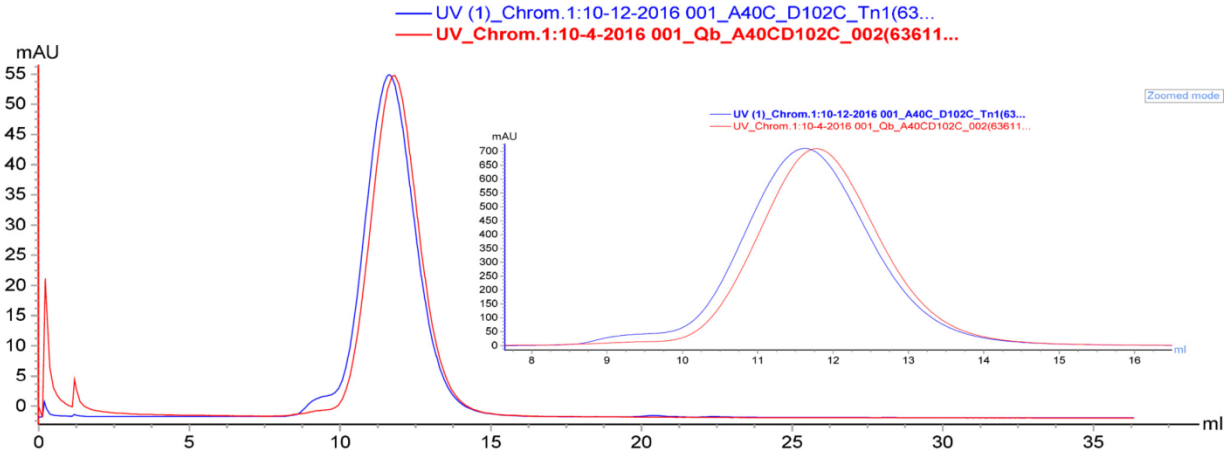

Figure 2.29: (Cont'd)

Qβ(T75K) and Qβ(T75K)-Tn1

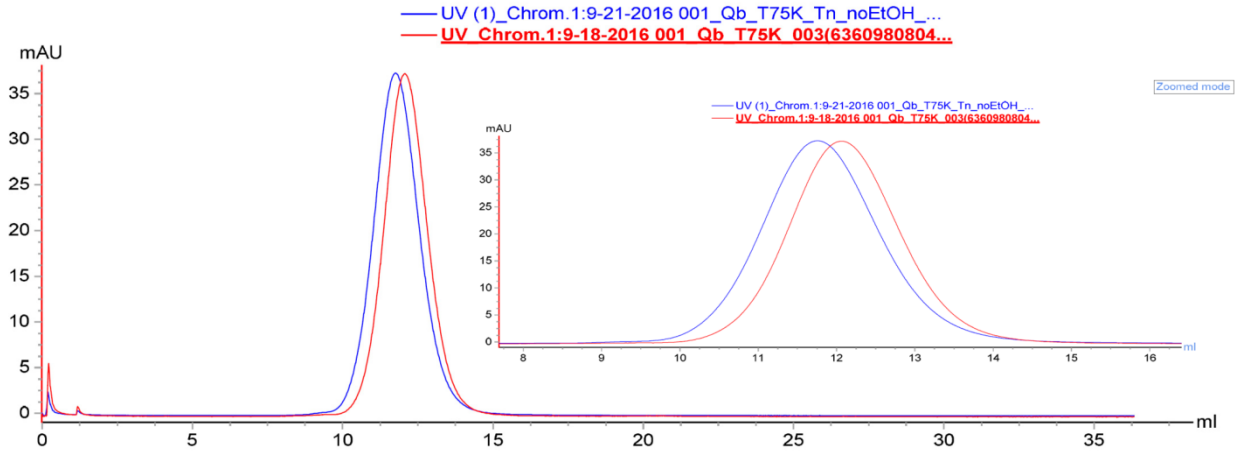

Qβ(A117K) and Qβ(A117K)-Tn1

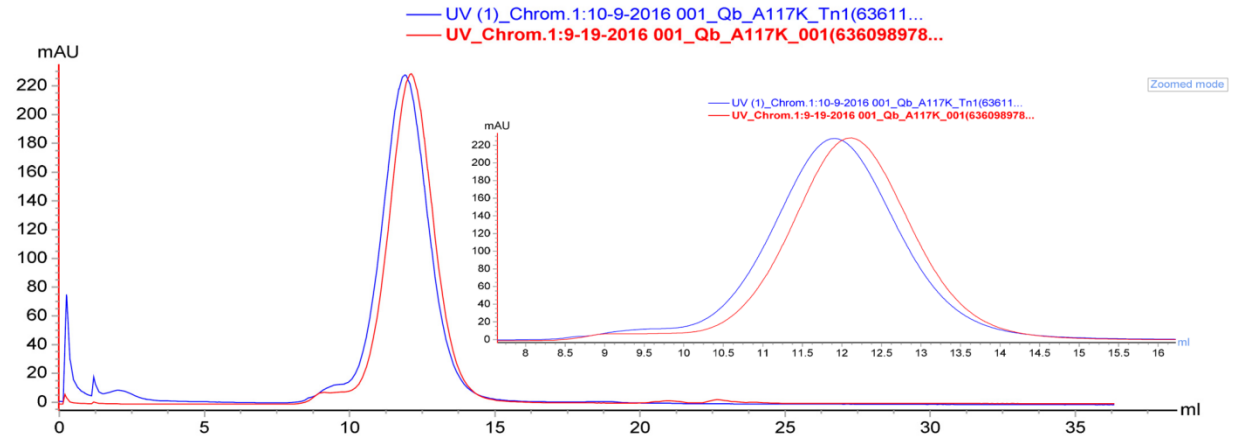

Figure 2.29: (Cont'd)

Qβ(P119K) and Qβ(P119K)-Tn1

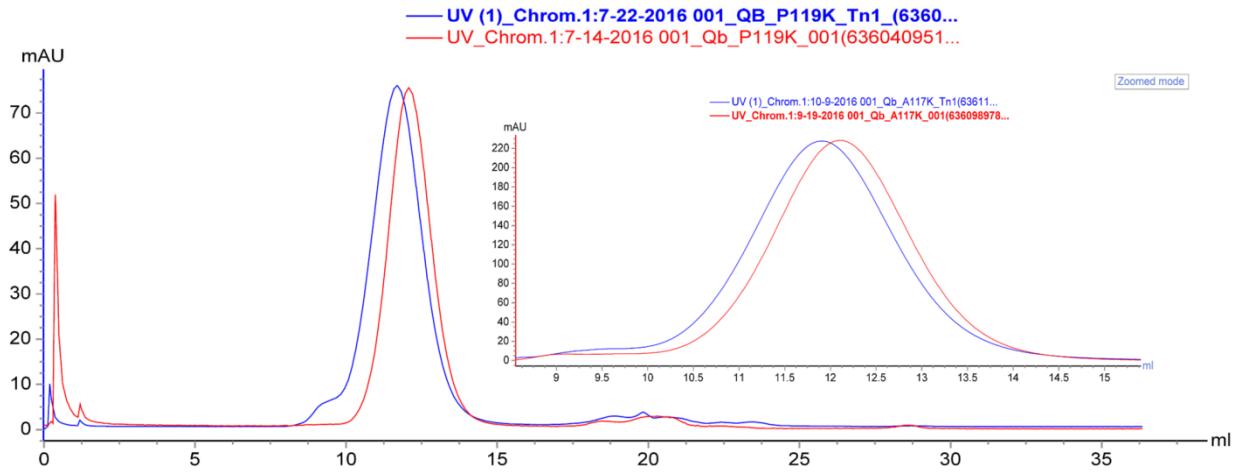

APPENDIX B

Liquid chromatography–mass spectra

Qβ_WT_Tn1

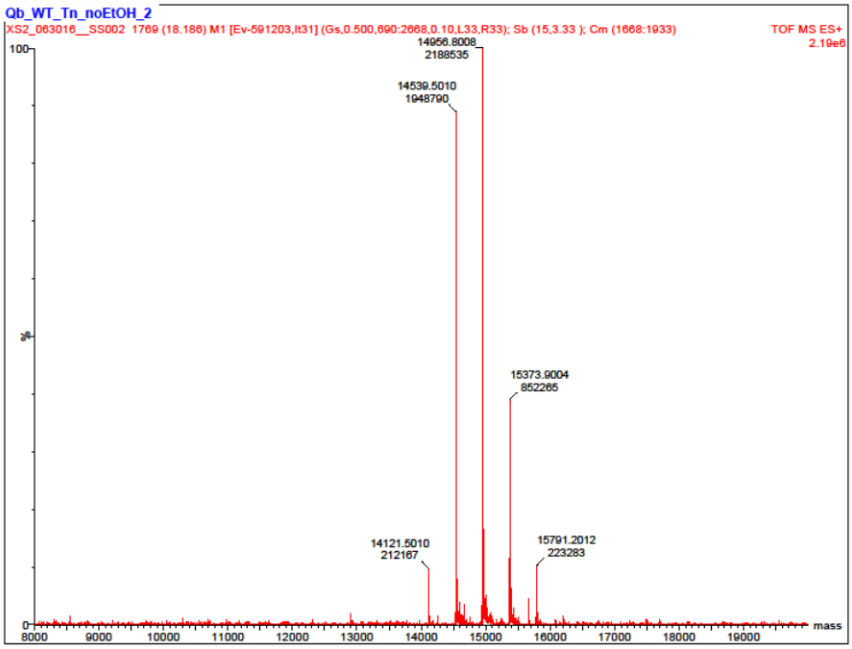

Figure 2.30: Mass spectra of wild-type Qβ-Tn1 and varied Qβ mutant-Tn1 after applying MaxEnd1 algorithm.

Figure 2.30: (Cont'd)

Qβ_T7K_Tn1

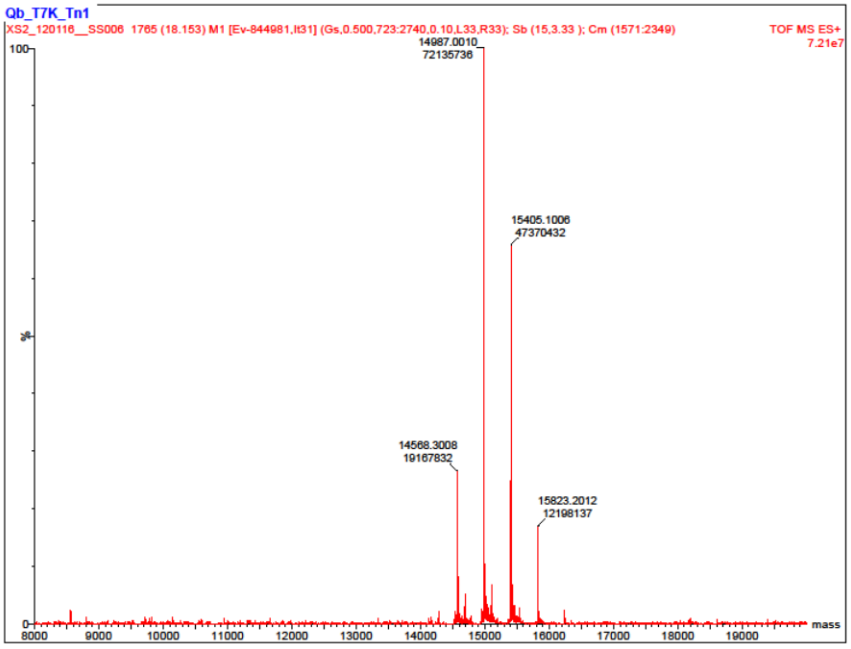

Qβ_N10K_Tn1

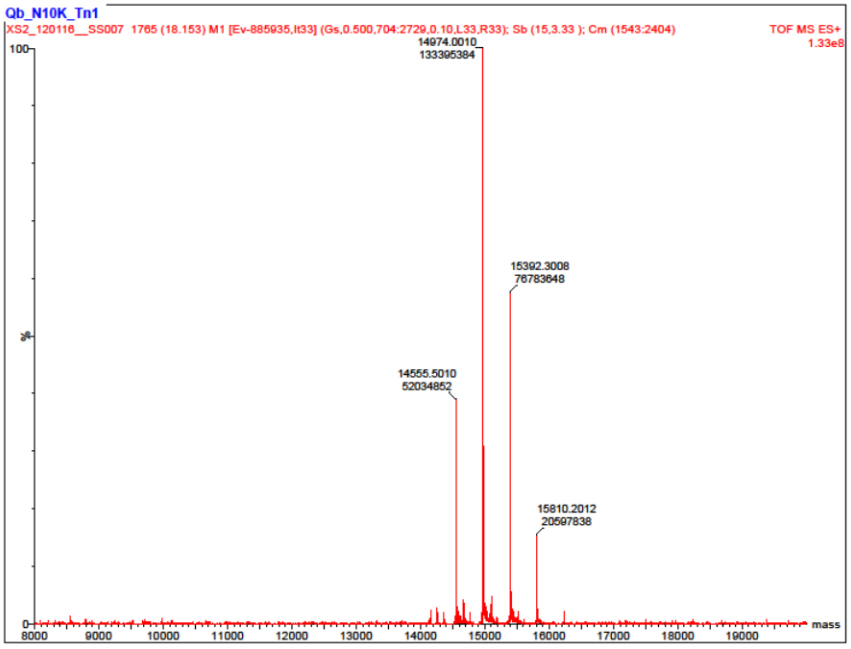

Figure 2.30: (Cont'd)

Qβ_K13R/A40C/D102C_Tn1

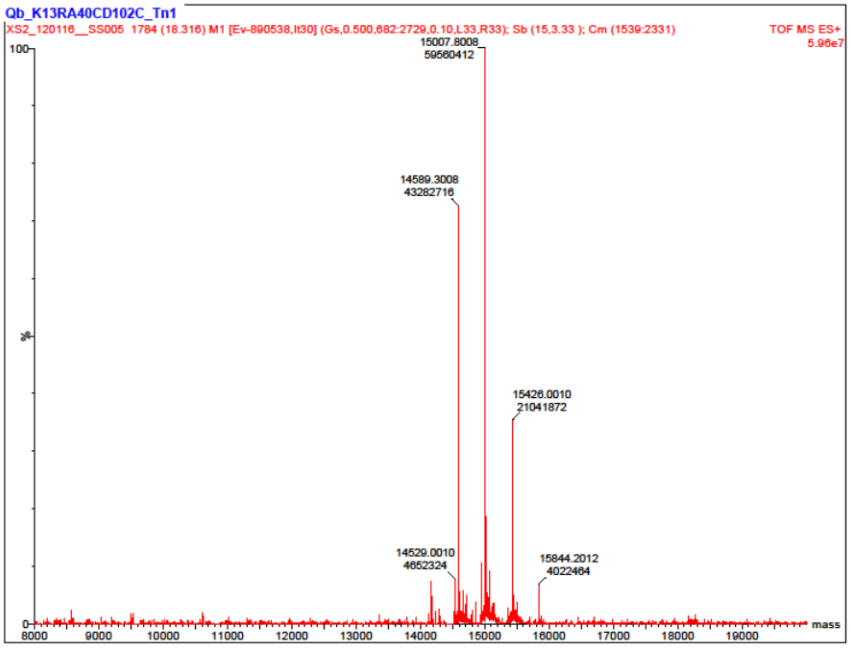

Qβ_A38K_Tn1

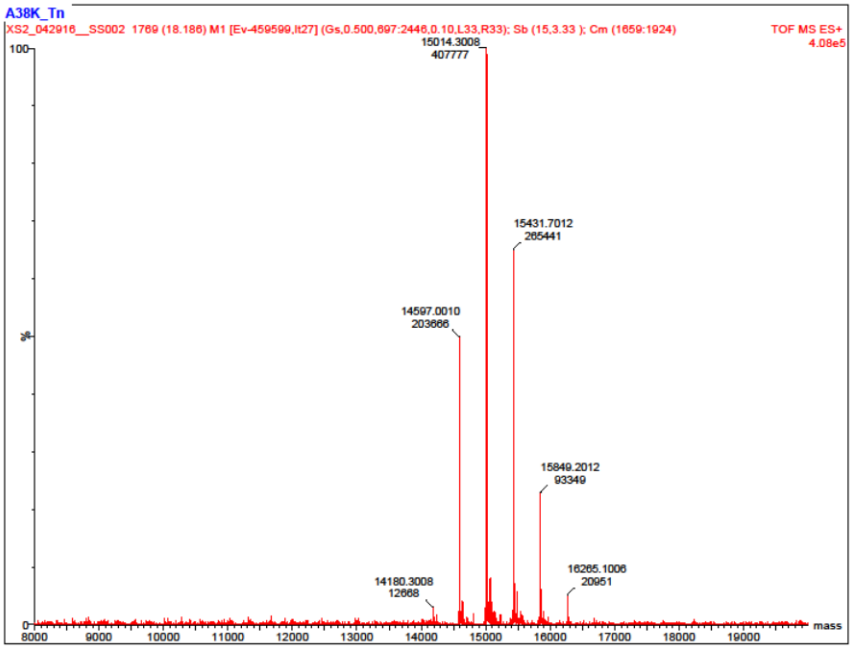

Figure 2.30: (Cont'd)

Qβ_A38K/A40C/D102C_Tn1

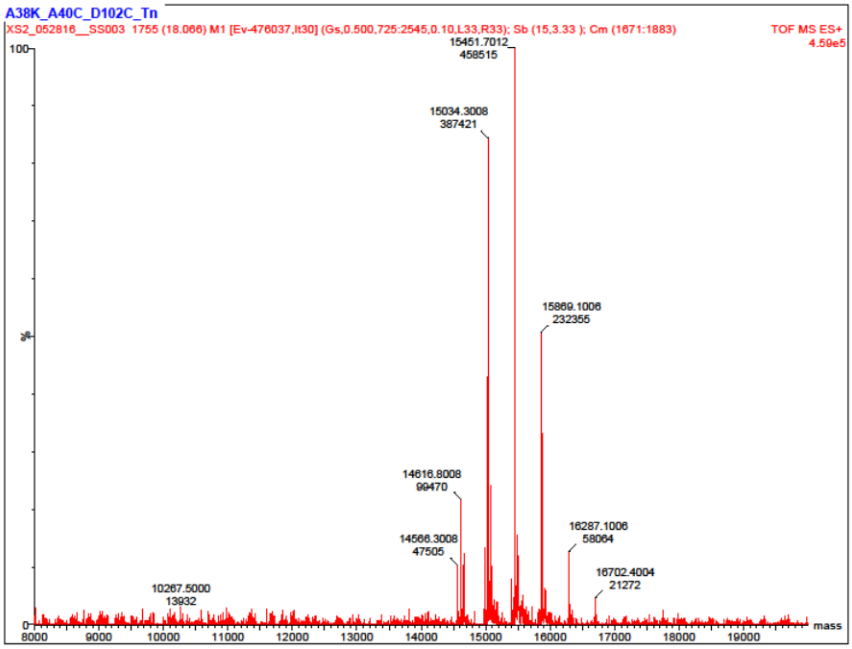

Qβ_A38K/A40C/D102C_Tn2

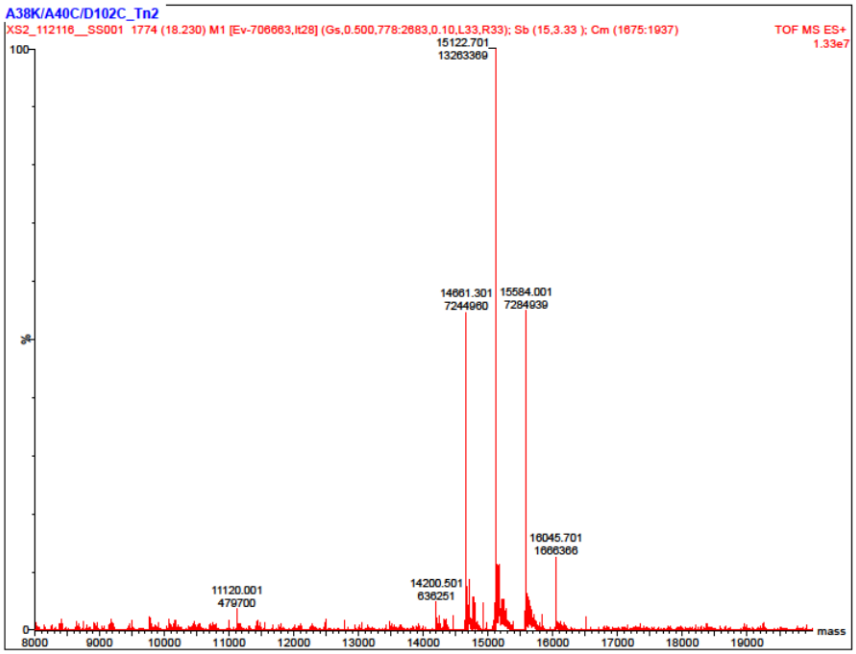

Figure 2.30: (Cont'd)

Qβ_A40C/D102C_Tn1

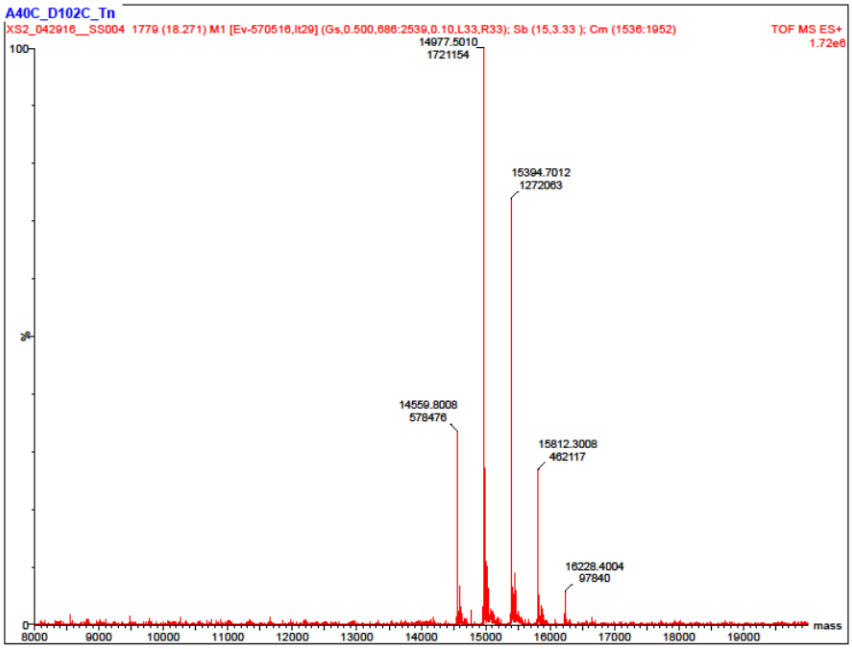

Qβ_A40C/D102C_Tn2

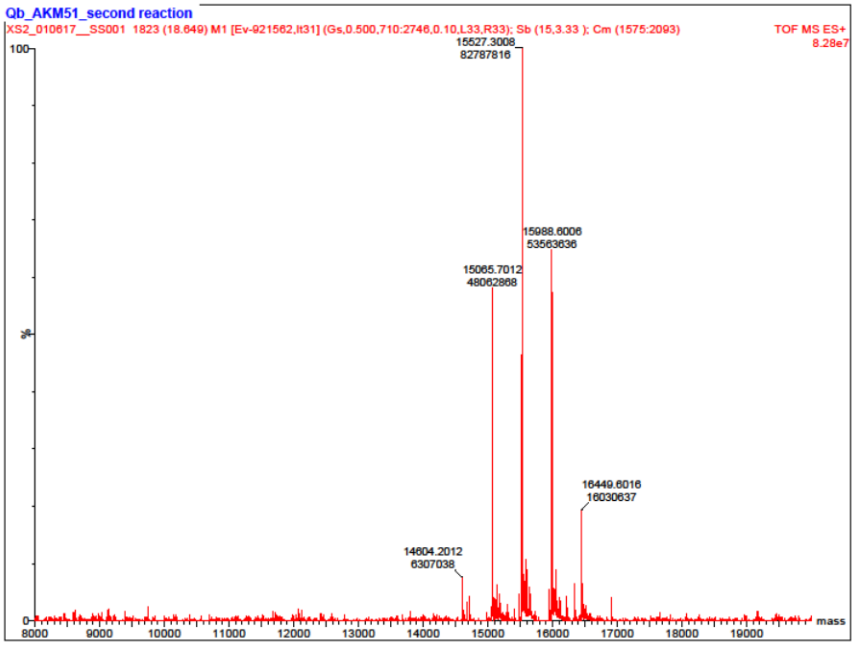

Figure 2.30: (Cont'd)

Qβ_A40S/D102S_Tn1

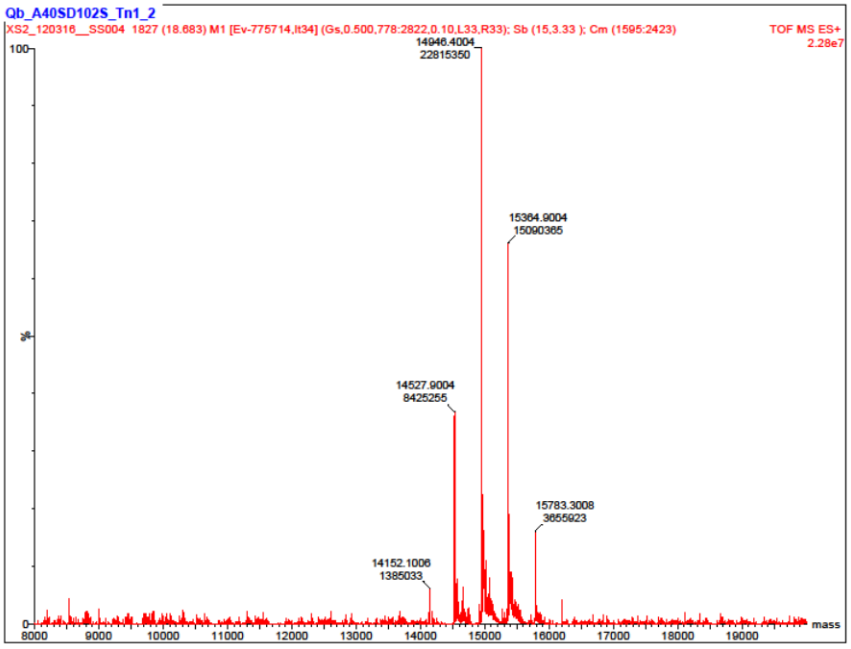

Qβ_T75K_Tn1

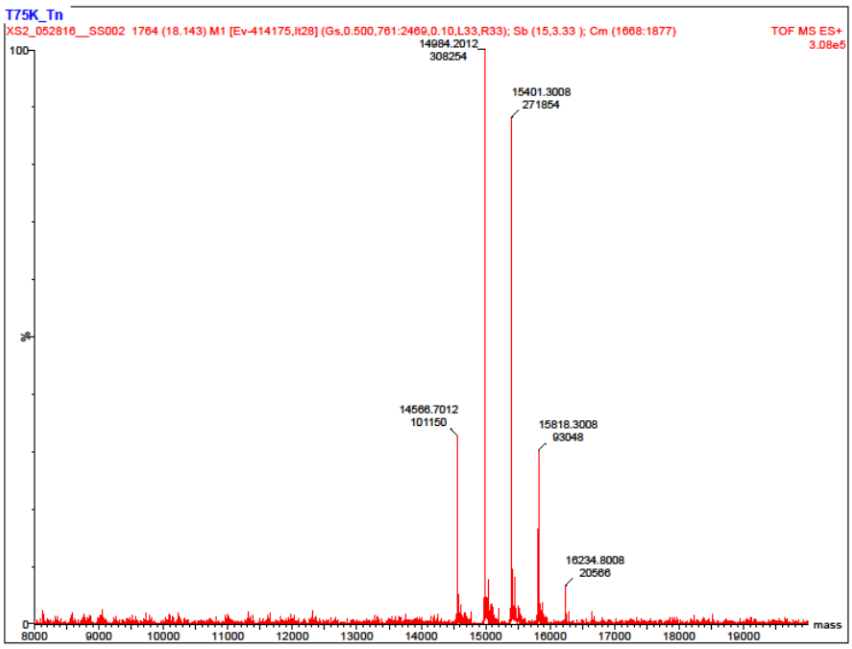

Figure 2.30: (Cont'd)

Qβ_A117K_Tn1

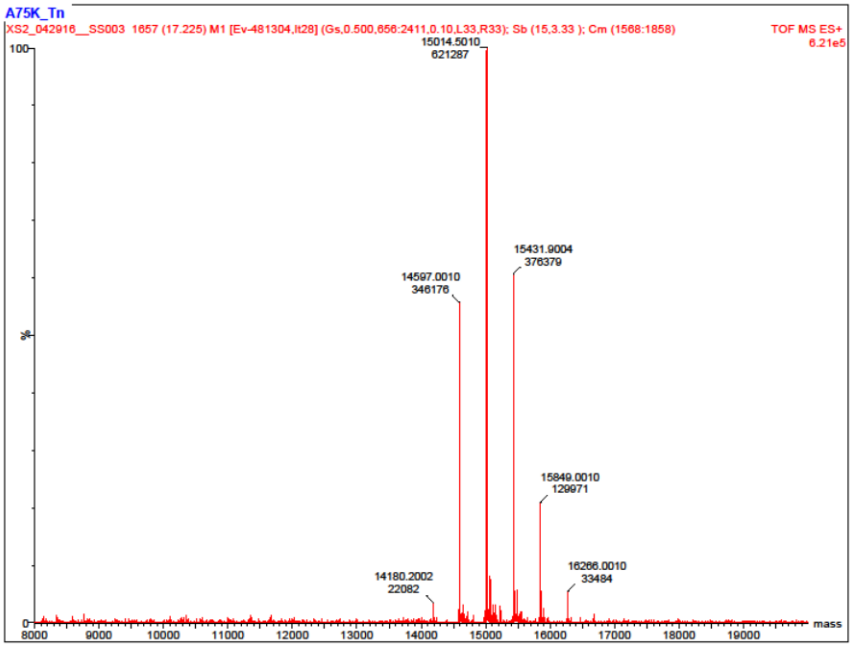

Qβ_P119K_Tn1

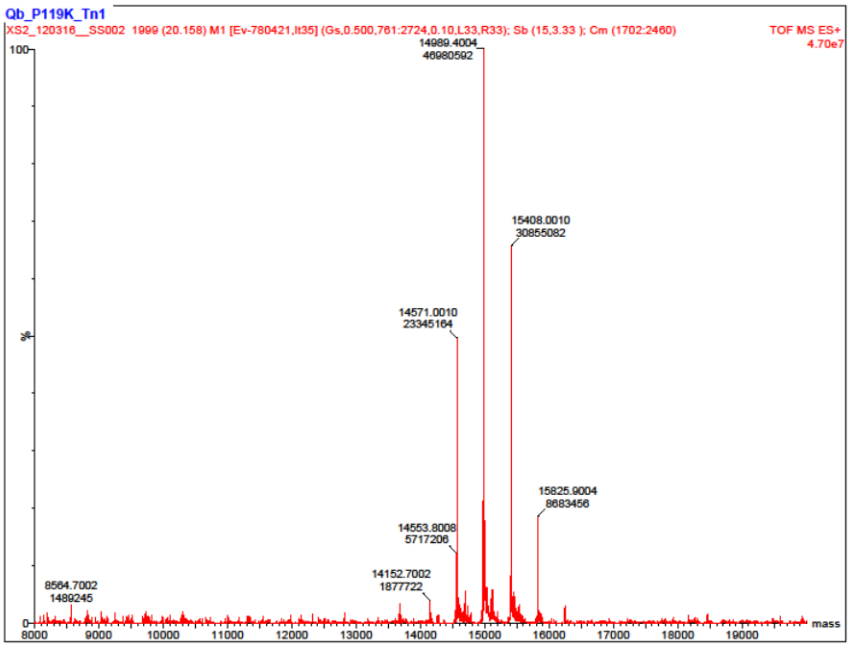

APPENDIX C

NMR spectra

*N-(Fluoren-9-ylmethoxycarbonyl)-O-(3,4,6-tri-O-acetyl-2-azido-2-deoxy-α-D-galactopyranosyl-L- serine benzyl ester (**SI-11**):*

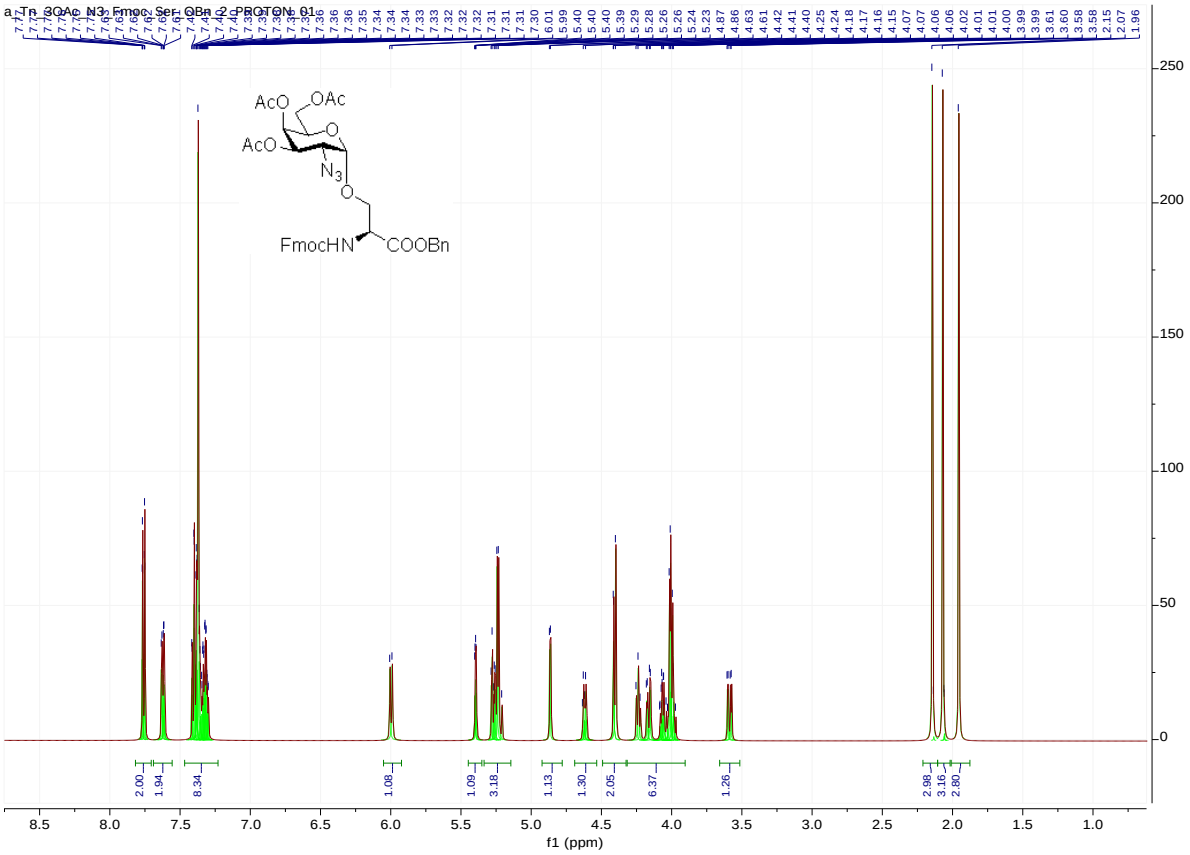

Figure 2.31: ^{1}H NMR spectrum of compound **SI-11**

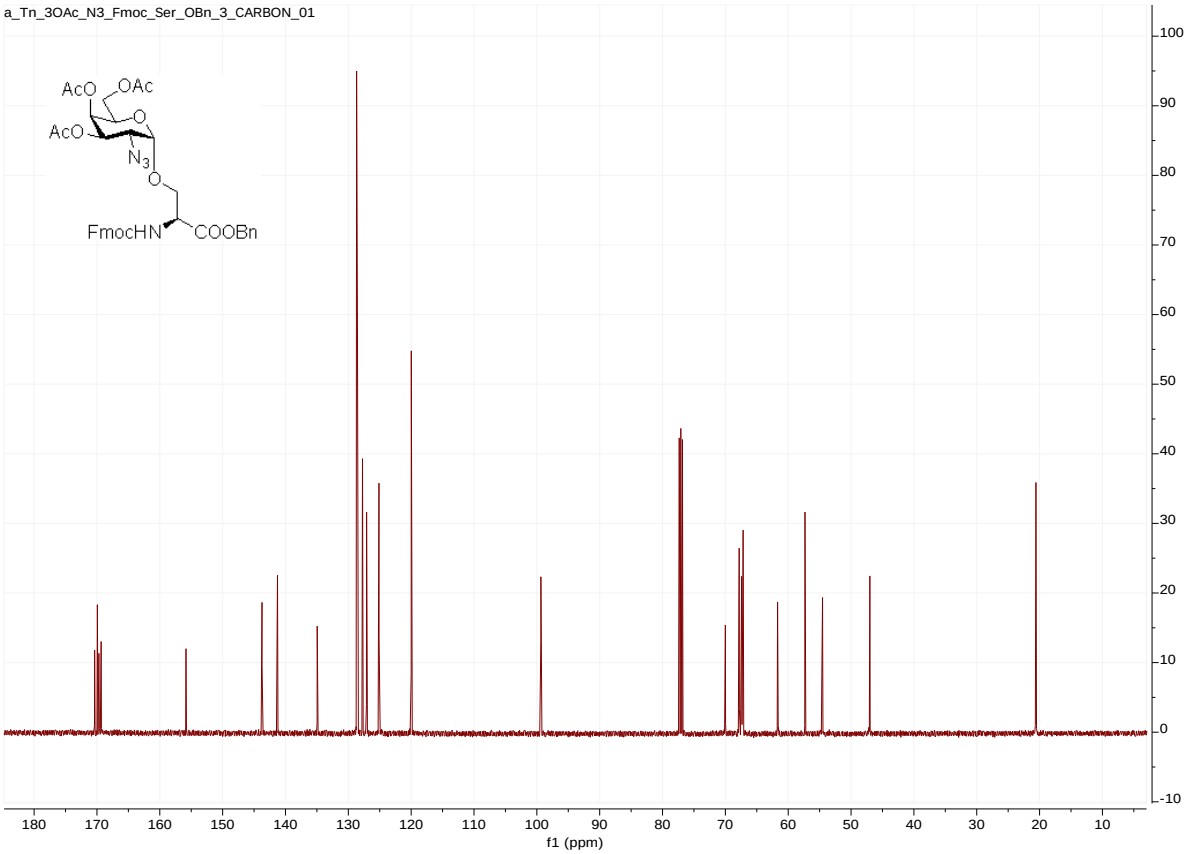

Figure 2.32: ^{13}C NMR spectrum of compound **SI-11**

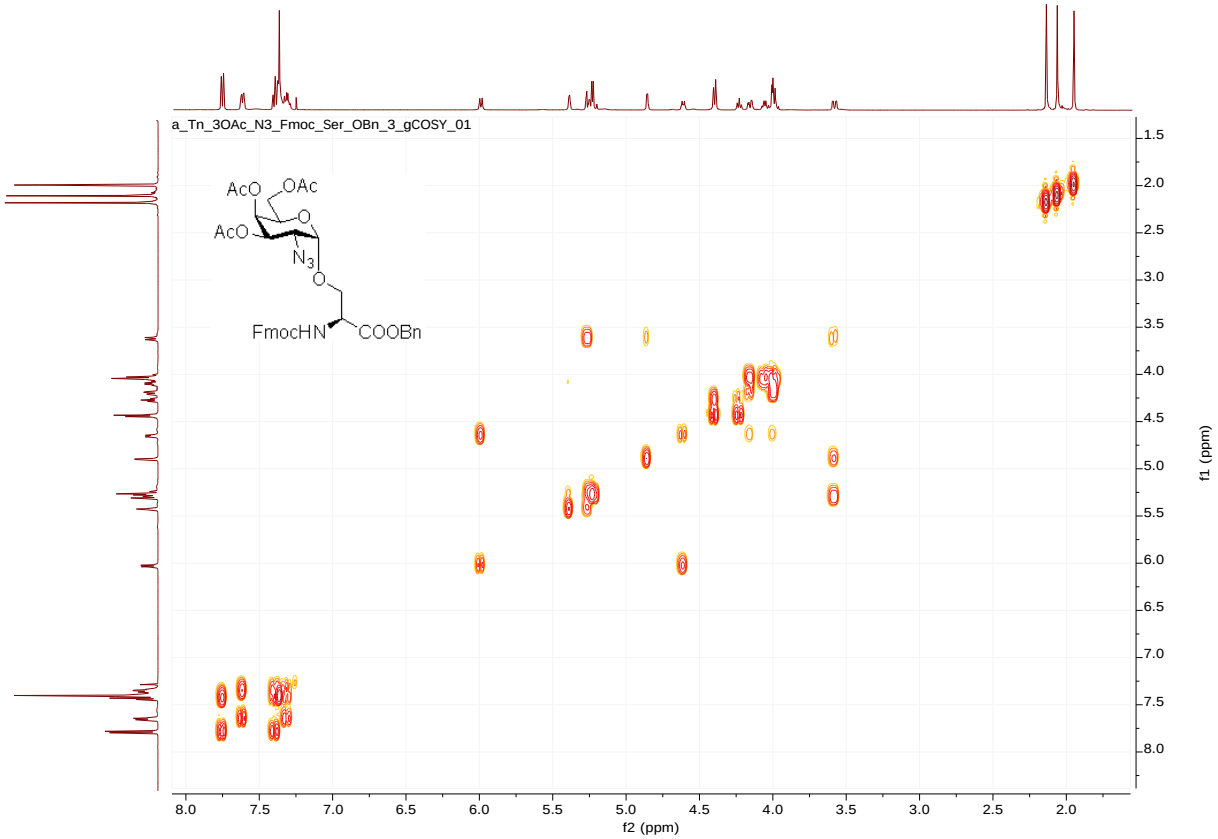

Figure 2.33: ^{1}H-^{1}H COSY NMR spectrum of compound **SI-11**

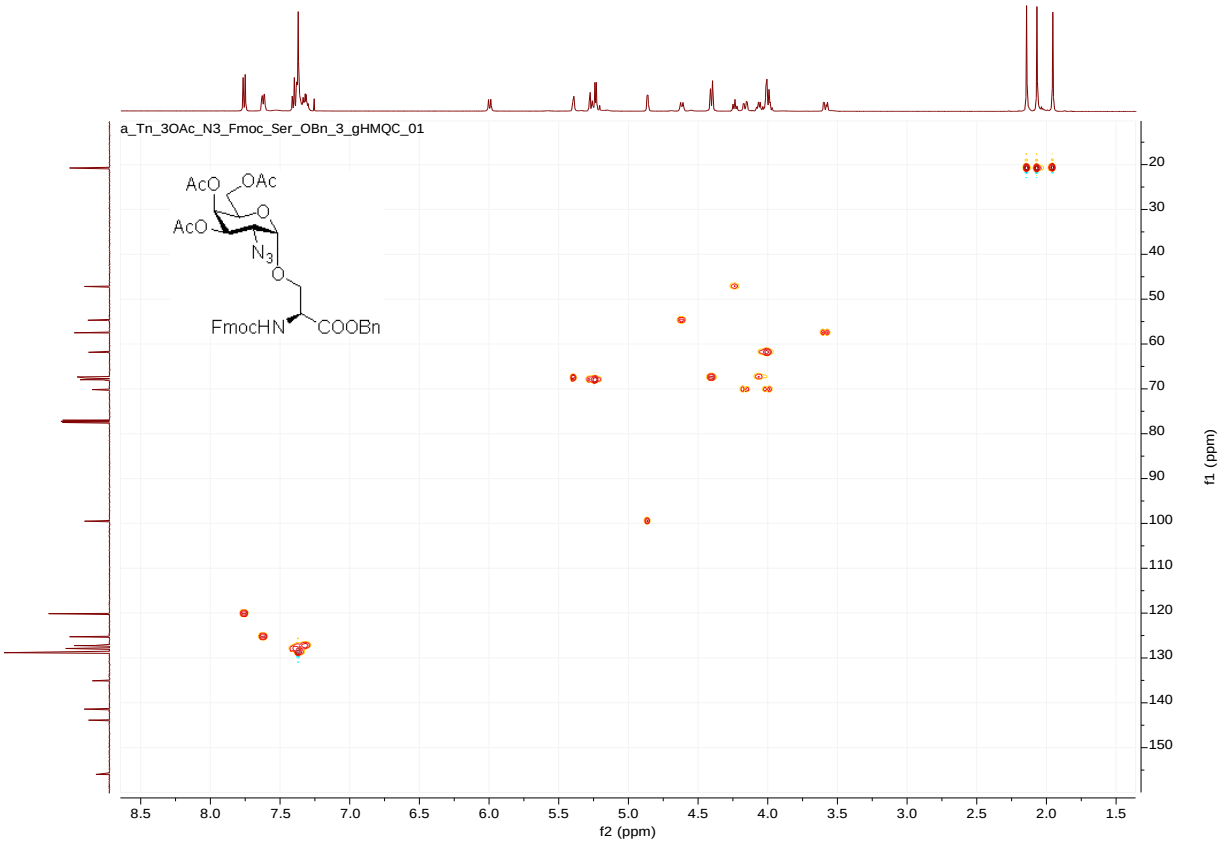

Figure 2.34: gHMQC NMR spectrum of compound **SI-11**

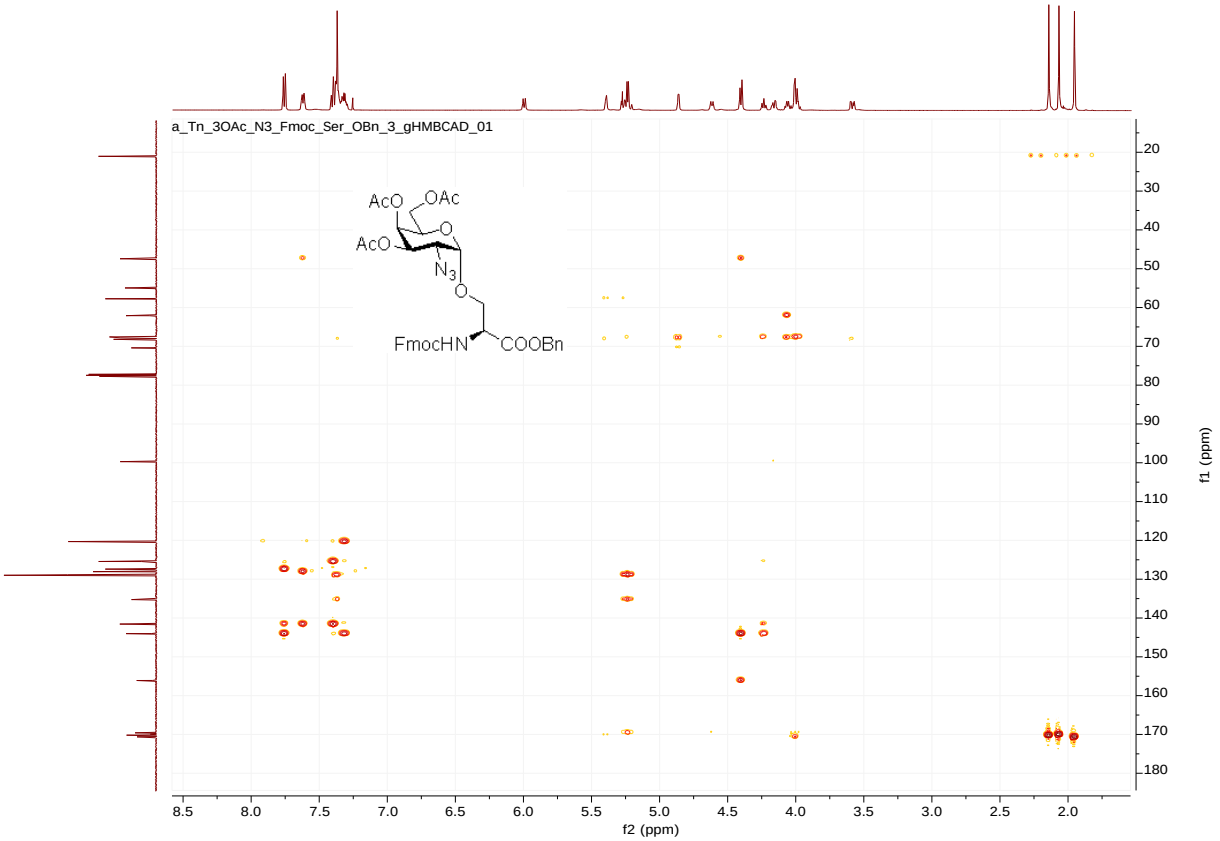

Figure 2.35: gHMBC NMR spectrum of compound **SI-11**

*N-(Fluoren-9-ylmethoxycarbonyl)-O-(3,4,6-tri-O-acetyl-2-acetamido-2-deoxy-α-D-galactopyranosyl-L-serine benzyl ester (**SI-12**):*

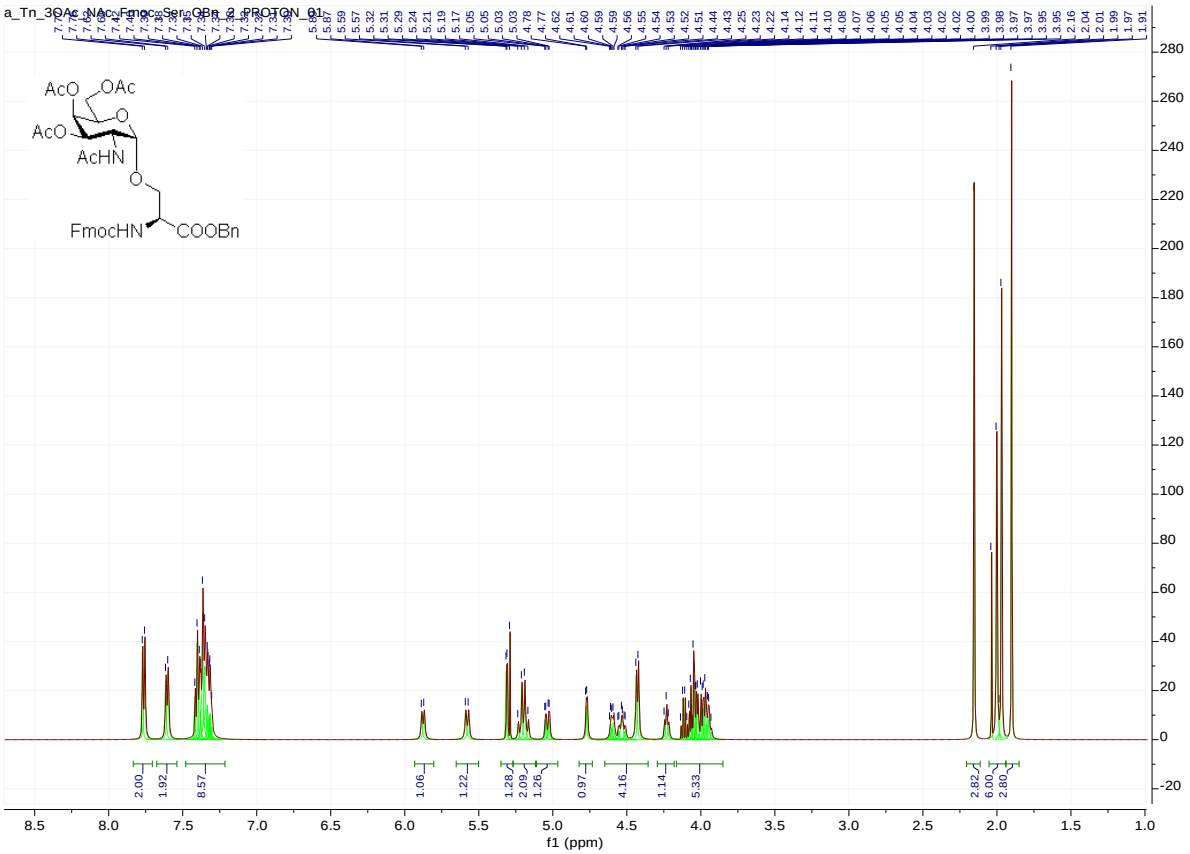

Figure 2.36: ^{1}H NMR spectrum of compound **SI-12**

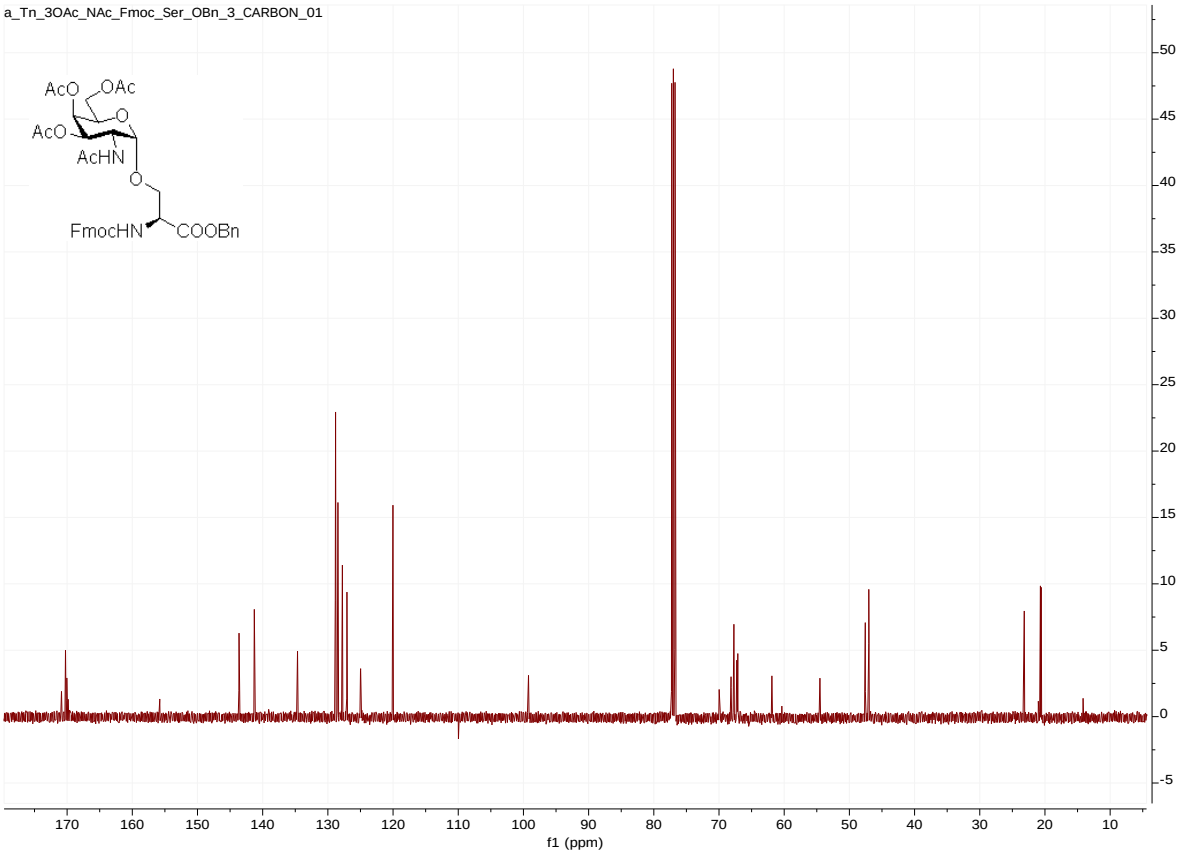

Figure 2.37: ^{13}C NMR spectrum of compound **SI-12**

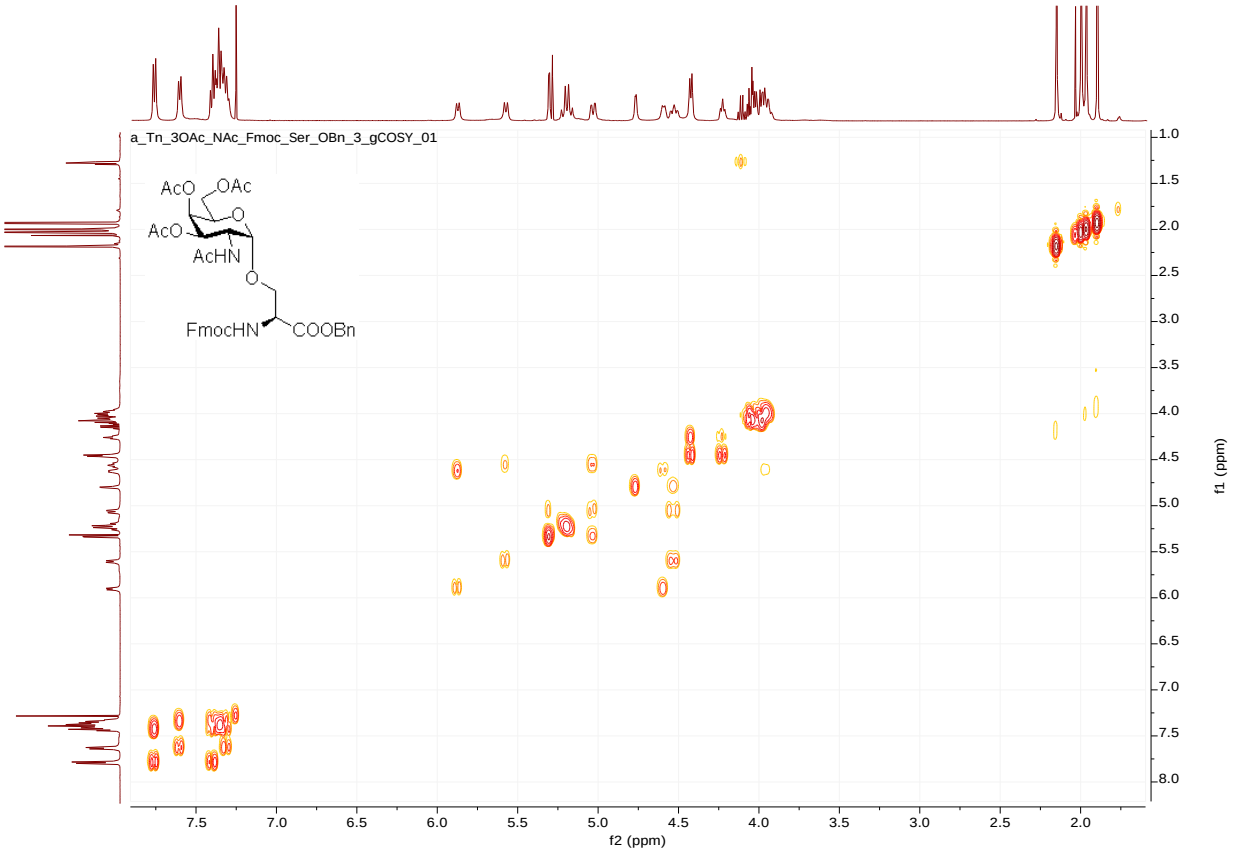

Figure 2.38: ^{1}H-^{1}H COSY NMR spectrum of compound **SI-12**

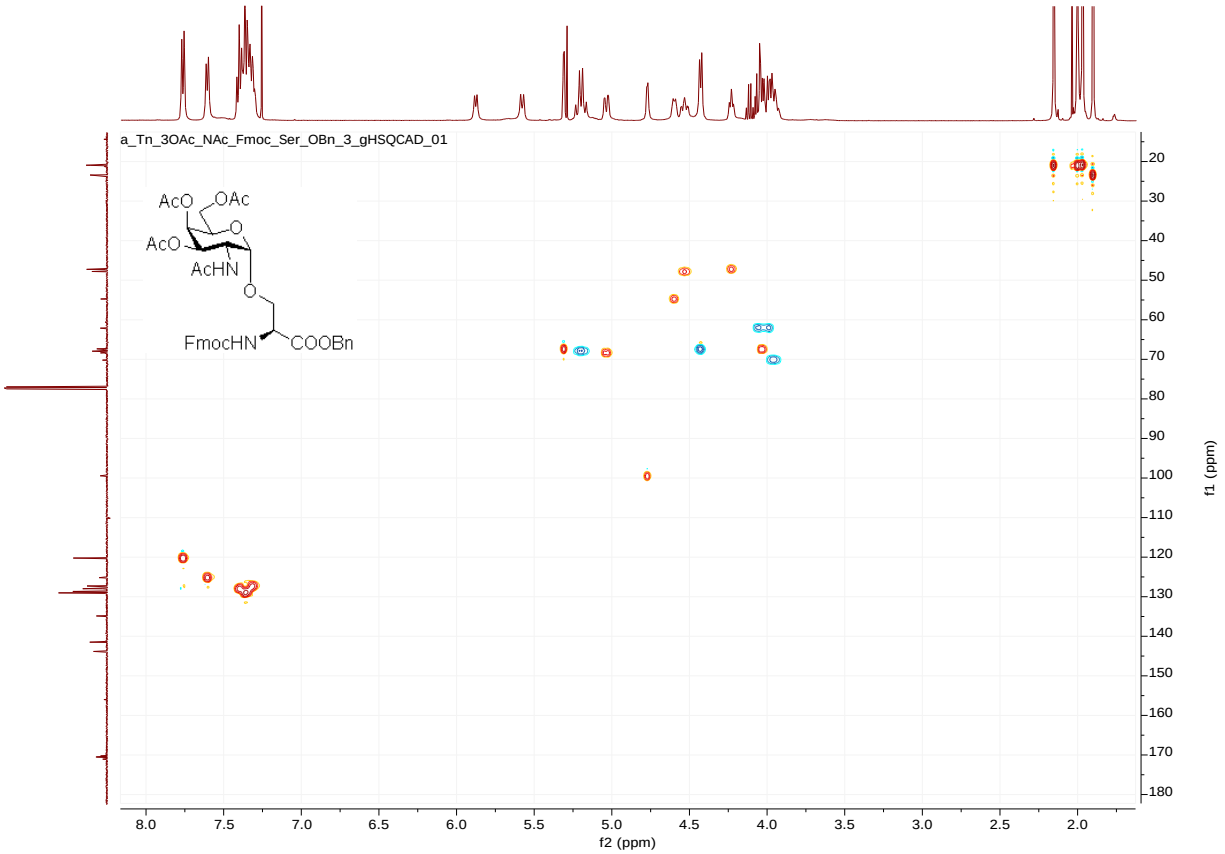

Figure 2.39: gHMQC NMR spectrum of compound **SI-12**

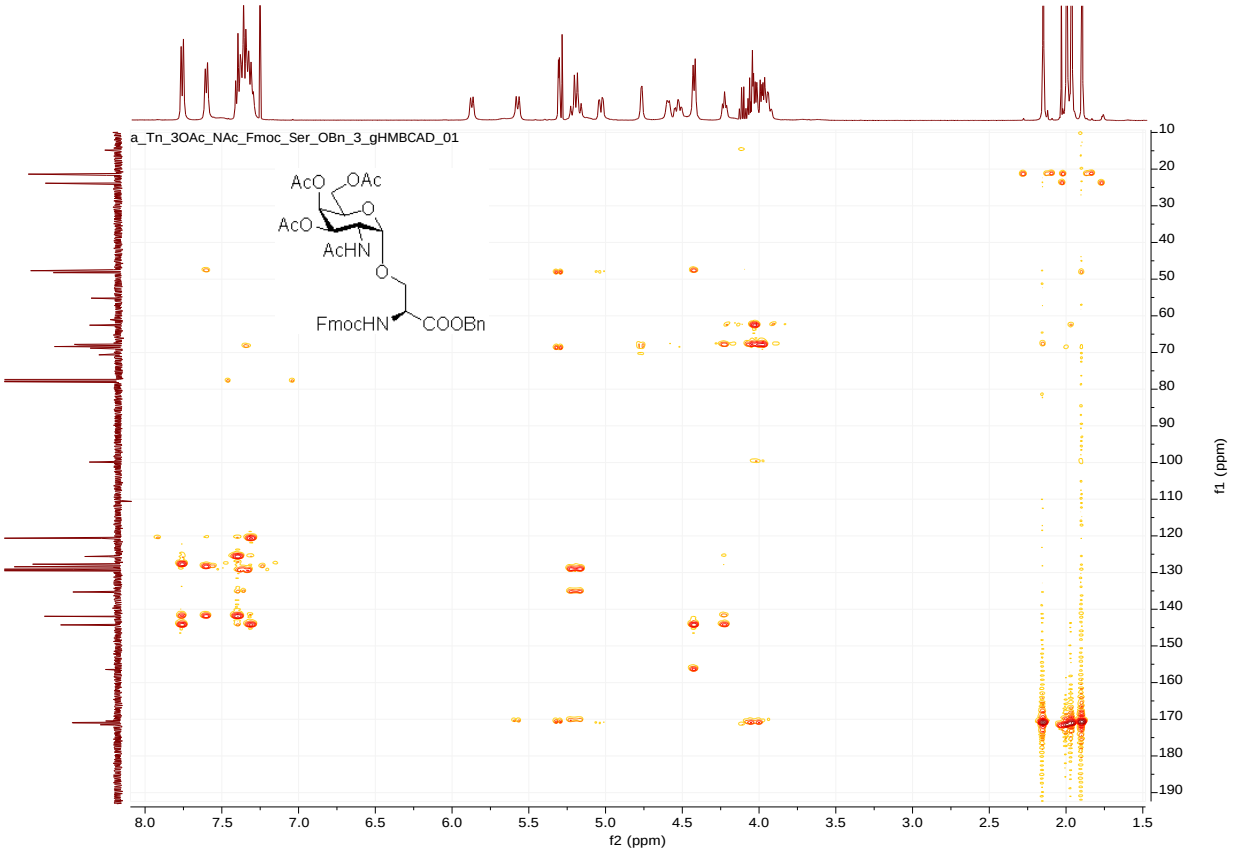

Figure 2.40: gHMBC NMR spectrum of compound **SI-12**

*N-(Fluoren-9-ylmethoxycarbonyl)-O-(3,4,6-tri-O-acetyl-2-acetamido-2-deoxy-α-D-galactopyranosyl-L-serine 2-ethanolyl amide (**SI-14**):*

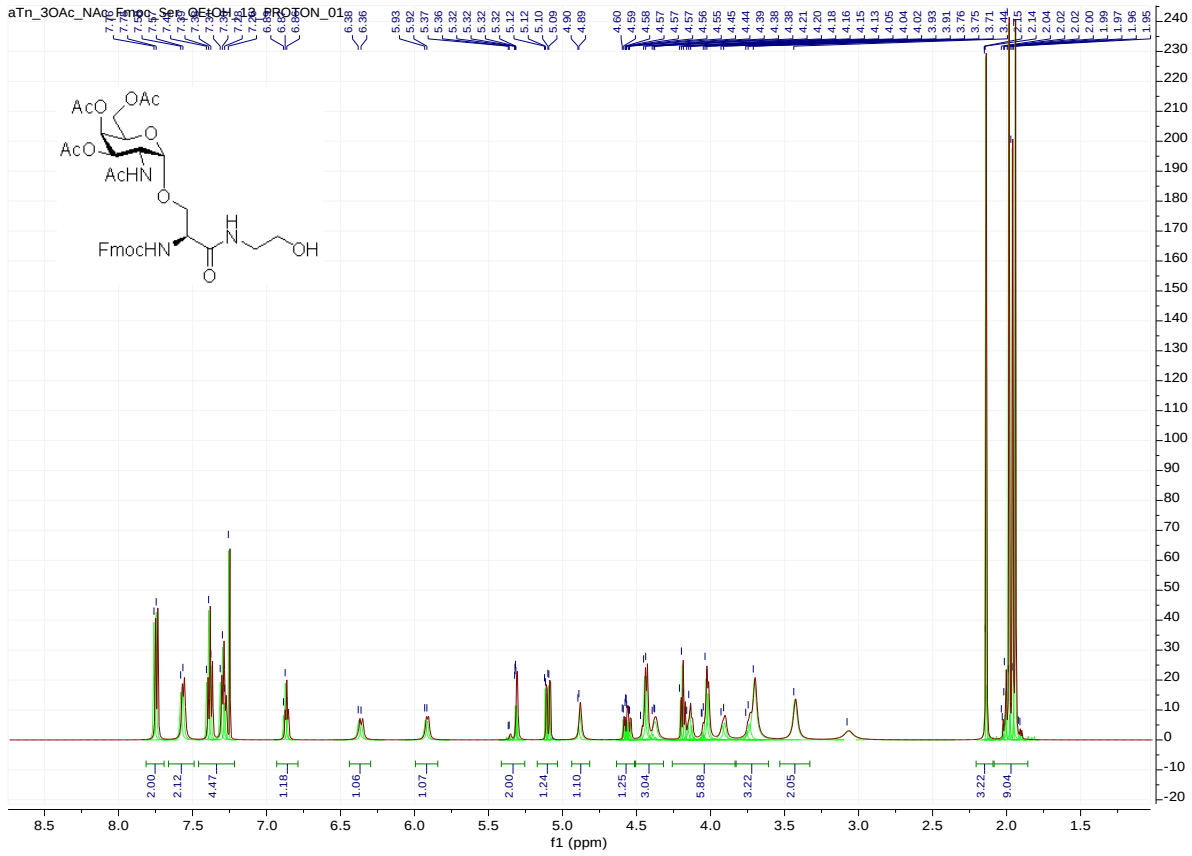

Figure 2.41: ^{1}H NMR spectrum of compound **SI-14**

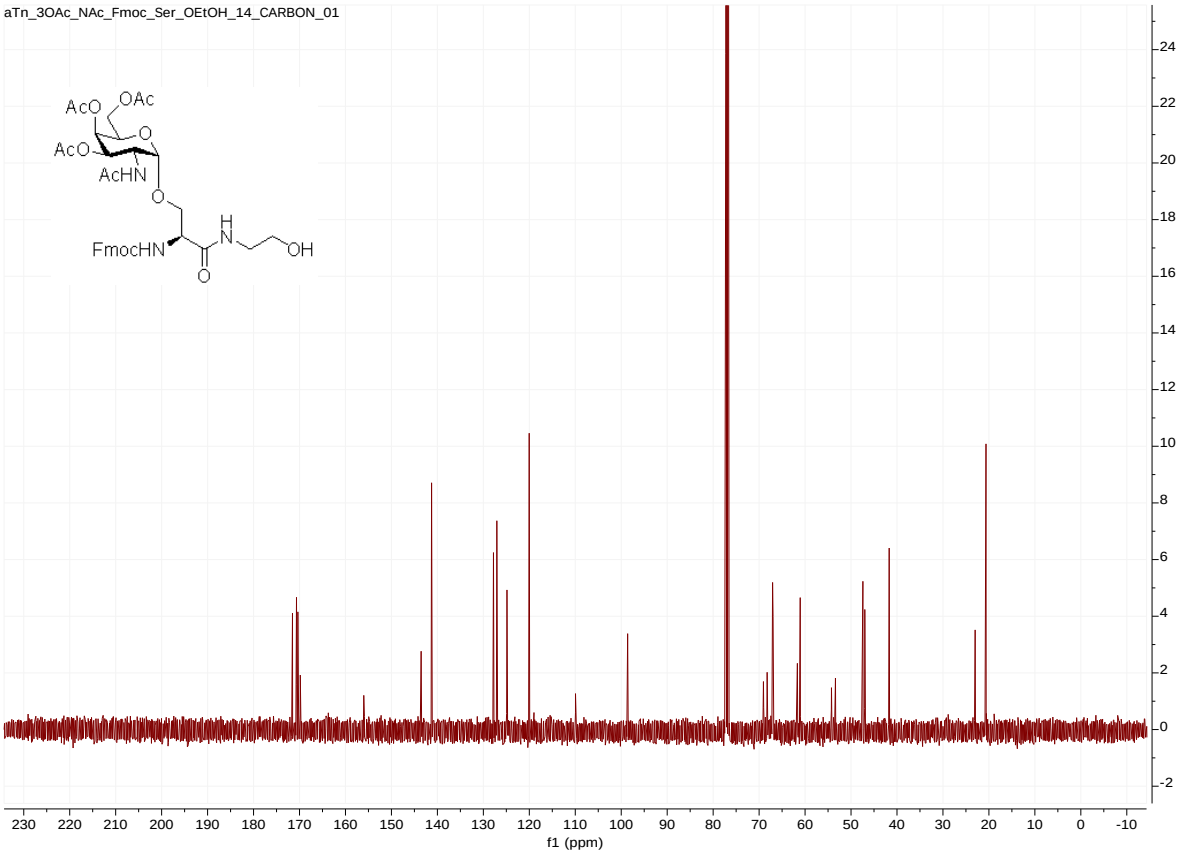

Figure 2.42: ^{13}C NMR spectrum of compound **SI-14**

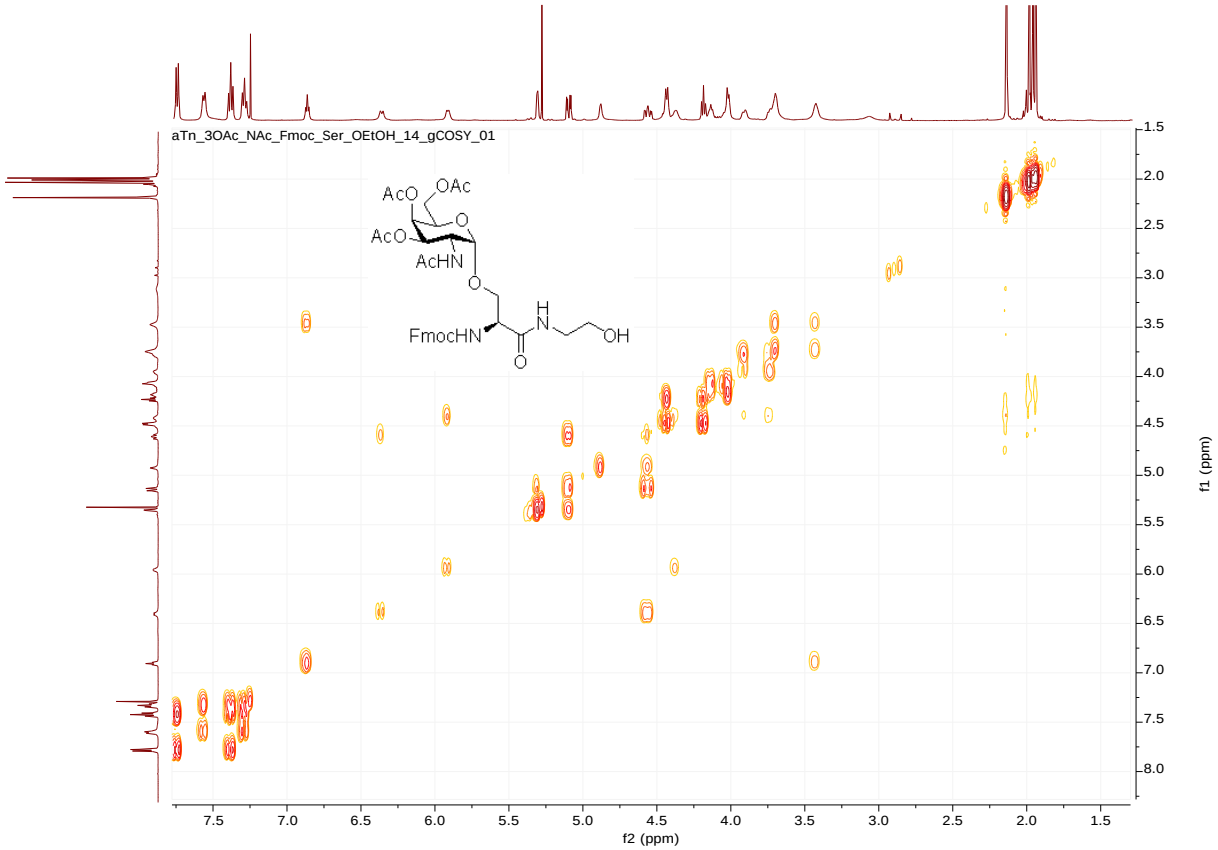

Figure 2.43: ^{1}H-^{1}H COSY NMR spectrum of compound **SI-14**

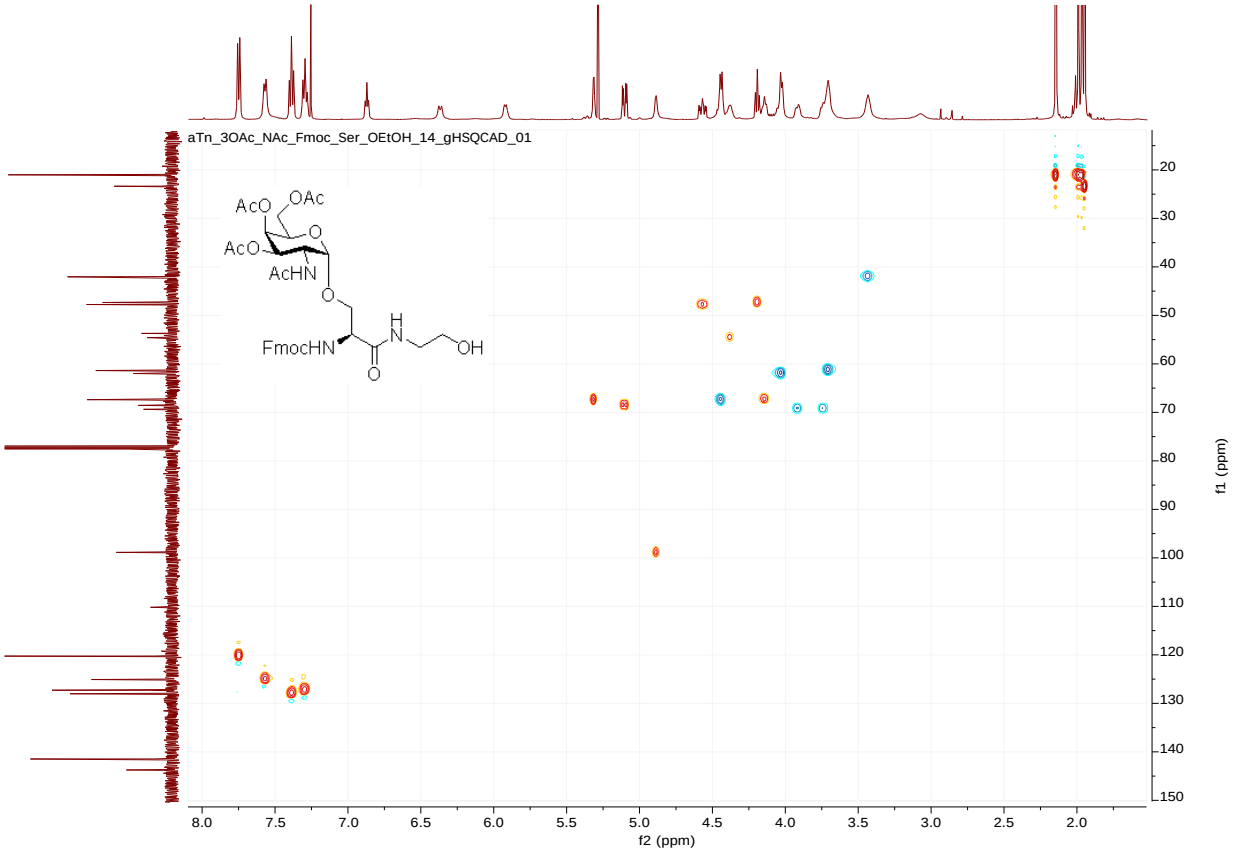

Figure 2.44: gHMQC NMR spectrum of compound **SI-14**

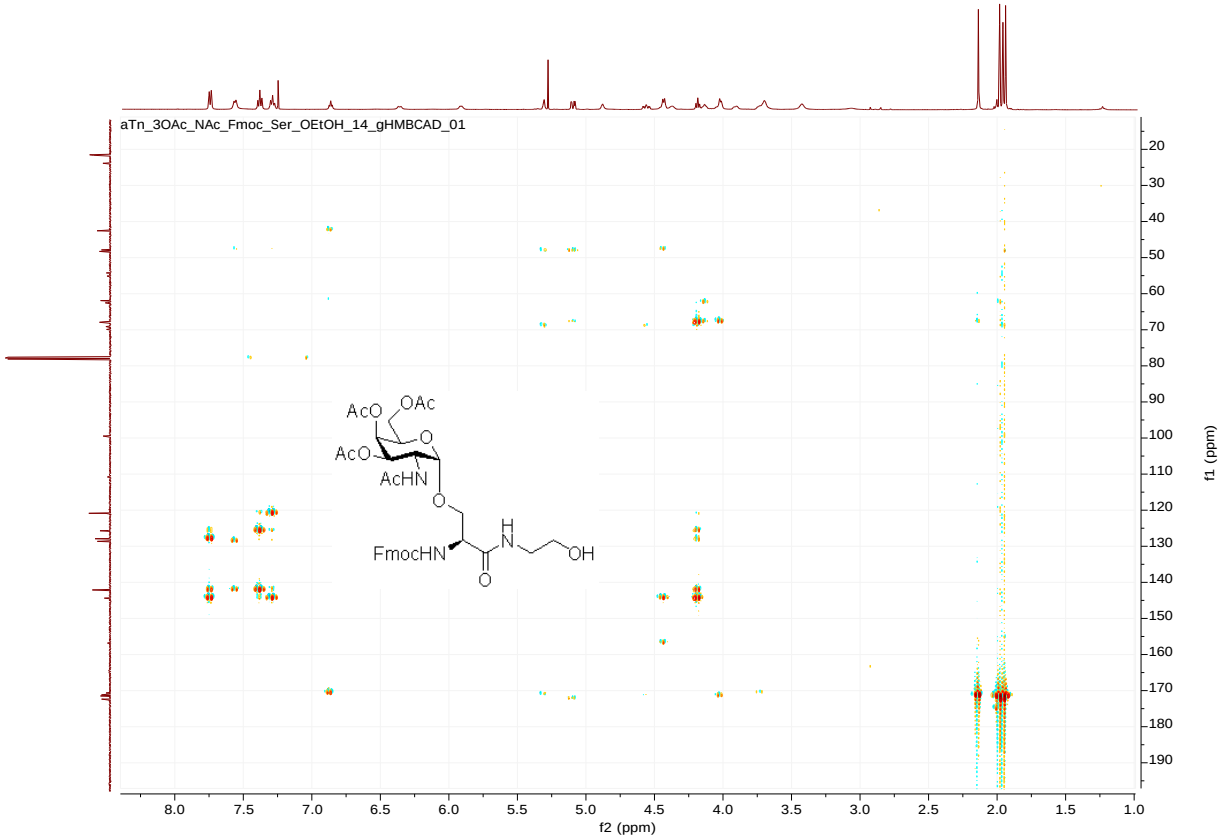

Figure 2.45: gHMBC NMR spectrum of compound **SI-14**

*O-2-acetamido-2-deoxy-α-D-galactopyranosyl-L-serine (**Tn1**):*

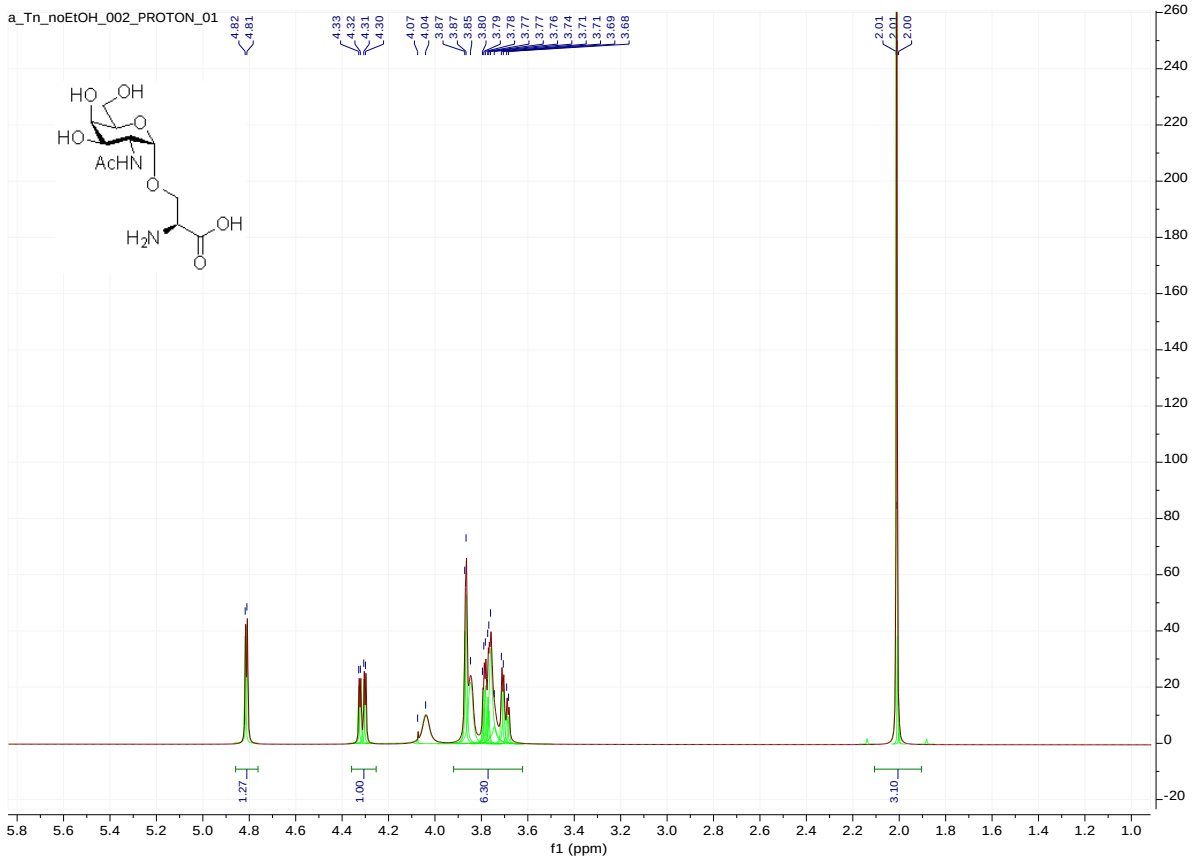

Figure 2.46: ^{1}H NMR spectrum of compound **Tn1**

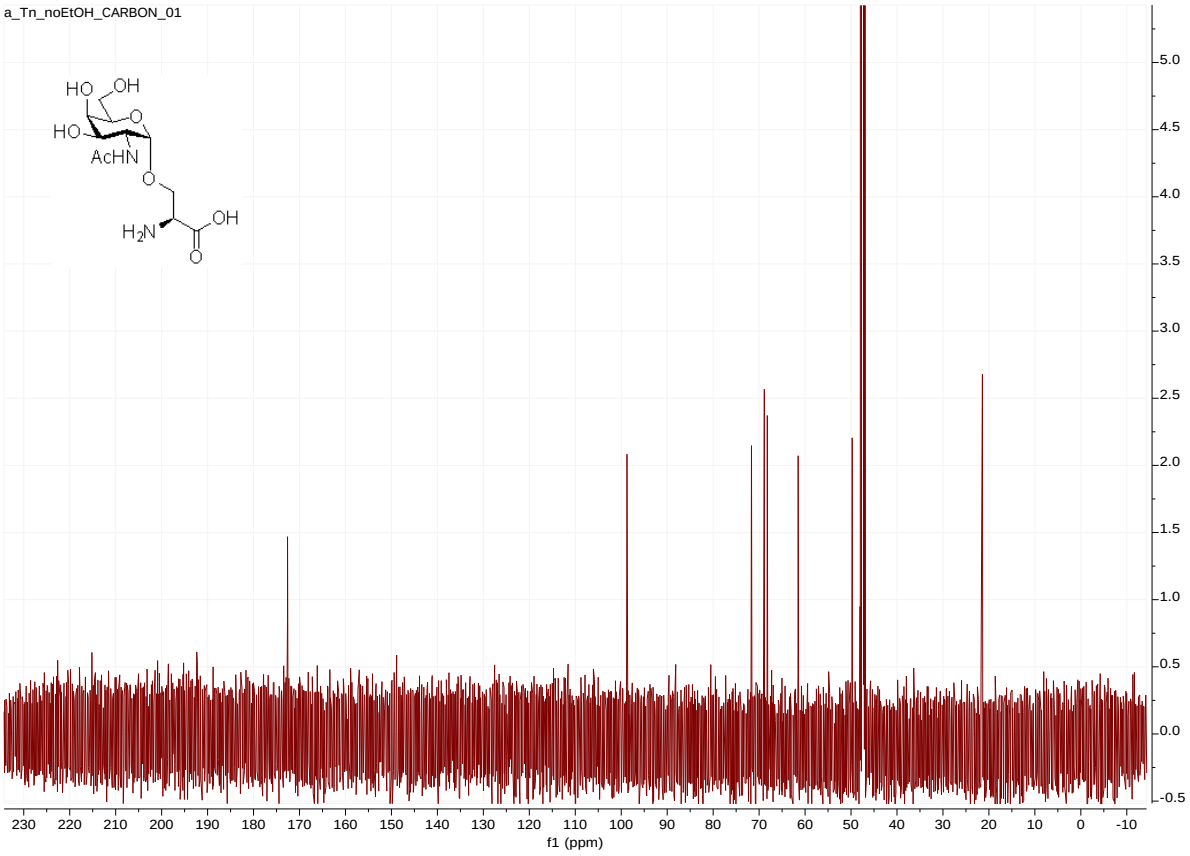

Figure 2.47: ^{13}C NMR spectrum of compound **Tn1**

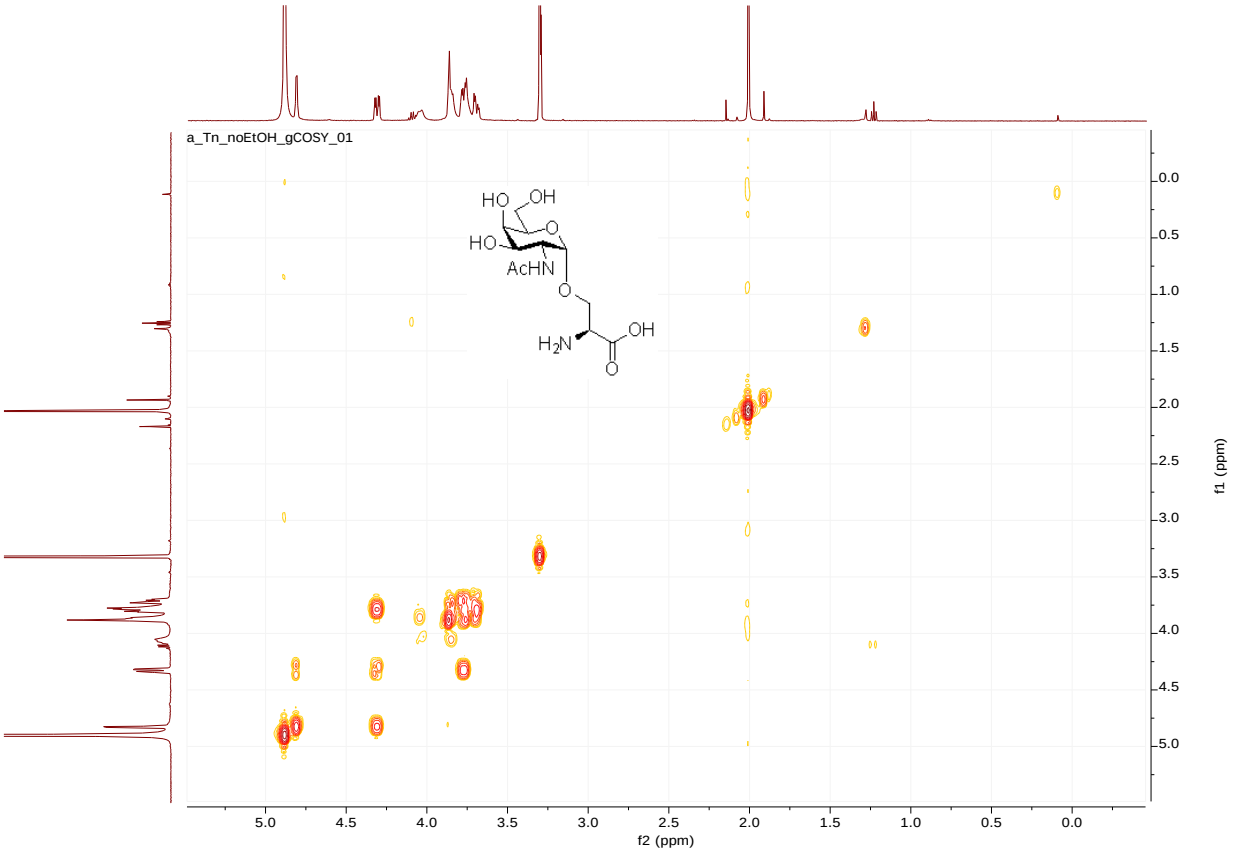

Figure 2.48: ^{1}H-^{1}H COSY NMR spectrum of compound **Tn1**

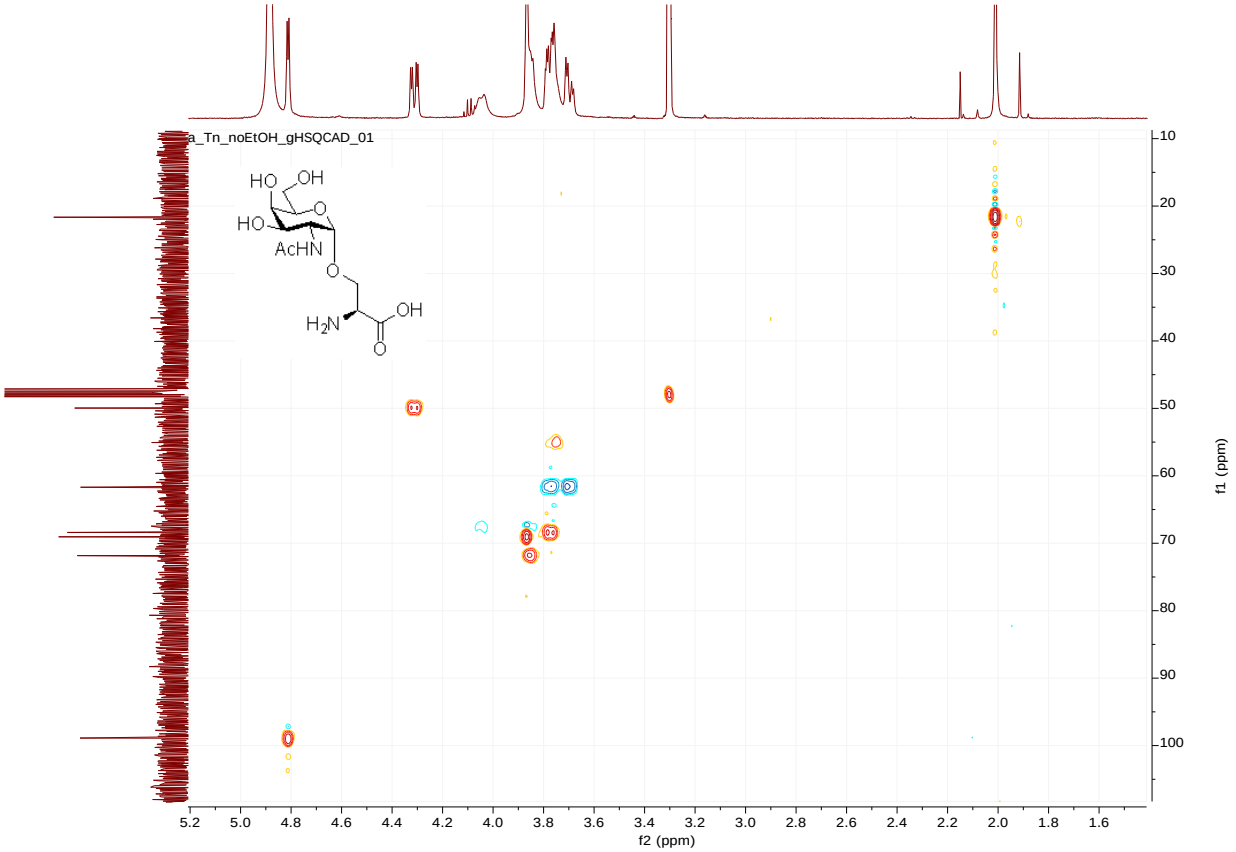

Figure 2.49: gHMQC NMR spectrum of compound **Tn1**

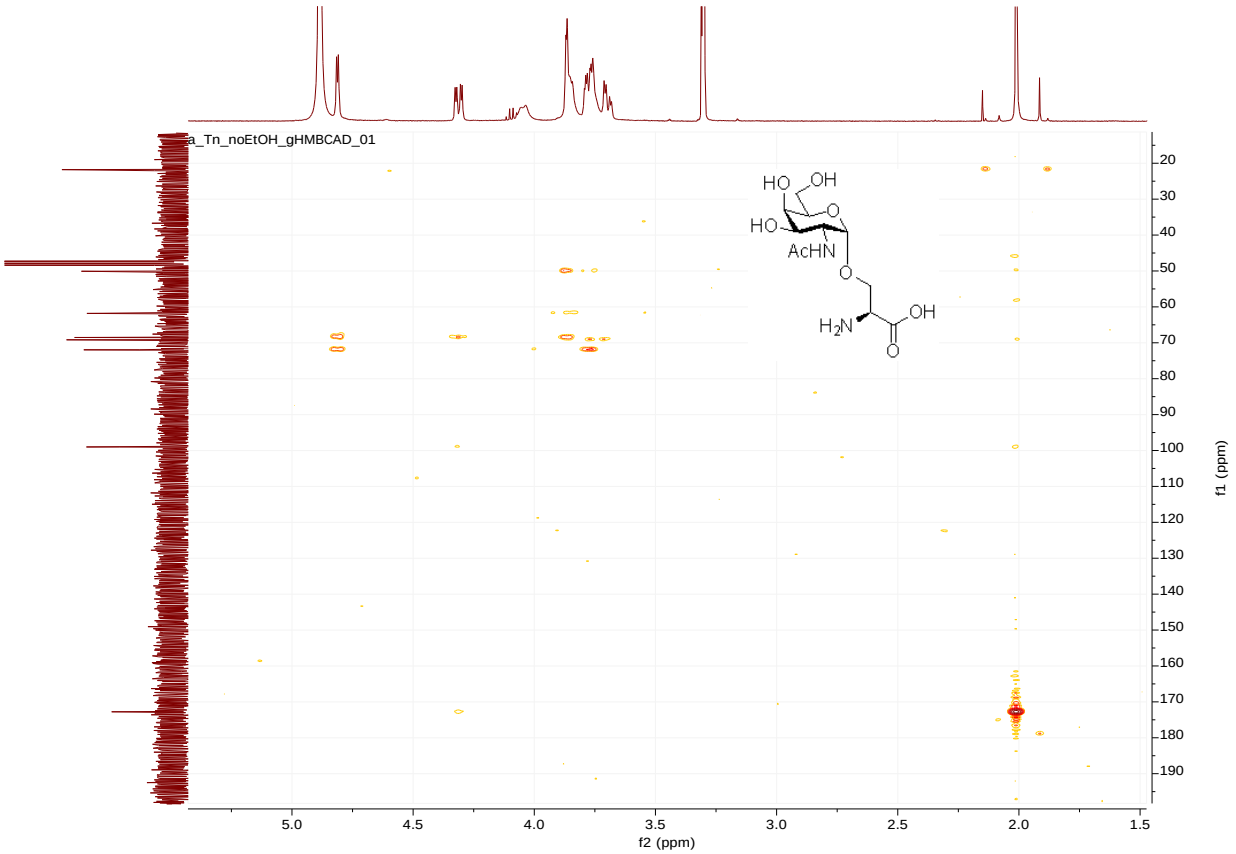

Figure 2.50: gHMBC NMR spectrum of compound **Tn1**

*O-2-acetamido-2-deoxy-α-D-galactopyranosyl-L-serine 2-ethanolyl amide (**Tn2**):*

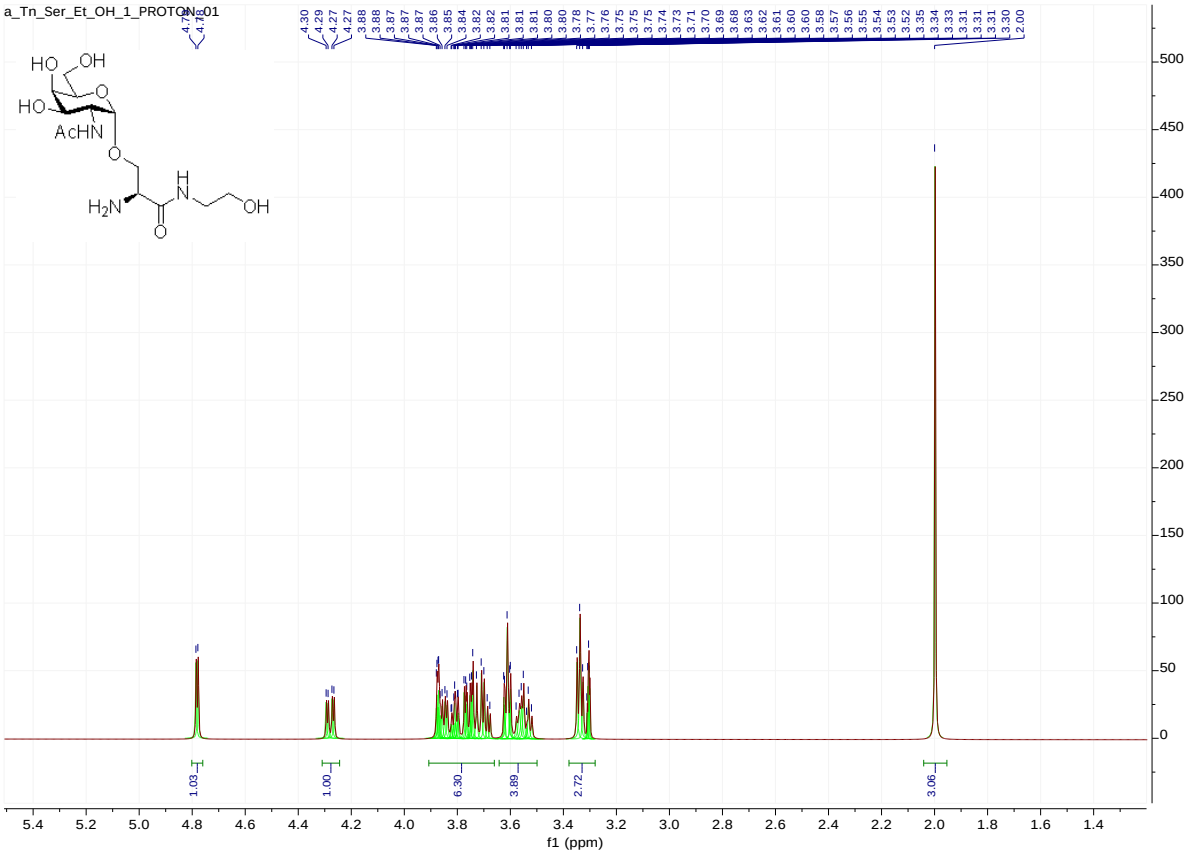

Figure 2.51: ^{1}H NMR spectrum of compound **Tn2**

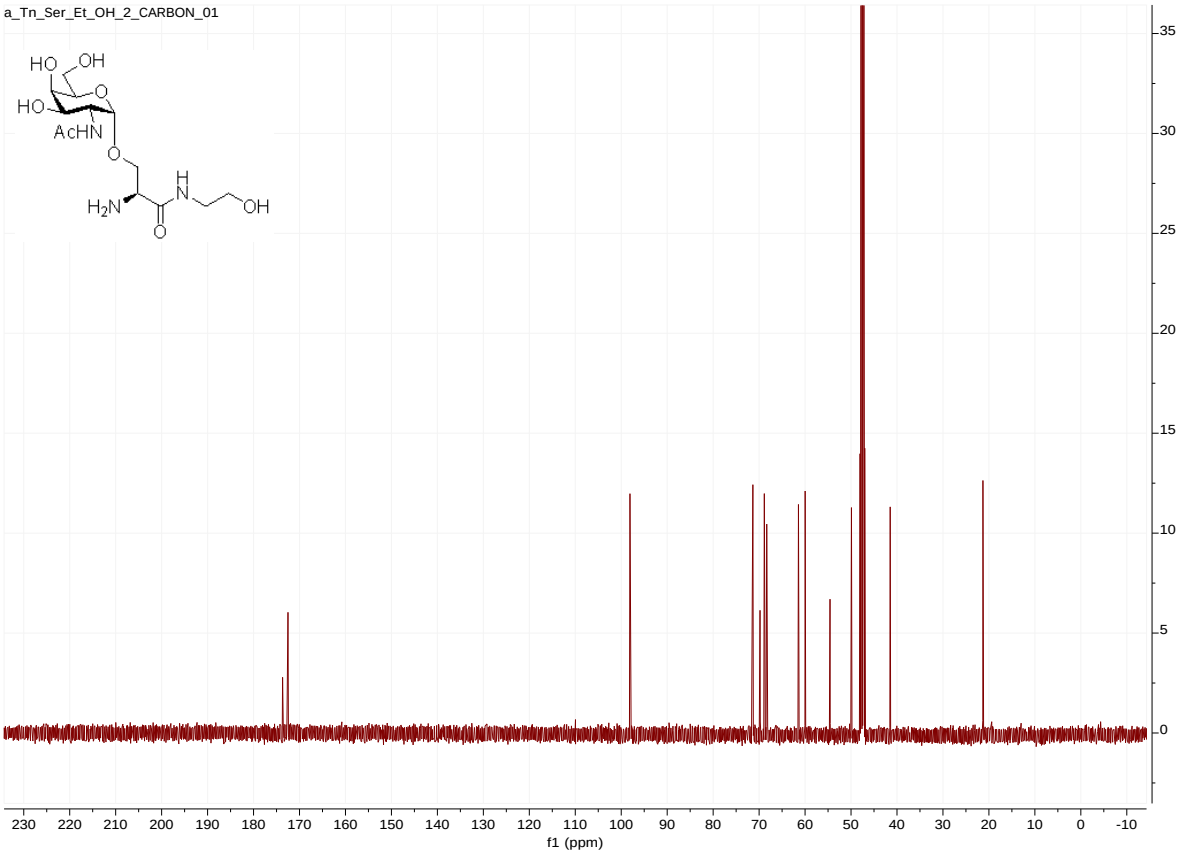

Figure 2.52: ^{13}C NMR spectrum of compound **Tn2**

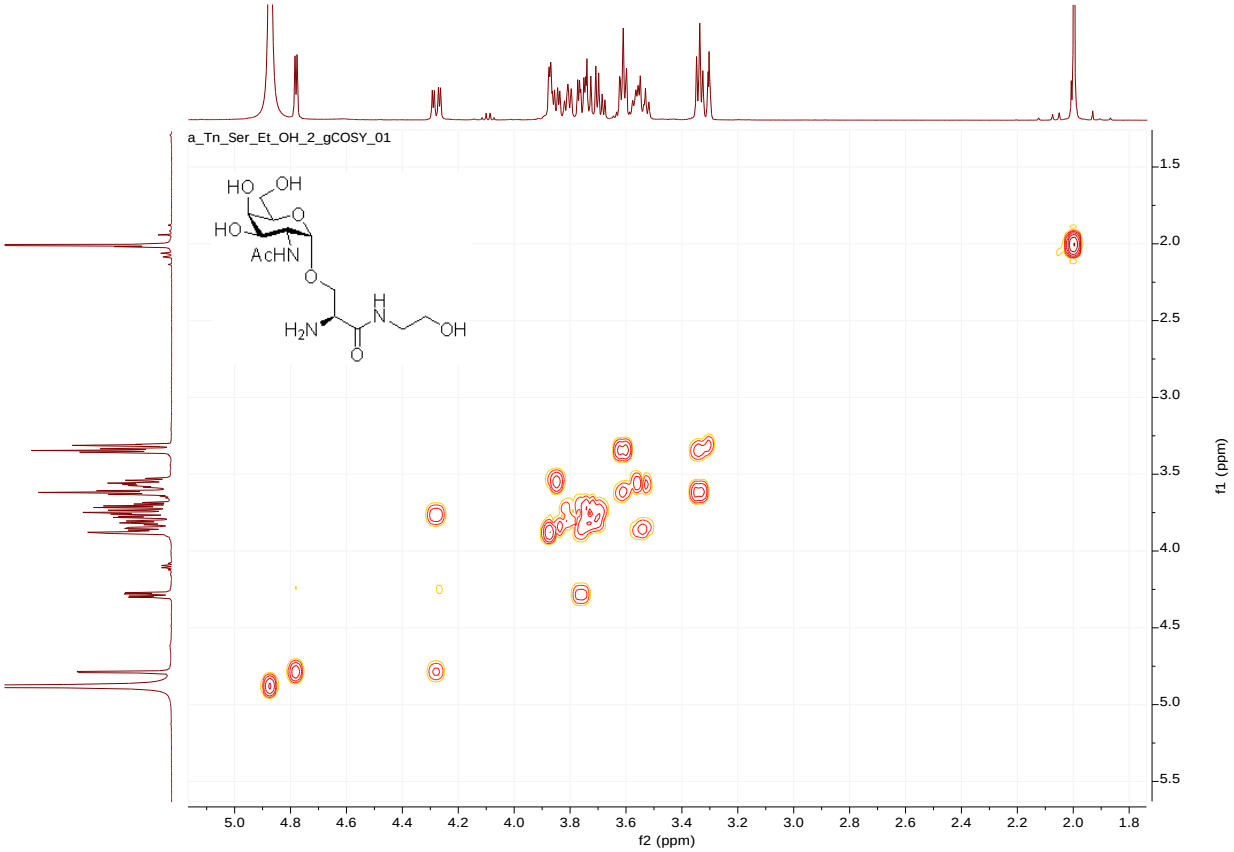

Figure 2.53: ^{1}H-^{1}H COSY NMR spectrum of compound **Tn2**

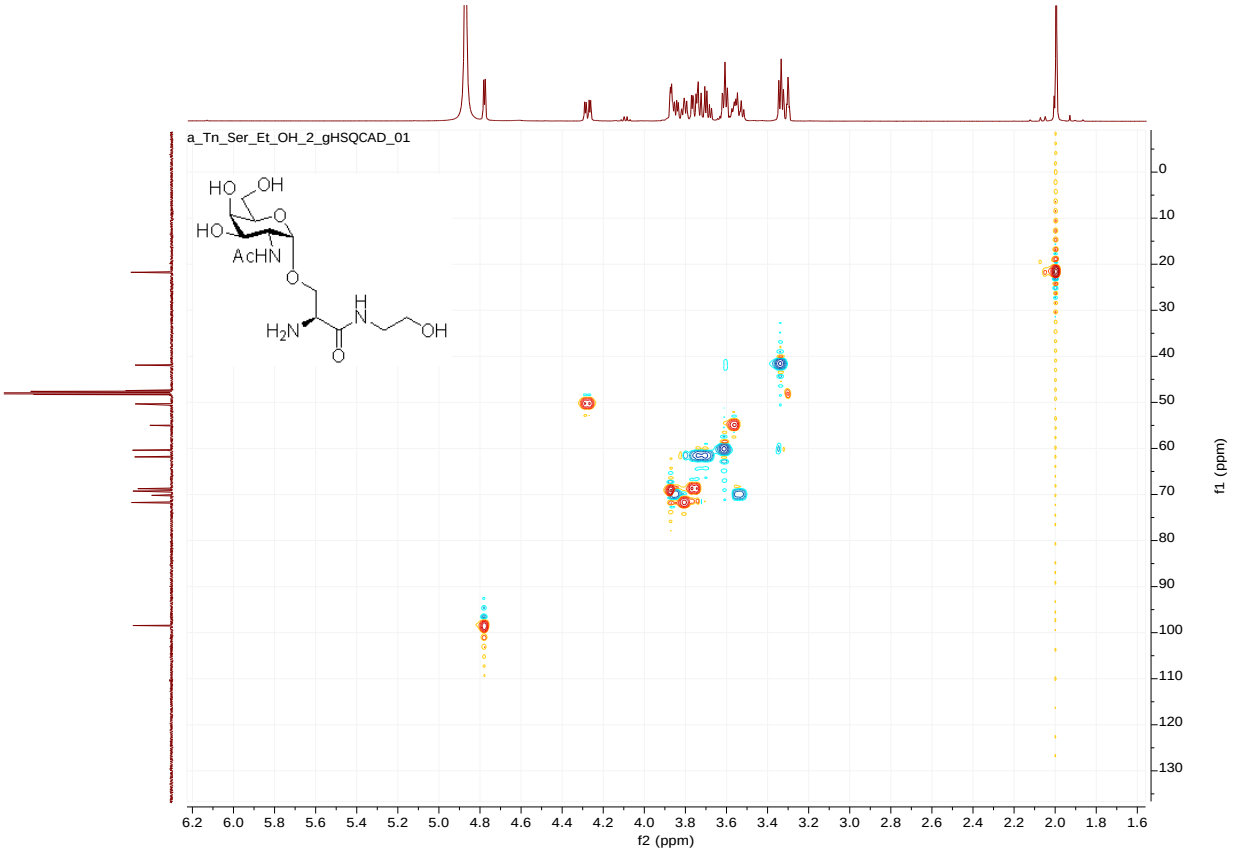

Figure 2.54: gHMQC NMR spectrum of compound **Tn2**

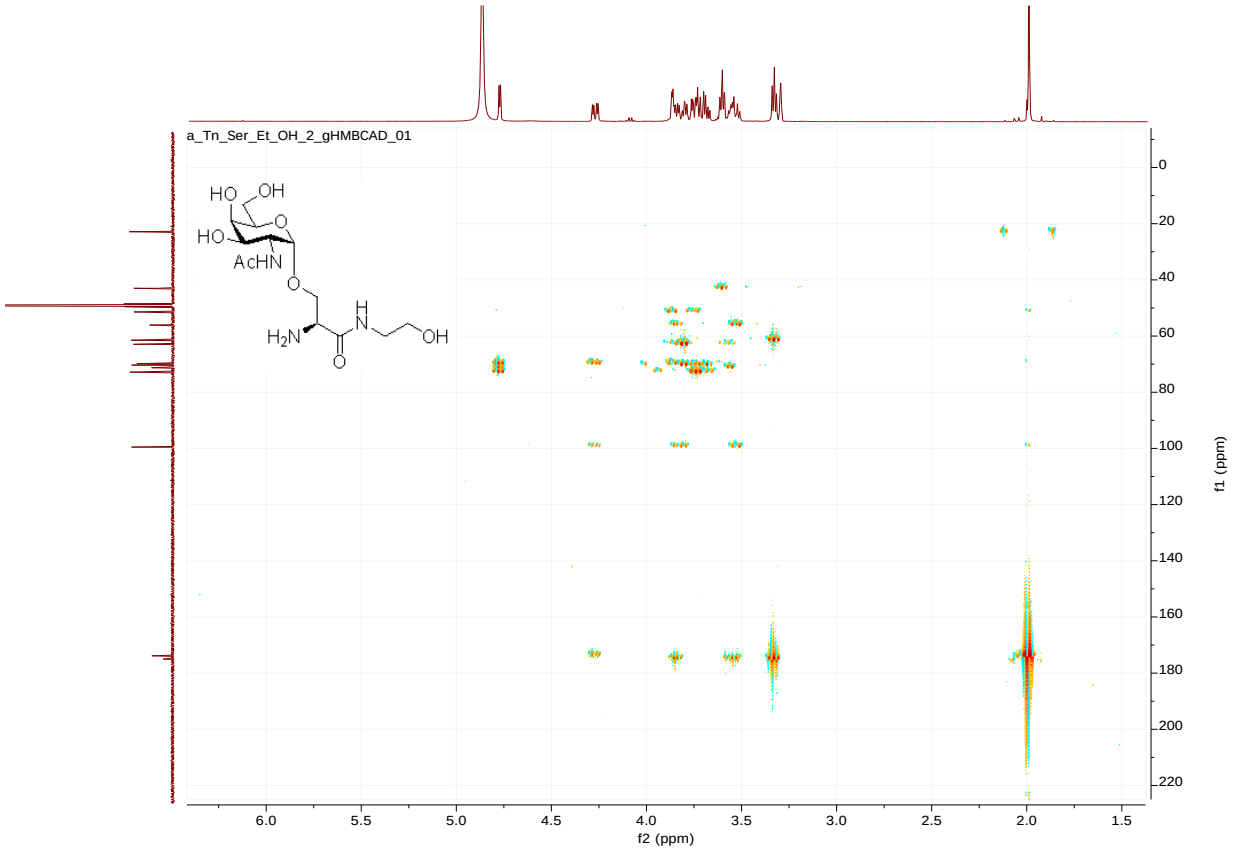

Figure 2.55: gHMBC NMR spectrum of compound **Tn2**

N-(N-Hydroxysuccinimidyl-adipoyl)-O-2-acetamido-2-deoxy-α-D-galactopyranosyl-L-serine ***(Tn1-NHS)****:*

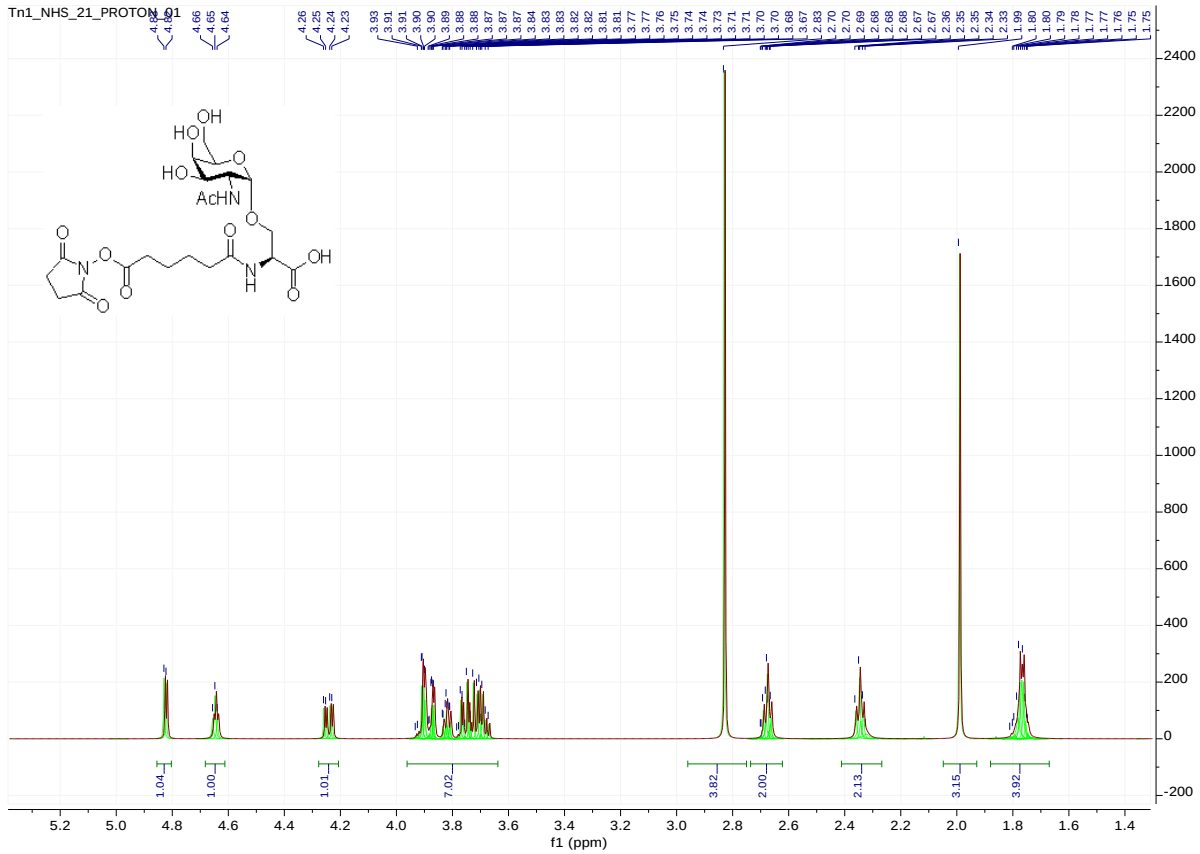

Figure 2.56: ^{1}H NMR spectrum of compound **Tn1-NHS**

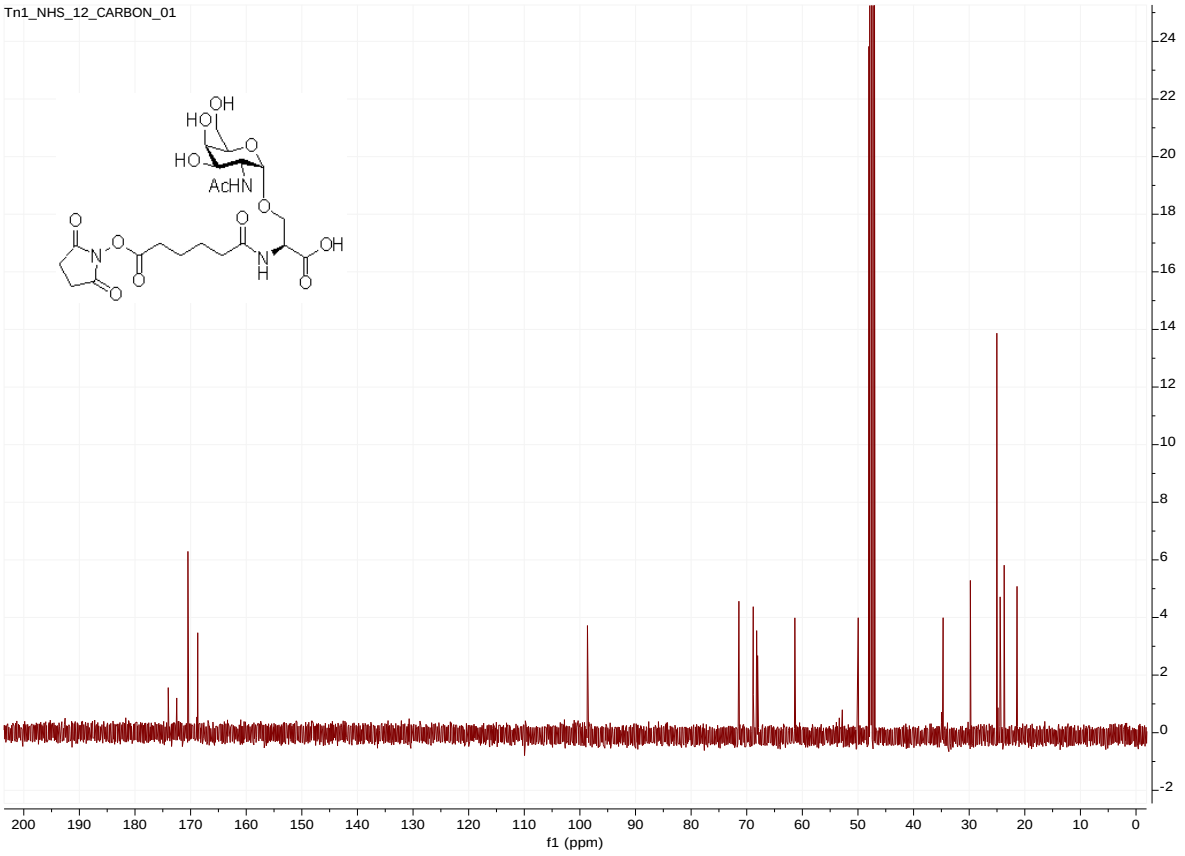

Figure 2.57: ^{13}C NMR spectrum of compound **Tn1-NHS**

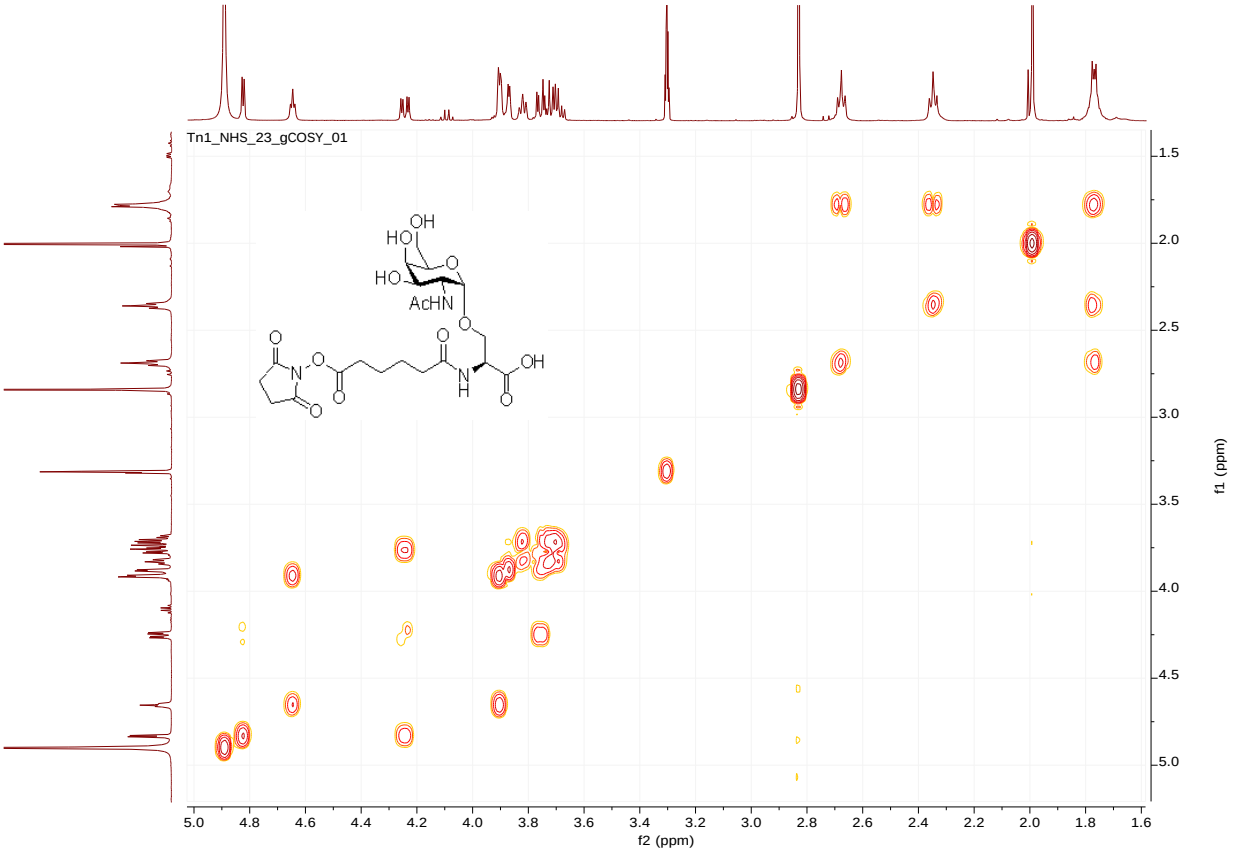

Figure 2.58: ^{1}H-^{1}H COSY NMR spectrum of compound **Tn1-NHS**

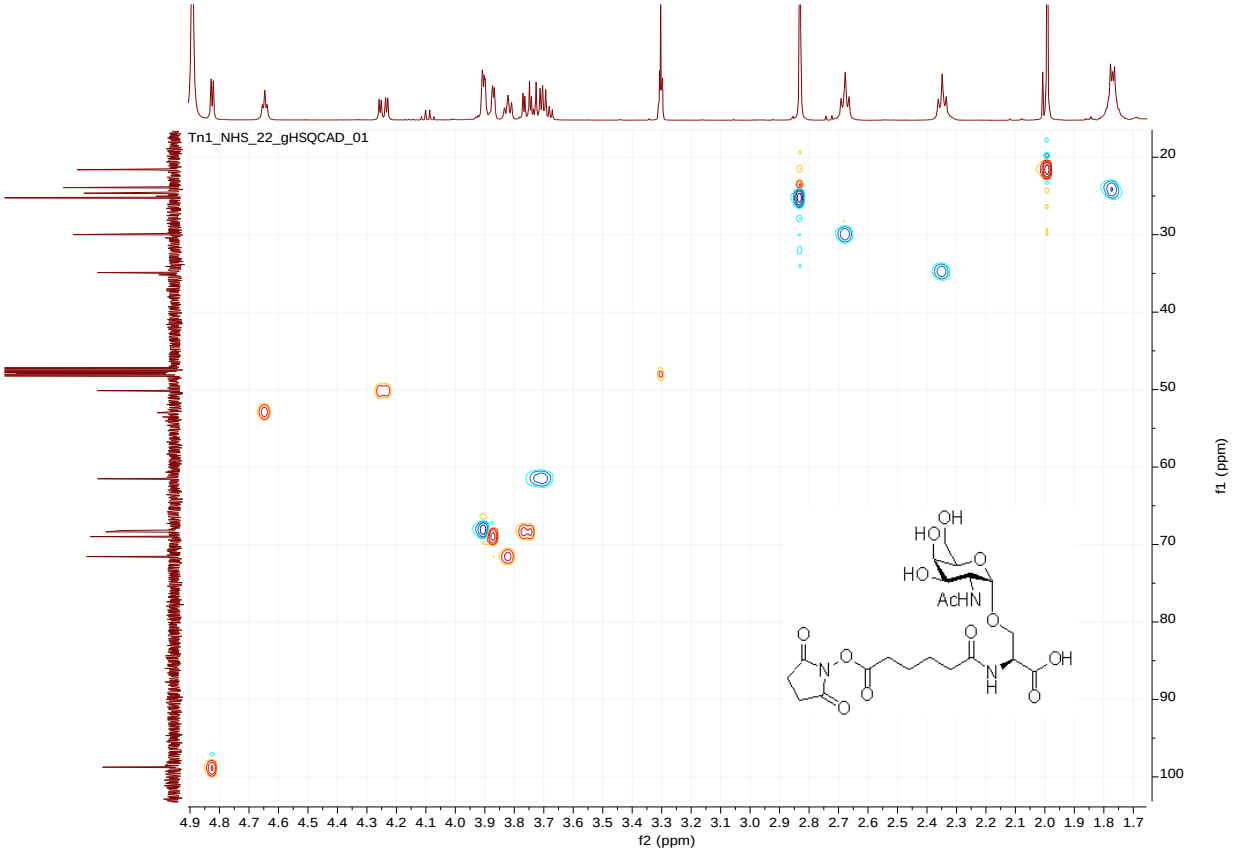

Figure 2.59: gHMQC NMR spectrum of compound **Tn1-NHS**

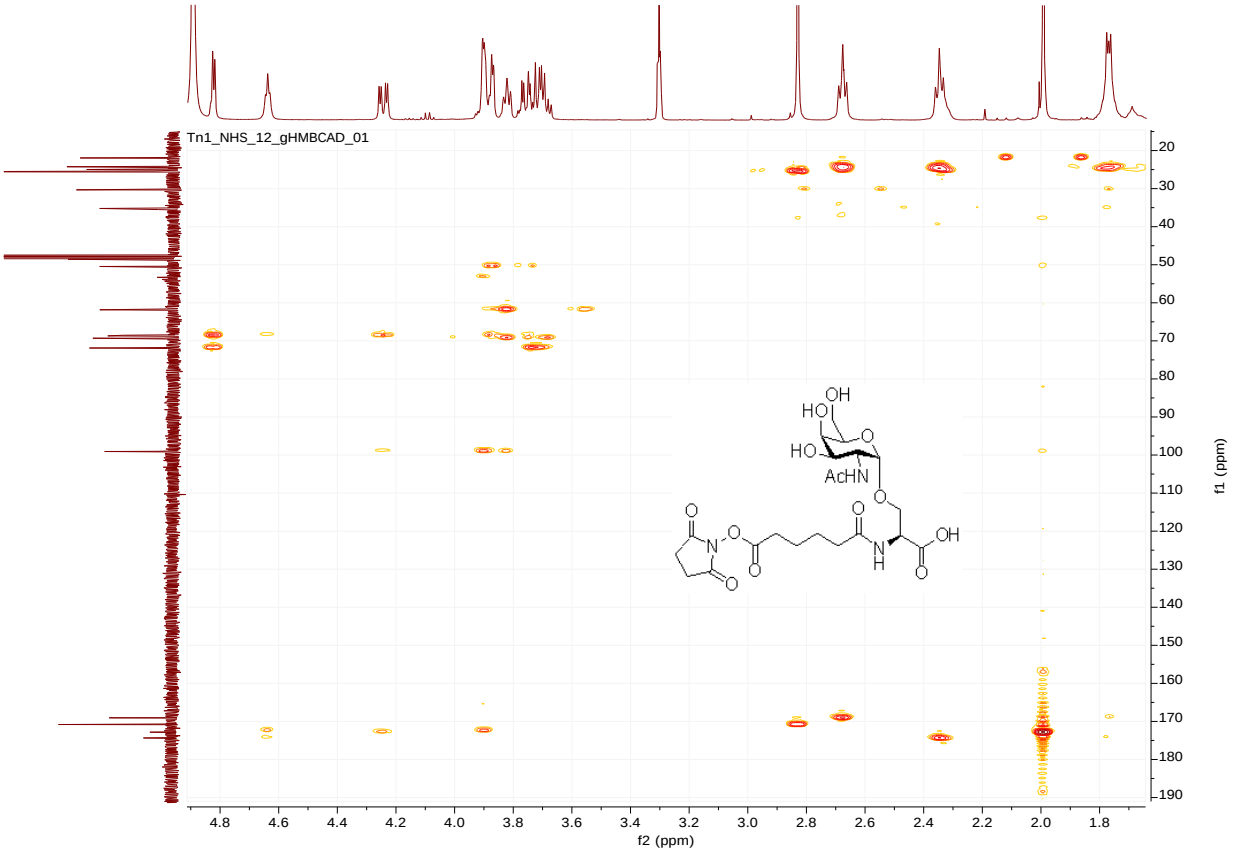

Figure 2.60: gHMBC NMR spectrum of compound **Tn1-NHS**

*N-(N-Hydroxysuccinimidyl adipatyl)-O-2-acetamido-2-deoxy-α-D-galactopyranosyl-L-serine 2-ethanolyl amide (**Tn2-NHS**):*

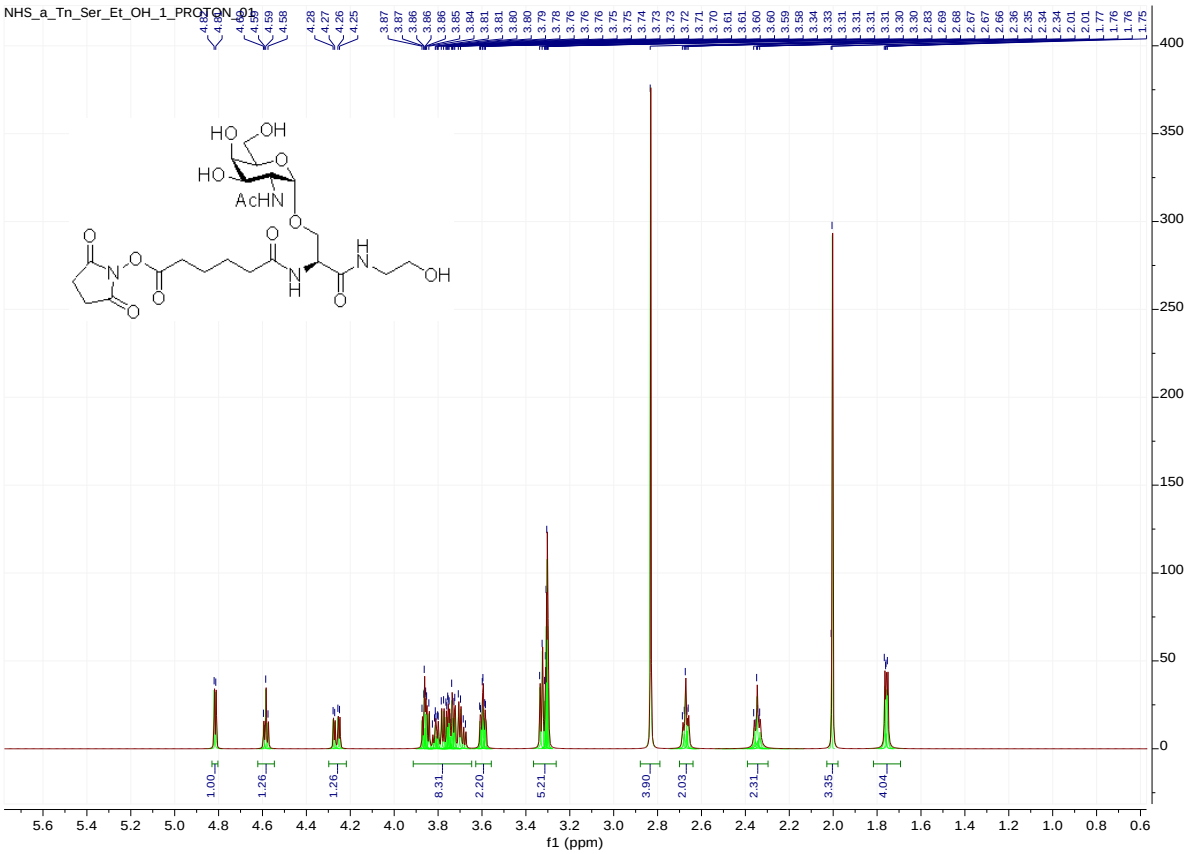

Figure 2.61: ^{1}H NMR spectrum of compound **Tn2-NHS**

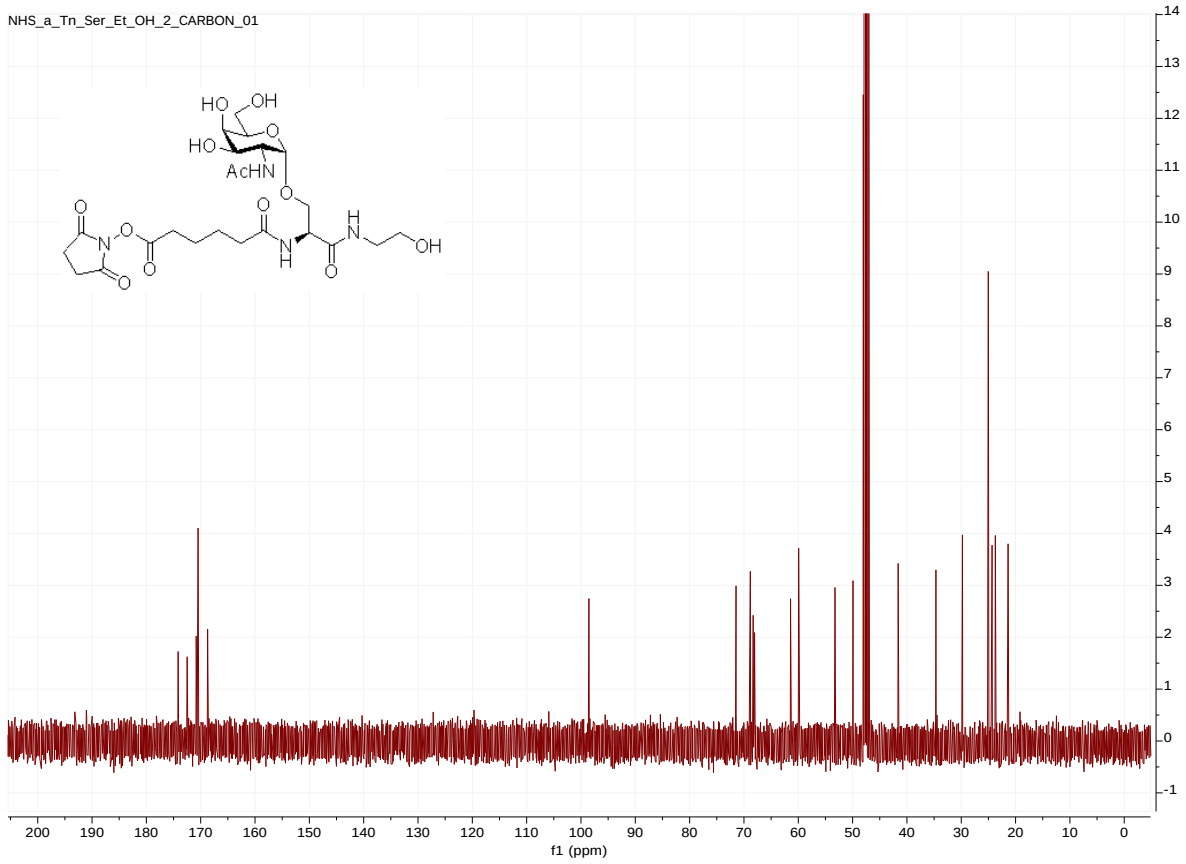

Figure 2.62: ^{13}C NMR spectrum of compound **Tn2-NHS**

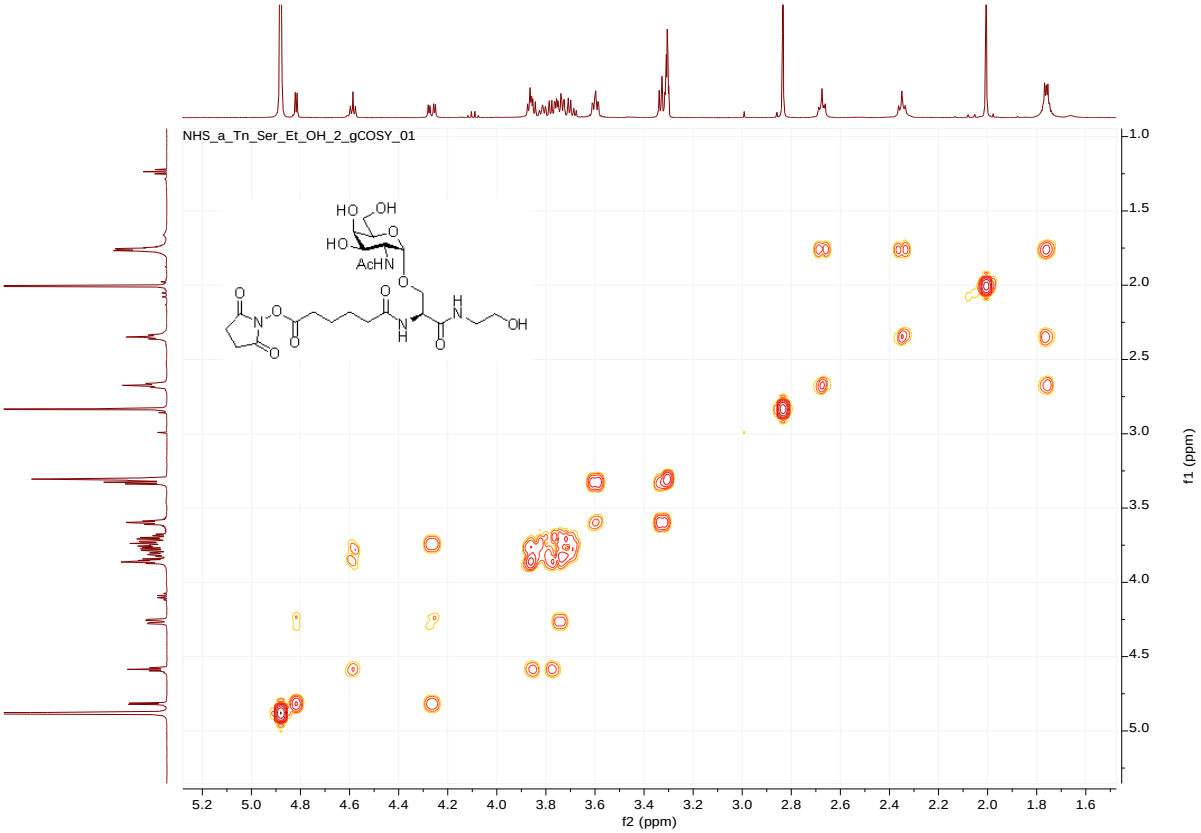

Figure 2.63: ^{1}H-^{1}H COSY NMR spectrum of compound **Tn2-NHS**

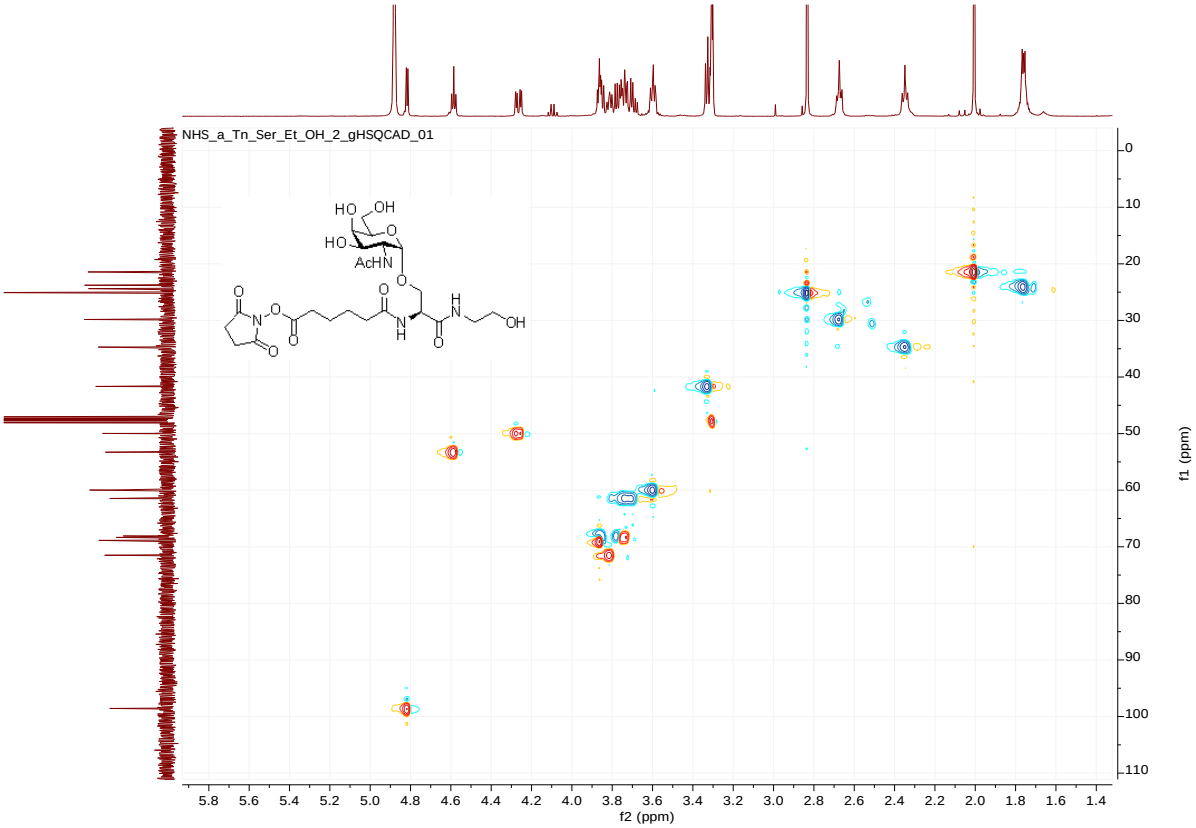

Figure 2.64: gHMQC NMR spectrum of compound **Tn2-NHS**

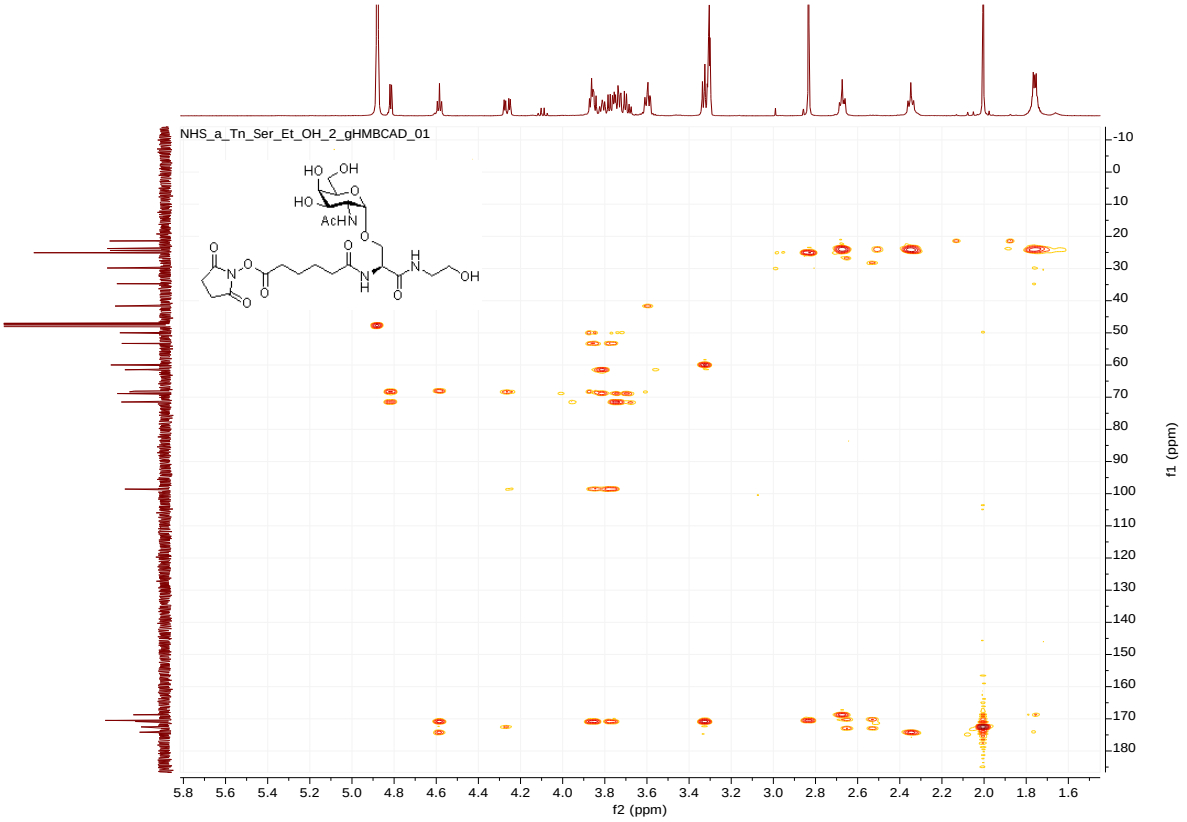

Figure 2.65: gHMBC NMR spectrum of compound **Tn2-NHS**

REFERENCES

REFERENCES

1. Bachmann, M. F.; Zinkernagel, R. M., Neutralizing antiviral B cell responses. *Annual Review of Immunology* **1997,** *15* (1), 235-270.

2. (a) Jegerlehner, A.; Storni, T.; Lipowsky, G.; Schmid, M.; Pumpens, P.; Bachmann, M. F., Regulation of IgG antibody responses by epitope density and CD21-mediated costimulation. *European Journal of Immunology* **2002,** *32* (11), 3305-3314; (b) Bachmann, M.; Rohrer, U.; Kundig, T.; Burki, K.; Hengartner, H.; Zinkernagel, R., The influence of antigen organization on B cell responsiveness. *Science* **1993,** *262* (5138), 1448-1451.

3. Vogelstein, B.; Dintzis, R. Z.; Dintzis, H. M., Specific cellular stimulation in the primary immune response: a quantized model. *Proceedings of the National Academy of Sciences of the United States of America* **1982,** *79* (2), 395-399.

4. Zabel, F.; Kündig, T. M.; Bachmann, M. F., Virus-induced humoral immunity: on how B cell responses are initiated. *Current Opinion in Virology* **2013,** *3* (3), 357-362.

5. Shirbaghaee, Z.; Bolhassani, A., Different applications of virus-like particles in biology and medicine: Vaccination and delivery systems. *Biopolymers* **2016,** *105* (3), 113-132.

6. Tan, M.; Jiang, X., Subviral particle as vaccine and vaccine platform. *Current Opinion in Virology* **2014,** *6*, 24-33.

7. (a) Fiedler, J. D.; Higginson, C.; Hovlid, M. L.; Kislukhin, A. A.; Castillejos, A.; Manzenrieder, F.; Campbell, M. G.; Voss, N. R.; Potter, C. S.; Carragher, B.; Finn, M. G., Engineered mutations change the structure and stability of a virus-like particle. *Biomacromolecules* **2012,** *13* (8), 2339-2348; (b) Rohovie, M. J.; Nagasawa, M.; Swartz, J. R., Virus-like particles: Next-generation nanoparticles for targeted therapeutic delivery. *Bioengineering & Translational Medicine* **2017**, 1-15.

8. (a) Lim, F.; Spingola, M.; Peabody, D. S., The RNA-binding site of bacteriophage Qβ coat protein. *Journal of Biological Chemistry* **1996,** *271* (50), 31839-31845; (b) Overby, L. R.; Barlow, G. H.; Doi, R. H.; Jacob, M.; Spiegelman, S., Comparison of two serologically distinct ribonucleic acid bacteriophages I. properties of the viral particles. *Journal of Bacteriology* **1966,** *91* (1), 442-448; (c) Lau, J. L.; Baksh, M. M.; Fiedler, J. D.; Brown, S. D.; Kussrow, A.; Bornhop, D. J.; Ordoukhanian, P.; Finn, M. G., Evolution and protein packaging of small-molecule RNA aptamers. *ACS Nano* **2011,** *5* (10), 7722-7729.

9. (a) Hung, P. P.; Ling, C. M.; Overby, L. R., Self-assembly of Qβ and MS2 phage particles: possible function of initiation complexes. *Science* **1969,** *166* (3913), 1638-1640; (b) Medrano, M.; Fuertes, M. Á.; Valbuena, A.; Carrillo, P. J. P.; Rodríguez-Huete, A.; Mateu, M. G., Imaging and quantitation of a succession of transient intermediates reveal the reversible self-assembly pathway of a simple icosahedral virus capsid. *Journal of the American Chemical Society* **2016,** *138* (47), 15385-15396.

10. Golmohammadi, R.; Fridborg, K.; Bundule, M.; Valegård, K.; Liljas, L., The crystal structure of bacteriophage Qβ at 3.5 å resolution. *Structure* **1996,** *4* (5), 543-554.

11. Akache, B.; Weeratna, R.; Deora, A.; Thorn, J.; Champion, B.; Merson, J.; Davis, H.; McCluskie, M., Anti-IgE Qb-VLP conjugate vaccine self-adjuvants through activation of TLR7. *Vaccines* **2016,** *4* (1), 3.

12. Jegerlehner, A.; Maurer, P.; Bessa, J.; Hinton, H. J.; Kopf, M.; Bachmann, M. F., TLR9 signaling in B cells determines class switch recombination to IgG2a. *The Journal of Immunology* **2007,** *178* (4), 2415-2420.

13. (a) Blander, J. M.; Medzhitov, R., Toll-dependent selection of microbial antigens for presentation by dendritic cells. *Nature* **2006,** *440* (7085), 808-812; (b) Bachmann, M. F.; Jennings, G. T., Vaccine delivery: a matter of size, geometry, kinetics and molecular patterns. *Nature Reviews Immunology* **2010,** *10* (11), 787-796.

14. (a) Hofstetter, H.; Monstein, H. J.; Weissmann, C., The readthrough protein A1 is essential for the formation of viable Qβ particles. *Biochimica et Biophysica Acta (BBA) - Nucleic Acids and Protein Synthesis* **1974,** *374* (2), 238-251; (b) Weiner, A. M.; Weber, K., A single UGA codon functions as a natural termination signal in the coliphage Qβ coat protein cistron. *Journal of Molecular Biology* **1973,** *80* (4), 837-855.

15. Dai, X.; Li, Z.; Lai, M.; Shu, S.; Du, Y.; Zhou, Z. H.; Sun, R., In situ structures of the genome and genome-delivery apparatus in a single-stranded RNA virus. *Nature* **2017,** *541* (7635), 112-116.

16. Vasiljeva, I.; Kozlovska, T.; Cielens, I.; Strelnikova, A.; Kazaks, A.; Ose, V.; Pumpens, P., Mosaic Qβ coats as a new presentation model. *FEBS Letters* **1998,** *431* (1), 7-11.

17. Udit, A. K.; Brown, S.; Baksh, M. M.; Finn, M. G., Immobilization of bacteriophage Qβ on metal-derivatized surfaces via polyvalent display of hexahistidine tags. *Journal of Inorganic Biochemistry* **2008,** *102* (12), 2142-2146.

18. Ashcroft, A. E.; Lago, H.; Macedo, J. M. B.; Horn, W. T.; Stonehouse, N. J.; Stockley, P. G., Engineering thermal stability in RNA phage capsids via disulphide bonds. *Journal of Nanoscience and Nanotechnology* **2005,** *5* (12), 2034-2041.

19. Maurer, P.; Jennings, G. T.; Willers, J.; Rohner, F.; Lindman, Y.; Roubicek, K.; Renner, W. A.; Müller, P.; Bachmann, M. F., A therapeutic vaccine for nicotine dependence: preclinical efficacy, and phase I safety and immunogenicity. *European Journal of Immunology* **2005,** *35* (7), 2031-2040.

20. Kündig, T. M.; Senti, G.; Schnetzler, G.; Wolf, C.; Prinz Vavricka, B. M.; Fulurija, A.; Hennecke, F.; Sladko, K.; Jennings, G. T.; Bachmann, M. F., Der p 1 peptide on virus-like particles is safe and highly immunogenic in healthy adults. *Journal of Allergy and Clinical Immunology* **2006,** *117* (6), 1470-1476.

21. Ambuhl, P. M. a.; Tissot, A. C. b.; Fulurija, A. b.; Maurer, P. b.; Nussberger, J. c.; Sabat, R. d.; Nief, V. a.; Schellekens, C. b.; Sladko, K. b.; Roubicek, K. b.; Pfister, T. b.; Rettenbacher, M. b.; Volk, H.-D. e.; Wagner, F. f.; Muller, P. b.; Jennings, G. T. b.; Bachmann, M. F. b., A vaccine for hypertension based on virus-like particles: preclinical efficacy and phase I safety and immunogenicity. *Journal of Hypertension* **2007,** *25* (1), 63-72.

22. Skibinski, D. A. G.; Hanson, B. J.; Lin, Y.; von Messling, V.; Jegerlehner, A.; Tee, J. B. S.; Chye, D. H.; Wong, S. K. K.; Ng, A. A. P.; Lee, H. Y.; Au, B.; Lee, B. T. K.; Santoso, L.; Poidinger, M.; Fairhurst, A.-M.; Matter, A.; Bachmann, M. F.; Saudan, P.; Connolly, J. E., Enhanced neutralizing antibody titers and Th1 polarization from a novel *Escherichia coli* derived pandemic influenza vaccine. *PLoS ONE* **2013,** *8* (10), e76571.

23. (a) Jeon, S. H.; Arnon, R., Immunization with influenza virus hemagglutinin globular region containing the receptor-binding pocket. *Viral Immunology* **2002,** *15* (1), 165-176; (b) Chiu, F.-F.; Venkatesan, N.; Wu, C.-R.; Chou, A.-H.; Chen, H.-W.; Lian, S.-P.; Liu, S.-J.; Huang, C.-C.; Lian, W.-C.; Chong, P.; Leng, C.-H., Immunological study of HA1 domain of hemagglutinin of influenza H5N1 virus. *Biochemical and Biophysical Research Communications* **2009,** *383* (1), 27-31; (c) Jegerlehner, A.; Zabel, F.; Langer, A.; Dietmeier, K.; Jennings, G. T.; Saudan, P.; Bachmann, M. F., Bacterially produced recombinant influenza vaccines based on virus-like particles. *PLoS ONE* **2013,** *8* (11), e78947.

24. Astronomo, R. D.; Kaltgrad, E.; Udit, A. K.; Wang, S.-K.; Doores, K. J.; Huang, C.-Y.; Pantophlet, R.; Paulson, J. C.; Wong, C.-H.; Finn, M. G.; Burton, D. R., Defining criteria for oligomannose immunogens for HIV using icosahedral virus capsid scaffolds. *Chemistry & Biology* **2010,** *17* (4), 357-370.

25. Spohn, G.; Schori, C.; Keller, I.; Sladko, K.; Sina, C.; Guler, R.; Schwarz, K.; Johansen, P.; Jennings, G. T.; Bachmann, M. F., Preclinical efficacy and safety of an anti-IL-1β vaccine for the treatment of type 2 diabetes. *Molecular Therapy — Methods & Clinical Development* **2014,** *1*, 14048.

26. Cavelti-Weder, C.; Timper, K.; Seelig, E.; Keller, C.; Osranek, M.; Lassing, U.; Spohn, G.; Maurer, P.; Muller, P.; Jennings, G. T.; Willers, J.; Saudan, P.; Donath, M. Y.; Bachmann, M. F., Development of an Interleukin-1[beta] vaccine in patients with type 2 diabetes. *Molecular Therapy* **2016,** *24* (5), 1003-1012.

27. (a) Qian, Y.-W.; Schmidt, R. J.; Zhang, Y.; Chu, S.; Lin, A.; Wang, H.; Wang, X.; Beyer, T. P.; Bensch, W. R.; Li, W.; Ehsani, M. E.; Lu, D.; Konrad, R. J.; Eacho, P. I.; Moller, D. E.; Karathanasis, S. K.; Cao, G., Secreted PCSK9 downregulates low density lipoprotein receptor through receptor-mediated endocytosis. *Journal of Lipid Research* **2007,** *48* (7), 1488-1498; (b) Kwon, H. J.; Lagace, T. A.; McNutt, M. C.; Horton, J. D.; Deisenhofer, J., Molecular basis for LDL receptor recognition by PCSK9. *Proceedings of the National Academy of Sciences* **2008,** *105* (6), 1820-1825.

28. Crossey, E.; Amar, M. J. A.; Sampson, M.; Peabody, J.; Schiller, J. T.; Chackerian, B.; Remaley, A. T., A cholesterol-lowering VLP vaccine that targets PCSK9. *Vaccine* **2015,** *33* (43), 5747-5755.

29. Mond, J. J.; Lees, A.; Snapper, C. M., T cell-independent antigens type 2. *Annual Review of Immunology* **1995,** *13* (1), 655-692.

30. Kagan, E.; Ragupathi, G.; Yi, S. S.; Reis, C. A.; Gildersleeve, J.; Kahne, D.; Clausen, H.; Danishefsky, S. J.; Livingston, P. O., Comparison of antigen constructs and carrier molecules for augmenting the immunogenicity of the monosaccharide epithelial cancer antigen Tn. *Cancer Immunology, Immunotherapy* **2005,** *54* (5), 424-430.

31. (a) Kuduk, S. D.; Schwarz, J. B.; Chen, X.-T.; Glunz, P. W.; Sames, D.; Ragupathi, G.; Livingston, P. O.; Danishefsky, S. J., Synthetic and immunological studies on clustered modes of mucin-related Tn and TF *O*-linked antigens: The preparation of a glycopeptide-based vaccine for clinical trials against prostate cancer. *Journal of the American Chemical Society* **1998,** *120* (48), 12474-12485; (b) Lo-Man, R.; Vichier-Guerre, S.; Perraut, R.; Dériaud, E.; Huteau, V.; BenMohamed, L.; Diop, O. M.; Livingston, P. O.; Bay, S.; Leclerc, C., A fully synthetic therapeutic vaccine candidate targeting carcinoma-associated Tn carbohydrate antigen induces tumor-specific antibodies in nonhuman primates. *Cancer Research* **2004,** *64* (14), 4987-4994; (c) Lo-Man, R.; Vichier-Guerre, S.; Bay, S.; Dériaud, E.; Cantacuzène, D.; Leclerc, C., Anti-tumor immunity provided by a synthetic multiple antigenic glycopeptide displaying a tri-Tn glycotope. *The Journal of Immunology* **2001,** *166* (4), 2849-2854.

32. Geyer, H.; Wuhrer, M.; Kurokawa, T.; Geyer, R., Characterization of keyhole limpet hemocyanin (KLH) glycans sharing a carbohydrate epitope with Schistosoma mansoni glycoconjugates. *Micron* **2004,** *35* (1–2), 105-106.

33. Yin, Z.; Nguyen, H. G.; Chowdhury, S.; Bentley, P.; Bruckman, M. A.; Miermont, A.; Gildersleeve, J. C.; Wang, Q.; Huang, X., Tobacco mosaic virus as a new carrier for tumor associated carbohydrate antigens. *Bioconjugate Chemistry* **2012,** *23* (8), 1694-1703.

34. Culver, J. N., Tobacco mosaic virus assembly and disassembly: Determinants in pathogenicity and resistance. *Annual Review of Phytopathology* **2002,** *40* (1), 287-308.

35. Yin, Z.; Comellas-Aragones, M.; Chowdhury, S.; Bentley, P.; Kaczanowska, K.; BenMohamed, L.; Gildersleeve, J. C.; Finn, M. G.; Huang, X., Boosting immunity to small tumor-associated carbohydrates with bacteriophage Qβ capsids. *ACS Chemical Biology* **2013,** *8* (6), 1253-1262.

36. Yin, Z.; Chowdhury, S.; McKay, C.; Baniel, C.; Wright, W. S.; Bentley, P.; Kaczanowska, K.; Gildersleeve, J. C.; Finn, M. G.; BenMohamed, L.; Huang, X., Significant impact of immunogen design on the diversity of antibodies generated by carbohydrate-based anticancer vaccine. *ACS Chemical Biology* **2015,** *10* (10), 2364-2372.

37. Jegerlehner, A.; Wiesel, M.; Dietmeier, K.; Zabel, F.; Gatto, D.; Saudan, P.; Bachmann, M. F., Carrier induced epitopic suppression of antibody responses induced by virus-like particles is a dynamic phenomenon caused by carrier-specific antibodies. *Vaccine* **2010,** *28* (33), 5503-5512.

38. (a) Schutze, M. P.; Deriaud, E.; Przewlocki, G.; LeClerc, C., Carrier-induced epitopic suppression is initiated through clonal dominance. *The Journal of Immunology* **1989,** *142* (8), 2635-40; (b) Leclerc, C.; Schutze, M. P.; Deriaud, E.; Przewlocki, G., The *in vivo* elimination of CD4+ T cells prevents the induction but not the expression of carrier-induced epitopic suppression. *The Journal of Immunology* **1990,** *145* (5), 1343-9; (c) Galelli, A.; Charlot, B., Clonal anergy of memory B cells in epitope-specific regulation. *The Journal of Immunology* **1990,** *145* (8), 2397-405.

39. Evans, M. C., Recent advances in immunoinformatics: application of in silico tools to drug development. *Curr Opin Drug Discov Devel* **2008,** *11* (2), 233-41.

40. Haste Andersen, P.; Nielsen, M.; Lund, O., Prediction of residues in discontinuous B-cell epitopes using protein 3D structures. *Protein Science* **2006,** *15* (11), 2558-2567.

41. Carrillo-Tripp, M.; Shepherd, C. M.; Borelli, I. A.; Venkataraman, S.; Lander, G.; Natarajan, P.; Johnson, J. E.; Brooks, C. L.; Reddy, V. S., VIPERdb2: an enhanced and web API enabled relational database for structural virology. *Nucleic Acids Research* **2009,** *37* (suppl 1), D436-D442.

42. (a) Prasuhn, D. E.; Singh, P.; Strable, E.; Brown, S.; Manchester, M.; Finn, M. G., Plasma clearance of bacteriophage Qβ particles as a function of surface charge. *Journal of the American Chemical Society* **2008,** *130* (4), 1328-1334; (b) Udit, A. K.; Everett, C.; Gale, A. J.; Reiber Kyle, J.; Ozkan, M.; Finn, M. G., Heparin antagonism by polyvalent display of cationic motifs on virus-like particles. *ChemBioChem* **2009,** *10* (3), 503-510.

43. Hovlid, M. L. The chemical and genetic engineering of Qβ virus-like particles for cell targeting and delivery. The Scripps Research Institute, La Jolla,, 2014.

44. Jessen, B.; Faller, S.; Krempl, C. D.; Ehl, S., Major histocompatibility complex-dependent cytotoxic T lymphocyte repertoire and functional avidity contribute to strain-specific disease susceptibility after murine respiratory syncytial virus infection. *Journal of Virology* **2011,** *85* (19), 10135-10143.

45. Plevka, P.; Tars, K.; Liljas, L., Structure and stability of icosahedral particles of a covalent coat protein dimer of bacteriophage MS2. *Protein Science : A Publication of the Protein Society* **2009,** *18* (8), 1653-1661.

46. Link, A.; Zabel, F.; Schnetzler, Y.; Titz, A.; Brombacher, F.; Bachmann, M. F., Innate immunity mediates follicular transport of particulate but not soluble protein antigen. *The Journal of Immunology* **2012,** *188* (8), 3724-3733.

47. Craig, D. B.; Dombkowski, A. A., Disulfide by Design 2.0: a web-based tool for disulfide engineering in proteins. *BMC Bioinformatics* **2013,** *14* (1), 346.

48. (a) Da Ren, H. S. G., Paul Raimville, Tom Wheat, Reb J. Russell and Jeff R. Mazzeo *Mass spectrometry quantification of protein mixtures*; Water Corperation: Milford, MA, USA, 2004; (b) Wright, T. H.; Bower, B. J.; Chalker, J. M.; Bernardes, G. J. L.; Wiewiora, R.; Ng, W.-L.; Raj, R.; Faulkner, S.; Vallée, M. R. J.; Phanumartwiwath, A.; Coleman, O. D.; Thézénas, M.-L.; Khan, M.; Galan, S. R. G.; Lercher, L.; Schombs, M. W.; Gerstberger, S.; Palm-Espling, M. E.; Baldwin, A. J.; Kessler, B. M.; Claridge, T. D. W.; Mohammed, S.; Davis, B. G., Posttranslational mutagenesis: A chemical strategy for exploring protein side-chain diversity. *Science* **2016**.

49. Sungsuwan, S.; Yin, Z.; Huang, X., Lipopeptide-coated iron oxide nanoparticles as potential glycoconjugate-based synthetic anticancer vaccines. *ACS Applied Materials & Interfaces* **2015,** *7* (31), 17535-17544.

50. Brown, S. D. Bacteriophage Qβ: A versatile platform for nanoengineering The Scripps Research Institute, La Jolla,, 2010.

51. Sedlik, C.; Heitzmann, A.; Viel, S.; Ait Sarkouh, R.; Batisse, C.; Schmidt, F.; De La Rochere, P.; Amzallag, N.; Osinaga, E.; Oppezzo, P.; Pritsch, O.; Sastre-Garau, X.; Hubert, P.; Amigorena, S.; Piaggio, E., Effective antitumor therapy based on a novel antibody-drug conjugate targeting the Tn carbohydrate antigen. *OncoImmunology* **2016,** *5* (7), e1171434.

52. (a) Laubreton, D.; Bay, S.; Sedlik, C.; Artaud, C.; Ganneau, C.; Dériaud, E.; Viel, S.; Puaux, A.-L.; Amigorena, S.; Gérard, C.; Lo-Man, R.; Leclerc, C., The fully synthetic MAG-Tn3 therapeutic vaccine containing the tetanus toxoid-derived TT830-844 universal epitope provides anti-tumor immunity. *Cancer Immunology, Immunotherapy* **2016,** *65* (3), 315-325; (b) Hubert, P.; Heitzmann, A.; Viel, S.; Nicolas, A.; Sastre-Garau, X.; Oppezzo, P.; Pritsch, O.; Osinaga, E.; Amigorena, S., Antibody-dependent cell cytotoxicity synapses form in mice during tumor-specific antibody immunotherapy. *Cancer Research* **2011,** *71* (15), 5134-5143.

53. (a) Lo-Man, R.; Bay, S.; Vichier-Guerre, S.; Dériaud, E.; Cantacuzène, D.; Leclerc, C., A fully synthetic immunogen carrying a carcinoma-associated carbohydrate for active specific immunotherapy. *Cancer Research* **1999,** *59* (7), 1520-1524; (b) Posey, Avery D., Jr.; Schwab, Robert D.; Boesteanu, Alina C.; Steentoft, C.; Mandel, U.; Engels, B.; Stone, Jennifer D.; Madsen, Thomas D.; Schreiber, K.; Haines, Kathleen M.; Cogdill, Alexandria P.; Chen, Taylor J.; Song, D.; Scholler, J.; Kranz, David M.; Feldman, Michael D.; Young, R.; Keith, B.; Schreiber, H.; Clausen, H.; Johnson, Laura A.; June, Carl H., Engineered CAR T cells targeting the cancer-associated Tn-glycoform of the membrane mucin MUC1 control adenocarcinoma. *Immunity 44* (6), 1444-1454.

54. Tseng, Y.-S.; Agbandje-Mckenna, M., Mapping the AAV capsid host antibody response toward the development of second generation gene delivery vectors. *Frontiers in Immunology* **2014,** *5* (9).

55. (a) Sgroi, D.; Varki, A.; Braesch-Andersen, S.; Stamenkovic, I., CD22, a B cell-specific immunoglobulin superfamily member, is a sialic acid-binding lectin. *Journal of Biological Chemistry* **1993,** *268* (10), 7011-7018; (b) Crocker, P. R.; Mucklow, S.; Bouckson, V.; McWilliam, A.; Willis, A. C.; Gordon, S.; Milon, G.; Kelm, S.; Bradfield, P., Sialoadhesin, a macrophage sialic acid binding receptor for haemopoietic cells with 17 immunoglobulin-like domains. *The EMBO Journal* **1994,** *13* (19), 4490-4503.

56. (a) Macauley, M. S.; Crocker, P. R.; Paulson, J. C., Siglec-mediated regulation of immune cell function in disease. *Nature Reviews Immunology* **2014,** *14* (10), 653-666; (b) Poe, J. C.; Tedder, T. F., CD22 and Siglec-G in B cell function and tolerance. *Trends in Immunology* **2012,** *33* (8), 413-420; (c) Courtney, A. H.; Puffer, E. B.; Pontrello, J. K.; Yang, Z.-Q.; Kiessling, L. L., Sialylated multivalent antigens engage CD22 in trans and inhibit B cell activation. *Proceedings of the National Academy of Sciences* **2009,** *106* (8), 2500-2505; (d) Macauley, M. S.; Pfrengle, F.; Rademacher, C.; Nycholat, C. M.; Gale, A. J.; von Drygalski, A.; Paulson, J. C., Antigenic liposomes displaying CD22 ligands induce antigen-specific B cell apoptosis. *The Journal of Clinical Investigation* **2013,** *123* (7), 3074-3083.

57. Duong, B. H.; Tian, H.; Ota, T.; Completo, G.; Han, S.; Vela, J. L.; Ota, M.; Kubitz, M.; Bovin, N.; Paulson, J. C.; Nemazee, D., Decoration of T-independent antigen with ligands for CD22 and Siglec-G can suppress immunity and induce B cell tolerance in vivo. *The Journal of Experimental Medicine* **2010,** *207* (1), 173-187.

58. (a) Blixt, O.; Paulson, J. C., Biocatalytic preparation of N-glycolylneuraminic acid, deaminoneuraminic acid (KDN) and 9-azido-9-deoxysialic acid oligosaccharides. *Advanced Synthesis & Catalysis* **2003,** *345* (6-7), 687-690; (b) Collins, B. E.; Blixt, O.; Han, S.; Duong, B.; Li, H.; Nathan, J. K.; Bovin, N.; Paulson, J. C., High-affinity ligand probes of CD22 overcome the threshold set by cis ligands to allow for binding, endocytosis, and killing of B cells. *The Journal of Immunology* **2006,** *177* (5), 2994-3003.

59. Kaltgrad, E.; O'Reilly, M. K.; Liao, L.; Han, S.; Paulson, J. C.; Finn, M. G., On-virus construction of polyvalent glycan ligands for cell-surface receptors. *Journal of the American Chemical Society* **2008,** *130* (14), 4578-4579.

60. Matsumoto, Y.; Zhang, Q.; Akita, K.; Nakada, H.; Hamamura, K.; Tokuda, N.; Tsuchida, A.; Matsubara, T.; Hori, T.; Okajima, T.; Furukawa, K.; Urano, T.; Furukawa, K., pp-GalNAc-T13 induces high metastatic potential of murine Lewis lung cancer by generating trimeric Tn antigen. *Biochemical and Biophysical Research Communications* **2012,** *419* (1), 7-13.

61. (a) Hsia, Y.; Bale, J. B.; Gonen, S.; Shi, D.; Sheffler, W.; Fong, K. K.; Nattermann, U.; Xu, C.; Huang, P.-S.; Ravichandran, R.; Yi, S.; Davis, T. N.; Gonen, T.; King, N. P.; Baker, D., Design of a hyperstable 60-subunit protein icosahedron. *Nature* **2016,** *535* (7610), 136-139; (b) Bale, J. B.; Gonen, S.; Liu, Y.; Sheffler, W.; Ellis, D.; Thomas, C.; Cascio, D.; Yeates, T. O.; Gonen, T.; King, N. P.; Baker, D., Accurate design of megadalton-scale two-component icosahedral protein complexes. *Science* **2016,** *353* (6297), 389-394; (c) Zhang, L.; Lua, L. H. L.; Middelberg, A. P. J.; Sun, Y.; Connors, N. K., Biomolecular engineering of virus-like particles aided by computational chemistry methods. *Chemical Society Reviews* **2015,** *44* (23), 8608-8618.

62. Asensio, M. A.; Morella, N. M.; Jakobson, C. M.; Hartman, E. C.; Glasgow, J. E.; Sankaran, B.; Zwart, P. H.; Tullman-Ercek, D., A selection for assembly reveals that a single amino acid mutant of the bacteriophage MS2 coat protein forms a smaller virus-like particle. *Nano Letters* **2016,** *16* (9), 5944-5950.

63. Luthe, D. S., A simple technique for the preparation and storage of sucrose gradients. *Analytical Biochemistry* **1983,** *135* (1), 230-232.

64. Ludek, O. R.; Gu, W.; Gildersleeve, J. C., Activation of glycosyl trichloroacetimidates with perchloric acid on silica (HClO4–SiO2) provides enhanced α-selectivity. *Carbohydrate Research* **2010,** *345* (14), 2074-2078.

65. Mukai, S.; Flematti, G. R.; Byrne, L. T.; Besant, P. G.; Attwood, P. V.; Piggott, M. J., Stable triazolylphosphonate analogues of phosphohistidine. *Amino Acids* **2012,** *43* (2), 857-874.

66. Miermont, A.; Barnhill, H.; Strable, E.; Lu, X.; Wall, K. A.; Wang, Q.; Finn, M. G.; Huang, X., Cowpea mosaic virus capsid: A promising carrier for the development of carbohydrate based antitumor vaccines. *Chemistry – A European Journal* **2008,** *14* (16), 4939-4947.